NASA TP-1999-209202

Advanced Cosmic-Ray Composition Experiment for Space Station (ACCESS)

ACCESS Accommodation Study Report

Under the direction of

Thomas L. Wilson
NASA Johnson Space Center
Houston, Texas

and

John P. Wefel
Louisiana State University
Baton Rouge, Louisiana

June 1999

Available from:

ii

Foreword

As we approach the 21st century, NASA has embarked upon an ambitious plan known as the Space Science Enterprise whose goals are aimed at answering a number of fundamental questions. These include the study of the origin of the Universe, the evolution of galaxies, stars, and solar systems, and the destiny of the Earth in the cosmos. An unprecedented opportunity in space exploration is now presenting itself. It is a time when breathtaking discoveries are being made in space about our own solar system and Universe while similar advances are coming forth in all the sciences and technologies back on Earth.

To this end, the construction and completion of the International Space Station (ISS) represents an important next step, and an opportunity to pursue missions of scientific exploration at the threshold of space, unhampered by the Earth's atmosphere. It is there, in low Earth orbit, that measurements of greater precision and longer duration are feasible which may bring together the disciplines of particle physics, astrophysics, and cosmology in much the same way that the orbiting Hubble Space Telescope has opened new vistas in astronomy.

One such experiment entitled the Advanced Cosmic-Ray Composition Experiment for Space Station (ACCESS) is proposed to measure the very high-energy nuclei in space (or "cosmic rays") and their relative abundances, comprising all of the elements in the periodic table. This large-area instrument will be designed for a four-year exposure in orbit, with the goal of determining the origin and acceleration mechanism for these particles at energies far above anything producible by Earth-based accelerators. This report summarizes our preliminary study of the accommodations such as power, weight, and other infrastructure provided for ACCESS by the ISS and the related Space Shuttle interfaces during launch, deployment, and return.

We are pleased to conclude that ACCESS in its current, preliminary baseline design can readily be accommodated by the ISS and Shuttle for a wide range of instrument configurations of varying size and weight—all of which are defined in the report which follows.

Table of Contents

Table of Contents

(continued)

Table of Contents

(continued)

Table of Contents

(continued)

Tables

Table of Contents

(continued)

Table of Contents
(continued)

Table of Contents

(continued)

Figures (continued)

Summary

In 1994 the first high-energy particle physics experiment for the Space Station, the Alpha Magnetic Spectrometer (AMS), was selected by NASA's Administrator as a joint collaboration with the U.S. Department of Energy. The AMS program was chartered to place a magnetic spectrometer in Earth orbit and search for cosmic antimatter. A natural consequence of this decision was that NASA would begin to explore cost-effective ways through which the design and implementation of AMS might benefit other promising payload experiments evolving from the Office of Space Science.

The first such experiment to come forward was Advanced Cosmic-Ray Composition Experiment for Space Station (ACCESS) in 1996. It was proposed as a new mission concept in space physics to attach a cosmic-ray experiment of weight, volume, and geometry similar to the AMS on the International Space Station (ISS), and replace the latter as its successor when the AMS is returned to Earth. This was to be an extension of NASA's suborbital balloon program, with balloon payloads serving as the precursor flights and heritage for ACCESS. The balloon programs have always been a cost-effective NASA resource since the particle physics instrumentation for balloon and space applications are directly related.

The next step was to expand the process, pooling together expertise from various NASA centers and universities while opening up definition of the ACCESS science goals to the international community through the standard practice of peer review. This process is still ongoing, and the accommodation study presented here will discuss the baseline definition of ACCESS as we understand it today. Further detail on the history, scope, and background of the study is provided in Appendix A.

Introduction to ACCESS

ACCESS science goals

The puzzle of cosmic radiation

The origin and composition of the cosmic rays has continued to be one of the most important problems in astrophysics since their discovery[1-3] in 1912. Although we have learned a great deal about the nature of cosmic rays, much remains a mystery. It was believed for some time by Lemaitre[4,5], as one of the founding fathers of the Big Bang theory, that the cosmic rays were relics left over from the origin of the Universe. However, as experiment and observation improved to the present day, it is now thought that these highly energetic nuclei, stripped of their electrons, are accelerated by the shock fronts of supernovae (SN) or exploding stars. Although this may be the source of energy, cosmic-ray origin is still unknown. The all-particle flux is illustrated in Figure 1, representing the collective knowledge we currently have as measured from a number of sources such as Earth-based, balloon-borne, and a few space-based detectors.
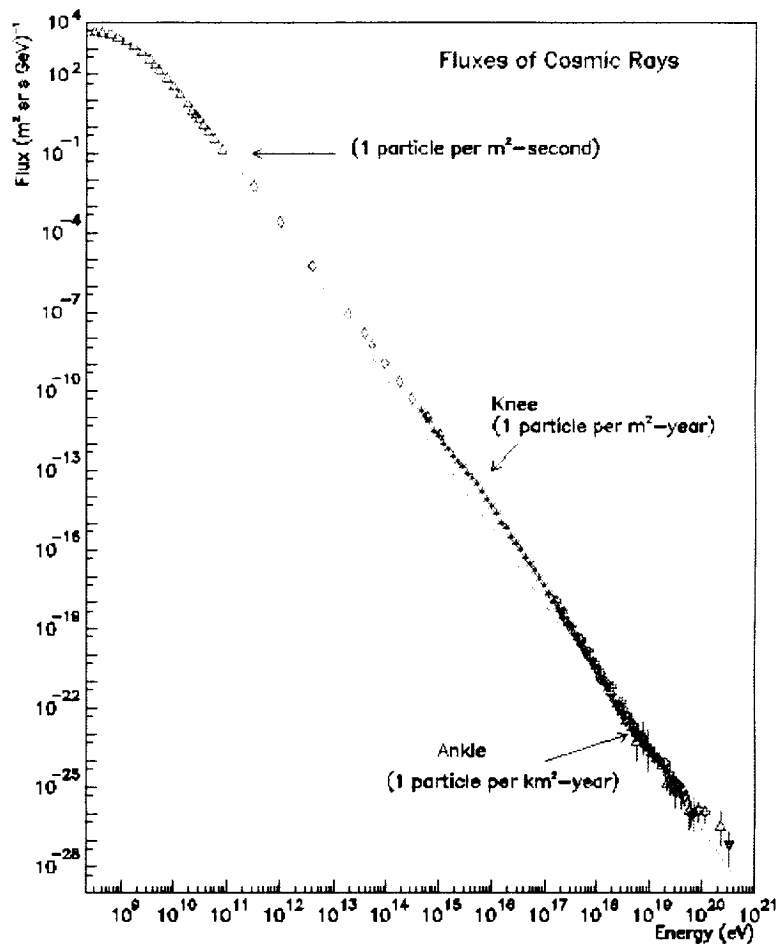
Figure 1. The all-particle flux of cosmic rays[6].

The ACCESS science mission

ACCESS is a new mission concept[7-11] whose science goals are to address many of the remaining questions about these cosmic rays which bathe our planet Earth. It is envisioned as the next-generation cosmic-ray observatory for measuring the elemental composition of the cosmic rays to very high energies, while acquiring valuable information on the individual element abundances throughout the periodic table. In particular, it is a goal of ACCESS to explore the possibility that SN shock fronts (Figure 2) are the acceleration mechanism for the bulk of cosmic rays with energies in the region of the "knee" in Figure 1.

Other ACCESS science goals can be summarized as follows:

- Test SN shock acceleration models at energies up to 10^{15} eV.

- Measure energy dependence of secondary to primary elements.

- Distinguish between first ionization potential (FIP) source injection versus acceleration from dust grains.

- Measure separately elements synthesized by s-process (slow) and r-process (rapid).
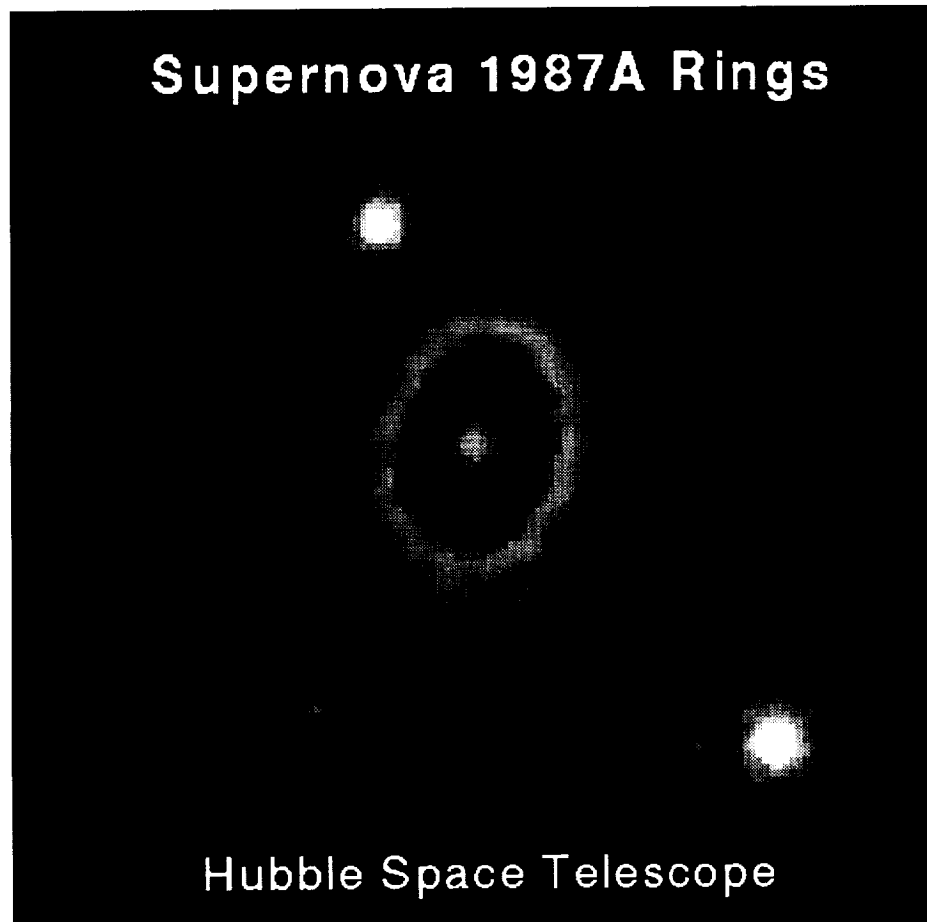
Figure 2. Supernova 1987A.

3

The more abundant nuclei, lighter than Fe, will be measured to energies of about 10^{15} eV. ACCESS will be capable of detecting fluxes of ultra-heavy (UH) nuclei more massive than Fe, and will do this with high charge (Z) resolution. This should allow important new measurements of elements at least to Z=83 (Bi). These data will prove valuable in our understanding of the nucleosynthesis of such elements and their abundances in the Universe.

The ACCESS mission will consist of a large-area detector (several square meters) deployed on the ISS for at least 4 years' duration. The result should be a cosmic-ray observatory in low Earth orbit (LEO) with a collecting power (area x exposure time) approaching 10,000 m^2-sr-days. From Figure 1, such a collecting power should result in about 10 measurements in the neighborhood of the cosmic-ray "knee" during this mission. ACCESS would be launched on board the Space Shuttle, and attached to the ISS sometime after final assembly of that orbiting laboratory. Present plans expect this deployment of ACCESS to occur around the year 2005.

The baseline ACCESS instrument

The baseline ACCESS instrument addressed in this study will consist of three detectors. The first is a Bi germanate (BGO) calorimeter for measuring the energy spectra of H and He, and limited numbers of heavier elements, up to 10^{15} eV. The second is a transition radiation detector (TRD) capable of measuring the energy spectra of Li to Fe. The third detector is the charge module (CM) or "Z" identification module (ZIM) for element identification of UHs and the lighter cosmic rays. Figure 3, depicting the collective instrument, illustrates one of the four structural options considered in this study as a baseline design for ACCESS instrument geometry.

Since the CM is located at the top of the ACCESS instrument, it must be capable of measuring the charge (Z) of all incident particles, from H through U, with dynamic range > 10^4. Overall, the CM is optimized for measurement of UH nuclei, and the charge measurements for the lighter particles are needed by the TRD and calorimeter modules. The CM contains two layers of Si detectors that provide excellent charge resolution up to Z>80. The Si detector near the bottom of the module provides a redundant charge measurement and identifies particles which interact. Two layers of scintillating fiber hodoscopes, located on the top and bottom, are used to determine the incident particle trajectory, and two Cherenkov detectors measure the particle velocity. For a 1000-day exposure the CM should collect more than a hundred Pt and Pb events with single-charge resolution.

The TRD module consists of six radiator layers, each of which is followed by a stack of gas-filled proportional tubes to measure the transition radiation X-ray photons. Alternate proportional tube layers are oriented at right angles so that the trajectory of the incident particle can be determined. Scintillators at the top and bottom measure the charge upon entry and exit from the module. Transition radiation is emitted for a high-energy charged particle passing between two regions of differing indices of refraction. The photon yield is proportional to Z^2 and the Lorentz factor (γ, gamma) of the particle and to the number of layers ('transitions'). The TRD covers a broad energy range up to a gamma of about 50,000 and should be able to observe Li and heavier nuclei.
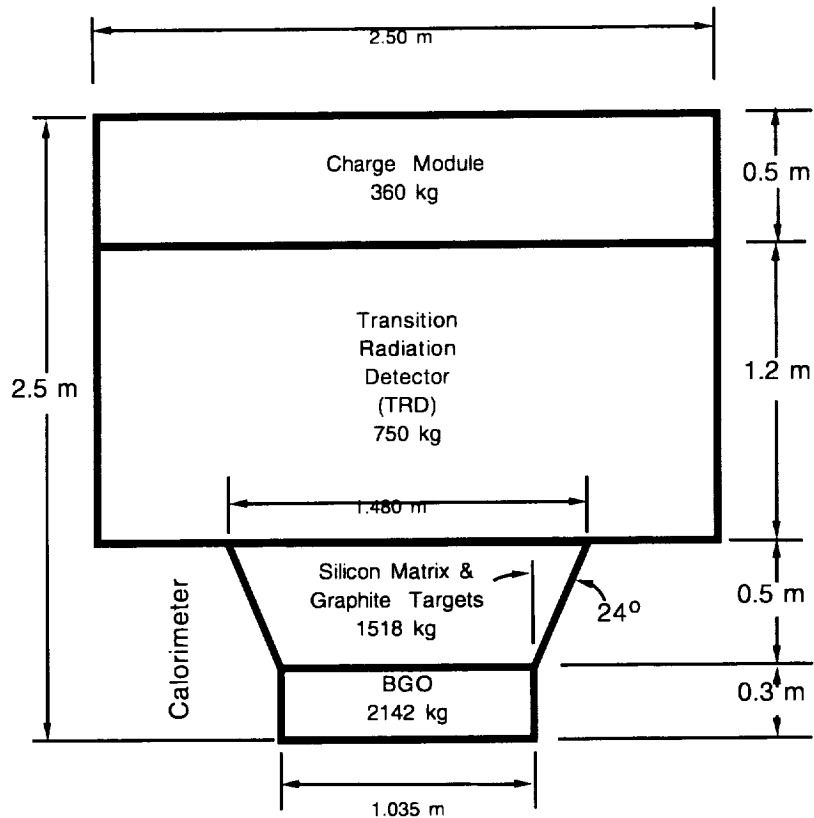
Figure 3. One of four instrument configurations assumed in the baseline ACCESS study.

The hadron calorimeter is composed of a one-interaction-length target of inert C (carbon) followed by a fully active, segmented calorimeter constructed from BGO crystals. Scintillator hodoscope planes are interspersed within the C to provide a fast trigger, and a Si matrix detector above the target provides a charge measurement for events that may have, or may have not, passed through the CM. The thickness of the BGO is selected to obtain better than 63% energy resolution to the highest energies. The target provides an interaction probability for H of about 50%, so for a 1000-day exposure the collecting power of the calorimeter is about 500 m^2-sr-days.

Additional information and detail on the three separate ACCESS detector systems, the BGO calorimeter, the CM, and the TRD, are provided in Appendix B, along with a composite representation of the consolidated instrument. The different structural options are defined in Appendix G.

Science detail

"How do cosmic rays gain their enormous energies?" "What is the source of the material that goes into their 'cosmic accelerator' to become high-energy cosmic rays?" "How do these high-energy particles propagate within, and escape from, our Galaxy?" Those are some of the principal science questions that the ACCESS mission is designed to address. The astrophysical implications are of central importance to the "Structure and Evolution of the Universe" theme in NASA's Office of Space Science.

5

Cosmic rays contain the nuclei of atoms covering all of the periodic table (H....Fe.....U) as well as electrons, X rays, gamma rays, anti-protons, positrons, and neutrinos. These are all at high energy, extending well beyond the energies available in terrestrial accelerators. The cosmic rays fill our Galaxy, as well as other galaxies, and are an important component in the dynamics of the Galactic disk. Cosmic-ray electrons are the source of the important radio synchrotron emission from all galaxies, and cosmic rays are a source of the high-energy photons observed in gamma-ray experiments. We know quite a bit about the cosmic rays from many decades of study, yet their exact source and the details of their acceleration to high energy remain a mystery. ACCESS is designed to tackle this problem by extending current knowledge to the high-energy and high-Z frontiers.
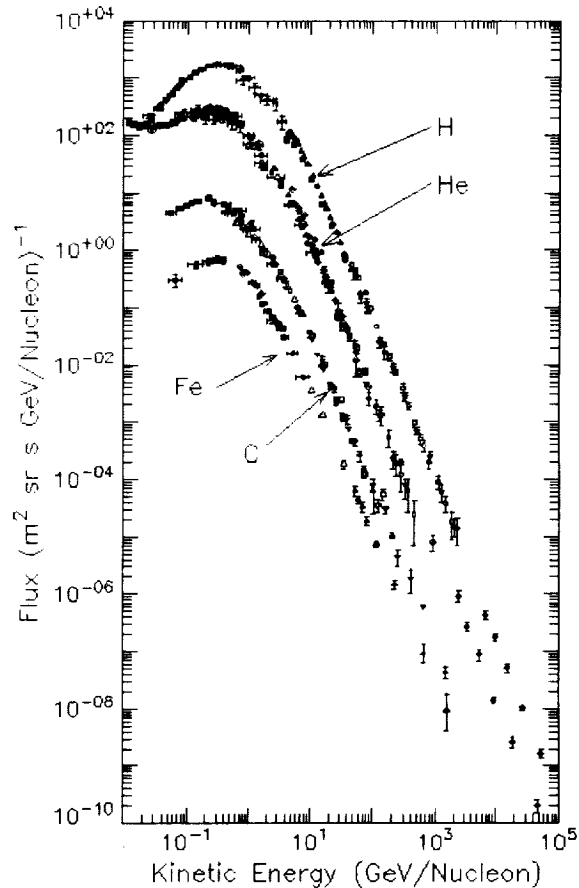
Figure 4. Differential energy spectra of H, He, C, and Fe.

One of the keys to unlocking the acceleration question is measurements of the energy spectra of individual elements. Figure 4 is a compilation of data on the differential energy spectrum of H, He, C and Fe[12,13]. At low energies ($<$ GeV/nucleon) the spectra roll over due to solar modulation effects. Above ~10 GeV/nucleon the spectra are power laws. To look at still higher energies, we must utilize the all-particle spectrum (which can be measured with ground-based air shower arrays). What is found appears to be a "knee" or change in index of the power law in the vicinity of 10^{15} eV/particle. This is illustrated in Figure 5 where the flux has been multiplied by $E^{2.75}$ to flatten or "remove" the power law in the region of the spectral change[14].

The steeper spectrum then extends up to near 10^{19} eV without another change. It is the energy region beyond the data shown in Figure 4 up to the "knee" region of Figures 1 and 5 that is the target of the ACCESS energy spectra measurements.

Figure 5 also gives the proton gyroradius in an assumed 3 micro-gauss interstellar magnetic field, which, for the energies being studied, is less than a few parsecs. This implies that the particles are easily confined in our Galaxy. More important is the scale at the bottom, which indicates that these high-energy events have intensities between 1 per m^2-sr-day and 1 per m^2-sr-month. That is, they are "rare," requiring large-area detectors and long exposure times for detailed study.

The current theoretical model that purports to explain the cosmic-ray spectra below the knee involves particle acceleration in SN remnants (SNRs) by the shock waves propagating from the explosion into the surrounding matter, e.g. the interstellar medium[15,16]. This "shock wave acceleration" is predicted to yield power-law energy spectra, and there is sufficient energy available in SN to replenish the energy in the cosmic rays. The mechanism of shock acceleration has been observed to work within the heliosphere, e.g., at planetary bow shocks, at interplanetary shocks in the solar wind, and at the solar wind termination shock. It is believed to be a prevalent process in astrophysical plasmas on all scales throughout the universe. It is a characteristic of diffusive shock acceleration that the resulting particle energy spectrum is much the same for a wide range of parameters, or shock properties. This energy spectrum, when corrected for leakage from the Galaxy, is approximately consistent with the observed spectrum of galactic cosmic rays shown in Figure 4.
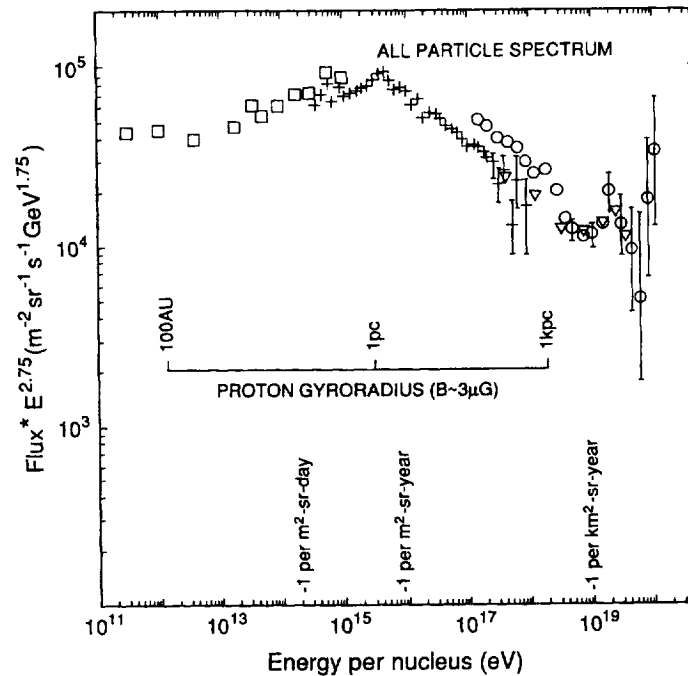
Figure 5. All-particle spectrum in total energy per particle showing the "knee."

This attractive model predicts a cutoff in the power-law spectrum. The shock-accelerated particles pick up a small increment of energy each time they cross the shock boundary, in a random-walking (diffusing) process. Thus, the maximum energy accessible in a given situation depends on the rate at which the particles diffuse back and forth across the shock (i.e., on the magnetic field) and on how long the acceleration mechanism acts. For a SN shock, the time and distance scales are much longer than the scales encountered in the heliosphere, so the corresponding energies are much larger. However, the available acceleration time is limited by the time taken for the blast wave to propagate outward and to weaken to the point that it is no longer an efficient accelerator. In the most commonly used form of the theory, the characteristic energy is about $Z \times 10^{14}$ eV, where Z is the particle charge[17]. This implies that the cosmic-ray composition would begin to change beyond about 10^{14} eV, the limiting energy for protons; Fe would start to steepen at an energy 26 times higher. Thus, we expect the H spectrum to fall off first (in total energy), followed by He and the higher-Z nuclei. As the energy increases, the fraction of heavy nuclei also increases. This is the characteristic signature of the SNR shock acceleration process that ACCESS is designed to detect.

Whether the "knee" feature in the all-particle spectrum is related to the termination of the SN acceleration mechanism is one of the questions that must be solved. However, the cosmic rays do extend to much higher energies, and this implies that, if the SN blast wave mechanism "cuts off" as expected, a new source must be invoked for the still higher energy particles. One idea is that these could be accelerated by the collective action of several SN blast waves. Since all components would come from the same class of source, both below and through the knee region, then the relative composition would depend on energy in a prescribed way. Furthermore, since the acceleration is mediated by the magnetic field, then the spectra of all species should be the same when compared as a function of magnetic rigidity.

Another view suggests that if the progenitor were a massive star with a strong wind (like SN 1987A), then the explosion would not be into the general interstellar medium, but rather into the atmosphere swept out by the wind of the progenitor star. In this situation, one would expect the acceleration rate to be determined at first by the magnetic field of the progenitor's wind, which might be significantly higher than that in the interstellar medium. Consequently, the acceleration rate could be higher, and the particles could reach higher energies than are achieved for an explosion into the general interstellar medium.

Finally, compact objects, especially neutron stars in various environments, have also been suggested as a possible new source of accelerators to supply particles above the knee region. Possibilities include: (1) the spin-down power of rapidly rotating neutron stars to accelerate particles in pulsar magnetospheres; and (2) the accretion power in binary systems in which matter from a companion star is falling onto the surface of a compact partner.

Whatever the case, it will be the direct composition measurements at energies approaching the "knee" which will provide the first clues to this new source of particles.

Figure 6 is a 1993 compilation of high-energy results for the charge ranges, H, He, CNO, Ne-S and the Fe group by Swordy[6]. The data are based on a variety of experimental techniques including passive emulsion chambers, ionization calorimeters, a magnetic spectrometer, a ring-imaging Cerenkov detector, TRDs, and Cerenkov counters. Note that the flux values are multiplied by $E^{2.75}$ and the scale is energy per nucleon. (A horizontal line corresponds to an $E^{-2.75}$ energy spectrum, with smaller power-law indices having a positive slope.)

A cursory view of Figure 6 indicates that the highest energy data extend up to roughly 10^{14} eV for protons and lower energies for the heavier components. Note the unexpected behavior, in that the flux of He relative to protons increases with energy. At low energy, below $\sim 10^2$ GeV/nucleon, the H and He show about the same slope. Above about 100 GeV/nucleon, however, the H becomes almost flat (i.e. $E^{-2.75}$ spectrum), while the He continues to increase (i.e. about $E^{-2.65}$ spectrum). This behavior has been interpreted as evidence for two different types of sources or acceleration mechanisms[18] for H and He.
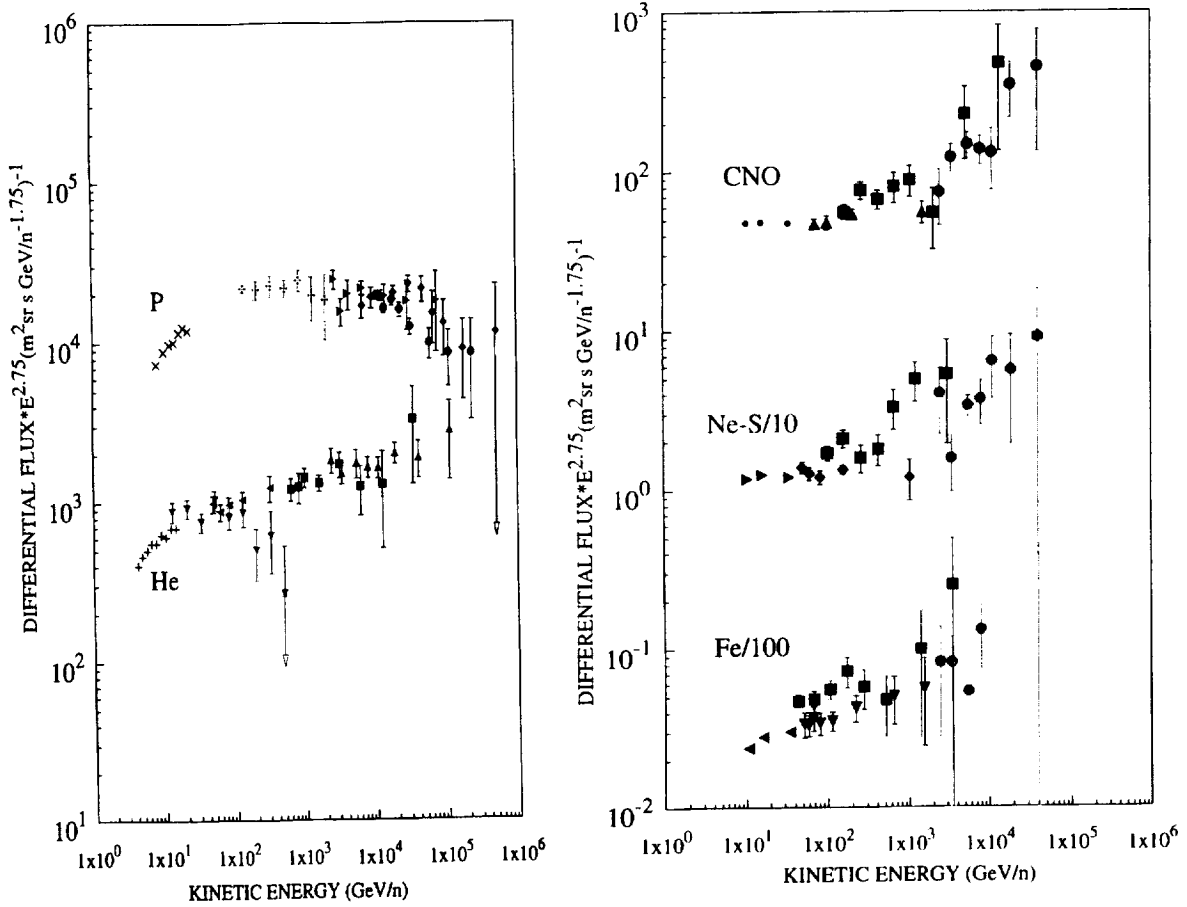
Figure 6. Compiled high-energy spectra for H and He (left) and CNO, Ne-S, and Fe group (right).

At the highest energies in Figures 6 (few x 10^4 GeV/nucleon), the proton spectrum appears to roll-off or bend, but this occurs at an energy that is a factor of ~ 2 below the expected cutoff for SNR shock acceleration. Note that He shows no tendency to change slope, within the limited statistics, to the highest energies shown. However, one must be careful in interpreting these data since the statistics for the highest energy points are very small, i.e. a few particles per bin. More recent data[19] do not show the tendency for the proton spectrum to roll off.

It is clear from Figure 6 that the spectra of the groups of heavier elements are similar to He but show a trend toward flatter spectra with increasing energy. Specifically, the spectral slopes at

higher energies seem to be close to values around 2.5 to 2.6, significantly flatter than the values reported at lower energies by previous space experiments[20,21]. However, again, the results are statistically limited and there may be normalization uncertainties between the different experiments.

The data in Figure 6 are intriguing. They suggest that something may be changing in this high-energy region around the knee, possibly related to the SNR shock acceleration process. Clearly, unraveling these questions requires comprehensive new data for the individual elements, H-Ni, extending to as high an energy as possible.

An equally compelling question for ACCESS is the nature of the material injected into the cosmic-ray accelerator. Here the important measurement is the relative composition of the cosmic rays themselves, at all energies. Previous work at low energy (<10 GeV/nucleon) has determined the relative abundances of each of the elements up to Zn, and of groups of elements beyond Z=30 to the end of the periodic table. Figure 7, for example, gives a compilation of results for the UH, Z≥30, region, compared to the relative abundances measured in the solar system, shown as the histogram[17]. These measurements were obtained by two previous satellite experiments[23,24]. Note that the scale is normalized to a million Fe nuclei, demonstrating the rarity of these UH cosmic rays and, again, the need for large-area detectors exposed for long durations in space. The best of these previous measurements were not able to separate the odd-Z elements from the neighboring even-Z elements over the full charge and energy range, which limits the conclusions that can be derived from the data. Measurements with single-charge resolution, spanning the periodic table, are a principal goal for ACCESS.
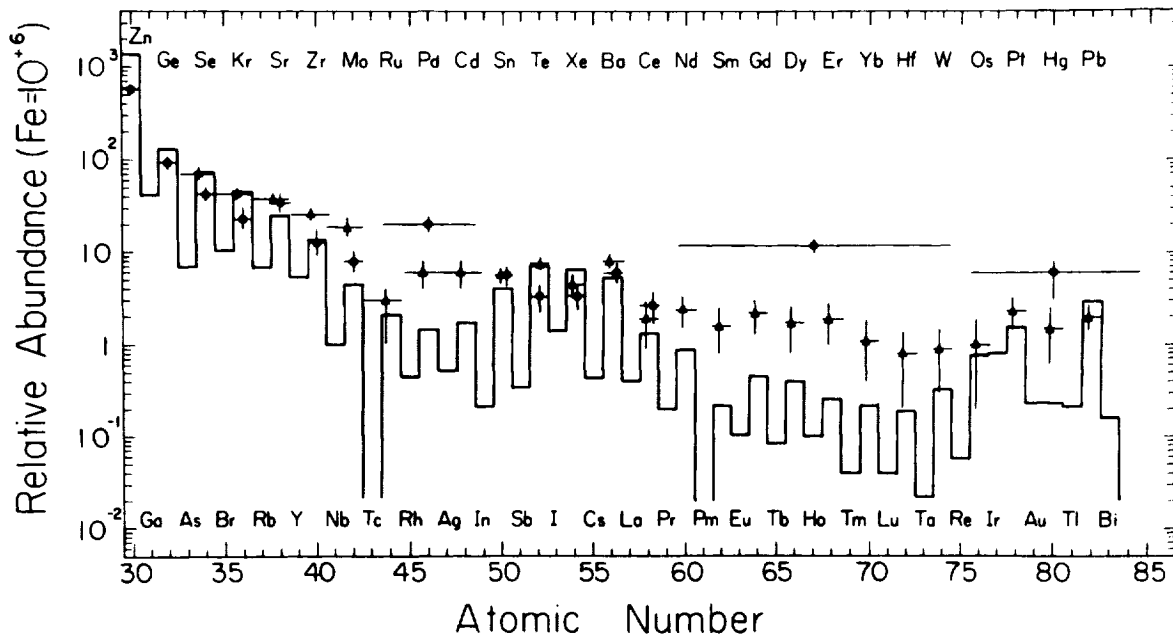
Figure 7. Compiled measurements of nuclei beyond the Fe peak.

The UH elements are particularly interesting since they are formed mainly by neutron capture reactions, unlike the lower-Z elements which are synthesized by charged particle reactions. From an analysis of the solar system abundance distribution, the neutron capture reactions have occurred in two distinct processes, called the r- and s-processes. The r-process is characterized by neutron capture rates much faster than the beta decay rates so that nuclei are driven far from the valley of beta stability. The s-process, however, is a longer-term exposure since the neutron capture rates are less than the beta decay rates producing synthesis of elements along the valley of beta stability. The UH cosmic rays of Figure 7 are evidence for the presence of both s-process and r-process components, but the data are not precise enough to determine the exact mixture. If the cosmic-ray material is indeed solar system-like, we would expect the mix to be similar to the solar system. On the other hand, if there is a component of freshly synthesized matter among the cosmic rays, e.g. from SN, then a different mixture would be indicated. ACCESS measurements of the individual element abundances should allow the r- and s-process contributions to be evaluated at low energy.

It has been known for many years that the cosmic rays arriving at Earth contain both primary nuclei that originated at the source and secondary nuclei formed en route by nuclear interactions of the primary nuclei with atoms in the interstellar medium through which they propagate. This transformation process has been studied experimentally by means of measurements of nuclei that are purely secondary, such as Li, Be, B, F, and the sub-Fe elements (Sc,V), all of which are extremely rare in the universe, but are orders of magnitude more abundant among the cosmic rays.

Figure 8 shows one such secondary-to-primary ratio, B/C, as a function of energy25. From the peak near 1 GeV/nucleon, the ratio decreases both to lower energies, due to the energy dependence of the cross sections combined with ionization energy loss and solar modulation, and to higher energies, due to escape from the confinement region. Cosmic-ray propagation at
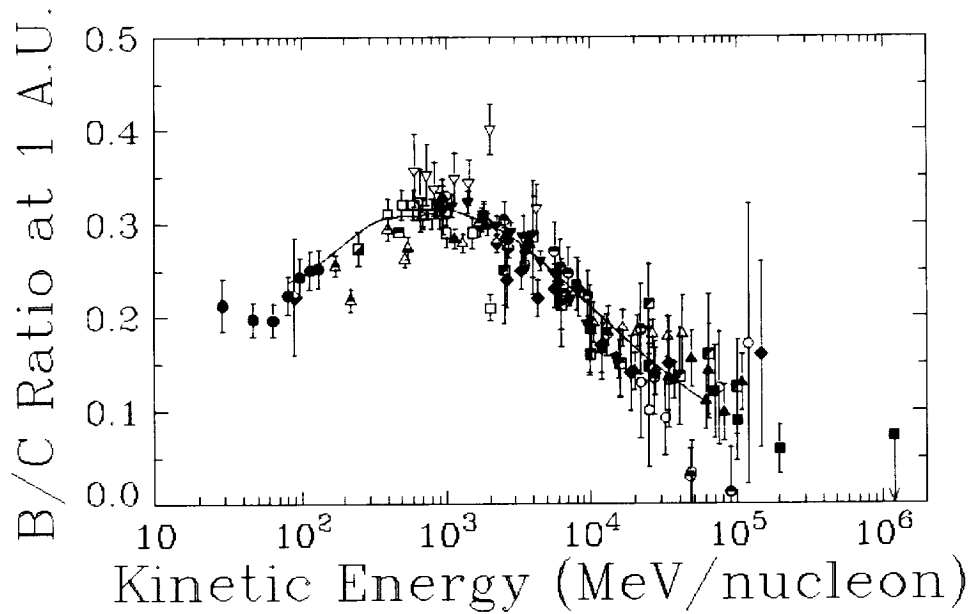
Figure 8. The B/C secondary-to-primary ratio as a function of energy.

energies above 1 TeV/nucleon is dominated by escape from the Galaxy. The mean escape length decreases with increasing energy up to ~100 GeV/nucleon[26], and it has been suggested that the flattening of the heavy nuclei spectra in Figure 6 could be explained by a less severe decline in the escape length above 1 TeV/nucleon, an energy range for which there are currently no reliable data. ACCESS will be able to extend the measurements of Figure 8 to higher energies to investigate this energy dependence.

Transport models for cosmic-ray propagation in the Galaxy have been developed which, in essence, work backwards from the measured composition, unfold the secondary component, and determine the relative abundances of the elements at the source(s) of the cosmic rays[12]. These models utilize the secondary-to-primary ratios, such as Figure 8, and incorporate the large body of nuclear fragmentation cross section data[25]. Uncertainties on the derived source abundances range from 5%-20% for the abundant, mostly primary species to factors of two or more for elements with large secondary contributions[27]. However, these source abundances provide a means to study the cosmic-ray source matter.

A comparison of this cosmic-ray source composition to matter in the solar system shows that there are systematic differences. The source matter is rich in elements like Fe, Ni, Al, Mg, and deficient in H, He, C, O, and Ar. This pattern can be organized by the FIP of the elements, a recent example[28] of which is presented in Figure 9. Plotted is the ratio of the cosmic-ray source abundance to the solar system abundance, normalized to H. The abundances divide into three regions: low-FIP elements, which are most overabundant; high-FIP elements, which are much less overabundant; and a transition region between the two groups. This FIP dependence does a moderately good job of organizing the abundances, but it is by no means perfect. (The very low abundance of H, the normalization point, and He stand out.) Deviations, of course, may be due to remaining uncertainties in the abundance measurements themselves. Note particularly the uncertainties for many of the UH elements. ACCESS measurements will certainly improve these values.

The FIP pattern in Figure 9, when viewed in a thermal, collisional excitation model, requires temperatures of about 10,000 °K. This suggests an origin in stellar atmospheres rather than in the interstellar medium, if ionization is the controlling mechanism. However, this may not be correct. Although FIP appears to be an organizing parameter, it may not be the astro-physically important one, i.e. FIP may be an alias for something else. FIP is closely correlated with volatility or condensation temperature, for example. The low-FIP elements tend to be the least volatile (refractories) and have higher condensation temperatures. This suggests that the FIP dependence could be implying that some of the cosmic-ray source matter has been condensed into dust grains. This would require preferential acceleration of atoms sputtered from the grains, as has been suggested in a recent model for SNR-based cosmic-ray acceleration[29]. Whether or not the cosmic-ray source matter is in the gaseous state or bound into grains is a very important question for determining the environment in the acceleration region, particularly if SNRs are involved.

Distinguishing between the "grain or gas" origin is possible since there are a few elements that break the FIP-versus-condensation-temperature correlation. These elements, e.g. As, Br, Rb, In, and Cs, are mainly in the UH region of the charge spectrum and are, for the most part, the rarer, odd-Z elements. With the single-element resolution planned for ACCESS's CM, obtaining

good measurements of elements such as these will be possible, for the first time. This should allow ACCESS to address the "grain" hypothesis.
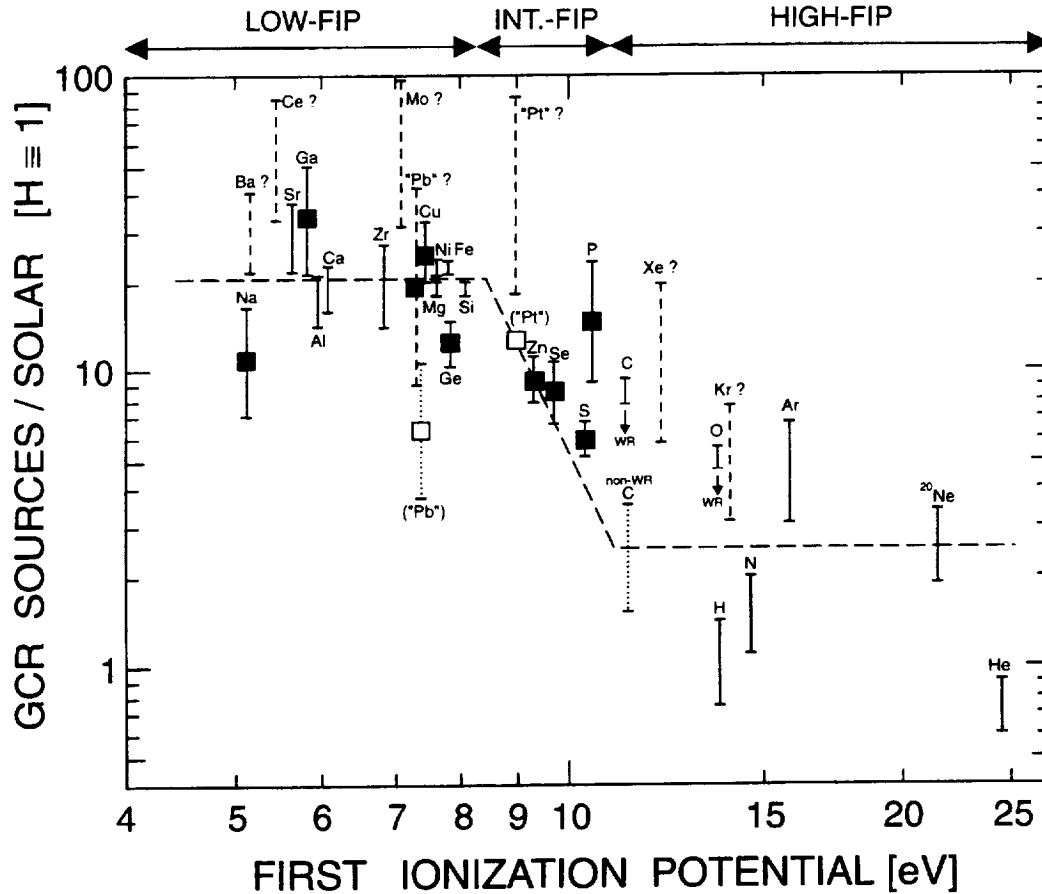
Figure 9. Galactic cosmic-ray source abundances divided by solar abundances vs FIP.

In summary, ACCESS holds the promise of answering some of the long-standing questions in cosmic-ray astrophysics: the cosmic-ray accelerator, propagation in the Galaxy, source abundances, nucleosynthesis, and the importance of interstellar grains. This is already a large science return. However, it may be possible to utilize ACCESS to measure electrons as well. The combination of a calorimeter in conjunction with TRDs has been employed previously for studying electrons, and such measurements are being investigated as a secondary science goal. At energies of a TeV (10^{12} eV) and above, electrons cannot propagate very far in the interstellar magnetic fields, so electrons observed at these energies would come only from "nearby" sources.

Overall, the new information ACCESS provides may dramatically change our understanding of the Galactic cosmic rays.

ACCESS Mission Plan: Baseline

As originally conceived, ACCESS was intended to be an ISS payload that would replace the AMS[30] when the latter is retrieved and brought back to Earth following a three-year stay. Under this scenario, ACCESS would in fact occupy the same ISS attached payload site as AMS. However, as the ACCESS conceptual design has matured, the consensus of opinion is that ACCESS must be prepared to occupy ISS attached payload sites on either side (port or starboard) in order to maintain program schedules, should the AMS experiment stay longer than expected on orbit. ACCESS is being planned for a four-year stay.

Figure 10 depicts the current ISS conceptual configuration with ACCESS attached at payload Site S3 UI (S for starboard, U for upper, and I for inboard). Should both ACCESS and AMS be resident on ISS at the same time, ACCESS will then be assumed to take its position temporarily on the port side of the Space Station at Site P3 UI (P for port).
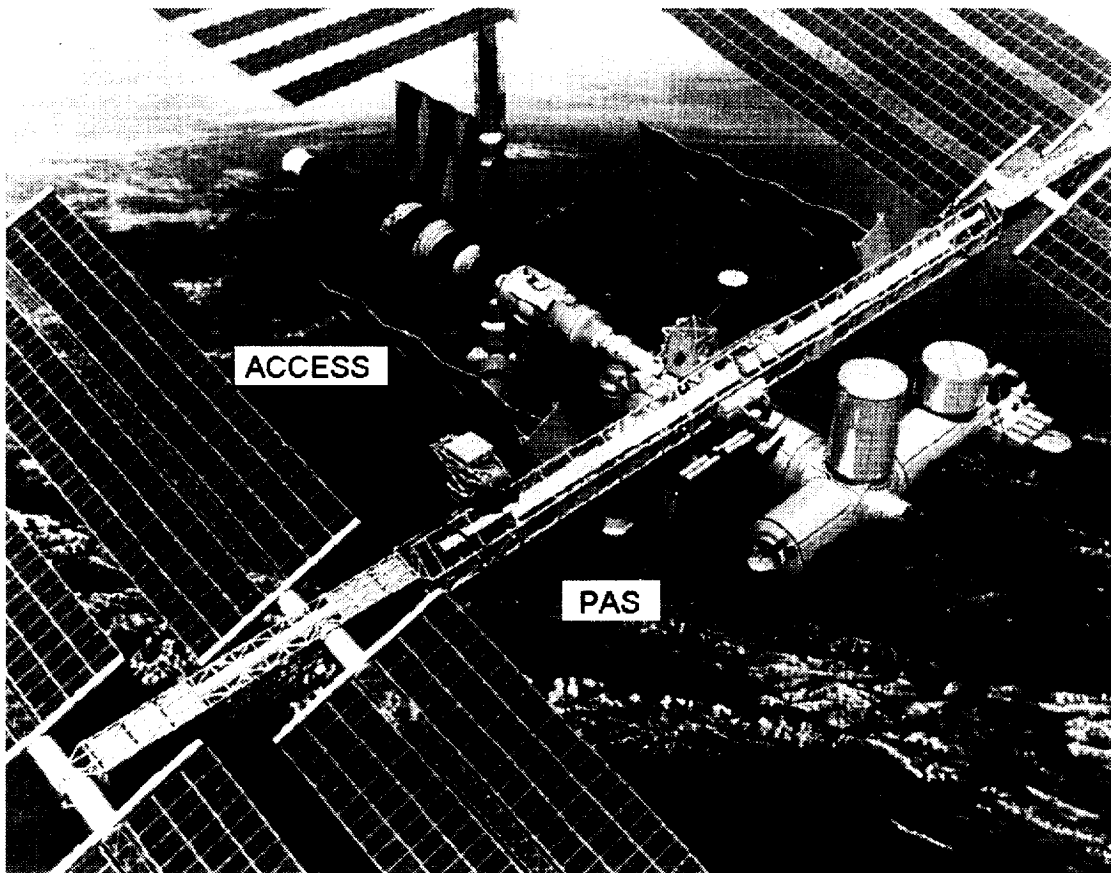
Figure 10. Currently planned ISS configuration with ACCESS attached at Site S3.

ISS Resources and Constraints

General

Upon its completion, the ISS will be the largest orbiting laboratory in LEO ever constructed. This build-up process (Appendix C), already begun with the successful launch of the first element Zarya on November 20, 1998, will take approximately five or six years until completion around April 2004 with the attachment of the U.S. habitation module after some 43 assembly flights.
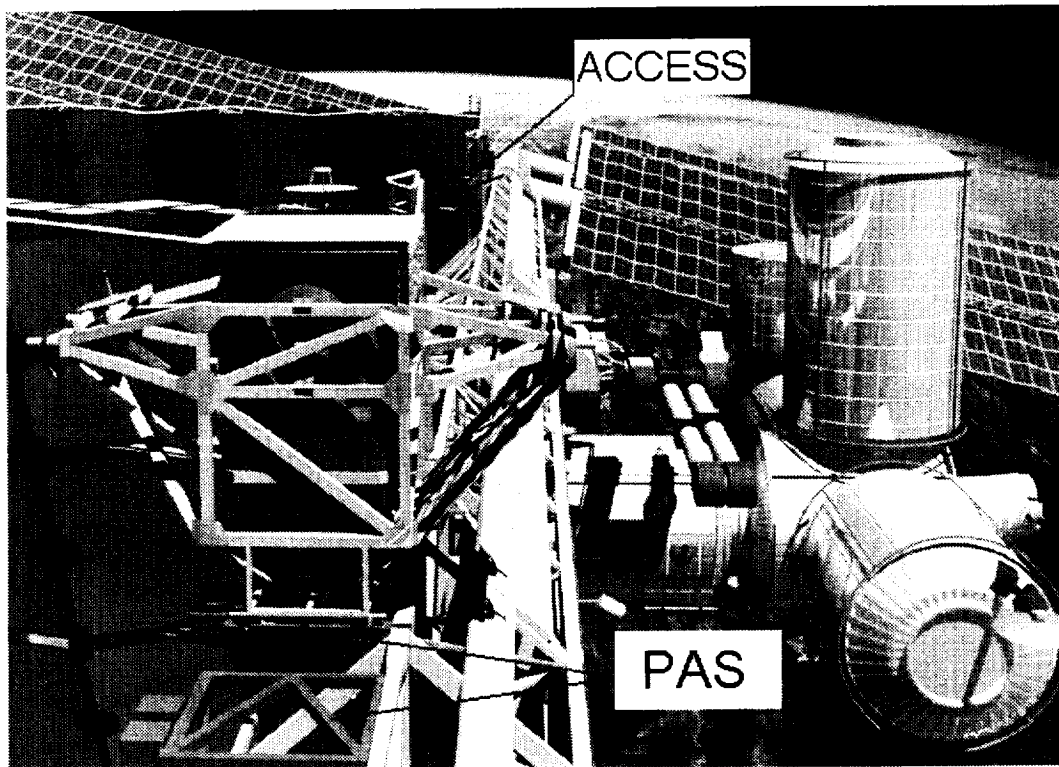
Figure 11. One possible configuration of ACCESS on the S3 truss site.

The ISS structure will be a very large-scale science and engineering outpost in LEO at the threshold of space, which will provide experiments such as ACCESS an impressive view of the astrophysical Universe, illustrated in Figure 11. The scale of the ISS is indicated by the following statistics.

• *Mass*	*1,040,000 lb*		• *Power*	*110 kilowatts*
• *Length*	*356.4 feet*		• *Altitude*	*220 n. mi. (mean)*
• *Width*	*290 feet*		• *Crew*	*Up to seven*
• *Height*	*131 feet*		• *Orbits/day*	*18*

Basic resource provisions

Having been launched by the Space Shuttle, ACCESS will be deployed robotically and attached to the payload attach system (PAS) which is located on the integrated truss segment of the ISS. The PAS provides the essential hardware and functional requirements interface, giving the 'life blood' resources available from the ISS to the payload. These are hardware structural support, power, and data interfaces. ISS provisions and accommodations combine to establish a stable orbiting platform with altitude and attitude control for ACCESS, depicted within its support carrier as a payload in Figure 11 above.

The payload integration hardware at the PAS is further illustrated in Figure 12, showing the capture latch assembly, the V-guides, and umbilical mechanism assembly (UMA). The UMA is the critical device that provides electrical power as well as telemetry data and command interfaces for ISS payloads, consisting of an active portion on the PAS itself, which connects with a passive portion on the payload's carrier.
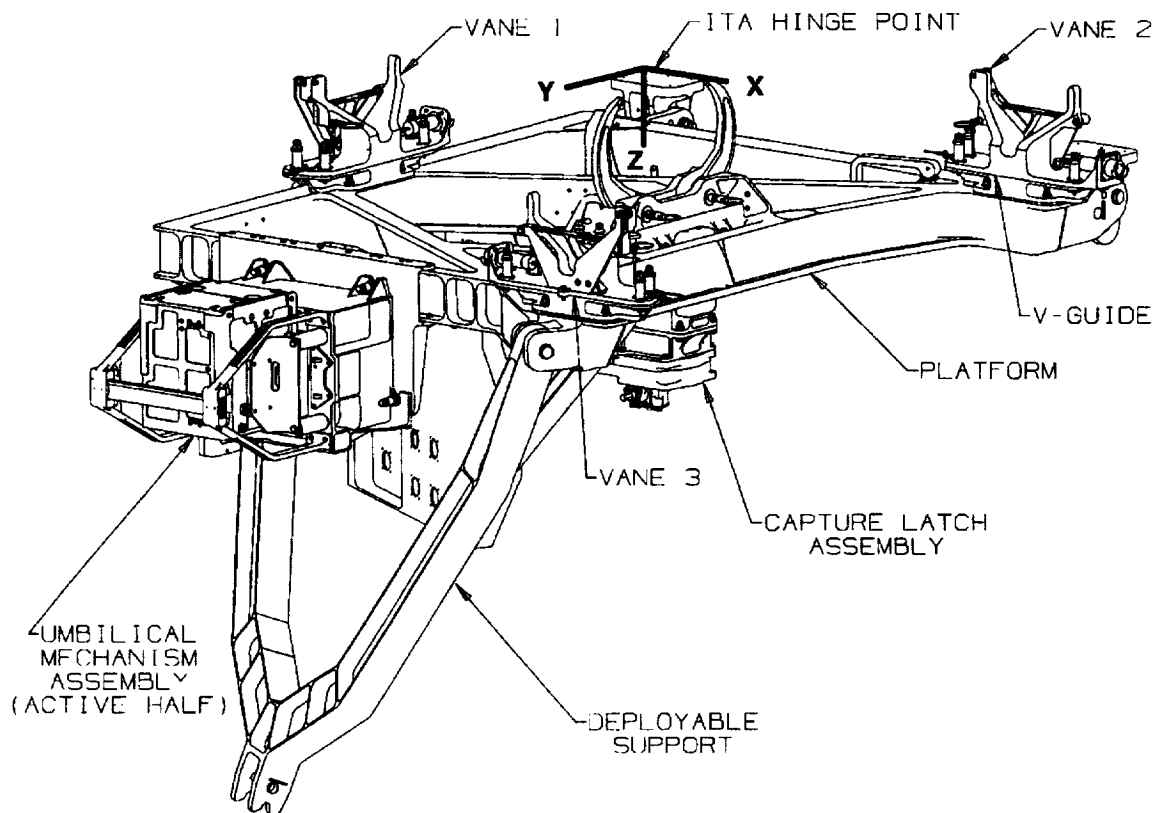
Figure 12a. ISS PAS integration hardware.

S3/P3 truss attach sites

The ISS truss attach site accommodations at the PAS UMA interface (Figure 12) are given in Table 1.

Table 1. Summary of Site S3/P3 Payload Accommodations

• Power	113 VDC (effective) at 3 kW to each site
	80% duty cycle at 1 kW, 100 W keep-alive
• Mass	See the "Carrier issues" section of this report.
• Volume	2.6m x 4.3m x height
• Low-rate data	MIL-STD-1553B (command, control, & telemetry)
	<1 Mbps, 2 twisted shielded-wire pairs payload multiplexer/demultiplexer (MDM)
• High-rate data	43 Mbps via fiber optic link to Ku-band data link
• Thermal control	Passive
• SSP* 57003	Controlling document
• SSP 52000-PAH-TAP	Controlling document
• SSP 52000-IRD-TAP	Controlling document
• SSP 52000-PAH-LSP	Controlling document

*Space Station Program (document)
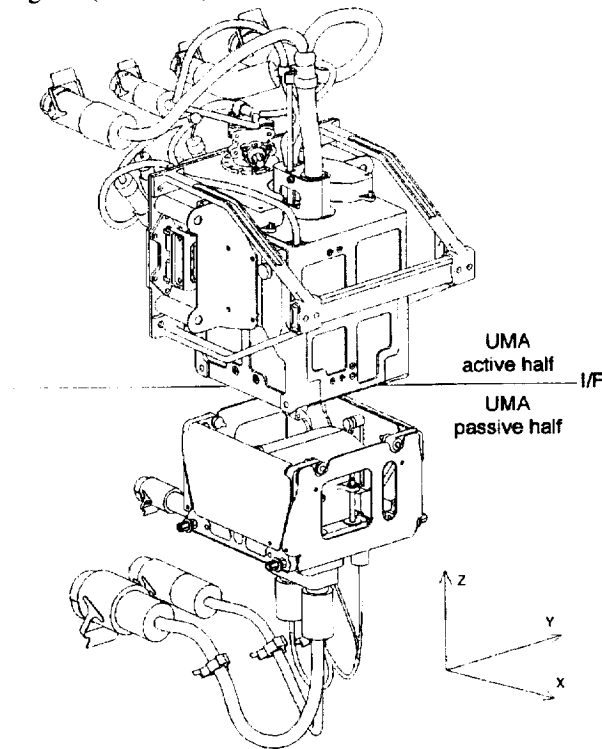
Figure 12b. Detail of the UMA in Figure 12a.

A functional block diagram of the PAS and UMA interfaces is provided in Appendix H.3.

ISS environments

The pertinent ISS operational characteristics which influence the ACCESS mission are summarized below, with controlling documents defined in Appendix D.

Orbit and ephemeris

• Inclination	51.6 degree, near circular
• Geocentric altitude	350-460 km (190-248 n.mi.), periodic re-boosts
• Perturbations	Gravitational, atmospheric drag, solar cycle
• Limitation, constraint	Soyuz de-orbit (maximum altitude of 470-480 km)

Space radiation environment

• ISS design altitude	500 km (Space Station Program Office and Boeing-Prime requirement)
• Trapped radiation belts	Protons and electrons, requiring ~250 mils shielding
• Auroral zone	Protons and electrons, higher concentration
• South Atlantic Anomaly	Protons and electrons, higher concentration
• Solar flares	Low- and high-energy nuclei; heavy ions
• Galactic cosmic rays	Low- and high-energy nuclei; heavy ions
• Risk mitigation	Shielding (low-energy flux); multi-path redundancy and ops work-around, power off (high-energy flux)
• SSP 30512	Controlling document

Micrometeoroid and debris environment

• SSP 30425, Rev. B	Controlling document
• Whipple shields	Present method of risk mitigation

Induced plasma environment

• ISS floating potential	Controlled by plasma contactors ($\pm$ 40 volts)

External contamination constraints

• Molecular contamination	Quiescent 1×10^{-14} g/cm^2 s (~ 30 angstroms/year)
• " "	Nonquiescent 1×10^{-6} g/cm^2 s (~100 angstroms/year)
• Molecular column density	1×10^{14} molecules/cm^2
• Particulate background	One 100 micron particle per 10^{-5} steradian per orbit

Electromagnetic radiation environment

• Radio-frequency emissions	Radiated susceptibility field limits (volts/meter), all
• SSP 41000	Controlling document
• SSP 57003	Controlling document

Basic ACCESS constraints

It is already known that there will be periods of reduced payload accommodation for ACCESS. This includes a "keep-alive" condition (with minimal power accommodation) during STS (Shuttle) launch, rendezvous, docking, and deployment to the attached payload site. Also, an overall ISS duty cycle of 75%-80% has been estimated for such attached payloads. The actual duty cycle is unknown at the present time, because it is a function of how many payloads will be present on the ISS. It could be as much as 500 W and as little as 100 W. The "golden rule" is to design the keep-alive dependence to be as small as possible. The power accommodation for keep-alive will be written into the Program Initiation Agreement (PIA).

The current baseline mission plan for ACCESS has been to remain unpowered during launch to the ISS, although there has been discussion of a powered keep-alive requirement prior to PAS and UMA activation in order to stabilize the temperature of the pressurized gas supply in the TRD instrument throughout the mission. NASA may also consider performing a post-launch payload functional test prior to unberthing from the Shuttle payload bay. Such power is available as an STS accommodation if it becomes necessary, although the situation is made somewhat awkward by three fundamental differences that currently exist between the Space Shuttle and the ISS:

- STS power is 28 VDC while ISS PAS power is 120 VDC.
- STS high-rate data travels via copper wire while the ISS uses fiber optics.
- STS low-rate data and command is via the payload signal processor and payload data interleaver, while the ISS uses a 1553 data bus.

See Appendix H for further discussion of STS power and data accommodations.

Following a four-year mission lifetime, ACCESS is to be removed from the attach site and returned to Earth. At the end of its mission, the science payload will be returned to the instrument provider. A final postflight calibration verification is under consideration.

A detailed discussion of all ISS environments in the space segment (LEO) which constrain its payloads is given in Appendix G.

ACCESS Accommodation on STS

Carrier issues

Summary

The carrier is the mechanical support structure that contains the ACCESS instrument, as shown in Figure 11. The carrier combined with the science instrument constitutes the total ACCESS payload. It must be suitable for both the ACCESS launch vehicle (STS) and the ISS PAS. It must also obviously have the structural and mechanical properties to withstand the stress and vibration loads of launch, on-orbit operations, descent, and landing. However, as with any aircraft or spacecraft cargo it must comply with certain center-of-gravity (CG) envelopes and volume constraints (Appendix F). This is the familiar "weight-and-balance" problem known to pilots everywhere, which precludes a loss of dynamic vehicle control.

These Shuttle/ISS mass-property constraints are summarized in Table 2.

Table 2. Critical Mass Properties Constraints

- *Upmass limitations*
- *Maximum allowable PAS payload mass*
- *CG constraints*
- *Volume constraints*
- *The payload CG should be high in the Shuttle bay, and low on the ISS PAS.*

The first four conditions drive the ISS weight limit. The "upmass" is the negotiated mass allocable to a U.S. payload on the subject utility flight (UF) in the ISS assembly sequence (Appendix C) or thereafter. The fifth drives the payload CG to fall along or near the trunnion sill-level in the Shuttle cargo bay.

That last constraint derives from the fact that, by design, the dynamic load performance for the Space Shuttle (launch, re-entry, and landing) is not equivalent to that for the ISS (quiescent and on-orbit re-boost). The Johnson Space Center (JSC) ACCESS Accommodation Study Team resolved this restraint at the outset[9]: *Simply turn the ACCESS instrument sideways when in the Shuttle bay.* Because most of the mass of the baseline ACCESS instrument resides in the calorimeter it easily passes the ISS constraint since it is at the "bottom" of the carrier in Figure 11 and is pressed up against the PAS.

The second category of payload carrier issues involves the frequency response of its structural design and the materials used. These constraints are summarized in Table 3. All ISS and STS payloads must go through a number of safety reviews, Phase-zero through Phase-III (see Safety, Table 20 below, for timing of phases). Depending upon the flight readiness of their structural design and the materials chosen, a payload can pass or fail these reviews.

Table 3. Critical Shuttle Load and Materials Constraints

- *All Shuttle payloads are required to perform static testing (per NSTS [National Space Transportation System]-14046).*

- *All Shuttle payloads are required to perform a modal test and correlate their finite element model (FEM) for all modes below 50 Hz (per NSTS-14046).*

- *All Shuttle payload structure must comprise material complying with properties from Military Handbook 5G, or undergo independent safety reviews.*

- *All fasteners must comply with the JSC fastener integrity program (JSC 73642).*

The material usage in Item 3 of Table 3 must be verified in accordance with applicable requirements in the appropriate controlling documentation (Payload Specific ICD [Interface Control Document], NSTS-14046, NSTS-1700.7B, or SSP-50021 for SSP cargo elements).

Shuttle bay geometry

It has been assumed in this Accommodation Study that the trunnion spacing in the Shuttle payload bay must be identical to the unique support structure (USS) carrier (addressed in detail below under ISS carrier options). This is not a firm requirement, but the baseline ACCESS mission plan previously discussed (Figure 10) was meant to cover the launch and retrieval scenario in which ACCESS would be swapped out for the first major ISS particle physics payload, the AMS. This assumption requires that the geometry of the AMS and ACCESS have identical trunnion hardware interfaces in the Shuttle cargo bay.

It is possible to change the Shuttle attach points for any new carrier, however. The AMS USS has five trunnions that attach to the Shuttle payload bay. The two primary trunnions (which carry Shuttle X and Z loads) are located toward the back of the payload bay. The two secondary trunnions (which carry Shuttle Z loads) are 70.8 inches forward of the primary trunnions. The keel trunnion (which carries Shuttle Y loads) is centered between the four longeron trunnions. Clearly, if ACCESS utilizes the USS (Figure 13), then this assumption would not be an issue. If ACCESS uses a new carrier structure, the trunnion spacing and orientation is still fixed by the design of the USS per this baseline mission plan assumption.

STS robotic interface

The robotic interfaces to the Shuttle are described in NSTS-21000-IDD-ISS, Sections 13 and 14. This document also deals with a variety of different issues related to the remotely operable electrical umbilical (ROEU) and the Shuttle and Station grapple fixtures which are the direct hardware STS-to-payload interface for robotic cargo logistics, transfer, and handover to the ISS, as well as retrieval, descent, and landing.

STS power and command & data handling (C&DH) interface

The STS power and C&DH accommodation is unique and different from the ISS.

The ROEU is an umbilical connector that provides capability for transferring STS power (28 VDC) to the payload. It also accommodates a 1553 data bus, and a copper-wire high-rate interface while the payload is still in the payload bay of the Shuttle. This is one form of "keep-alive" power. Currently the Shuttle has two different types of grapple fixtures, the flight releasable grapple fixture (FRGF) and the electrical flight releasable grapple fixture (EFGF, also 28 VDC). The EFGF's movable grapple shaft extends and retracts an electrical connector to the payload.

As discussed previously under "Basic ACCESS Constraints," 120 VDC power is not provided in the Shuttle payload bay unless it is outfitted with an assembly power converter unit (APCU) for converting the STS 28 VDC power to 120 VDC. Similarly for the data, there is a data incompatibility at this interface. The Shuttle bay must be outfitted with a data conversion unit (DCU) to convert payload high-rate fiber optic data to the STS copper-wire interface in order to bootstrap it into the Ku-band downlink or to record it in the shirtsleeve environment of the crew cabin. The Shuttle, furthermore, must be outfitted with an Orbiter interface unit (OIU) in order to get the 1553 low rate command and data into the Orbiter S-band uplink and downlink.

Therefore, under existing STS design the Shuttle Orbiter must be equipped with an APCU, an ROEU, a DCU, and an OIU to power up the ACCESS payload while still in the Shuttle payload bay and transmit any of its high-rate science data downlink (e.g., as a functional test before deployment to the ISS), unless it operates off of 28 VDC and 120 VDC. If, on the other hand, ACCESS were only concerned with a keep-alive thermal control capability (e.g., heaters) along with a low-rate housekeeping S-band downlink, the APCU could be eliminated if the payload heater system could operate off of the ROEU's 28 VDC.

See Appendix H for further discussion of STS power and data interfaces.

STS hardware interfaces

The subject of STS hardware interfaces is discussed in the Carrier analysis section of this report and in Appendix H.

ACCESS Accommodation on ISS

Experiment carrier structures (ECSs)

Summary

The initial task of this feasibility study was to determine if the ACCESS experiment could utilize the existing design of the USS (Figure 13) prepared, developed, and flown by JSC on a precursor flight for the first high-energy particle physics experiment (AMS) destined for the ISS. As the science definition of ACCESS progressed through the study, however, it became obvious that several carrier options were available. These are defined in detail in Appendix E. This report will focus upon two of these. The first is the original USS design, because it was the going-in concept. The second is a totally new design called an ECS, described below.

- We recommend the ECS.
- Comparison of the USS with ECS is given in Tables 4 and 5.
- JSC carrier deliverables are given in Table 6.

USS

This study has demonstrated that, with modifications, the USS can accommodate the ACCESS experiment[31]. However, in order for the ACCESS payload to fit within the existing USS design, size, and weight, certain limitations must be placed on the ACCESS experiment. Recent developments with the PAS on the S3 segment of the ISS will increase the overall cost to the ACCESS payload under the USS option. Since it was developed for another experiment, adapting the USS to ACCESS is less mass-efficient than a carrier designed specifically for ACCESS.
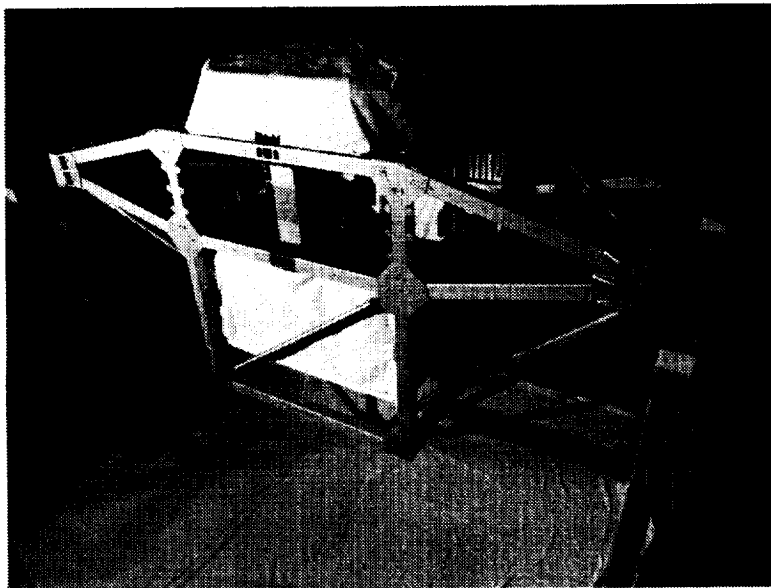
Figure 13. USS design.

23

ECS

A new ECS design was therefore investigated, several versions of which are presented. One ECS (Option 3) was chosen as the best potential candidate for the ACCESS support structure, but all are viable. The design goals for the ECS were to minimize the overall weight of the support carrier while providing for flexibility in the event of unforeseen changes to the experiment design. Another important goal for the design of the ECS was to ensure that the PAS can accommodate the experiment structurally while minimizing the overall design cost.

The ECS has several advantages that are included in Table 4.

Table 4. ECS Advantages

- *Lightweight*
- *Easy to build*
- *Low cost*
- *Extremely flexible to accommodate changes in the experiment design*
- *Utilization of existing test fixtures and ground handling equipment (GHE)*
- *No research and development program, special testing, or special certification necessary (since constructed with proven methods and materials)*

Cost and readiness (schedule)

The current estimated cost to modify the USS for accommodation of the ACCESS mission is $2.1-$2.4 million. A certified structure can be ready for shipment 12 months after definition of the experiment and the interfaces to the USS. Because of the size and weight limitations of the USS and the increased cost to modify the USS to accommodate new PAS requirements (discussed below), the USS becomes an increasingly limiting support structure.

The current estimated cost to build the new ECS is $2.2-$2.6 million. A certified structure can be ready for shipment 19 months after definition of the experiment and the interfaces to the ECS.

Table 5 below recapitulates the JSC carrier costs and readiness for side-by-side comparison.

Table 5. USS versus ECS Comparison Summary

- *USS cost: $2.1M - $2.4M*
- *USS readiness: 12 months*
- *ECS cost: $2.2M - $2.6M*
- *ECS readiness: 19 months*

Mechanical interface to the ISS

As mentioned, the current proposed attach site for ACCESS on the ISS is at the upper-inboard S3 Site (Figure 11). All attached payloads at this site connect with the ISS through the PAS interface illustrated in Figure 12.

The ISS program is currently working on Change Request 1135 (CR1135) that will finalize the interface requirements for the PAS attach sites[32]. CR1135 will define the weight and CG limits, the total volume envelopes, the mobile transporter envelopes, and the extravehicular activity (EVA) and extravehicular robotic activity envelopes and requirements. Final results of CR1135 should be available by spring or summer 1999. ACCESS accommodation requirements will not be ultimately known until this ISS re-definition is completed. From discussions with Boeing (Huntington Beach) in September 1998, it is obvious that the current design of the USS launched on STS-91 on June 2, 1998, will not meet new PAS requirements expected under CR1135. When the USS was designed, it was acceptable for the USS keel trunnion to extend into the plane of the PAS (Figure 14). The USS was also well within the published weight and CG capabilities of the PAS. With changes to the PAS requirements, the intrusive keel is no
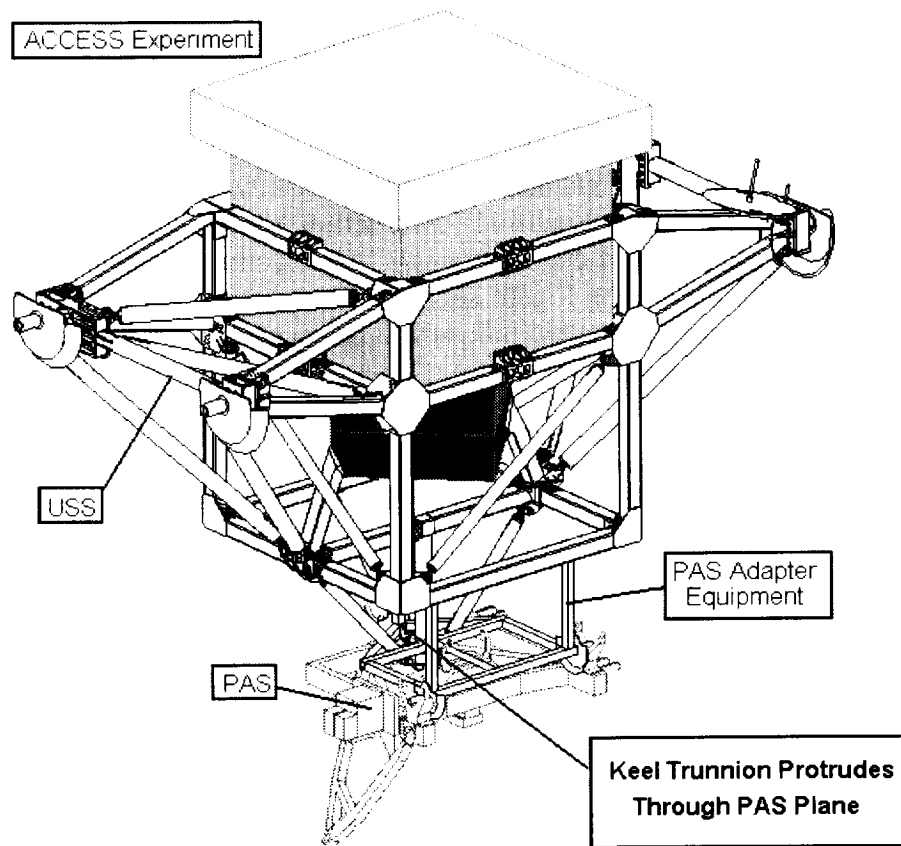
Figure 14. USS/ACCESS with PAS.

longer acceptable because it comes within inches of the PAS latching motor. Therefore, a retractable keel assembly will be necessary to use the USS as a carrier. It is estimated that the retractable keel will be an extremely costly burden on the USS. It is also likely that the weight

and CG capabilities[33] (Appendix F) that were initially issued in 1995 and then updated in 1997 (SSP 42131) will become much more restricted for attached ISS payloads. This means that the overall CG of any attached payload may have to be much closer to the PAS plane than originally specified for USS design.

In addition to changes in the PAS envelope requirements, new equipment that the attached payload may have to provide has been identified. This equipment could add considerable cost to the attached payload. In order to ensure two-fault tolerance on the S3 PAS sites, ACCESS may be required to provide an EVA unloadable and removable capture bar, which is a totally new requirement. This capture bar is part of the passive half of the PAS that is mounted to the ACCESS payload structure. The capture bar will probably have to be prelaunch-adjustable to ensure that the proper preload is applied to the ACCESS experiment once it is on orbit and attached to the PAS. These new changes could prove to be fairly costly.

If ACCESS protrudes into the EVA pathways, it will probably be necessary to add EVA handrails, tether attach points, and portable foot restraint attach points to the experiment or support structure. Video cameras or targets may also be necessary for the berthing operations. Currently it is uncertain who is responsible for the cost of these items. ACCESS will, at least, be responsible for the cost of their integration onto the payload. It may also be necessary for ACCESS to pay for the development and/or recurring manufacturing cost of some of these items.

ACCESS on the USS

The ACCESS experiment weight and volume envelope that was used in our USS study (Option 1, Appendix E) is shown in Figure 15. A structural model of Option 1 was developed and added to the structural model of the USS design. After a structural assessment was performed in the configuration shown in Figure 16, it was demonstrated that the USS can be used for the ACCESS payload. Several modifications will be necessary to accommodate the ACCESS experiment. An attempt was made to minimize the cost associated with these changes, but the following changes are necessary:

1) The calorimeter should be rotated 45 degrees (Figures 14, 16) to provide a better load path. It was determined that this modification to the experiment configuration will not adversely affect the science.

2) In addition to the eight existing attach points on the USS, two additional attach points would be necessary (Figure 16). The interface between the calorimeter and the TRD should be centered on the middle horizontal joint as shown in Figure 16.

3) Redesign of the primary and secondary sill joints and the V-braces will be necessary to accommodate the loads from the ACCESS experiment configuration. The CG of the ACCESS experiment is considerably lower than the USS was designed to accommodate. This means that high loads will be applied to the support structure in places that were not designed to take high loads.

ACCESS on USS

Total Payload Mass Estimate: 4979 kg (10952 lbs.)

Overall approximate weights and dimensions for the preliminary structural assessment of the ACCESS Experiment integrated on the existing Unique Support Structure (USS).

All envelopes are squares in the X-Y plane.
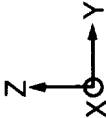
Orbiter coordinate system. +X is out of the paper.

There is another 200 kg of avionics, thermal control system, gas resupply system, debris shields, and contingency mass for a total ACCESS Experiment mass of 3850 kg (8488 lbs).

For this preliminary assessment, all mass is assumed to be uniformly distributed throughout each of the envelopes shown.

141 kg (310 lbs) is required to adapt ACCESS to the USS. 146 kg (321 lbs) is required to make the USS deployable and to attach it to the PAS. With an existing USS weight of 832 kg (1834 lbs) the total integration hardware mass is 1121 kg (2465 lbs). Therefore the total ACCESS Payload mass is 4979 kg (10952 lbs).

All envelopes are squares in the Y-Z plane.

Charge Module 200 kg

Transition Radiation Detector (TRD) 500 kg

Silicon Matrix & Graphite Targets 950 kg

BGO 2000 kg

Calorimeter

0.3 m
1.2 m
0.5 m
0.3 m

2.00 m
1.65 m

2.3 m

1.0 m

Figure 15. ACCESS experiment for USS option.

27

Experiment to
Carrier Attach
Points

Secondary
Sill Block

Modified Lower
V-Brace
Attachment

PAS Adapter
Equipment

ACCESS Experiment

Primary
Sill Block

PAS

USS
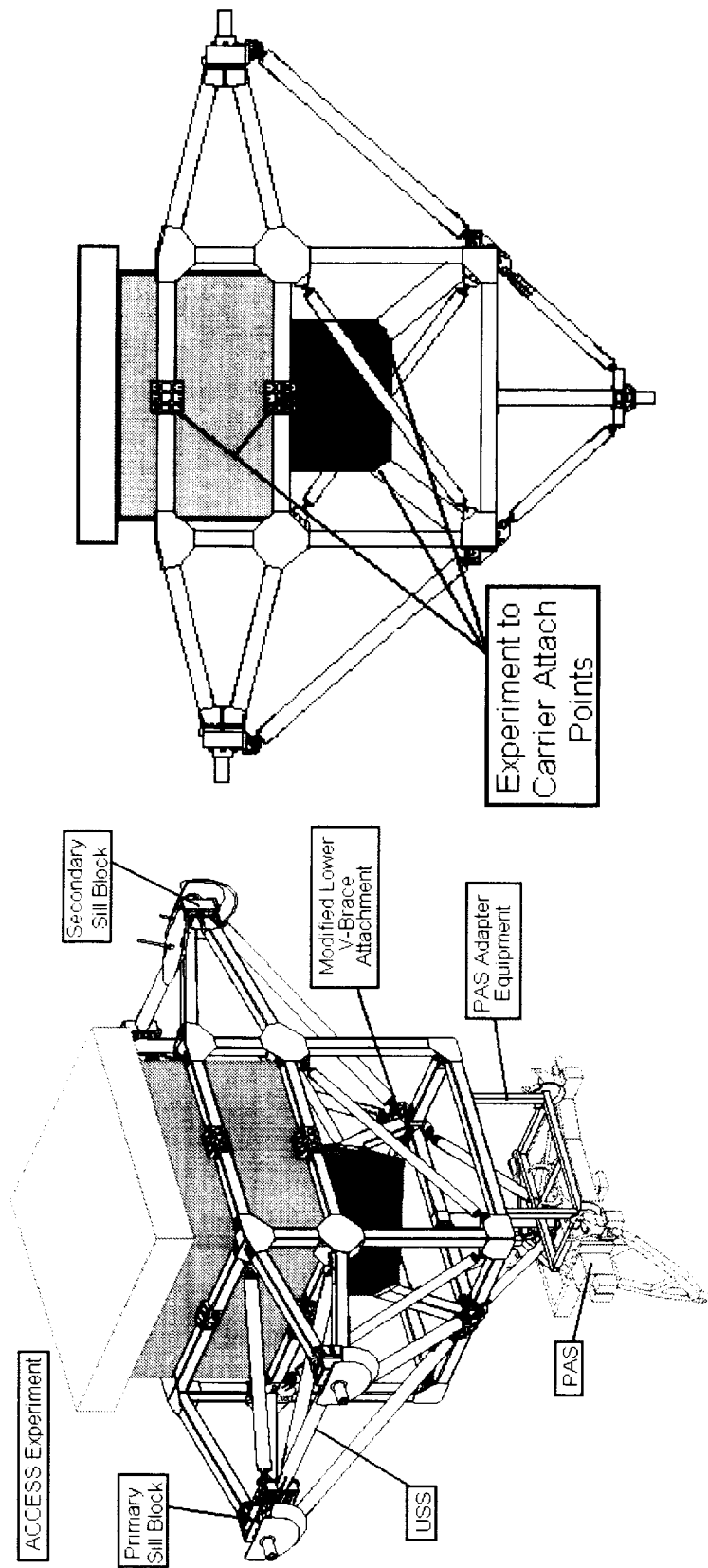
* PAS Model is preliminary and Keel Trunnion is shown passing through the PAS; a retractable keel
probably will be necessary in the final PAS.

Figure 16. USS/ACCESS option.

A FEM has been developed for this configuration. The first natural frequency of the payload is 10.1 Hz, and the structure has only five modes below 50 Hz. From Table 3, every Shuttle payload is required to perform a modal test and correlate the FEM for all modes below 50 Hz. This means that the Option 1 configuration would provide for a relatively simple modal correlation. That directly corresponds to less analysis and testing, and thus less cost to the project.

Preliminary results show all positive margins assuming such modifications are made to the USS. It is also important to note that the USS is relatively insensitive to structural stiffness changes of the science experiment portion as it evolves during development. A consequence is that the experiment support structure *per se* (hardware required to hold the three instruments in Appendix B together, not the carrier portion) can be fairly light. The science hardware can then be a larger percentage of the total weight allotted to each experiment.

In addition to the changes necessary to accommodate the ACCESS experiment, a retractable keel would be necessary to provide the necessary attach location for the PAS (as discussed previously). That in turn would require keep-alive power from the Shuttle in order to extend the keel (Appendix H). A retractable keel also means more failure modes, all of which require additional crew training. These added requirements would result in additional cost to the USS modification for Option 1.

Weight

Table 6 shows a weight summary for the ACCESS payload on the USS. The current USS weight is a measured value. The additional weight to modify the USS is broken into the weight necessary to accommodate the ACCESS experiment and the weight necessary to make the ACCESS payload deployable on the PAS. Since the USS is not optimized to carry the ACCESS experiment, the total weight for the support structure is a fairly large percentage (22.50%) of the total weight of the payload.

Table 6: ACCESS Weight Summary on the USS

Item	Weight lb (*kg*)	% of Total Weight
Experiment Hardware	**8488** (*3858*)	77.50
USS Weight	**1834** (*834*)	16.74
Weight to Adapt ACCESS to USS	**310** (*141*)	2.83
Weight to Make ACCESS Deployable to PAS	**321** (*146*)	2.93
Total Payload Weight	**10952** (*4979*)	100.00

USS advantages

Although the USS does require some redesign to accommodate the ACCESS experiment, there are still several advantages of using an existing design for the ACCESS support structure. ACCESS could take advantage of the fact that most of the design work for the support structure has already been completed, and only modification design work is necessary. This would primarily afford the payload savings of time because it is not necessary to design a completely new structure. All of the GHE and test equipment that has already been developed for the USS

could be reused. This is a significant amount of design and analysis work that would not be necessary.

USS limitations

Although the USS can accommodate the ACCESS experiment as shown in Figure 15, the Principal Investigator (PI) for the TRD expressed a strong interest in a larger detector than shown. The USS is physically not large enough to accommodate a larger TRD (by volume). Additionally, the USS was designed to carry the majority of the weight of the experiment at the eight upper attach locations. The modifications necessary to support the ACCESS TRD dimensional changes add undue weight to the original USS carrier.

Cost and schedule

As part of this accommodation study, an attempt was made to estimate the cost and schedule needed to modify the USS to accommodate ACCESS. The total cost of modifying the USS for ACCESS will be approximately $2.1 to $2.4 million, depending on the modifications that are ultimately necessary, the final payload weight, and the final experiment design. This cost is based on actual experience with across-the-bay payloads that JSC has flown recently (1998) in space. The cost includes the necessary modifications to accommodate the ACCESS instrumentation and the modifications necessary to incorporate the PAS into the USS.

A certified USS can be ready for shipment 12 months after the definition of the experiment and the definition of the experiment-to-USS interfaces.

JSC carrier deliverables

The JSC total 'turnkey' carrier cost is broken out as deliverables in Table 7. The term 'turnkey' refers to the utilization of existing JSC design, certification, and integration (DC&I) methodology, personnel, and templates.

Table 7. JSC Carrier Deliverables (End-to-End Product)

- *Design with interfaces to the experiment, the Space Shuttle, and the ISS*
- *All necessary structural analysis*
- *Complete fabrication and assembly*
- *Complete structural certification*
  - *Modal survey testing*
  - *Static testing*
  - *All special test equipment (STE)*
  - *Ground support equipment (GSE) and GHE*
  - *Component testing*
  - *Materials testing*
  - *Modal correlation*
  - *Space Shuttle and ISS verification process support*

30

ACCESS on new ECS

Because the USS was not specifically designed to carry the ACCESS experiment and because ACCESS appears to be evolving toward a larger collecting power (a larger detector seems desirable to improve the science results), several different ECSs have been analyzed under this Accommodation Study. The main design goals of the ECS are to minimize the overall weight of the support structure, while providing for maximum flexibility in the event of unforeseen changes to the final experiment instrument. Several different experiment options have been considered[10,11], but Figure 17 shows the final experiment configuration that has been chosen to provide the best alternative (Option 3, Appendix E). As the figure shows, the experiment dimensions and total weight have increased over those shown in Figure 15 (USS option).

To accommodate the experiment as shown in Figure 17, thirteen different ECS structures were assessed (Appendix E). Figures 18, 19, and 20 show the ECS structure that the ACCESS Accommodation Study Team has chosen. To satisfy the design goals that were set for the ECS, the following design decisions have been made:

- Utilize common aerospace materials for ease of manufacturing and overall project cost savings (primarily Aluminum 7075-T7351).

- Attempt to utilize only material properties directly from Military Handbook 5G to avoid any additional testing that will be required for more exotic materials. Portions of the USS incorporate material thicknesses that are not shown in 5G, so reduced material properties were deemed necessary. These reduced material properties unnecessarily affected the design margins.

- Attempt to show preliminary design margins of 20% to 40% and decrease the margins as the design matures.

The ECS provides a stiff support structure, but it will rely on the ACCESS experiment to provide some internal structural support. As more integration is performed between the carrier structure and the internal ACCESS instrument structure, the overall weight of the payload will be optimized.

The ECS configuration will be horizontal in the payload bay of the Shuttle. This means that the ACCESS experiment will be pointed toward the Space Shuttle crew cabin. In the USS configuration, the experiment was pointed straight up out of the payload bay. As Figure 21 shows, the horizontal configuration allows for better adaptability to the PAS. As discussed earlier, it is likely that the PAS weight and CG requirements will become more limiting than previously published (e.g., CR 1135). If this occurs, it is in the best interest of any attached payload to have its mass and CG as close to the PAS as possible. In the horizontal ECS configuration, the PAS attachment point is on the bottom of the calorimeter. Since the calorimeter is the heaviest portion of ACCESS, the PAS is very close to the payload CG. This feature is desirable, as mentioned earlier in the discussion of Table 2. The result can be seen in Figure 21 where the ACCESS payload is shown on the S3 truss of the ISS.

ACCESS on ECS

Total Payload Mass Estimate: 6014 kg (13232 lbs.)
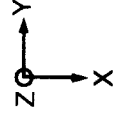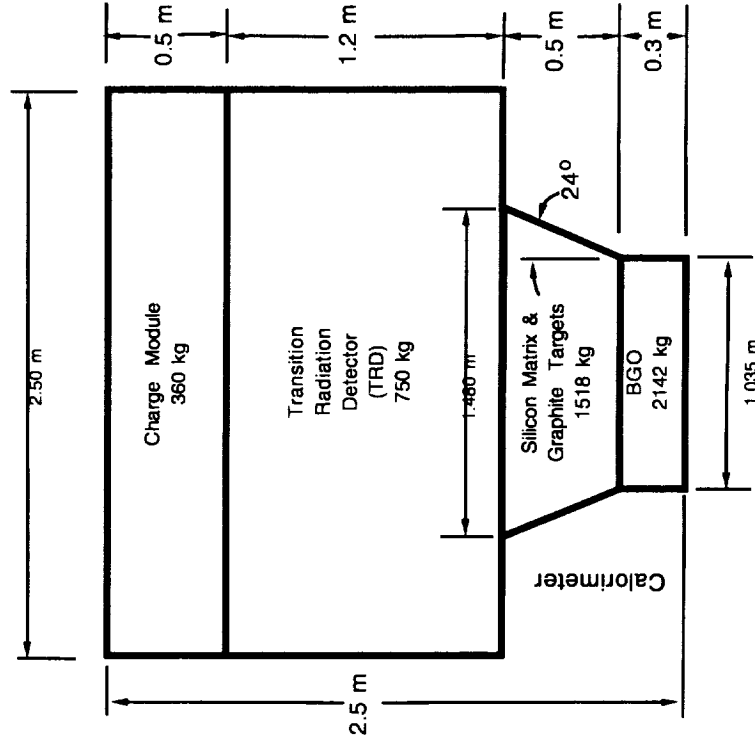
Orbiter coordinate system.
+Z is out of the paper.

There is another 250 kg of avionics, thermal control system, gas resupply system, debris shields, and contingency mass for a total ACCESS Experiment mass of 5031 kg (11069 lbs).

For this preliminary assessment, all mass is assumed to be uniformly distributed throughout each of the envelopes shown.

An ECS to carry this experiment mass would weigh 865 kg (1903 lbs). 118 kg (260 lbs) is required to make the ECS deployable and to attach it to the PAS. Therefore the total ACCESS Payload mass is 6014 kg (13232 lbs).

All envelopes are squares
in the Y-Z plane.

Figure 17. ACCESS experiment for ECS option.

32
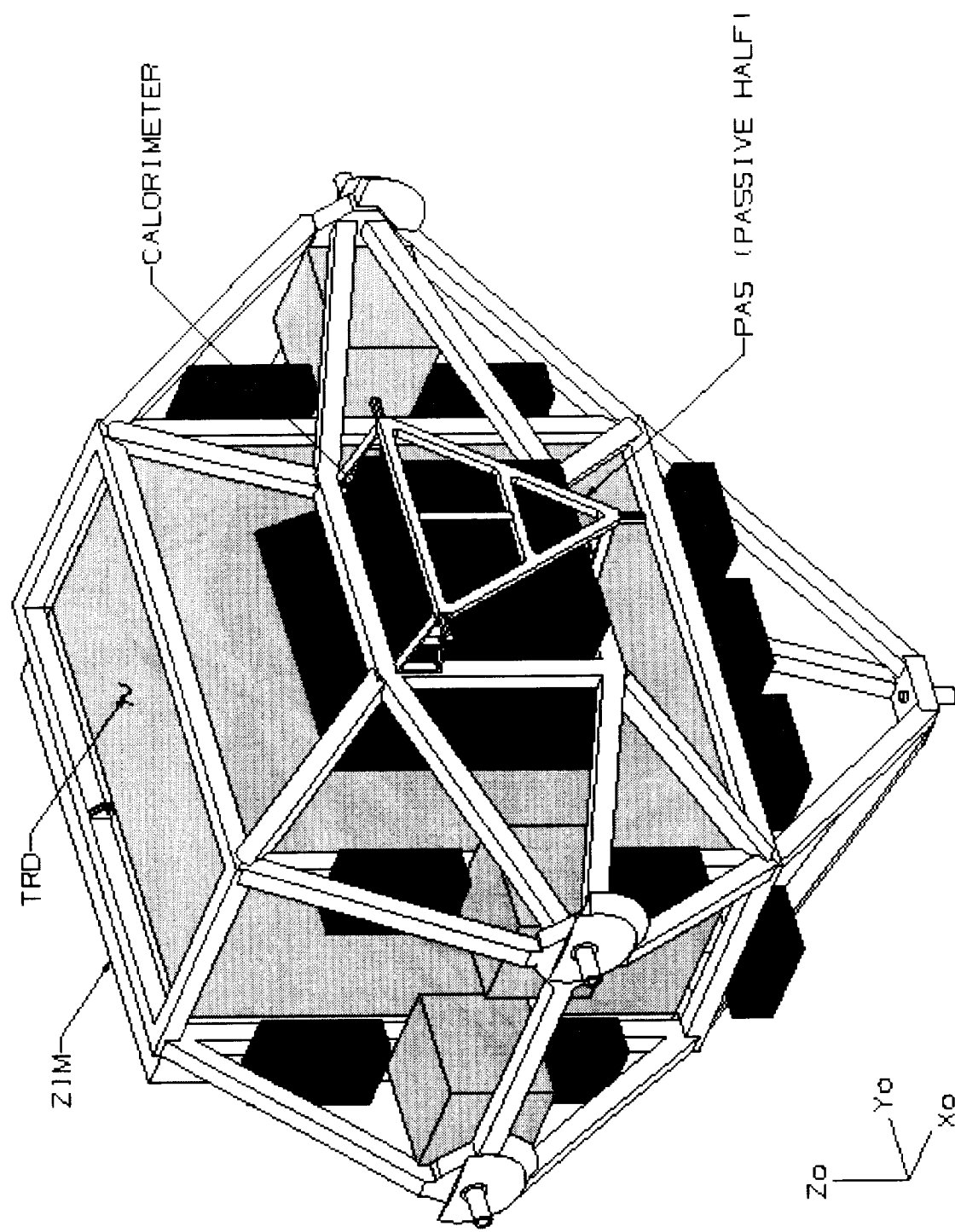
Figure 18. ECS design.

33
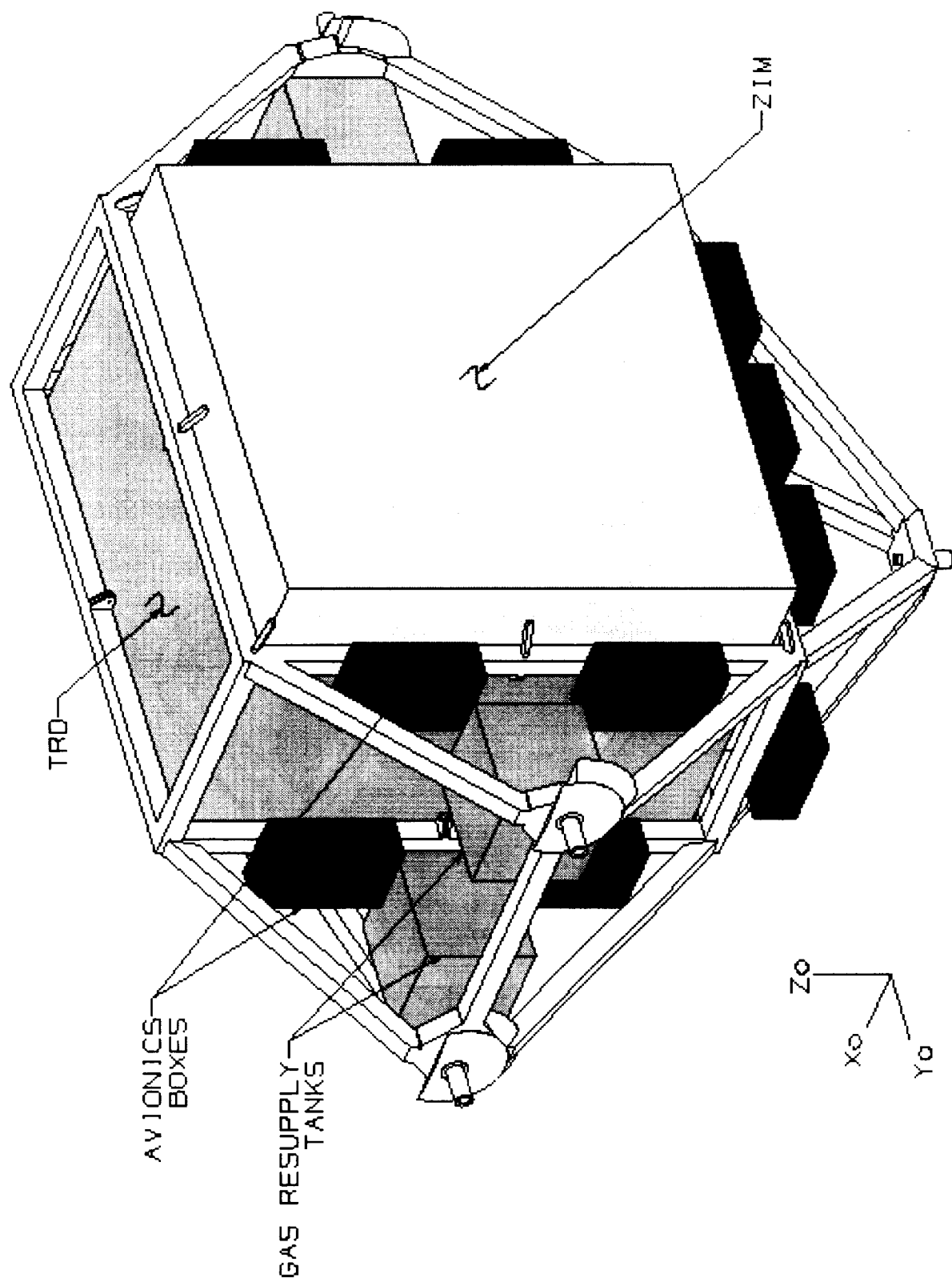
Figure 19. ECS, topside view.

TRD

AVIONICS BOXES

GAS RESUPPLY TANKS

ZIM

Zo

Xo

Yo

34
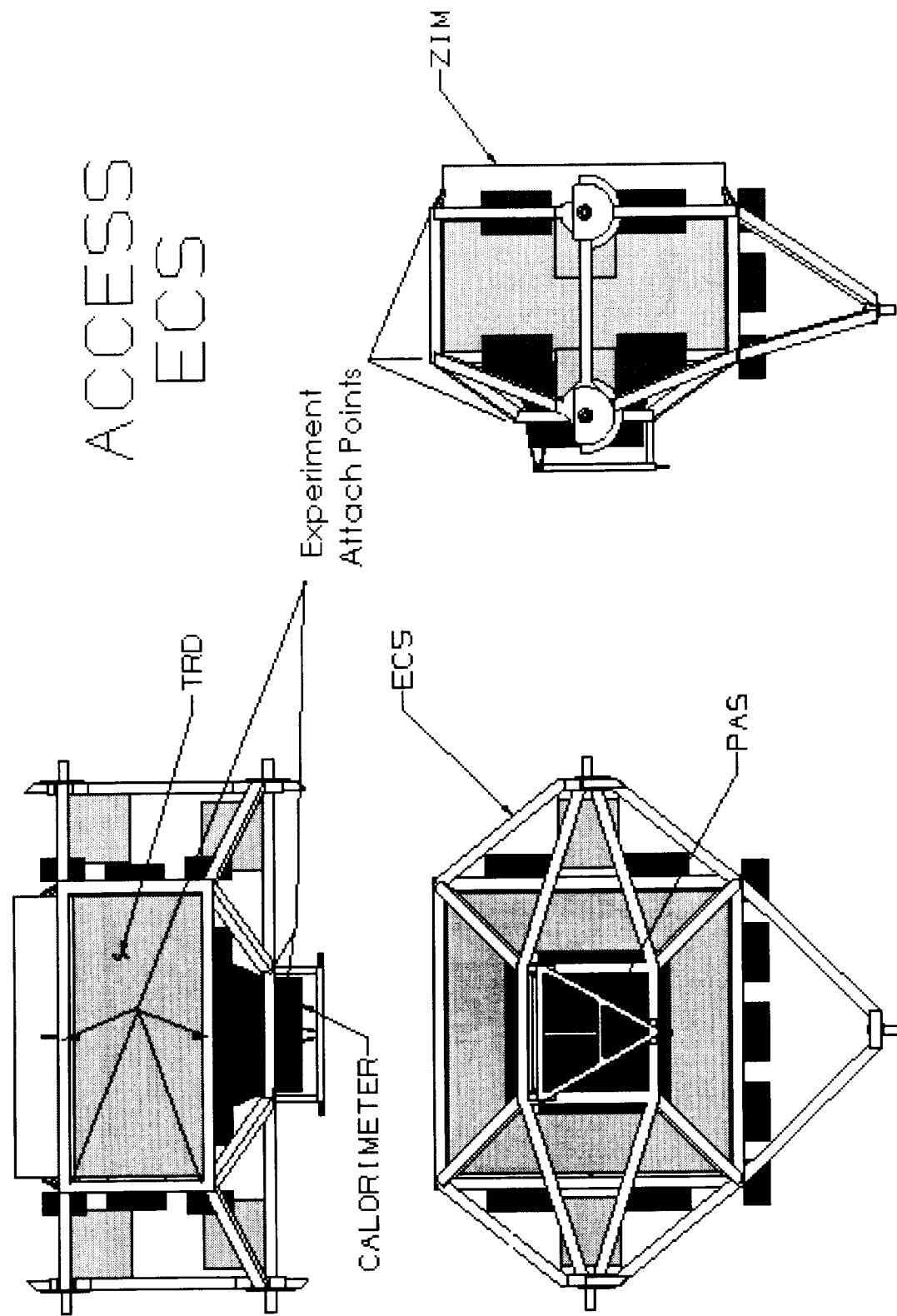
Figure 20. ECS-to-experiment attach points.

35

Figure 21. ECS/ACCESS attached to PAS on S-3 segment.
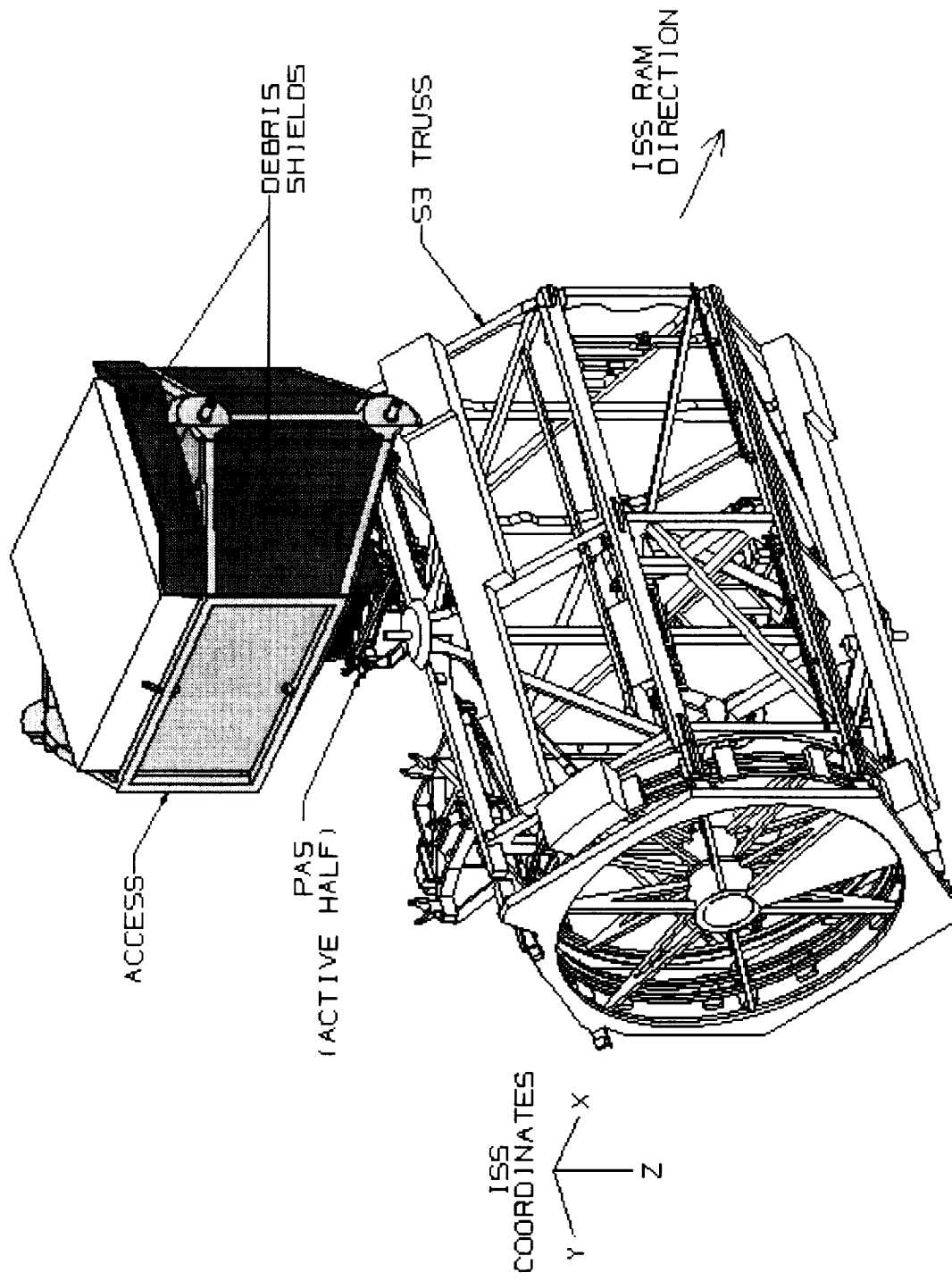
Note: Only orbital debris shields are shown. Micrometeoroid shields will be considered for zenith-arriving trajectories, but were not shown due to uncertainty about the placement of the shields over the ZIM. Thermal louvers are on the wake side.

A FEM has been developed for this configuration. The first natural frequency of the payload is 9.9 Hz, and the structure has only six modes below 50 Hz. Like the USS, this means that the ECS/ACCESS configuration would provide for a relatively simple modal correlation. This directly corresponds to less analysis and testing, and thus less cost to the project. Preliminary results show all positive margins above 20% for this configuration.

Weight

Table 8 gives a weight summary for the ACCESS experiment within the ECS. The total experiment weight is allocated as shown in Figure 17. As the table indicates, the ECS weight is a much smaller percentage of the total weight (16.34%) than was the modified USS (22.50%). The total weight of the ECS and PAS integration hardware is 2163 lb with a total payload weight of 13,232 lb. The total weight of the modified USS and PAS integration hardware is 2465 lb with a total payload weight of 10,952 lb. The ECS provides a support structure weight savings of over 300 lb while increasing the total payload weight by 2280 lb. This shows the significant weight advantage of designing a dedicated structure for the ACCESS payload.

Table 8: ACCESS Weight Summary on the ECS

Item	Weight lb (kg)	% of Total Weight
Experiment Hardware	11069 (5031)	83.66
ECS Weight	1903 (865)	14.38
Weight to Make ACCESS Deployable to PAS	260 (118)	1.96
Total Payload Weight	13232 (6014)	100.00

It should be noted that some of the other ECS configurations studied (Appendix F) relied more heavily on the ACCESS internal instrument structure to share some of the loads. Although this can bring the weight down, it depends heavily upon a closely knit science integration team, and should one instrument's schedule slip significantly, the collective program cost can be increased dramatically. The total weight of the lightest ECS (including PAS integration hardware) is 1808 lb (14.04% of total weight) with a total payload weight of 12,877 lb. Details on this structure are available[34]. Further definition of the ACCESS internal experiment structure will lead to an even lighter ECS.

ECS advantages

The ECS provides several key advantages simply because it optimizes the carrier design for the specific ACCESS instrumentation. The structure is lightweight, easy to build, relatively low cost, and is extremely flexible to accommodate changes in the three respective experiment designs. In addition, because the ECS will be built with proven methods and materials, the structure does not require the added cost of a research and development program, or a special testing and certification program. The ECS also provides the most viable option to accommodate the yet undetermined PAS requirements in the ISS program. Because the ECS utilizes the same Shuttle attach points as the USS, the existing GHE and test hardware can be used for the ECS. This represents a saving of a significant amount of design and analysis work.

37

Cost and schedule

Once again, an attempt was made to estimate the cost and schedule needed for the ECS to accommodate the ACCESS experiment (Table 8). The total cost to build the ECS for ACCESS will be approximately $2.2 to $2.6 million depending on the final payload weight and the final experiment design (broken out as deliverables in Table 7). This cost is based on actual JSC flight experience.

A certified ECS can be ready for shipment 19 months after the definition of the experiment and the definition of the experiment-to-ECS interfaces.

Thermal control

Summary

Over its four-year mission, ACCESS will experience the full range of ISS environments (Appendix G). It must be designed to withstand and function within all of them. The study below was performed to identify the range of particular thermal effects that ACCESS will encounter and possible means of dealing with them. Such an assessment of the overall thermal feasibility of ACCESS is essential due to the temperature sensitivity of its instruments. This payload has extremely tight thermal requirements that must be considered in both its overall payload design and its internal detector design.

- Insulation and possibly heat pipes can be used to minimize thermal gradients.

- Total heat rejection can be achieved with reasonably sized radiators.

- A louvered radiator adds mass and complexity, but would reduce required heater power.

- Thermal design within each detector is extremely important to ensure minimum temperature gradients and adequate heat rejection.

ACCESS thermal configuration

From the three separate baseline ACCESS instruments described in Appendix B (CM or ZIM, TRD, and calorimeter), a total integrated thermal instrument for the study was defined as depicted in Figure 22. As was shown in Figures 18-20, the detectors, avionics, thermal control hardware, and other miscellaneous items will all be supported and attached to the ISS by the ECS. For purposes of this thermal study, only the detectors were evaluated. Baseline Option 3 dimensions, mass, and power dissipation were used (Table 9 and Appendix E). The temperature limits arrived at by the Accommodation Study Team PIs are shown in Table 10. Detailed thermal evaluation of the internal detector structure (such as that described in Appendix B) and the avionics boxes (such as shown in Figure 19) were not part of this thermal analysis because these are still undergoing conceptual design.
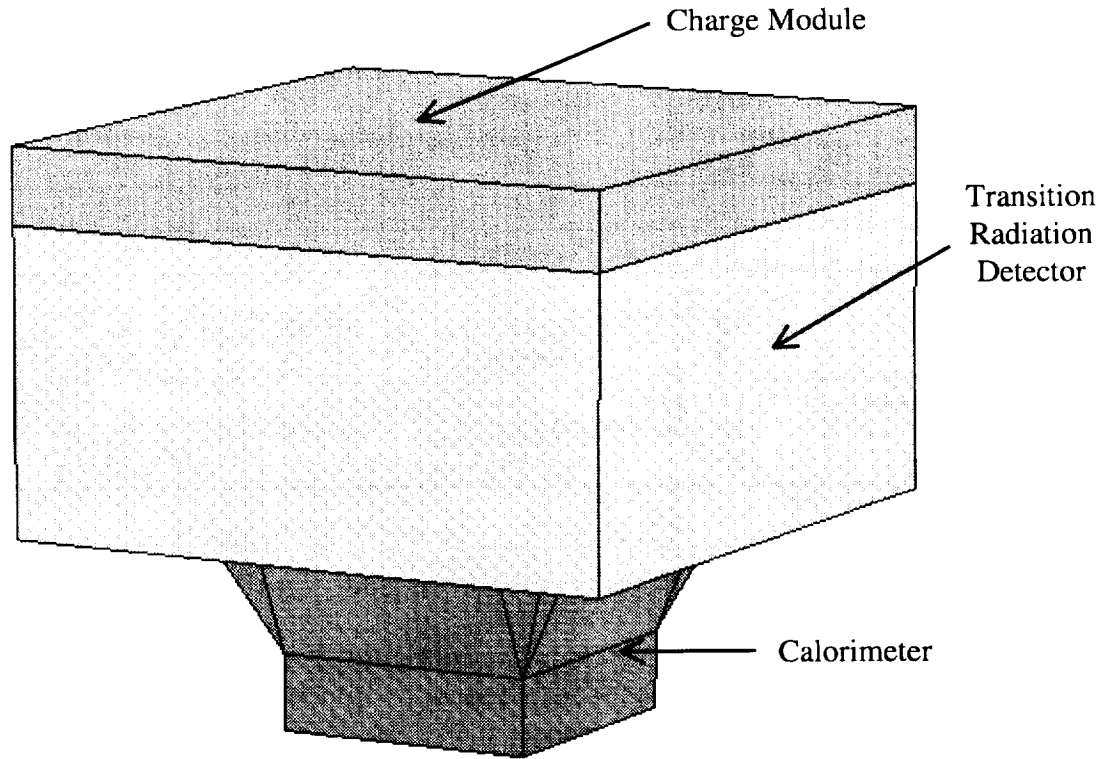
Figure 22. Integrated ACCESS instrument (Option 3) for thermal analysis.

Table 9. Dimensions, Power Dissipation, and Mass for Baseline ACCESS Thermal Study (Option 3)

Subsystem	Dimensions (m)	Exposed Surface Area (m^2)	Power (watts)	Mass (kg)
CM (ZIM)	2.5 x 2.5 x .5	9.25	58	360
TRD	2.5 x 2.5 x 1.2	16.06	200	750
Calorimeter: Si Matrix BGO	1.257 x 1.257 x .55 1.035 x 1.035 x .3	2.75 2.31	38 32	1518 2142
Remote Electronics: ZIM Calorimeter	N/A N/A	N/A N/A	58 50	N/A N/A
TOTAL:			436	4770

Table 10. Temperature Limits for Baseline ACCESS Study

Subsystem	Operating Target Temperature (°C)	Min/Max Operating Temperature (°C)	Min/Max Survival Temperature (°C)	Operating Temperature Gradient (°C)	Allowed Temperature Variation (°C)
CM (ZIM)	5	-5/+20	-30/+30	<10	N/A
TRD	5	-5/+20*	-30/+30*	N/A	N/A
Calorimeter: Si Matrix BGO	10 10	-25/+30 -10/+30	-40/+40 -40/+50	<2 N/A	<1-2 / orbit <2-3 / 45 days <5 / year
Remote Electronics: ZIM Calorimeter	20 20	-30/+45 -5/+40	-40/+70 -45/+75	N/A N/A	N/A N/A

* Assumed value for TRD

ISS thermal environment

The ISS will be at an Assembly Complete configuration by the time ACCESS is launched. Our geometric thermal model is illustrated in Figure 23 for a static, feathered-array configuration. At an altitude of roughly 435 km (235 nautical miles), the ISS will orbit the Earth every 93 minutes with the +Z-axis pointing at Earth and the +X-axis along the velocity vector. The actual ISS attitude can vary by as much as ± 15° around the X and Z axes, and +15°/-20° around the Y axis.[35]

The natural orbital environment (solar constant, Earth albedo, Earth infrared, or IR) and local coupling effects due to ISS hardware itself, drive the thermal environment. The solar constant is the radiation emitted from the Sun that reaches Earth. Earth albedo is the percentage of the incident sunlight that is backscattered out into space again. Earth IR is the energy re-emitted from Earth as long-wavelength IR radiation. Table 11 summarizes the nominal natural environment used for this analysis. Local effects must be calculated using appropriate geometry and optical properties.

Table 11. ISS Nominal Natural Environment

Solar constant	1367 W/m^2
Earth albedo	27%
Earth IR	241 W/m^2

A large contributor to variations in the ISS thermal environment is the solar beta angle. Beta angle is defined as the smallest angle between the orbit plane and the solar vector (Figure 24). For any spacecraft, the beta angle at a given time will be governed by launch inclination, launch date and time, and the time of year. Figure 25 shows a sample of beta-angle progression.
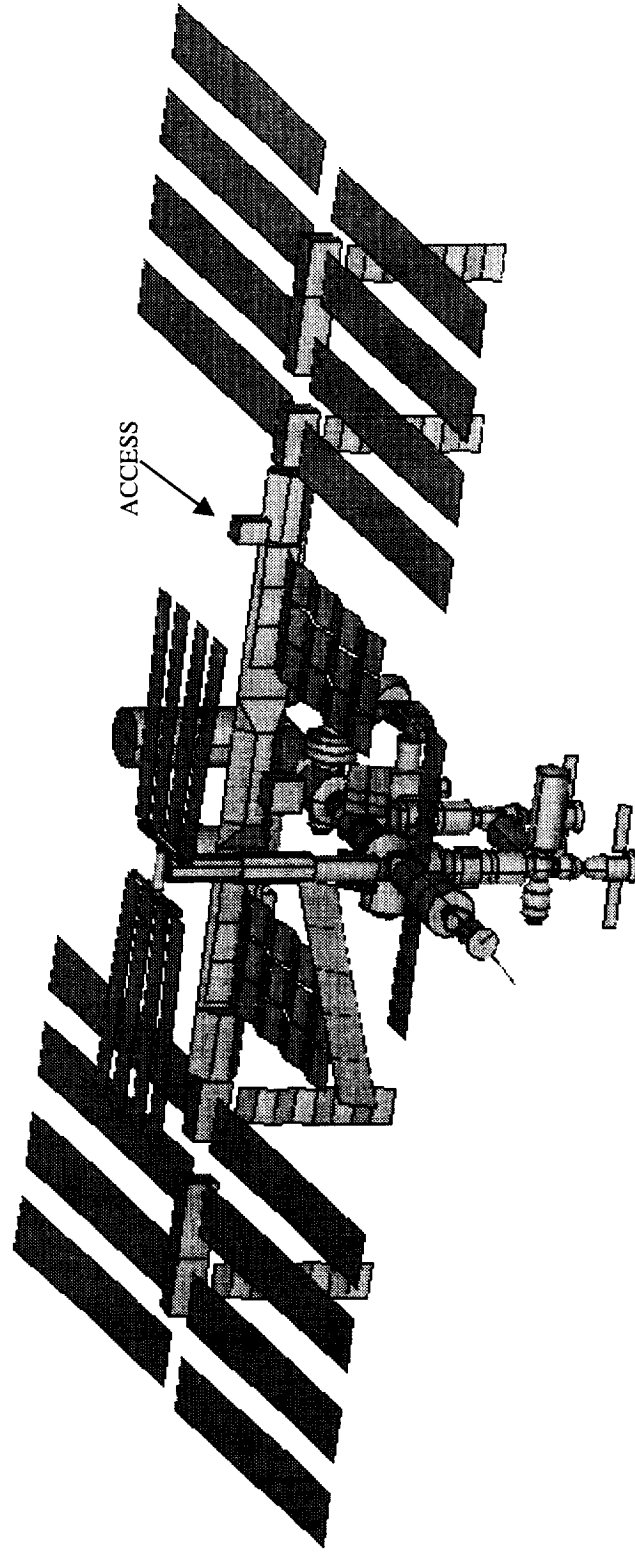
ACCESS

Figure 23. ISS geometric model for ACCESS thermal analysis, Assembly Complete.

41

For the ISS, this angle will change periodically from -75° to +75°. At beta angles greater than 70°, parts of the ISS will be in sunlight for the entire orbit.
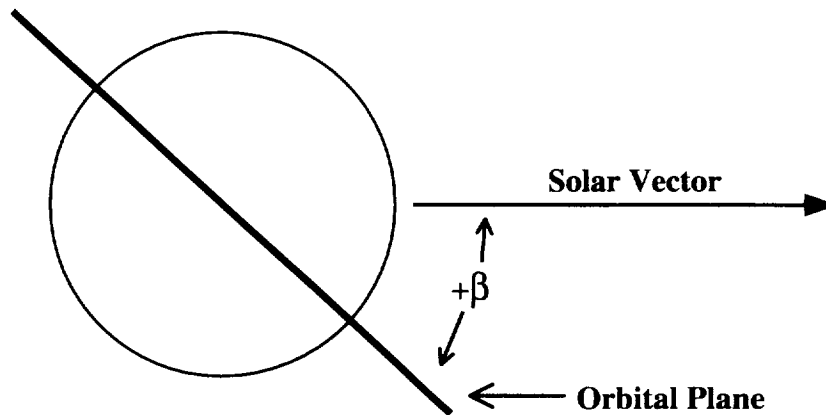
Figure 24. Beta angle definition.
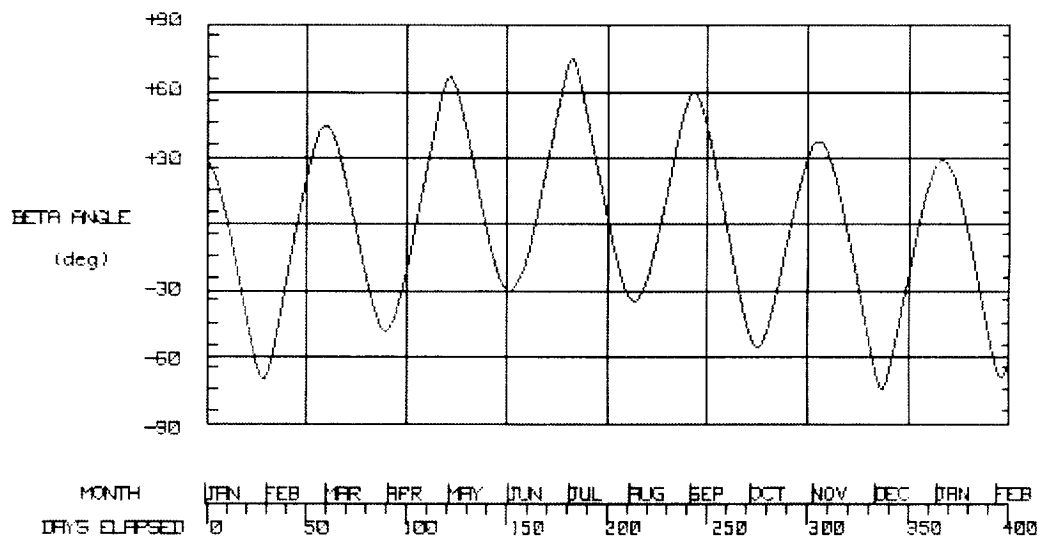
Figure 25. Sample beta angle progression with time.

The payload attach sites on both the S3 and P3 trusses are located outboard of the ISS radiators and inboard of the solar arrays. Both radiators and solar arrays will articulate continuously and will influence the ACCESS thermal environment. Payloads attached next to ACCESS

could also have a significant effect. At this point it is uncertain what payloads will be located next to ACCESS and how long they may remain there.

ACCESS will also have to withstand other environments prior to installation on the ISS. Shuttle Orbiter environments while undocked from the ISS can be controlled by Shuttle attitude. Once docked, however, ACCESS could remain in the Shuttle payload bay and/or on a temporary attach site for several days. These ISS operational scenarios also need to be accounted for.

Thermal survey

A detailed survey was performed of possible ISS thermal environments for ACCESS. The thermal model in Figure 25 which includes the ISS Assembly Complete geometry and a representative ACCESS payload, was used to determine the six-directional thermal environment at the S3 attach site[36]. The S3 and P3 locations were assumed to be symmetric. In all, 196 cases covering beta angles from -75° to +75° and ISS attitude variation extremes were surveyed. Average sink temperatures based on various optical properties were used as criteria to identify worst-case hot and cold environments. These environments were then imposed on a more detailed ACCESS model to size radiators and heaters. The hot case was used to find the amount of radiator area necessary to keep the experiment at its desired operating temperature. This configuration was then exposed to the cold-case environments to find the necessary heater power to maintain the desired operating and survival temperatures.

Thermal assumptions

ACCESS was evaluated as three independent detectors with properties as defined in Tables 9 and 10. Since their operating and survival temperatures are similar, no heat flow was considered between detectors. Electronics the baseline study PIs identified as being able to be mounted apart from the detectors were also evaluated and treated independently (Figure 19 and 20).

The CM (ZIM) and TRD detectors where modeled as single isothermal internal nodes, connected to external surfaces and radiators. The calorimeter was modeled as two separate systems, the Si matrix and the BGO crystals. Each of these was also modeled as a single isothermal node connected to external nodes and a radiator. External surfaces were assumed to be insulated with 10-layer multilayer insulation (MLI) to minimize gradients. Outer surface optical properties were assumed to be those of beta cloth. Beginning of life (BOL) optical properties (α/ε =0.34/0.92) were used for the cold case while end of life (EOL) (α/ε =0.4/0.88) properties were used for the hot case. Radiators were assumed to have optical properties of Z93 white paint (α/ε = 0.17/0.92). Silver Teflon would provide better radiator properties but, due to its highly specular nature, it may not be acceptable for use on the ISS. Optical properties for louvered radiators were adjusted to take into account conduction between blades and radiator, blocked views to space, and reflections off blades[37]. The outer surfaces of the louver blades were assumed to be black anodized aluminum. A summary of optical properties used in this study is shown in Table 12.

Table 12. Assumed Optical Surface Properties

Surface	Solar Absorptivity (α)	IR Emissivity (ε)
Beta Cloth (BOL)	0.34	0.92
Beta Cloth (EOL)	0.40	0.92
Z93 White Paint	0.17	0.92
Louvered Radiator (open)	0.17	0.64*
Louvered Radiator (closed)	0.1*	0.1*

* Effective values

Radiators were assumed to be located facing the ISS wake (-X) direction. Other possible radiator directions are less desirable for various reasons. The nadir (+Z) and outboard (+Y) directions appear to be too warm, and the ram (+X) and zenith (-Z) sides will probably require debris shields (Figure 21). Thermal resistance between internal nodes and radiators was neglected in this study. This is a non-conservative assumption, which must be taken into account for detailed thermal design.

Thermal results

The hot case was found to occur at a beta angle of $-75°$, with the ISS in a $-15°$ yaw (Y), $15°$ pitch (P), and $15°$ roll (R) attitude. By imposing this environment on the ACCESS thermal model, the required radiator area to maintain detectors at their desired operating temperature was calculated. The cold-case environment (Beta 75°, YPR of $-15°, -20°, 15°$) was then imposed on the model using radiator areas from the hot-case analysis. With detectors powered on, the amount of additional heater power necessary to maintain the operating temperature was determined. Heater power necessary to maintain survival temperatures when detectors are not powered was also found. A summary of these results is shown in Table 13.

Table 13. Required Radiator Area and Heater Power

Subsystem	Radiator Area (m²)		Operating Heater Power (W)		Survival Heater Power (W)	
	no louver	w/ louver	no louver	w/ louver	no louver	w/ louver
CM	0.45	0.75	73	0	53	11
TRD	1.6	2.7	210	0	165	15
Calorimeter: Si Matrix	0.31	0.54	33	0	8	0
BGO	0.22	0.37	31	0	16	0
Electronics	.34	0.55	2	0	30	0
Total	2.92	4.91	347	0	242	26

Results show that a total-radiator surface area (no louvers, no heaters) is sufficient to reject 436 W in a hot environment. Radiator surface area could be the surface of a detector or a dedicated radiator. Actual radiator surface area will have to be larger to account for thermal resistance between heat sources and radiators. Detailed modeling and thermal design can determine this. Heater power (347 W operating and 242 W survival) is required to maintain detectors at minimum temperatures. Results indicate that almost no heater power is required if louvers are implemented. This is due to radiator temperature being high enough to heat detectors. This is unrealistic, and heaters would probably still be needed to minimize thermal gradients and temperature variation within detectors. This too would have to be determined by detailed analysis.

The orbital temperature variation seen for all detectors was found to be minimal (<1°C). This was expected because of the simplified model nodalization, high mass and relatively small, insulated surface areas.

Thermal design considerations

Because the thermal environments at the payload attach sites will vary significantly with changing solar beta angle, the detectors need to be insulated to minimize gradients and orbital variations. This insulation will protect ACCESS from the external environment, but will also keep the heat generated by the experiments themselves from dissipating. Radiators then become necessary to remove the excess heat. Isolating the electronics away from the detectors maximizes the allowable insulation and minimizes radiator and heater requirements. Using louvered radiators reduces the heater power necessary, yet adds complexity to the system. The use of either a common radiator, or individual radiators per detector, needs to be evaluated and optimized.

Getting heat from detectors to the radiators could be challenging. Solid conduction paths (aluminum, copper, etc.) between heat sources and radiators would require that radiators be located as close to the detector as possible, and could cause a significant increase in mass. Any 250-mil aluminum avionics shielding from trapped electron-proton radiation, however, could serve as such a conduction path. Heat pipes are a viable low-mass option using a closed two-phase liquid-flow system to move large amounts of heat from one location to another. The driving force for moving fluids is capillary action, which is greatly affected by gravity. Ground testing of non-horizontal heat pipes is therefore a major concern. Heat pipes should also be considered for minimizing gradients within ACCESS detectors and in the radiators themselves.

ACCESS avionics & power

Avionics is an acronym for "aviation electronics" which has also come to be all-encompassing, meaning aerospace electronics. Avionics necessarily requires distributed electrical power. For the ACCESS baseline study, it was determined that a central avionics and power box was necessary to manage the ISS accommodation resources (power and data) provided in the PAS UMA interface shown in Figure 12 and indicated schematically in Figure 26.
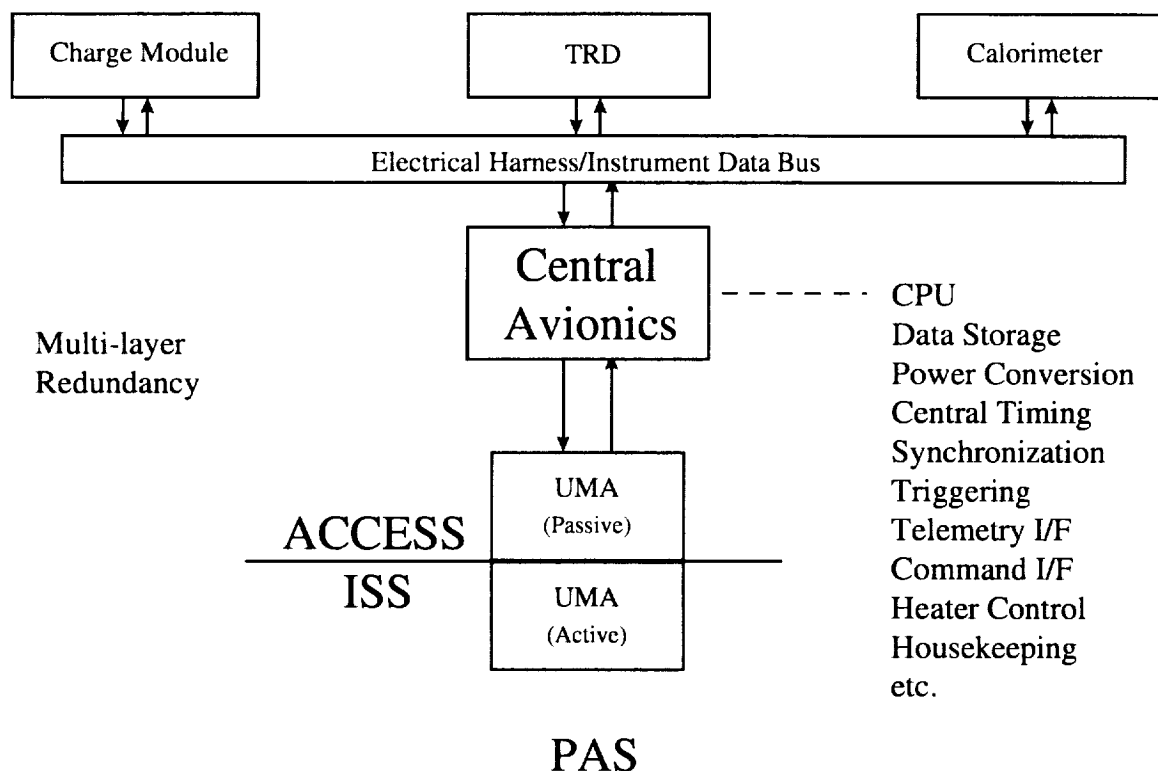
Figure 26. Functional ACCESS avionics, data, and power overview.

These PAS resources (Figure 26) are distributed to the three instruments in the functional fashion shown and the two-way data links are established. A detail of the central avionics box is given in Figure 27. When necessary, its functions include central microcomputer processing, data storage, power conversion, central timing, synchronization, triggering, telemetry data and command interface, heater control, and general housekeeping. PAS power and data interfaces include a utility power feed for pass-through to the attached payload via the UMA. Both the electrical and the C&DH interface between the PAS UMA and the ACCESS payload are handled by means of the avionics & power box (Figure 26 and 27). Trigger control can be run along the electrical harness.

Electrical power

The ISS provides 113-124 VDC utility accommodation power as measured at the PAS UMA. Power quality is specified in the ISS External Payload Interface Definition Document. As shown in Figure 27, this electrical power is either fed through directly or undergoes a power conversion in the power module. At the time of writing this report, the Accommodation Study Team PIs are unclear as to whether they want converted power, or they want to do their own conversion, or both. The power is then routed via an electrical harness (Figure 26) to the respective instrument or instruments. An optional 28 VDC STS electrical power interface is also shown in order to alleviate STS accommodation incompatibilities discussed in Appendix H.2. A 28 and 120 VDC heater control system could then operate off of both STS and ISS power accommodations without additional conversion.

Central Avionics Concept
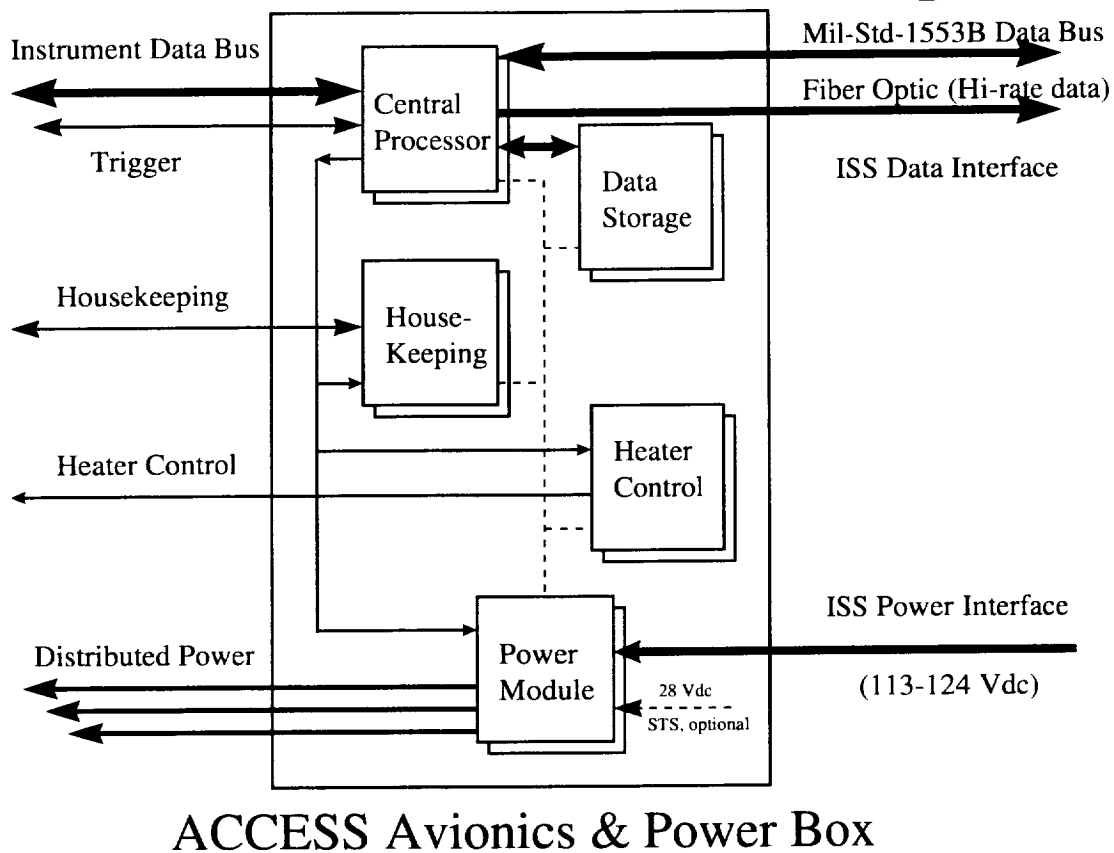
Figure 27. ACCESS avionics & power box concept.

Present estimates indicate that the ACCESS avionics will require 436 W for normal operations. An additional 200-400 W may be required to maintain the proper operating temperature. When the electronics are off, 200-400 W of keep-alive power appear to be required, depending upon the final thermal control system design.

Data interfaces

In addition to the power interface, there are potentially three command and data interfaces between the ACCESS payload and the ISS: a fiber-optic high-rate forward link (uplink), a fiber-optic high-rate return link (downlink), and a MIL-STD-1553B data bus for both forward and return low-rate data. The high-rate fiber-optic forward link will not be addressed here because there is no obvious use for it on ACCESS and the ISS Ku-band forward link has not been defined at this time. (The medium-rate link [E-net] is not available to external payloads.) Therefore, the interfaces of concern in the avionics & power box concept of Figure 27 are DC power, the 1553 data bus, and the high-rate return link.

Command, control, and monitoring

Figure 28 is a simplified block diagram of the entire ISS payload C&DH system. Figure 29 illustrates the portion of the ISS C&DH system that basically supports ACCESS. Connections to other payloads are not shown.

Figure 28. ISS C&DH system, payload data subsystem summary.

There are two ISS payload MDMs. MDM 2 is a backup and is brought on line manually in the event that MDM 1 fails. Unlike the MDMs, the two automated payload switches (APSs) are used simultaneously.

The active payload MDM obtains low-rate data via the 1553 data bus at a maximum rate of 20 kilobits per second (kbps). In the unlikely event that there is any ACCESS data associated with crew or vehicle safety, this particular data will be routed to the ground via the command and control MDMs (C&C MDMs) and the S-Band telemetry system. All the ACCESS data acquired via the 1553 data bus will be combined with the rest of the 1553 data acquired by the payload MDM from other payloads and will be transmitted to an APS via fiber. Operationally, the active payload MDM should always be switched to one of the eight APS output lines.

High-rate telemetry is sent directly from ACCESS on the fiber-optic interface to the APS shown in Figure 29. As currently planned, only two of the payload direct links to the APS will be switched to the communications outage recorder (COR) and Ku-band telemetry system at any one time. The return-link rate allocated to the APS output at this time is 43 megabits per second (Mbps).

48

Figure 29. ACCESS/ISS C&DH interfaces (simplified) in Figure 27.

The HCOR, which is the operational version of the COR, will have the capability to store 220 Gbits of data. Because of communications outage and the fact that multiple payloads will be competing for resources on the APS output channels, as much data storage as practical should be provided within the ACCESS payload (Figure 27). Multiple playback rates will be required.
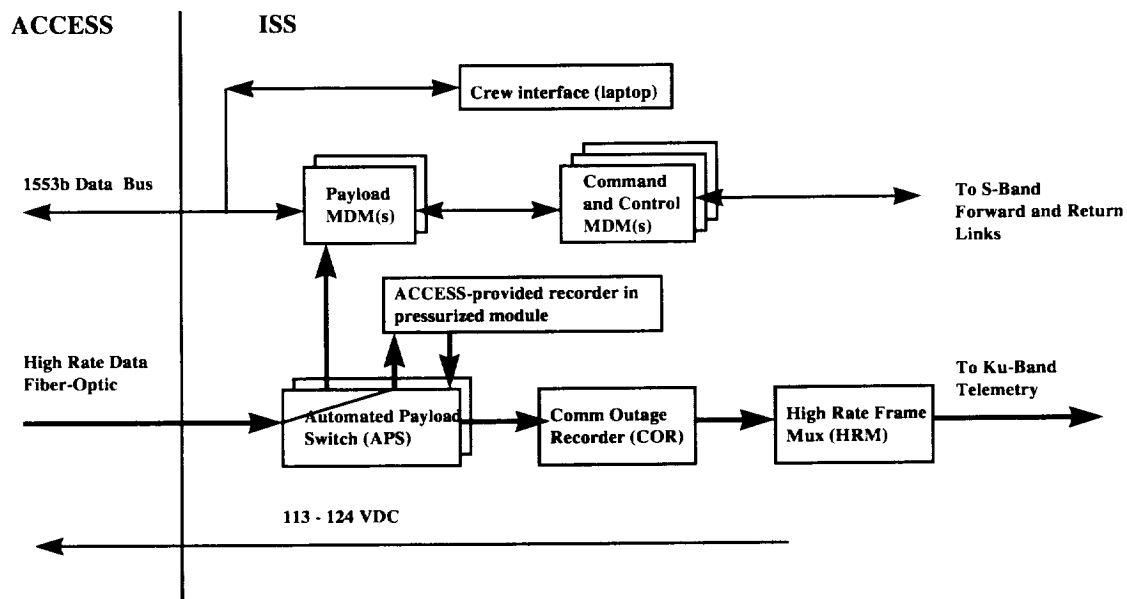
Figure 30. Alternate ACCESS/ISS C&DH interfaces (simplified) in Figure 27.

An alternate high-rate telemetry connection is illustrated in Figure 30. The high-rate data is passed via the APS to equipment in one of the pressurized modules where it can be recorded for deferred playback or on media that the crew can return to the ground. The advantage of this

49

approach is that the design options are not frozen-in years prior to launch. Up-to-date recording equipment can be used, and even upgraded as advancing technology permits, by astronauts in their shirtsleeve environment.
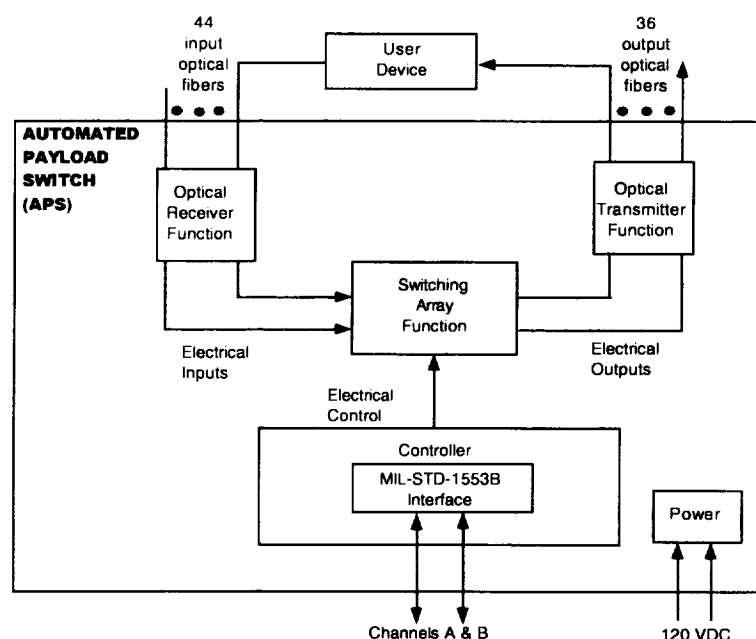
Figure 31. Typical APS connectivity.

The disadvantage of such an approach is that pressurized module accommodations will be required as well as another APS connection. Figure 31 indicates a typical APS connection.

Ground commands are sent through the ISS S-band system and are implemented using the 1553 data bus interface (Figures 27, 28, and 29). Command words are 64 words long (including 11 words of overhead). Eight commands per second are available for all payloads combined.

Crew interfaces

The ISS flight crews are intimately involved in all ISS payloads. Table 14 clarifies this.

Table 14. ISS Flight Crew Interfaces

- *From the ISS cupola, the crew will be manually involved in the remote, robotic attachment of an ACCESS payload at the PAS.*
- *The crew has a C&DH interface.*
- *The crew has a failure mode function for all payloads.*
- *The crew will probably be in physical contact with the payload at the PAS.*
- *The payload cannot jeopardize the safety of the crew.*

An ISS-issued laptop computer connected to the payload MDM 1553 data bus (Figures 22, 23, and 24) as a portable computer system (PCS) provides crew C&DH interface capability for a limited amount of data display and command.

50

Environmental issues

ISS environmental issues that impact the ACCESS payload are presented in Appendix G. Some are simple and straightforward, while others are far-reaching and significant. Strategy consists of control plans and mitigation plans. Only three examples will be discussed here. Additional environmental issues, safety reviews, and control procedures that impact ACCESS design, development, and operations are deferred to Appendix G.

Control plans (electromagnetic interference, or EMI, example)

EMI

A straightforward example is EMI, which will be a fundamental consideration during the detailed design and development phase (Implementation Phase: design, development, test, and evaluation, or DDT&E) of ACCESS. An SSP EMI control plan (EMICP, SSP 57010 cited in Appendix D of this study report) outlines the process required by the ISS community to ensure electromagnetic compatibility (EMC) between ACCESS and other ISS systems as well as other ISS payloads.

Hazard mitigation plans

An example of a far-reaching consequence of the on-orbit LEO environment is the hazard to payload instrumentation and avionics represented by particle radiation. Sources include the Earth's trapped radiation belts, the Sun, and the Galaxy (Figures 32 and 33). For this circumstance
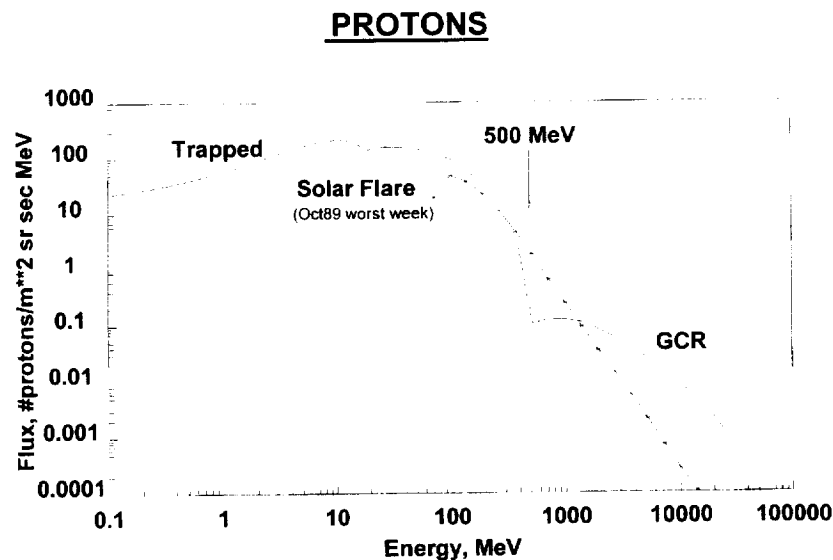
PROTONS

Figure 32. Proton flux in LEO as a function of energy[40].

there is no control plan. Rather, risk mitigation rests in payload design, operations procedure, shielding strategy, and an existing JSC radiation-level measurement plan.

HEAVY IONS
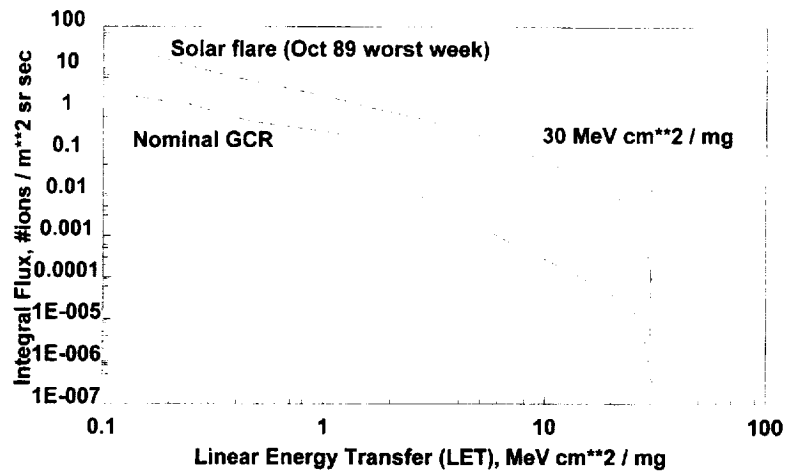
Figure 33. Particle flux[40] in LEO as a function of linear energy transfer (LET)[39].

Radiation hazards

For the purpose of this ACCESS Accommodation Study, a radiation hazard analysis for payload avionics and electronic components was conducted based upon JSC computer simulation codes for the Earth's trapped radiation belts (Appendix G, Ionizing Radiation). By definition, this study was conducted for an ISS altitude of 500 km, which is a programmatic requirement. That altitude is a firm ISS hardware-imposed limit arising from the fact that the Russian Soyuz cannot go above 470-480 km and still de-orbit. Therefore, the trapped electron and proton fluxes (Figures G.8-G.11) along with the shielding curves (Figures G.12-G.14) can be used directly as a worst-case data analysis for a 2-σ margin of allowable dose. The SSP requirement for ISS altitude will always place it lower than those figures, thereby removing it further from the trapped radiation belts, which reduces the hazard.

Phase 1 of the ISS program was the joint U.S.-Russian *Mir* program orbiting at an altitude similar to the ISS (*Mir*: 51.65 degree @ ~ 381 km). One objective of Phase 1 was to define the radiation-level environment as a hazard. JSC's Space Radiation and Analysis Group (SRAG) did this; the data are available[38], and the same SRAG detectors are slated for the ISS (the TEPC and CPDS—see Acronyms, Appendix J). The CPDS is already on board the ISS (second-element launch, Flight 2A in Appendix C). It has a five-year life-cycle, and the ACCESS Accommodation Study Team has discussed how CPDS-II might be modified to complement and support ACCESS requirements when CPDS is upgraded in 2003.

Having introduced the ISS radiation hazard and the JSC SRAG measurement plan, how should ACCESS cope with the problem of a cosmic ray that penetrates payload electronics as illustrated in Figure 34?

The subject is well understood and has been thoroughly discussed[39]. We now introduce the concept of a hazard mitigation plan (HMP). These are diverse, and the topic has a rich heritage. O'Neill has pointed out[40] that two philosophies have emerged over the past 30 years for radiation HMPs: (1) The chip-by-chip method using a preferred parts list (PPL); and (2) The system-level

approach using commercial off-the-shelf (COTS) equipment from an approved parts list (APL). Both methods have been used successfully in spaceflight. These are contrasted in Table 15.
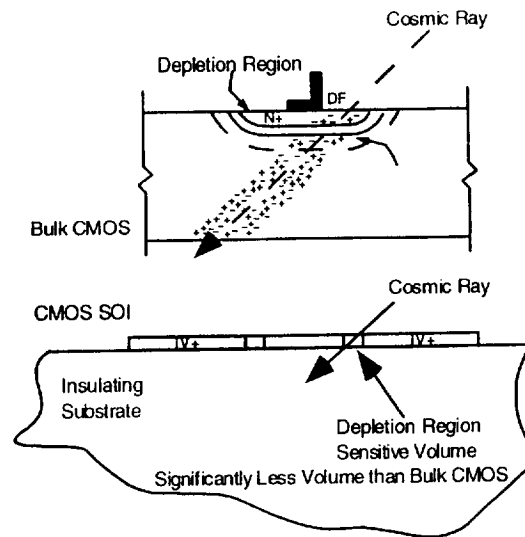
Figure 34. Radiation hardening and avionics failure mitigation.

Table 15. Contrast Between Radiation HMPs

Approved Parts Strategy	*Preferred Parts Strategy*
• *Use rad-hard approved parts*	• *Use rad-hard preferred parts*
• *System-level testing (APL)*	• *Chip-by-chip certification (PPL)*
• *Test "whole thing"*	• *Design is NASA-unique*
• *No latchups to LET ~ 15 years*	• *No latchups to LET > 35*
• *MTBF* ~ 10 years*	• *MTBF ~ ?? years*
• *Practical, latest technology*	• *Expensive, frozen-in*
• *Fallacy: Proton-beam only*	• *Fallacy: Non-existent parts*
*mean time between failures	

Radiation hardening (for rad-hard parts) is an avionics design strategy aimed at minimizing single-event phenomena (utilizing epitaxial layers, complementary metal oxide semiconductor silicon-on-sapphire insulator, dielectric isolation, guard rings, cross-coupled resistors, oxide composition and thickness assessment, and voltage derating).

The PPL method is well-known, being the chip-by-chip rad-hard certification procedure meeting military standards to some high LET (e.g., LET ~ 36). It was the NASA culture until approximately three years ago. It results in virtually 100% assurance of mitigation. However, it is cost-prohibitive; and it freezes-in the design early in the design, development, test, and certification (DDT&C) to such an extent that the avionics parts may no longer exist when the payload gets to its implementation phase or DDT&E (see Note 1). This happens in a robust technology when industry has stopped producing the parts commercially in lieu of better products.

The APL method is newer, having appeared in the ISS era as part of the "faster, smaller, cheaper" method. Basically, one places "the whole thing" (e.g., avionics box, PC, printer, etc.) in a 200 MeV proton beam. It is an integrated, system-level beam test performed with the entire electronics system operating[41]. It emulates an LET of 15 MeV-cm^2/mg, catching all failure modes with MTBF $\le$ 10 years. It also provides data for predicting system-level on-orbit failure rates.

The advantages of the two DDT&C approaches are compared in Table 16. In both strategies, all designs are assumed to be "radiation smart": (a) error detection and correction for critical RAM (random access memory and cache); (b) protected executable code; (c) system redundancy (self-checking, watchdog timers, etc.); and (d) shielding (optimal). Shielding up to ~250 mils as shown in Figure 35 does help for the trapped-belt radiation. Obviously, when known electrical, electronic, and electromechanical (EEE) rad-hard components are available and cost-effective, they can be used in both methods.

Table 16. Comparison of DDT&C Radiation Hazard Mitigation Strategy

System-level COTS	*Chip-level, LET-specific*
• *System-level, high confidence*	• *Chip-level, 100% confidence*
• *Chip-level, undefined*	• *System-level, undefined*
• *Flexibility*	• *Frozen-in*
• *COTS*	• *Unavailable parts*
• *Test cost - $300/hour*	• *Test cost - 1 WYE/chip*
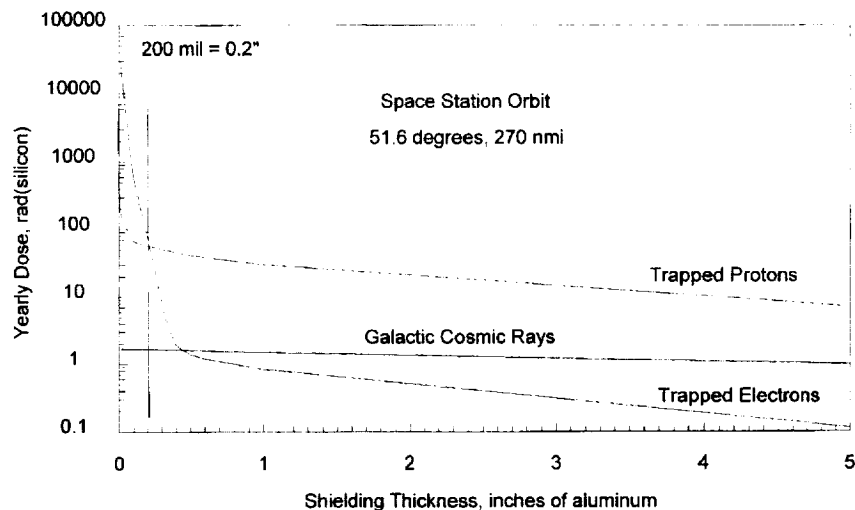
Figure 35. Effectivity of shielding in the trapped belts at ISS altitudes.

In summary, there is no PPL in the ISS program. There is an APL (at the Boeing Radiation Effects Laboratory website, with URL links and pointers elsewhere). The current ionizing radiation requirements are given[40] in Table 17.

Table 17. Ionizing Radiation Requirements

- *Avionics "... shall meet performance and operability requirements while operating within the natural radiation environments as specified in ... "*

- *Shuttle*

  - *NSTS 07700 Volume X Books 1 & 2*

  - *Flux vs. LET for 57 degree x 500 km orbit, solar minimum, 100 mil shielding*

  - *SEE (single event effects) only*

- *Space Station*

  - *SSP 30512 Rev. C*

  - *Flux vs. LET for 51.6 degree x 500 km orbit, solar minimum, 50 mil shielding or actual shielding*

  - *SEE and Total Dose*

The spacecraft avionics requirements in Table 17 are not relegated upon science payloads. For the ACCESS payload, the Accommodation Study Team recommends a hybrid combination of the system-level (COTS APL) and chip-level (rad-hard PPL) radiation HMPs. This allows for the obvious use of known, inexpensive rad-hard circuity components (e.g., rad-hard EEE PROMs [programmable read-only memory]) when they are COTS—but in the system-level APL method defined for the ISS program. Rad-hard components are not required, however, if the system can pass the proton beam test. The method is currently being adopted at JSC for the MARIE-Mars 2001 program[42]. It is summarized[10,40] in Table 18.

Table 18. Recommended Radiation HMP for ACCESS

- *Apply SSP 30512, Rev. C.*

  - ≤ 250 *mils shielding*

  - *Appendix G, Figures G.9 and G.10*

- *Adopt system-level performance requirements, not "rad-hardness" of components.*

  - *Allow flexibility.*

  - *Allow reasonable, quantified risk.*

  - *Allow use of robust modern technology.*

- *Adopt rad-hard components as an option, when cost-effective and COTS.*

- *Adopt SEE strategy.*

  - *A little bit of shielding helps, low-energy (~ 250 mils Al equivalent)*

  - *Ops work-arounds, high-energy events*

  - *Fail-operational, fail-safe design (multipath circuit design)*

The ISS APL can be found at the Boeing Radiation Effects Laboratory website (Appendix K), with links to the ESA database as well as to parts lists at Jet Propulsion Laboratory, the Electronic Radiation Response Information Center, and the Goddard Space Flight Center (GSFC).

Micrometeoroid and orbital debris (MMOD) hazards

The MMOD hazard in the ISS environment is particularly relevant to ACCESS because the baseline TRD instrument (Appendix B.3) contains a pressurized tank system. Until such a TRD conceptual design is brought into compliance with the NSTS and SSP safety review process, ACCESS will not fly on STS or the ISS.

Details of the subject hazard models are defined in SSP 030425, Rev. B, Section 8, and the debris model is available elsewhere[43]. An initial risk assessment for ACCESS[44] was the basis for the debris shields depicted in Figure 21. These are referred to as 'Whipple' shields or 'bumpers' (cf. photos in Johnson[43]). For instrumentation with a field of view (FOV), these function much like an automobile windshield on a freeway, which keeps flying particles from entering the eyes of the driver. Some 200 ISS shielding types are available (Whipple, multi-shock, mesh double bumper, stuffed Whipple, etc.) using ceramic cloth, metallic mesh, fabric, toughened insulation blankets, and aluminum. The toughening enhancement adds Nextel to the thermal blanket, between the beta cloth and the MLI.

The MMOD analysis process is summarized in Figure 36. It includes actual hypervelocity impact testing in JSC's Hypervelocity Impact Facility (HITF).
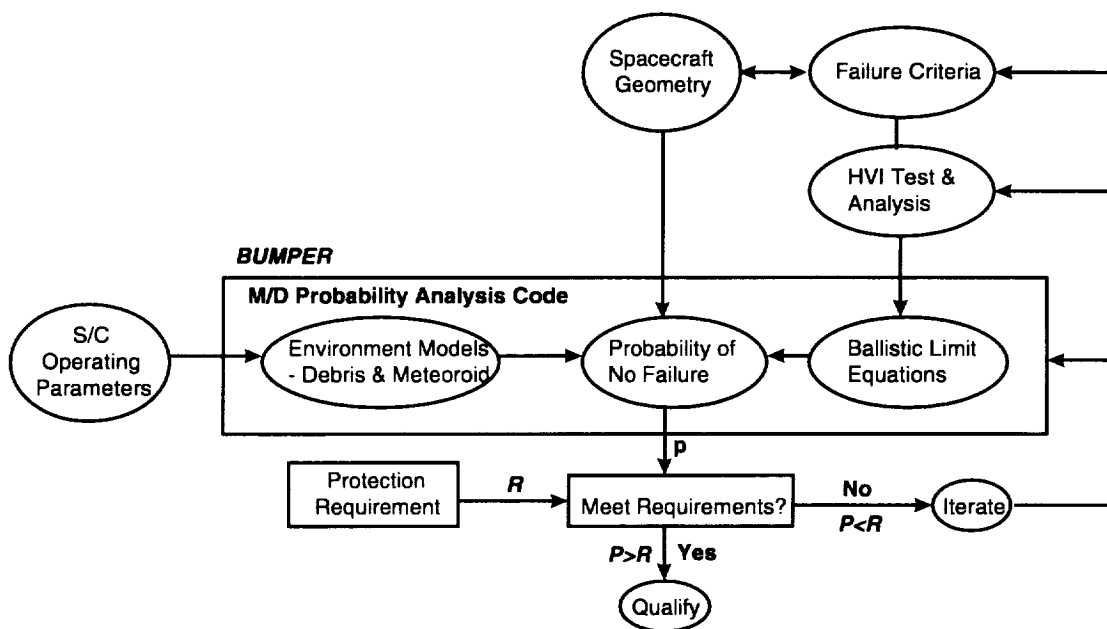
Figure 36. MMOD analysis process[44].

ACCESS pressurized gas system (TRD)

The toughening procedure mentioned above was applied to the flight qualification of Rocketdyne's plasma contactor unit (PCU) tank system[45-47] in the ISS electrical power system. The net result is functionally illustrated in Figure 37, showing the tank, Kevlar fabric, Nextel fabric, aluminum foil, and aluminum alloy shield. The spherical tank has been transformed into a system. It becomes a box (illustrated previously in Figures 19 and 20). Configuration details of the PCU box system are given in Appendix I.
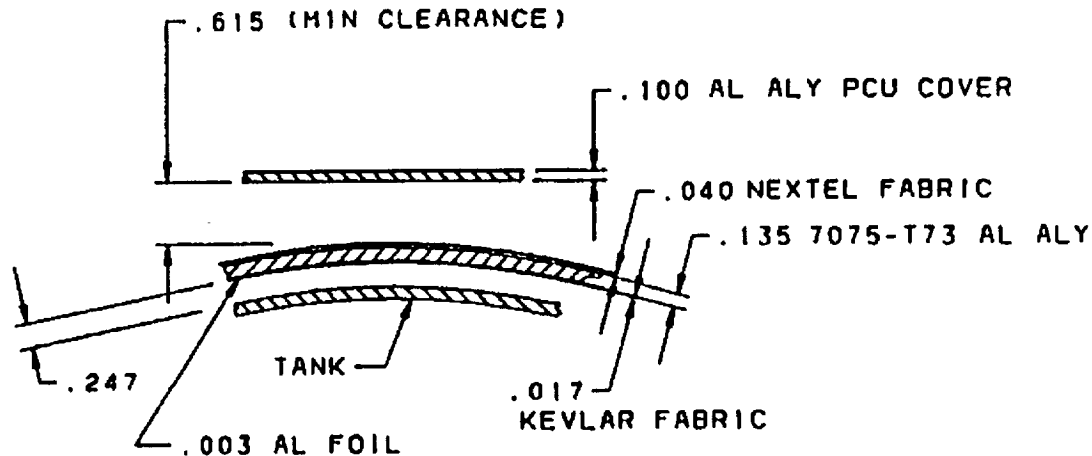
Figure 37. PCU MMOD design[44].

The ACCESS Accommodation Study Team recommends adopting the PCU tank system for the TRD instrument's use. The rationale is simply that the Boeing-Rocketdyne PCU tank system design has already gone through an ISS flight qualification procedure (Figure 36) to protect the high-pressure Xe tank on ISS, with a PCU-shielding probability-of-no-penetration (PNP) of 0.9988 over 10 years (exceeding the ISS safety requirement of PNP = 0.9955 over 10 years). Also, crew training for topping off or refilling the gas supply is essentially the same as for the ISS electrical power system. That results in another cost benefit.

Utilization of the PCU tank system for ACCESS constitutes a re-flight of the Rocketdyne unit and therefore considerably simplifies the safety review process (Table 19 below). Re-flight hardware usually begins at Phase III.

With respect to costs for the PCU system, these are virtually off-the-shelf. The following estimates in Table 19 have been arrived at[48]. The Xe gas costs are appreciable, for the flow tests, purity tests, acceptance tests, and qualification tests.

Table 19. Rocketdyne PCU Tank Costs

• *PCU tank system (3 flight boxes)*	*$120K*
• *PCU tank system (3 prototype boxes for tests)*	*$90K*
• *Xe refills (per fill-up $40+K)*	
• *Xe refills, total*	*$500K*
• *Total*	*$710K*

Robotic interfaces

The robotic interfaces with the ISS are functional and consist of hardware. These are described in NSTS-21000-IDD-ISS, Sections 13 and 14. Currently, the ISS only has one type of hardware grapple fixture, called the power and data grapple fixture. The requirements for this system are not fully defined. They will eventually be specified in SSP 57003. More details on this system are listed in the Carrier Issues section of this report and in Appendix H.

Safety

Station-wide safety is the subject and responsibility of NASA's safety review process. All payloads such as ACCESS that will be integrated into the Space Shuttle at Kennedy Space Center (KSC) for flight to the ISS must meet the flight and ground safety requirements of the following documents (Appendix D):

Flight Safety: NSTS 1700.7B; NSTS 1700.7B, ISS Addendum; and NSTS/ISS 18798B
Ground Safety: KHB 1700.7B
Flight and Ground Safety: NSTS/ISS 13830C

The flight and ground safety processes for payloads are specified in NSTS/ISS 13830C. The primary safety task is the preparation of payload safety data packages which contain descriptive information, identified hazard reports, and supporting data. These data packages are submitted to the NASA Flight and Ground Payload Safety Panels for review and approval at phased meetings. The maximum number of meetings that could be held is four for flight safety (Phase 0, I, II, and III) and four for ground safety (Phase 0, I, II, and III). These are not to be confused with procurement phases (Note 1). The phases are defined in 13830C, Section 6 and 7. The timing of the safety reviews is shown in Table 20.

Table 20. Timing of Payload Safety Reviews

- *Phase 0*   *Conceptual design established*

- *Phase I*   *Preliminary design established (preliminary design review level)*

- *Phase II*   *Final design established (critical design review level)*

- *Phase III* *Most of the testing, analyses, inspections, etc. completed; must be completed 30 days prior to start of payload activities at the launch site (usually assumed as delivery at launch site).*

The actual number of safety reviews depends upon the ACCESS payload complexity, technical maturity, hazard potential, and whether it is a re-flight. The latter (re-flights such as the PCU box in Appendix I) can begin at Phase III.

The safety review process includes hazardous payload commands which must be identified and annotated at the Phase I safety review and incorporated into the Payload Command and Data Integration Data File (SSP 52000-A04) and the Payload Data Library.

Testing and verification requirements are also specified in NSTS/ISS 13830C. The type and depth of verification is dependent upon the phase of the safety package and its review. Examples of some of the verifications are as follows:

- structural verification plan
- structural analyses and tests
- fracture control plan and report
- material assessments and tests for toxicity
- flammability and stress corrosion
- fault tolerance analyses and tests for electrical and mechanical systems

- battery tests and analyses
- EMI tests and analyses
- sharp edge inspections
- grounding and bonding tests
- sealed container and pressure vessel analyses and tests
- laser or ionizing radiation assessments and tests

The key to a successful payload safety program is prompt and complete submittal of information to the Payload Safety Panels via the safety data packages. Examples of the review process are as follows. Selection of Aluminum 7075-T7351 for the primary payload structural support material, chosen from accepted mature standards for spaceflight, would contribute to a successful safety review. The choice of a robust composite material for carrying primary structural loads that is not in the handbook for spaceflight standards could lead to numerous delays. As secondary structural load paths, composites may be satisfactory, however. "Failure" in the safety review process means the item is not approved for the next level of review for lack of spaceflight readiness. The consequence can be a major impact upon payload program schedules and costs.

Costly redesign and recertification work can be avoided by early identification of potential hazards and spaceflight readiness, as well as early approval of hazard controls and verification methods by the Payload Safety Panels. The NASA-JSC Mission Management Office (MMO) support concept is recognized for its ability to assist payload customers with all aspects of the flight and ground safety process.

Integration, verification, and test (IV&T)

Under the JSC templates for STS and ISS payload IV&T, the science instrument and the accommodation payload support structure (APLSS) finally come together at KSC. Figure 38 describes this IV&T process. That complete support structure consists of the ECS (or USS) in Figures 13-21 fully integrated with the ancillary avionics (power, data, and communications) in Figures 26-27.

The APLSS is actually an accommodation interface device or a payload interface device, which provides and maintains all of the accommodations for the payload science customer. This final integration begins at KSC, continues into the Shuttle payload bay, and is the resource for interfacing with the PAS and UMA (Figure 12) while on the ISS.

KSC operations

The flowchart in Figure 38 gives the overall flow of events for launch site operations. Mission management (defined below) will coordinate, plan, and see that all of these events are carried out. Most of the operations involve coordination between the experiment developers and the launch site operations personnel. The launch site operations personnel include safety, reliability, quality, operations per se, management, etc. The steps that are shown in the figure are meant to indicate a general process flow for the payload as it progresses through the launch site operations and emerges in the Shuttle payload bay. Additional steps may be necessary, and KSC operations and ground safety personnel must document and review specific procedures and operational details at that time.
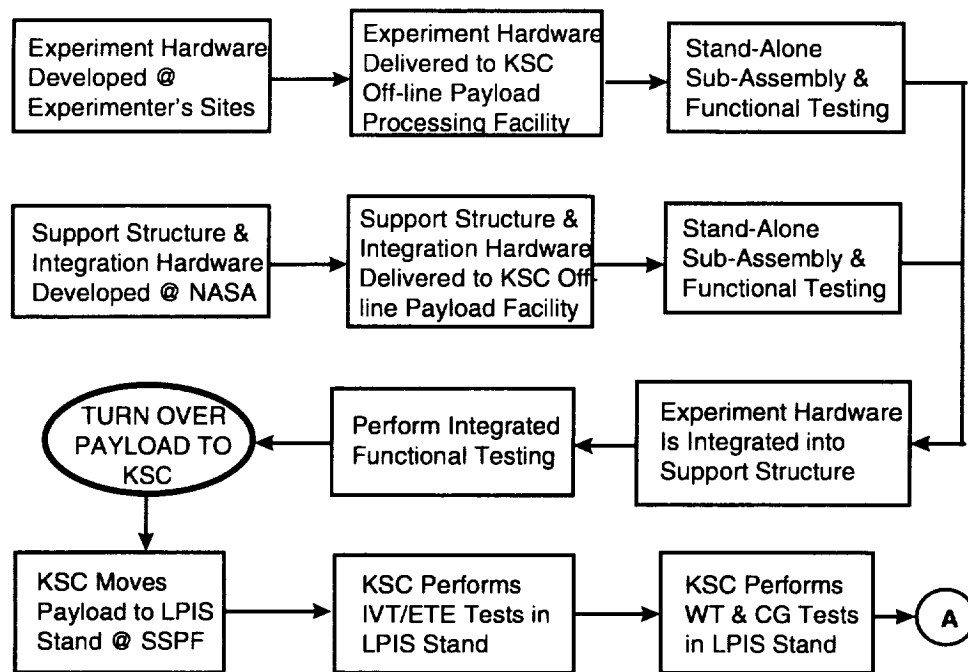
Figure 38a. Conceptual launch site operations flow chart for an ISS science payload (modeled from the actual STS-91 mission for the AMS Orbiter).
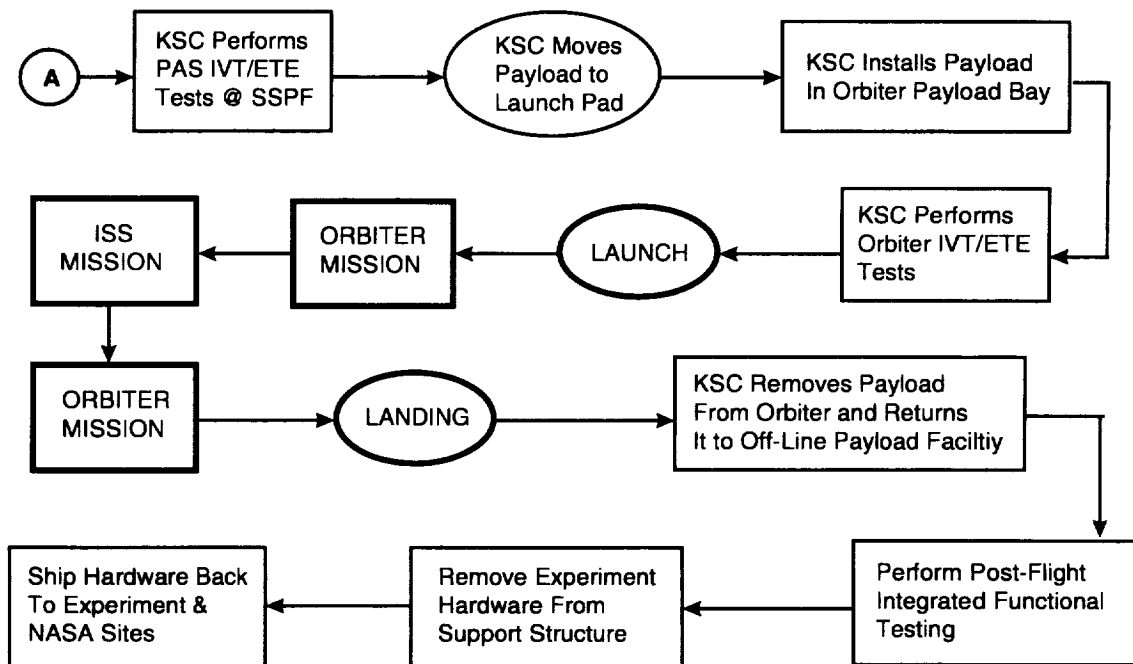
Figure 38b. Conceptual launch site operations flow chart for an ISS science payload (continued).

Mission management coordinates KSC operations and payload processing requirements through a series of Ground Operations Working Group (GOWG) meetings at KSC. These GOWG meetings are conducted throughout the payload development process. Payload processing and verification requirements are documented in the Payload Launch Site Support Plan and the Operations and Maintenance Requirements and Specifications Document.

Additional details of KSC operations are illustrated in the DC&I master schedule and KSC schedule under "ACCESS Conceptual Accommodation Schedule" given below.

ACCESS operations

A post-launch functional test of ACCESS prior to unberthing from the Shuttle payload bay may be performed. Following deployment at the PAS, one-orbit payload operations would proceed.

The initial phase of ACCESS operations involves experiment activation, commissioning, and preliminary checkout. This period will last probably 15 to 30 days, during which time the entire instrument is calibrated by adjusting thresholds and other operational instrument parameters. It probably will involve various forms of self-test. Interfaces between the three detectors (CM or ZIM, TRD, and CAL) will be verified as well.

ACCESS will then enter routine operations, requiring minimal monitoring and relatively small daily uplink capacity. What is important will be the downlink of the experiment data. ACCESS has a relatively low data rate and will perform little onboard processing. Delivery of the downlinked data (Figure 39 below) to an ACCESS operations and data distribution center will be necessary for detailed evaluation of the cosmic-ray experiment. This center will also perform operations and contingency planning in coordination with the ISS operations (ops) team and ISS schedules or time-lines. There also will be known periods of reduced science data recovery and ISS communication outage.

Full-scale ACCESS operations will then be carried out. Aside from monitoring cosmic-ray events and general housekeeping plus commands, an example of ops would be the proximity operations during Shuttle rendezvous and docking when the ISS solar arrays are feathered and ACCESS would be placed in a keep-alive mode. Another example would be the topping off or resupply of the TRD PCU tank system gas.

Failure modes are conditions that arise during mission operations when a spacecraft component breaks or malfunctions. The failure could be within the payload, or within the space or ground segment of the ISS. In either case, they can compromise the science objectives of the ACCESS experiment. Failure modes and effects analyses (FMEAs) need to be conducted to anticipate these and preclude as many as possible through a fail-operational design strategy. However, FMEAs were not a part of the ACCESS Accommodation Study and must be taken up in a subsequent phase of the program.

Science data interface

The end-to-end ISS payload data flow is illustrated in Figure 39 (MSFC-SPEC-2123B). This figure shows the functional ground and space segment architecture for ISS payload science data, involving the White Sands Complex (WSC), JSC's Space Station Control Center, GSFC, and the Marshall Space Flight Center (MSFC).

61

ISS ground segment

MSFC is responsible for the ISS ground segment payload data processing and distribution. This includes definition, design, development, and operations. To fulfill their responsibility, MSFC is developing the payload data services system (PDSS) shown in Figure 39. The PDSS is to be installed in the MSFC Huntsville Operations Support Center (HOSC) to support on-orbit ISS payload operations.
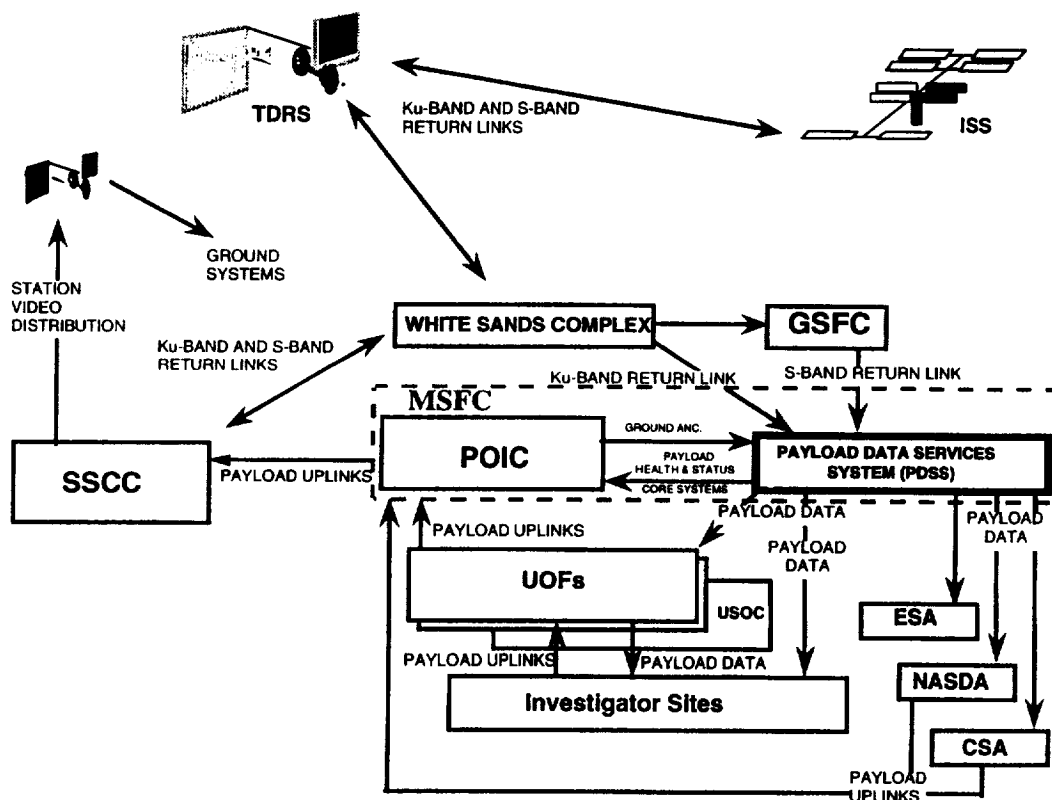
Figure 39. End-to-end ISS payload data flow.

The PDSS in Marshall's HOSC will receive, process, store, and distribute ISS Ku-band data to the user community. This includes a number of the sites and facilities shown in Figure 39, and in particular the science investigator sites for ACCESS. The PDSS will interface with the Payload Operations Integration Center (POIC) to handle, store, and distribute to the ACCESS user community ground ancillary data, payload health and status data, and ISS core systems data. In addition, the PDSS will process, store, and distribute the ISS COR data for the payload user community as part of the Ku-band downlink. Core systems data will be contained in the S-band stream while payload science data will be in the high rate Ku-band stream.

Onboard architecture (space segment)

The baseline ISS onboard payload architecture is depicted in Figure 40, which is similar to Figure 28 but focuses upon ISS module geometry. It consists of a central backbone payload

network comprised of payload command/control, high-rate data, and medium-rate data with mutiple ISPR-to-ISPR (international standard payload rack) communications media as shown. This was discussed earlier. Devices attached to these media are indicated, with acronyms defined in Appendix J.
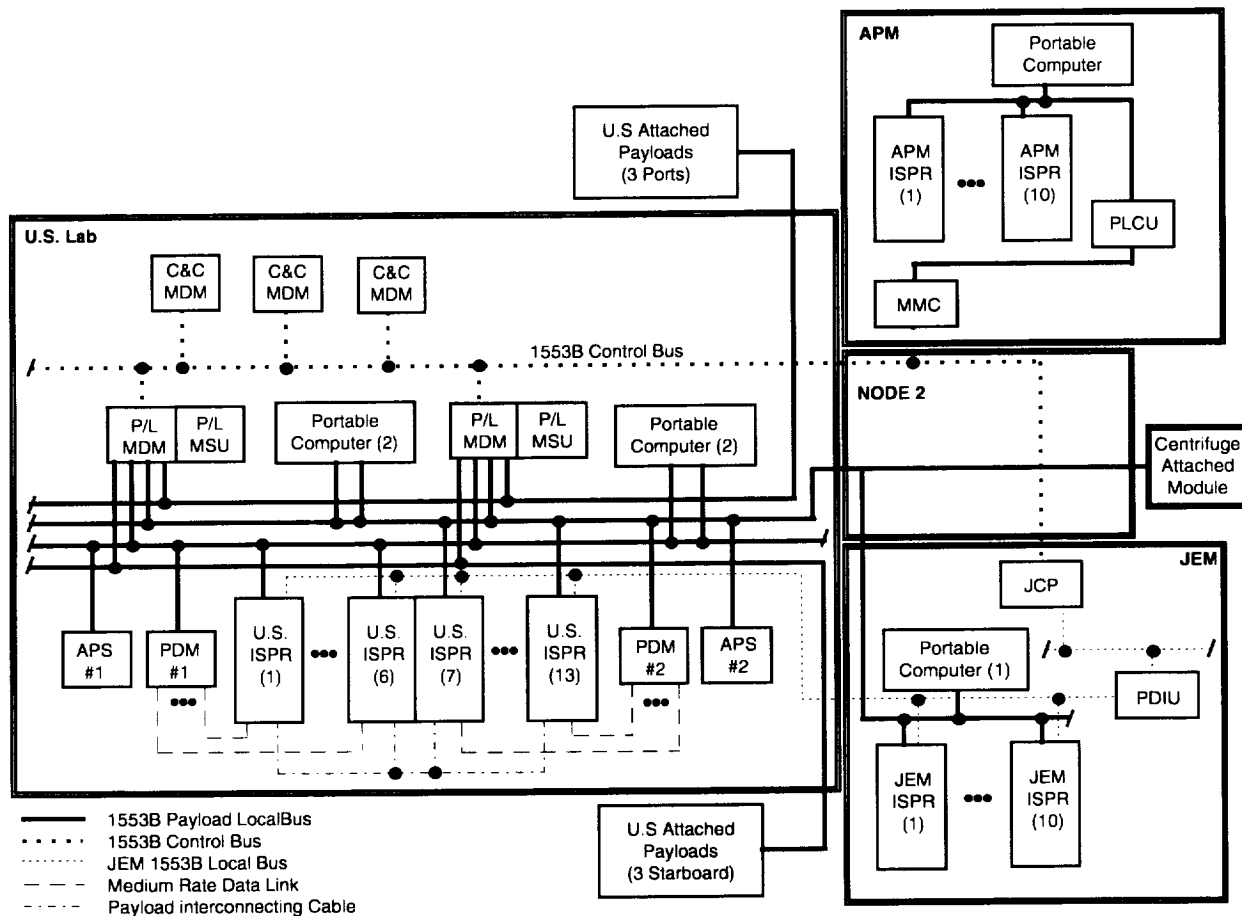
Figure 40. ISS onboard payload architecture.

Functional command flow

The C&C MDM provides the top-level control functions for the ISS. The Payload MDMs provide the primary interface with the system C&C MDMs for resource allocation and reception of ground-based commands and data for payloads such as ACCESS attached to its 1553B local buses. Payload MDM commanding, then, can be visualized as a four-step process in Figure 41 based upon the architecture in Figure 40. A command packet originates from the ground (WSC) or the crew PCS. Otherwise, it is a time-lined one. It then is routed to the appropriate Payload MDM, which directs it to the target payload on its local ISPR bus. For ACCESS, the packet would arrive on one of the three starboard ports shown in Figure 40.

The basic ISS command processing overview is summarized in Figure 42.
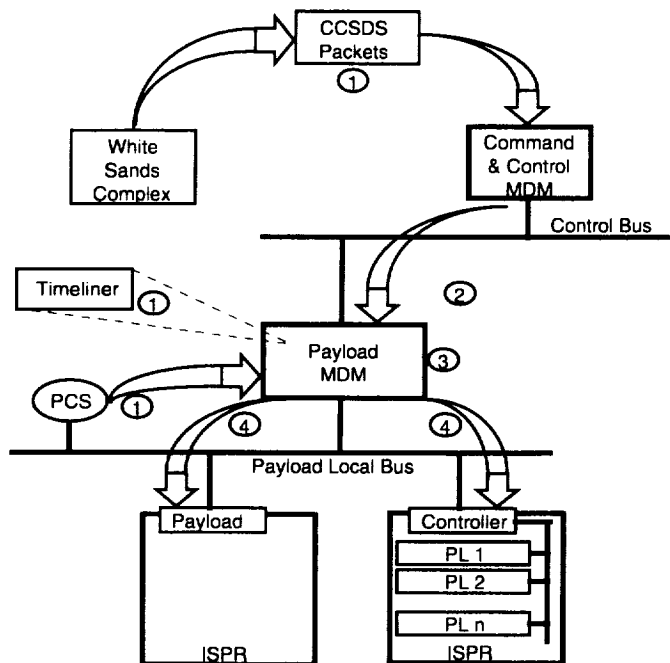
Figure 41. Payload MDM functional data flow.
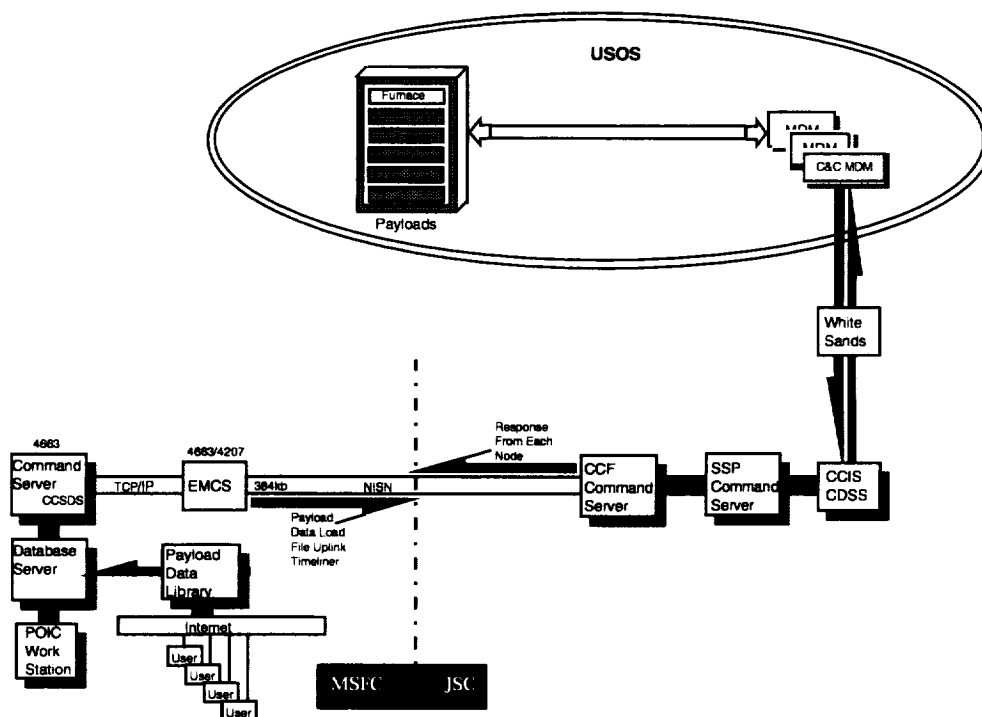
Figure 42. Functional ISS command flow.

NASA Mission Management Office

Summary

In order to maximize the potential for successful and timely deployment of the ACCESS payload on the ISS, the Accommodation Study Team recommends that the same single-interface managerial structure used effectively in the AMS program should be utilized for management of the analytical, physical, and operational interfaces required for ACCESS. Thus, it recommends that a NASA MMO, or its functional equivalent, be established for the ACCESS program and serve as interface or liaison to the Shuttle and ISS Program Offices. This would include overall mission integration for the ACCESS Program Office and ACCESS payload community. The MMO could be established at any NASA center, although it is presently at JSC. As a concept, JSC experience with STS and ISS payloads has shown that the MMO strategy is the most cost-effective approach for mission integration and accommodation.

Mission management functional tasks are given in Table 21.

Table 21. Mission Management Functional Tasks

- *Management interface to Shuttle and ISS programs*

- *Payload consultation for ACCESS payload community*

- *Payload safety representative to flight and ground safety panels*

- *Negotiation of payload integration requirements*

- *Payload physical integration management and mechanical interface development*

- *Payload training coordination*

- *Payload flight operation and mission support coordination*

- *Postflight support*

The Mission Manager provides the planning for the overall integration of the payload into the Space Shuttle and the ISS. This involves negotiating and documenting all payload interfaces with the Space Shuttle and ISS Program Offices. Typical interfaces include structural (or mechanical) design, thermal design, electrical power, command and data, and robotic and crew interfaces. Since the JSC MMO will have completed all these tasks for AMS as the first ISS attached payload, this valuable experience should lead to significant savings in time and cost to NASA and the ACCESS program.

The Mission Manager negotiates payload compliance with respect to Shuttle and ISS requirements. This effort involves in-depth knowledge of the applicable program requirements and their current interpretations to negotiate payload compliance successfully. ACCESS compliance with these requirements will be tracked in the Certification of Flight Readiness process, the flight and ground safety process, and the program-specific ICD waiver process. The Mission Manager provides the coordination between the ACCESS science instrument developers and the Shuttle and ISS Programs to complete this effort.

The Mission Manager provides assistance and advice to the ACCESS payload community related to payload mission success. This is based upon previous payload experience and interaction with Shuttle and ISS Program personnel. Included in the mission success task is the verification of payload compatibility with all Shuttle and ISS environmental conditions and requirements, including thermal, EMI, power quality, radiation, and orbital debris.

Management interface

The Mission Manager serves as a single-point-of-contact representing the ACCESS payload to the Shuttle and ISS Programs, and to the various support organizations involved in the integration, certification, testing, safety and operations of the payload. This effort involves representing the payload organization at various Shuttle and ISS Program meetings and interfacing with various program and support personnel to define, document, negotiate, and implement all payload requirements from the Shuttle or ISS Programs. The Mission Manager also assists the ACCESS payload community in understanding the capabilities and limitations of the Shuttle and ISS accommodations. The Mission Manager works with the Shuttle and ISS Programs to develop a program schedule of milestones and deliverables. The Mission Manager is responsible for providing guidance to the ACCESS payload community in meeting the required milestones and deliverables per the agreed-to program schedule and for providing status of progress as needed.

Payload consultation

The Mission Manager provides early design and operations consultation and guidance to the ACCESS payload community to ensure compatibility between the payload design and operations and the capabilities and requirements of the Shuttle and the ISS. This is necessary to eliminate or minimize the potential for physical, functional, or safety incompatibilities between the payload and the Shuttle or the ISS. This function involves providing detailed engineering design, testing, modeling, or analysis to assist the payload in verifying compatibility. The Mission Manager also assists the ACCESS community in configuring and packaging the payload into a cargo element capable of being analytically, physically, and operationally integrated into the Shuttle and ISS systems.

Payload safety

The Mission Manager negotiates payload compliance with flight and ground safety requirements. This effort begins early in the payload design process to incorporate all applicable safety requirements before the design is complete to ensure significant redesign effort and cost are not incurred. The MMO provides guidance to the ACCESS project to identify, and eliminate or control hazards or potential hazards associated with the ACCESS payload. The MMO assumes the lead role in developing all applicable flight and ground safety compliance documentation. It would be the payload representative to the Shuttle, ISS, and KSC Safety Review Panels.

Payload integration requirements development

The Mission Manager provides guidance to the payload developers in the development, documentation, and negotiation of payload requirements to be levied by the Shuttle and ISS Programs. This process involves meetings, telecons, and correspondence with Shuttle and ISS Program personnel and associated technical experts. During this process, the Mission Manager would act as the ACCESS payload representative to ensure that all payload requirements are met.

Payload physical integration

The Mission Manager oversees the physical integration of the ACCESS payload and all mission-particular integration and interface equipment into the Space Shuttle and onto the ISS. The Mission Manager would not perform the function of experiment integrator. Rather, the experiment integrator would be responsible to the ACCESS Program Office for the integration of the various subassemblies of ACCESS into an integrated payload. The integrated payload would include the CM, the TRD, the calorimeter, and the power, data thermal control, and gas resupply systems required for supporting the three main components. The MMO would be involved in designing, building, testing, and certifying unique flight hardware and GSE or GHE required to integrate the payload into the Space Shuttle and the ISS. This hardware includes payload thermal protection and control systems, the ECS, and power, command and data interfaces between the ACCESS payload and the Space Shuttle or the ISS.

The Mission Manager serves as the payload interface to KSC personnel for all launch site support and operations. This function would involve coordinating the definition, documentation, and implementation of all payload launch site testing, integration, and launch operations. This effort would be completed through standard payload integration plan (PIP), PIP Annex, PIA, and PIA Annex documentation and through various GOWG meetings, as payload launch site requirements and operations are developed.

Payload training coordination

The Mission Manager is responsible for training the astronaut crew and ground support personnel on the ACCESS payload. A training plan will be developed and implemented. ACCESS ground support personnel and the NASA flight crew will be trained on the real-time operation of the payload via simulations, both joint integrated simulations with the entire flight control team and internal stand-alone ACCESS simulations.

Payload flight operations and mission support

The Mission Manager assists the ACCESS payload community in the development, documentation, and verification of all payload nominal, contingency, and in-flight-maintenance procedures. The procedures are documented in the Shuttle and ISS Flight Data Files for use by the Shuttle and ISS flight crews. The responsible astronauts would exercise these procedures in crew training sessions and joint integrated simulations (JISs). The Mission Manager would coordinate and support all crew training sessions and applicable JISs.

The Mission Manager also assists the ACCESS payload community in the setup of the ACCESS Payload Operations Control Center (POCC) to support real-time operations. The

Mission Manager would work with the ACCESS payload community and the NASA program offices to arrange provision of required Shuttle and ISS data to the ACCESS POCC. The Mission Manager in the JSC Mission Control Center (MCC) would provide real-time mission support of the ACCESS delivery flight to the ISS through deployment, installation, checkout, and operation verification. The Mission Manager could also provide real-time support for the ISS on-orbit operations for ACCESS as required. Support for the ACCESS de-integration operations from the ISS and the return flight on the Shuttle would also be provided in the JSC MCC.

Payload postflight support

The Mission Manager provides postflight analysis and de-integration support for the ACCESS payload. This support includes KSC operations support for postflight de-integration of the ACCESS payload and interface hardware from the Shuttle and de-integration of and data retrieval from the payload. The Mission Manager also assists the payload developers in shipping payload hardware and support equipment from KSC to the payload developers' home institutional facilities.

ACCESS accommodation schedule template

The attached ACCESS program schedule template that follows is a preliminary draft of a top-level or major milestone schedule for the DC&I of the ACCESS payload. This schedule assumes that the ACCESS payload experiment integrator has already essentially completed the integration of the three major components (Appendix B) into a complete single payload, including data and power interfaces between components. At that point the MMO support would design the interfaces and integration hardware required to mate the payload with the Space Shuttle and the ISS. (See Integration, Verification, and Test, Figure 38.) This schedule assumes a Shuttle launch to the ISS in late 2006. The MMO would require a 36-month schedule to complete all of the DC&I activities associated with the ACCESS payload. The MMO can prepare a detailed schedule of all activities as the project progresses and the program requirements are better defined (Implementation Phase, DDT&E). Additional schedules will be required to address specifics of KSC preflight ground operations, real-time mission support, the Shuttle retrieval flight, and KSC post-landing operations.

ACCESS Conceptual Accommodation Schedule

Overview

JSC's successful flight from launch through landing of the AMS precursor mission (STS-91) in June 1998 will provide the schedule templates for the ACCESS Accommodation Study baseline. The assumption is that this process will be repeated for the ACCESS payload. These templates are actuals, describing in detail the specific process involved in the JSC DC&I of the recent AMS payload targeted as the first major ISS science payload following Assembly Complete.

For the purposes of the ACCESS Accommodation Study, an October 1, 2006, launch is baselined. This date derives from the original AMS schedule for a three-year stay at Site S3 UI, with a one-year extension in view of discussions that the AMS might remain longer for additional data collection. The templates are generic and can be readily shifted. For example, this could be an October 1, 2005, ACCESS launch date if AMS is retrieved in three years as originally planned. Another example could be a shift of the entire ISS schedule, or an ACCESS launch prior to AMS retrieval.

The schedule templates fall into three categories. They follow on the next 12 pages.

36-month schedule

Under a baseline assumption that the science instrument has been defined[8] and can keep pace with JSC DC&I master schedules, ACCESS can be launched in 36 months. Save for the science instrument costs being defined under the instrument study[8], this can be accomplished at the cost given in the "Estimated Costs" section, which follows in this report.

The four-page 36-month DC&I template which follows consists of a work breakdown structure (WBS) containing 42 elements. They range from design and safety reviews (WBS 1-8) to mission integration plan (WBS 9-11, 15-17), and ICD (WBS 12-14) definition along with program reviews (WBS 18). These are followed by the structural test article (WBS 19, 28-29), the payload support carrier and interface avionics design, fabrication, and test (WBS 20-22, 25-27, 30-31), delivery (WBS 32), and reporting (WBS 33). Then there are simulations (WBS 34-35), thermal blanket design (WBS 36), KSC testing and launch installation (WBS 37-40), interface verification test (IVT, WBS 41), and launch (WBS 42). Subsequent to launch is the single-page Mission Support Master Schedule.

60-month schedule

For reference, a 60-month template (L-59) appears in the AMS schedule below.

ACCESS PAYLOAD STUDY
Design, Certification, & Integration Master Schedule

CALENDAR YEAR

WB	Milestones	Q4	2004 Q1	Q2	Q3	Q4	2005 Q1	Q2	Q3	Q4	2006 Q1	Q2	Q3	Q4
1	Preliminary Design Review	◇												
2	Critical Design Review						◇							
3	Flight Safety Review at JSC Phase 0/I	◇												
4	Ground Safety Review & GOWG at KSC Phase 0/I		◇											
5	Flight Safety Review at JSC Phase II						◇							
6	Ground Safety Review & GOWG at KSC Phase II							◇						
7	Flight Safety Review at JSC Phase III										◇			
8	Ground Safety Review & GOWG at KSC Phase III											◇		
9	MIP Inputs					◇								
10	MIP Updates							◇						
11	MIP B/L								◇					
12	ICD Inputs						◇							
13	ICD Updates							◇						
14	ICD B/L								◇					

ACCESS PAYLOAD STUDY
Design, Certification, & Integration Master Schedule

CALENDAR YEAR

WBS		Q4	2004 Q1	Q2	Q3	Q4	2005 Q1	Q2	Q3	Q4	2006 Q1	Q2	Q3	Q4
15	Milestones													
15	MIP Annexes Inputs													
16	MIP Annexes Updates													
17	MIP Annexes B/L													
18	Program Reviews													
18.1	FDRD													
18.2	CIR													
18.3	FPSR													
18.4	Flight Operations Review													
18.5	Flight Readiness Review													
19	ACCESS STA: Fabrication, Assembly, Structural Certification Testing													
20	Design/Analyze Carrier Flight Hardware													
21	Design, Breadboard, & Test Prototype ISS Interface Avionics													
22	Lab Development at NASA for Carrier and Avionics Buildup													
23	Design GHE Hardware													

ACCESS PAYLOAD STUDY
Design, Certification, & Integration Master Schedule

CALENDAR YEAR

WB	Milestones	2004				2005				2006			
		Q4	Q1	Q2	Q3	Q4	Q1	Q2	Q3	Q4	Q1	Q2	Q3	Q4
24	Fabricate & Assemble GHE Hardware												
25	Fabricate, Component Test, and Assemble Carrier Flight Hardware												
26	Procure Parts, Fabricate, Assemble, & Test Qual/Fit & Flight ISS Interface Avionics												
27	Design and Fabricate Carrier Assembly Fixture												
28	Modal Test on the Carrier in the Test Stand with STA at JSC												
29	Static Test on the Carrier in the Test Stand with STA at JSC												
30	Structural Math Model Correlation & Verification Loads Analysis (VLA)												
31	Carrier and ISS Interface Avionics Processing at JSC prior to delivery to KSC												
32	Flight & FSE Hardware & Software Delivery to ACCESS POCC												
33	Submit Integration Reports: Stress Analysis, Thermal, and EMI												
34	STS-00 Joint Integrated Simulations (JIS)												
35	Design and Fabricate ACCESS WETF Mockup												
36	Design and Fabricate ACCESS Mockup for Thermal Blanket Design												
37	ACCESS Flight Experiment Shipped to KSC & Perform Off-line Functional Tests												

ACCESS PAYLOAD STUDY
Design, Certification, & Integration Master Schedule

CALENDAR YEAR

WB	Milestones	Q4	2004 Q1	Q2	Q3	Q4	2005 Q1	Q2	Q3	Q4	2006 Q1	Q2	Q3	Q4
38	Install ACCESS Flight Experiment on Carrier											▫		
39	ACCESS Payload Functional Tests & Final Preparations											▫		
40	ACCESS IVT, ETE, & Weight & CG Test at CITE												▫	
41	ACCESS Installation, IVT, & ETE at Launch Pad												▫	
42	STS-00 Launch Shuttle/ISS Mission-00													◇

ACCESS PAYLOAD STUDY
Mission Support Master Schedule

ID	Milestones	2006			2007				2008				2009				2010				Calendar Year
		Qtr 3	Qtr 4	Qtr 1	Qtr 2	Qtr 3	Qtr 4	Qtr 1	Qtr 2	Qtr 3	Qtr 4	Qtr 1	Qtr 2	Qtr 3	Qtr 4	Qtr 1	Qtr 2	Qtr 3	Qtr 4	Qtr 1	
1	STS-00 Launch Day Shuttle/ISS Mission-00	◇																			
2	STS-00 Shuttle Mission Support	□																			
3	ISS Mission Support																				
4	Shuttle Retrieval Flight STS-00																◇				
5	KSC Post Landing Operation																	□			

Task ▬▬▬ Milestone ◆ Rolled Up Task ▬▬ Rolled Up Progress ▬▬

Progress ▬▬▬ Summary ◤▬▬◢ Rolled Up Milestone ◇

Project:
Date: 1/8/99

Page 1

AMS templates

The AMS templates fall into two categories, providing explicit details:

- The DC&I master schedule (STS-91 through ISS launch) is first, comprising the first three subsequent pages.

- The KSC schedule follows, representing the "off-line" and "on-line" integration there. These comprise the second set of subsequent, three-page totals. "Off-line" (see Appendix I) means the payload has been delivered to KSC but has not yet been turned over to NASA. "On-line" means the payload is at KSC and has been turned over to NASA.

DC&I master schedule

The three-page DC&I master schedule template reflects the actual end-to-end JSC turnkey process involved in the design and integration of a certified payload. The example shown was the AMS illustrated in Figure 13. This STS-91 launch, originally set for May 29, 1998, actually occurred on June 2, 1998, aboard Shuttle Orbiter "Discovery" (OV-103) following a brief KSC delay unrelated to the payload. As one can see, the template is less than 36 months (L-34).

The schedule illustrates how the science instrument and the accommodation support structure each emerge, and then converge upon KSC for final integration as a consolidated payload at the launch site. Final integration occurs along the conceptual lines of Figure 38.

The KSC schedule for off-line and on-line activities shown at the bottom of the master schedule is defined further in the KSC schedule.

Off-line KSC schedule

The off-line KSC schedule consists of a Schedule A and a Schedule B. Schedule A covers the period from science instrument delivery to turnover to JSC at KSC. Schedule B covers the subsequent period through turnover of the science instrument and the accommodation support structure to KSC at the Multi-Payload Processing Facility (MPPF). At the completion of the off-line KSC schedule, an integrated ACCESS payload exists.

On-line KSC schedule

The on-line KSC schedule carries the newly integrated ACCESS payload from completion of off-line processing to the launch pad. This is followed by installation at the launch pad, followed by Shuttle Orbiter IVT and end-to-end testing on the launch pad. At this point, the ACCESS payload is ready for launch.

ALPHA MAGNETIC SPECTROMETER (AMS) PAYLOAD ON STS-91 (S/MM-09)
DESIGN, CERTIFICATION, & INTEGRATION MASTER SCHEDULE
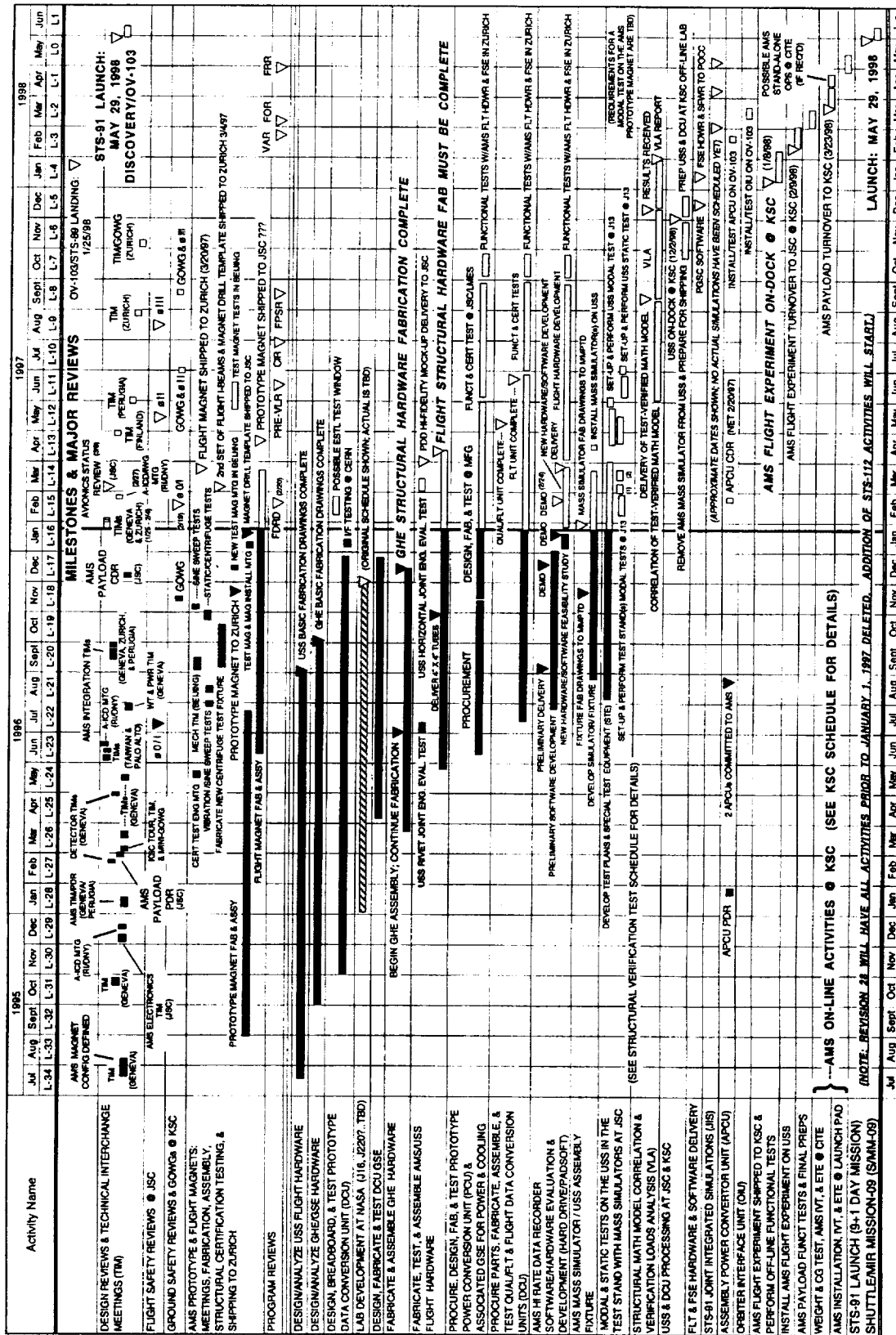
(BASED ON DECEMBER 19, 1996 FAWG)

(FLIGHT TO ISS ON ISS-19-UF-4/STS-112 IS SCHEDULED ON JANUARY 18, 2001)

76

ALPHA MAGNETIC SPECTROMETER (AMS) PAYLOAD ON STS-91 (S/MM-09) & STS-121 (ISS-21/UF-4)
DESIGN, CERTIFICATION, & INTEGRATION MASTER SCHEDULE

ALPHA MAGNETIC SPECTROMETER (AMS) PAYLOAD ON STS-91 (S/MM-09) & STS-121 (ISS-21/UF-4)

DESIGN, CERTIFICATION, & INTEGRATION MASTER SCHEDULE

(BASED ON JAN 15, 1998 FAWG, STS-91 KSC MASTER
MILESTONE SCHED DATED JAN 6, 1998, & STS-91
MANAGEMENT INTEGRATED SCHEDULE DATED JAN 5, 1998)

(NOTE: PREVIOUS REVISIONS COVER ALL
ACTIVITIES FROM JULY, 1995 THRU JAN, 1997,
AND JAN THRU AUG, 1997.)
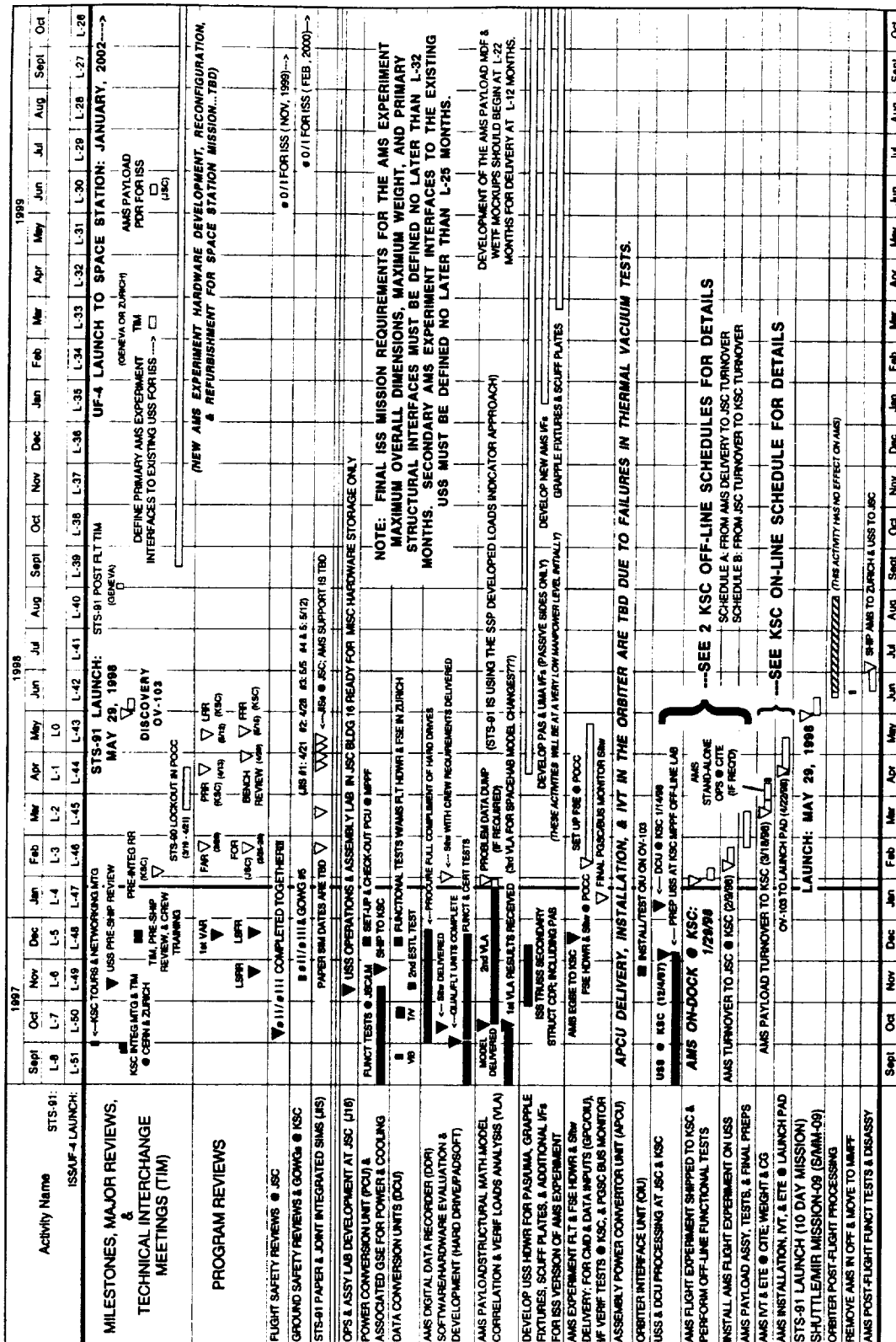
ALPHA MAGNETIC SPECTROMETER (AMS) PAYLOAD ON STS-91 (S/MM-09)   LAUNCH: 5/29/98

OFF-LINE INTEGRATION SCHEDULE A AT KSC: FROM AMS DELIVERY ON JAN 29 TO JSC TURNOVER

Chart date columns (Mondays):

Dec '97					Jan '98				Feb '98	
1	8	15	22	29	5	12	19	26	2	9
L-25	L-24	L-23	L-22	L-21	L-20	L-19	L-18	L-17	L-16	L-15

Activities and Procedures responsibility:

#	Activity Name	AMS	NASA MMO
1	SHIP, RECEIVE, & INSPECT USS HDWR @ MPPF; SET UP LAB		X
2	USS & GHE INITIAL PREPARATIONS		X
3	PERFORM SHARP-EDGE INSPECTION ON INTEG GHE & GSE		X
4	REMOVE USS LOWER DIAGONAL STRUTS & I-BEAMS		X
5	PCU SET-UP AND CHECK-OUT		X
	CHRISTMAS, NEW YEARS & VARIOUS HOLIDAYS	X	
6	RECEIVE & INSPECT AMS EGSE HDWR @ MPPF; SET UP LAB	X	
7	INSTALL SCAFFOLDING NEXT TO & OVER USS & GHE		X/KSC
8	DCU POST-SHIP FUNC TESTS & INSTALLATION ON USS		X
9	REPLACE FASTENERS ON USS & SAFETY WIRE		X
10	AMS EXPERIMENT @ KSC; MOVE FROM SLF TO MPPF	X	X
11	RECEIVE, UNPACK, & INSPECT HARDWARE; SET UP LAB	X	
12	AMS GSE SHARP EDGE INSPECTION		X
13	REMOVE AMS EXP FROM SHIPPING CRATE & SET ON FLOOR		X*
14	REMOVE AMS MAIN EXP FROM SHIPPING CENTERBODY		X*
15	SWAP BUSHINGS & INSTALL EXP STANDS (GUIDES)		X
16	KSC MEASURES FRINGE MAGNETIC FIELD		KSC
17	MOUNT & CONNECT MCCs ON I-BEAMS & PSBs ON LEGS	X	X*
18	REMOVE ATC & CARRIER FROM CRATES & SET UP ON FLOOR	X	X*
19	PLACE MAIN AMS EXPERIMENT OVER ATC	X	X*
20	CONNECT ATC CABLES TO MAIN AMS EXP	X	
21	CONNECT EGSE & PREP FOR POST-SHIP FUNCT TESTS	X	
22	PERFORM "MINI" POST-SHIP FUNC TESTS ON AMS EXP	X	
23	CLEAN USS FLIGHT HARDWARE TO GC LEVEL		X
24	REMOVE +Z & -Z LEPS FROM CRATES	X	X*
25	INSTALL HTC-83 ON -Z LEPS, BRKTS ON + & -Z LEPS (TEMP)	X	
26	PERFORM WEIGHT & CG ON -Z LEPS & +Z LEPS		X
27	ARRANGE & PAINT INSIDE OF +/- ZLEPS TO REDUCE DEBRIS	X	X*
28	INSTALL -Z LEPS IN LOWER CENTERBODY (PARTIAL)		X*
29	INSTALL ATC MOUNTING RAILS ON USS & NEXT TO GHE		X*
30	DISCONNECT CABLES, PREPARE AMS FOR TURNOVER		X
31	CLEAN AMS FLIGHT HARDWARE TO GC LEVEL	X	
32	AMS EXPERIMENT TURNOVER TO JSC @ KSC		X*

Chart annotations:

- USS, GHE, & GSE ON DOCK @ KSC: 12/4/97
- PCU CK-OUT
- (PCU ON DOCK @ KSC: 11/28/98)
- AMS GSE ON DOCK @ KSC: 12/15/97
- DCU ON DOCK @ KSC: 1/14/98
- AMS @ KSC SLF: JANUARY 29, 1998 @ 5 PM --->
- ALL THE AMS EXPERIMENT HARDWARE SHIPPING, TRANSFER, UNPACKING, AND SETUP ACTIVITIES AT THE MPPF WERE COMPLETED 1.4 DAYS AHEAD OF SCHEDULE. THIS ALLOWED THE AMS EXPERIMENT TO BE POWERED UP EARLY.
- (-Z) (+Z)
- (PAINTING THE +/-Z LEPS WAS A NEW, UNPLANNED TASK ADDED AT KSC. DESIGNS WERE DEVELOPED AND HARDWARE WAS LOCATED TO ROTATE THE AMS EXPERIMENT PRIOR TO USS INSTALLATION. HOWEVER, THIS WAS CANCELLED PRIOR TO IMPLEMENTATION.)
- NOTE: DATES AT TOP & BOTTOM ARE MONDAYS
- (SEE OFF-LINE SCHEDULE B FOR CONTINUATION.)

FEBRUARY 9, 1998

OFF-LINE SCHEDULE A (FINAL; AS COMPLETED)

(BASED ON JAN 15, 1998 FAWG & STS-91 KSC MASTER MILESTONE SCHED DATED FEB 11, 1998)

ALPHA MAGNETIC SPECTROMETER (AMS) PAYLOAD ON STS-91 (S/MM-09)   LAUNCH: 5/29/98

OFF-LINE INTEGRATION SCHEDULE B AT KSC - FROM JSC TURNOVER TO KSC TURNOVER

Activity Name	PROCEDURES AMS	PROCEDURES NASA MMO	Feb '98 / Mar '98 (schedule)
1. AMS EXPERIMENT TURNOVER TO JSC @ KSC		X*	FEBRUARY 9, 1998 (CONTINUED FROM OFF-LINE SCHEDULE A.)
2. ALL-UP AMS EXP INTEGRATED SYSTEM FUNCT TESTS	X	X*	
3. PERFORM WT & CG TESTS ON ATC	X		(+ & -Z LEPS WERE DONE EARLIER; MAIN EXP & OTHER COMPONENTS WERE DONE LATER.)
4. INSTALL ATC IN USS LOWER CENTERBODY (PARTIAL)		X*	(+ & -Z LEPS MOUNTING BRACKETS HAD TO BE RE-MACHINED.)
5. INSTALL LIGHT-TIGHT CLOTH BETWEEN ATC & -Z LEPS	X		
6. INSTALL 4 PSBs ON THE USS & SAFETY WIRE		X*	(TEMPORARY INSTALLATION) (FINAL INSTALLATION)
7. ROUTE ATC, HTC.83, & -Z LEPS CABLES	X		THE CRANE WAS RELEASED FOR THE MAIN AMS
8. INSTALL ELECTRONICS CRATES COVERS (TEMPORARY)	X	X*	EXPERIMENT INSTALLATION AFTER ONLY 5.5 HOURS.
9. WEIGH & INSTALL MAIN AMS EXPERIMENT IN USS		X*	(SHEAR PINS & MOST BOLTS) (REMAINING BOLTS & SAFETY WIRE)
10. COMPLETE ATC AND -Z LEPS INSTL, CABLES, & S-WIRE		X*	NASA HOLIDAY
11. INSTALL 2 MCCs ON THE I-BEAMS & SAFETY WIRE	X	X*	(EDU) (FLIGHT)
12. DESIGN & FAB NEW PSB THERMAL PLATES		X*	
13. COMPLETE LIGHT-TIGHT & MISC THERMAL COVERINGS	X	X*	(AS REQ'D)
14. ELECT MATES TO AMS; FINALIZE CABLE SUPPORTS	X	X*	(AS REQ'D)
15. SAFETY WIRE ALL POSSIBLE FASTENERS & CONN.		X	
16. INSTALL USS SHEAR PIN/BUSHING RETAINING CAPS		X	
17. REINSTALL USS LOWER DIAGONAL STRUTS		X	
18. INSTALL +Z LEPS ON TOP I-BEAMS, CABLE, & S-WIRE		X*	(THE INSTALLATION OF THE AMS
19. REMOVE USS WITH AMS EXPERIMENT FROM GHE		X	MAIN EXPERIMENT WAS COMPLETED
20. INSTALL FLIGHT SILL TRUNNIONS ON USS		X	6 DAYS AHEAD OF SCHEDULE. THE
21. RECONFIGURE GHE: LOW TO HIGH POSITION		X	BUILT-UP CONTINGENCY TIME WAS
22. REINSTALL USS WITH AMS EXP ON GHE		X	GIVEN BACK TO THE EXPERIMENTERS
23. INSTALL KEEL TRUNNION ASSY, LIFT PLUGS, & S-WIRE		X	TO COMPLETE ELECTRONICS &
24. INSTALL LOWER & DCU THERMAL BLKTS & GRND WIRES		X	SOFTWARE TASKS.) USS/AMS PLACED ON FLOOR PEDESTALS
25. INSTALL 2 SAAMDS ON +X & +Y I-BEAMS		X	THE WBSAAMD WON'T BE READY UNTIL CITE OR AT THE PAD.
26. INSTALL UPPER THERMAL BLKT & GRND WIRES		X	THE TOP BLANKET WILL BE INSTALLED AT CITE IF THE NEW LABELS ARE NOT READY IN TIME -->
27. INSTALL 14 ISS CONTAM. WITNESS PLATES & PHOTO	X/ISS		
28. SHARP EDGE INSPECTION ON ENTIRE AMS PAYLOAD		X	
29. FINAL CLEANING & PREPS FOR MOVE TO SSPF		X*	THE PAYLOAD ENVIRONMENTAL TRANSFER SYSTEM (PETS) WILL BE USED FOR MOVE TO SSPF --->
30. AMS PAYLOAD TURNOVER TO KSC AT MPPF		X*	MARCH 18, 1998 @ 08:00 AM
NOTE: DATES AT TOP & BOTTOM ARE MONDAYS			(SEE ON-LINE SCHEDULE FOR CONTINUATION.)

Timeline scale (top & bottom): Feb '98 — 9 (L-15), 16 (L-14), 23 (L-13); Mar '98 — 2 (L-12), 9 (L-11), 16 (L-10)

ALPHA MAGNETIC SPECTROMETER (AMS) PAYLOAD ON STS-91 (S/MM-09)

ON-LINE INTEGRATION SCHEDULE AT KSC - HYBRID FLOW WITH INSTALLATION AT LAUNCH PAD 39A

Activity Name	Mar '98					Apr '98					May '98				Jun '98	
	9	16	23	30	6	13	20	27	4	11	18	25	1	8
	L-11	L-10	L-9	L-8	L-7	L-6	L-5	L-4	L-3	L-2	L-1	L0		

ORBITER PROCESSING MILESTONES

APCUs INSTL'N & IVT ARE TBD

VAB ROLLOVER 4/15 ▽   TANKING TEST 5/6-9 ☐   LAUNCH 5/29 ▽
PAD 39A ROLLOUT 4/22 ▽   PLBD CLOSE 5/14 ▽

ON-LINE ACTIVITIES BEGIN HERE.
SEE OFF-LINE SCHEDULES A & B FOR ACTIVITIES UP TO THIS POINT.

PERIODIC ACCESS TO TAKE "HOUSEKEEPING MEASUREMENTS" AT THE PAD MAY BE AVAILABLE ON A NON-INTERFERENCE BASIS WITH ORBITER PROCESSING ACTIVITIES.

1. AMS SIMUL/BACKUP DCU/ORBITER IVT IN OPF
2. AMS PAYLOAD TURNOVER TO KSC @ MPPF — ▽MARCH 18, 1998 @ 08:00 AM
3. INSTALL AMS & GHE IN PETS @ MPPF
4. TRANSPORT AMS PAYLOAD TO SSPF/CITE
5. INSTALL AMS IN CITE & CONNECT CABLES — ☐19
6. AMS PAYLOAD IVT @ CITE — ☐20
7. AMS PAYLOAD END-TO-END TESTS @ CITE — ☐23
8. AMS STAND-ALONE OPS @ CITE (AS REQ'D)
9. CEIT AT OPF — ☐28
10. INSTALL WBSAAMD ON -X I-BEAM
11. COMPLETE ELECT CRATES COVER INSTL'N
12. AMS PAYLOAD WEIGHT & CG TEST @ SSPF — ☐14
13. INSTALL AMS IN PYLD CANISTER, CRF OPS
14. MOVE AMS TO LAUNCH PAD — ☐20
15. REPLACE 4 ISS CONTAM. WITNESS PLATES
16. AMS INSTALLATION AT LAUNCH PAD — AMS INSTALLED WITH SPACEHAB SM ----> ☐24

☐ <--- THIS ACTIVITY STILL MUST BE NEGOTIATED WITH KSC PERSONNEL

17. SPACEHAB IVT @ LAUNCH PAD — 2 ☐ ☐ 4
18. AMS IVT WITH ORBITER @ LAUNCH PAD — ☐11
19. AMS END-TO-END TEST @ LAUNCH PAD — ☐12   NASA HOLIDAY ☑
20. ORBITER PROCESSING @ LAUNCH PAD

LAUNCH: MAY 29, 1998 ▼
(5/29/98 EST; 5/29/98 GMT)

STS-91 LAUNCH (10 DAY MISSION)
SHUTTLE/MIR MISSION-09 (S/MM-09)

NOTE: DATES AT TOP & BOTTOM ARE MONDAYS.

THE ACTIVITIES AND DATES IN THIS SCHEDULE HAVE BEEN REVIEWED & APPROVED BY KSC, JSC, AND AMS EXPERIMENT PERSONNEL.
THE FINAL DATES WILL CONTINUE TO BE ADJUSTED AS THE FLIGHT DRAWS NEARER.

(BASED ON JAN 15, 1998 FAWG & STS-91 KSC
MASTER MILESTONE SCHED DATED FEB 11, 1998)

ON-LINE SCHEDULE

Estimated Costs

Estimated mission management costs

The estimated costs to NASA for the mission management accommodation function are now presented. These include the design, fabrication, and certification of the ECS, and the mechanical and functional integration of the ECS with the ACCESS science components.

A summary of the mission management cost estimate is provided in Table 22, which follows in 5 parts on the five subsequent pages (pp. 86-90). The cost estimate is presented there in detail, along with the assumptions upon which the costs were determined. Phase 1 for the ACCESS Accommodation Study is complete with this report. The phasing adopts NASA's re-definition of phased procurement (Procurement Notice [PN] 97-19, our Note 1).

- Table 22   Cost by fiscal year
- Table 22a   Phase 1   Phase A/B   Formulation (this report)
- Table 22b   Phase 2   Phase C/D   Implementation
- Table 22c   Phase 3   Phase E   Deployment to ISS
- Table 22c   Phase 4   Phase E   On-orbit mission operations and data analysis (MO&DA)
- Table 22d   Phase 5   Retrieval   Post-flight retrieval

This estimate does not include the costs to carry out the following, which are assumed to be functions that will be performed by GSFC[8] and funded separately.

- DDT&E of the ACCESS science instrument.
- Electrical and avionics integration.
- Thermal design, analysis, and hardware development.
- Systems engineering and hardware development to integrate the science components of ACCESS into an operational instrument.

The costs that follow are based upon the known, actual support costs for the AMS payload that JSC is currently responsible for. The ECS costs (Tables 4-8) are included.

The total mission management cost for the duration of the entire ACCESS program in real-year (RY) dollars is $9.455M.

Ancillary costs

The ACCESS Accommodation Study Team determined that the Rocketdyne PCU box was an acceptable alternative for the TRD gas tank supply. An estimated total cost of that portion for the instrument definition team[8] has been determined[48]. Cost details are given in Table 19. The total TRD PCU tank system cost is estimated to be $710K.

Table 22. ACCESS Mission Management Costs by Fiscal Year ($K)

ACTIVITIES	FY03	FY04	FY05	FY06	FY07	FY08	FY09	FY10	FY11	Total
Phase 2 – Experiment Development and Integration Support	224	308	275	239						1,046
Phase 3 - Deploy to ISS Mission		1,675	2,658	1,818	321					6,472
Phase 4 - On-Orbit ISS Support					303	317	328	341	89	1,378
Phase 5 - ACCESS Retrieval Mission								241	318	559
	224	1,983	2,933	2,057	624	317	328	582	407	9,455

Costs are escalated by 3% per annum, in RY dollars.

Basis of the JSC Science Payloads Management Division (JSC-SM) estimate for ACCESS payload development

- GSFC performs DDT&E for the ACCESS science instrument.
- JSC performs DDT&E for ACCESS accommodations.
- JSC-SM mentors the ACCESS PIs and the instrument developers on ISS, SSP, and KSC requirements, processes, and procedures.
- Phase 1 - Accommodation Study (this report); Phase 1 continues for the science instrument[8].
- Phase 2 - ACCESS experiment development and integration support continues.
- Phase 3 - Deployment to ISS mission; ACCESS uses an ECS on STS-TBD in October 2006.
- Phase 4 - On-orbit ISS MO&DA support; ACCESS remains on the ISS for 4 years of continuous operations.
- Phase 5 - ACCESS retrieval mission; ACCESS will be retrieved on STS-TBD in October 2010.
- GSFC performs electrical and avionics integration, thermal design, analysis, integration, and systems engineering for the ACCESS instrument.
- JSC performs mechanical design, fabrication, testing, analysis, and integration for the ECS.
- JSC-SM documents compatibility and negotiates compliance with ACCESS, ISS and SSP requirements.
- JSC-SM designs, manufactures, tests, and certifies mission-peculiar equipment (MPE), unique POCC equipment, GSE, GHE, STE, and mock-ups needed to adapt the experiment hardware to the Shuttle and the ISS.
- JSC-SM develops structural math models and completes structural, stress, fracture dynamics, thermal, EMI/EMC and material analyses and reports for the integrated payload.
- GSFC develops structural math models and completes structural, stress, fracture dynamics, thermal, EMI/EMC and material analyses and reports for the ACCESS experiment hardware.
- JSC-SM completes flight and ground safety and reliability analyses and reports for the integrated payload.
- JSC-SM develops inputs for the PIP, PIP Annexes, PIA, and PIA Annexes; supports KSC integration activities; and provides on-orbit mission operations from the POCC and customer support room (CSR).
- JSC-SM supports flight crew, POCC, and CSR training and simulations.
- JSC-SM supports postmission de-integration and hardware recovery, facilitates mission data annotation and distribution, and develops final mission reports for all phases.
- The estimate excludes costs for ISS, SSP, KSC, and other operation, test, and facility costs.
- This estimate includes JSC facility costs for ECS structural verification testing.
- The estimate includes a 10% contingency.

Table 22a. Phase 2 – Accommodation Development and Integration Support ($K)

ACTIVITIES	FY03	FY04	FY05	FY06	FY07	FY08	FY09	FY10	FY11	Total
1.0 Mission Management	74	100	90	75						339
2.0 Integration	35	45	40	38						158
3.0 Engineering Analysis	80	110	100	85						375
4.0 Operations	15	25	20	19						79
5.0 Contingency	20	28	25	22						95
Total Phase 2 Costs	224	308	275	239	0	0	0	0	0	1,046

Costs are escalated by 3% per annum, in RY dollars.

Basis of the JSC-SM estimate for Phase 2—accommodation development and integration support

- JSC-SM mentors the ACCESS PIs and the instrument developers on ISS, SSP, and KSC requirements, processes, and procedures.

- GSFC performs electrical and avionics integration, thermal design, analysis, integration, and systems engineering for the experiment.

- JSC performs mechanical design, fabrication, testing, analysis, and integration for the ECS.

- JSC-SM supports the experimenter's programmatic reviews and meetings.

- JSC-SM documents compatibility and negotiates compliance with ACCESS, ISS, and SSP requirements.

- JSC-SM develops structural math models and completes structural, stress, fracture dynamics, thermal, EMI/EMC and material analyses and reports for the integrated payload.

- GSFC develops structural math models and completes structural, stress, fracture dynamics, thermal, EMI/EMC and material analyses and reports for the ACCESS experiment hardware.

- JSC-SM completes safety and reliability analyses and reports for the integrated payload.

- JSC-SM develops experiment operations scenarios, timelines, and analyses.

- JSC-SM assists and reviews the experiment hardware design, manufacturer, and test.

- The estimate excludes costs for ISS, SSP, KSC, and other operations, tests, and facilities.

- This estimate includes JSC facility costs for ECS structural verification testing.

- The estimate includes a 10% contingency.

Table 22b. Phase 3 – Deployment to ISS Mission ($K)

ACTIVITIES	FY03	FY04	FY05	FY06	FY07	FY08	FY09	FY10	FY11	Total
1.0 Mission Management		300	353	400	103					1,156
2.0 Integration		775	1,320	498	78					2,671
3.0 Engineering Analysis		200	397	275	19					891
4.0 Operations		248	346	480	92					1,166
5.0 Contingency		152	242	165	29					588
Total Phase 3 Costs	0	1,675	2,658	1,818	321		0	0	0	6,472

Costs are escalated by 3% per annum, in RY dollars.

Basis of the JSC-SM estimate for Phase 3—deployment to ISS mission

- ACCESS flies using an ECS on STS-TBD in October 2006.

- GSFC performs electrical and avionics integration, thermal design, analysis, and integration, and systems engineering for the ACCESS instrument.

- JSC performs mechanical design, fabrication, testing, analysis, and integration for the ECS.

- JSC-SM mentors the ACCESS PIs and the experiment developments on ISS, SSP, and KSC requirements, processes, and procedures.

- JSC-SM documents compatibility of the ACCESS experiment hardware design with ISS and SSP requirements.

- JSC-SM supports payload, SSP, and ISS programmatic reviews and meetings.

- JSC-SM designs, manufactures, test, and certifies mission peculiar equipment, unique POCC equipment, GSE, GHE, STE, mock-ups, and training units needed to adapt the ACCESS experiment hardware to the ECS and ISS.

- JSC-SM develops structural math models and competes structural, stress, fracture dynamics, thermal, EMI/EMC and material analyses and reports for the integrated payload.

- GSFC develops structural math models and completes structural, stress, fracture dynamics, thermal, EMI/EMC and material analyses and reports for the ACCESS experiment hardware.

- JSC-SM completes flight and ground safety and reliability analyses and reports for the integrated payload.

- JSC-SM develops inputs for PIA and PIA Annexes; supports KSC integration activities; and provides on-orbit mission support from the POCC and CSR.

- JSC-SM supports flight crew, POCC, and CSR training and simulations.

- JSC-SM supports EVA contingency crew training.

- JSC-SM develops the final mission report.

- The estimate excludes costs for SSP, KSC, and other operations, testing, and facilities.

- This estimate includes JSC facility costs for structural verification testing.

- The estimate includes a 10% contingency.

Table 22c. Phase 4 – On-Orbit ISS Support ($K)

ACTIVITIES	FY03	FY04	FY05	FY06	FY07	FY08	FY09	FY10	FY11	Total
1.0 Mission Management					74	77	80	84	21	336
2.0 Integration					0	0	0	0	0	0
3.0 Engineering Analysis					0	0	0	0	0	0
4.0 Operations					201	211	214	224	60	910
5.0 Contingency					28	29	30	33	8	128
Total Phase 4 Costs	0	0	0	0	303	317	328	341	89	1378

Costs are escalated by 3% per annum, in RY dollars.

Basis of the JSC-SM estimate for Phase 4—on-orbit ISS support

- ACCESS remains on ISS for 4 years of continuous operations.

- GSFC performs electrical and avionics integration and systems engineering for the ACCESS instrument.

- JSC performs mechanical design, fabrication, testing, analysis, and integration for the ECS.

- JSC-SM resolves on-orbit anomalies in real time.

- JSC-SM supports experiment and ISS programmatic reviews and meetings.

- JSC-SM maintains MPE, GSE, GHE, and STE for the retrieval.

- JSC-SM maintains unique POCC equipment.

- JSC-SM facilitates annotation and distribution of mission data and reports.

- The estimate excludes costs for SSP, KSC, and other operations, testing, and facilities.

- The estimate includes a 10% contingency.

Table 22d. Phase 5 – ACCESS Retrieval Mission ($K)

ACTIVITIES	FY03	FY04	FY05	FY06	FY07	FY08	FY09	FY10	FY11	Total
1.0 Mission Management								123	181	304
2.0 Integration								0	0	0
3.0 Engineering Analysis								9	14	23
4.0 Operations								87	94	181
5.0 Contingency								22	29	51
Total Phase 5 Costs	0	0	0	0	0	0	0	241	318	559

Costs are escalated by 3% per annum, in RY dollars.

Basis of the JSC-SM estimate for Phase 5—ACCESS retrieval mission

- Retrieval will be on STS-TBD in October 2010.

- GSFC performs electrical and avionics integration and systems engineering for the ACCESS instrument.

- JSC performs mechanical design, fabrication, testing, analysis, and integration for the ECS.

- JSC-SM mentors the ACCESS PIs and the instrument developers on ISS, SSP, and KSC requirements.

- JSC-SM supports payload, SSP, and ISS programmatic reviews and meetings.

- JSC-SM re-certifies mission peculiar equipment, GSE, GHE, mock-ups, and training units needed to complete the retrieval.

- JSC-SM revises structural math models and completes structural, stress, fracture dynamics, thermal, EMI/EMC and material analyses and reports for the integrated payload.

- JSC-SM revises flight and ground safety and reliability analyses and reports for the integrated payload.

- JSC-SM develops inputs for PIA and PIA Annexes; supports KSC integration activities; and provides on-orbit mission support from the POCC and CSR.

- JSC-SM supports flight crew, POCC, and CSR training and simulations.

- JSC-SM supports EVA contingency crew training.

- JSC-SM supports payload de-integration at KSC and hardware recovery, facilitates data annotation and distribution, and develops the final mission report.

- The estimate excludes costs for SSP, KSC and other JSC operations, test, and facility costs.

- The estimate includes a 10% contingency.

Conclusions and Future Effort

The attached payload sites on the ISS will provide a unique platform for astrophysical observations of the cosmic rays from our Galaxy and the rest of the Universe, using ACCESS. In the field of cosmic-ray science, this experimental concept is a natural extension of several of the goals in NASA's Structure and Evolution of the Universe theme of the Space Science Enterprise[49]. It also represents another step forward in the evolution of our attempts to study the cosmic rays by taking advantage of improving technology and the advent of a space-based outpost such as the ISS beyond our atmosphere and in Earth orbit. It goes beyond the well-proven balloon experiments of short duration and limited capabilities in a natural way, and it takes cosmic-ray science to the frontier of space where such investigation belongs. Although there is nothing new in such a goal which has been the objective of scientists in the field since its inception 87 years ago[1], bringing the task to fruition is as important as it ever was.

At the completion of this baseline Accommodation Study and at this juncture in the progress of cosmic-ray science, the next step appears to be the identification of an ACCESS program strategy which is modest in cost and far-reaching in its consequences. The basic idea is still as simple as Victor Hess climbing to the mountaintop: Almost anyone can do it. But can anyone do it inexpensively? How do we accomplish the goal of a modest ACCESS program cost? As a preliminary Phase 1 summary, this report has identified an initial estimate of certain portions of that cost, derived from actual numbers and JSC flight experience for existing Shuttle and ISS payloads. It is likewise derived from a number of rigorous assumptions, payload expertise, and qualified study team personnel who have already made original contributions to the design and development of both the STS and the ISS programs.

If such experience can serve as a paradigm, then what conclusions can we draw to direct our future effort? Experience is not always a talisman for success. Nevertheless, it does have merit and the following summary in Table 23 addresses several of the issues that presently face the ACCESS program.

Table 23. Future Efforts

- *Identify a Phase 2 (DDT&E) program architecture.*
  - *Complete definition of the ACCESS science mission.*
  - *Define the end-to-end payload integration concept.*
- *Identify the NASA Centers that support the architecture.*
- *Implement the architecture.*
- *Be consistent with existing STS and ISS architecture.*

As was stated in this report, JSC can launch an ACCESS payload in 36 months under its template at the cost given. However, this is only true if and when the ACCESS science mission and instrument definition are mature enough to keep pace with that schedule. Such is not the case at the time of this writing in view of the fact that the ACCESS science definition is still under study[8]. Nevertheless, for a launch in November 2006 the JSC template allows until November 2003 for the ACCESS science and instrument definition to mature.

The second aspect of Table 23 that needs attention is the problem of heritage. The last bullet points out that the evolution of NASA's space exploration programs into the current STS and ISS era is one of human spaceflight. It is post-Challenger. It intimately is involved with human presence and therefore human safety. That means multitudes of a new kind of safety review. Older notions which derive from science payloads flown on unmanned spacecraft or balloon flights can prove to be out of date and very expensive on an ISS science mission. So these points of view need to change. The guiding principle of ISS integration strategy adopted in the Accommodation Study is that final test and verification happens at KSC and ultimately on orbit in the space segment—not the ground segment in a high-bay facility. As long as 30-year-old ideas about IV&T still plague us, an ACCESS science mission may prove to be a very expensive thing. The KSC integration concept has already been proven in NASA test flights. It works and presently appears to be cost-effective, thorough, and adequate for ISS science missions. The question for ACCESS then is how to arrive at a successful, cost-effective IV&T strategy that is consistent with existing STS and ISS architecture.

With these parting thoughts on future effort, we complete the baseline ACCESS Accommodation Study (Phase 1). All members and contributors of the baseline study team look forward to the next exciting phases and future effort (Table 23 and Notes 1-2) of the ACCESS program.

References

1. Hess, V. F., *Physik. Zeitschr.* **14**, 610 (1913); *Nobel Lectures - Physics* **2**, 351 (Elsevier, NY, 1965).
2. Ramaty, R., Kozlovsky, B., and Lingenfelter, R., *Physics Today* **51.4**, 30 (1998).
3. Wefel, J.P., *et al.*, in *The Astronomy and Astrophysics Encyclopedia*, Maran, S.P, ed., Van Nostrand, New York (1992).
4. Lemaitre, G., *Nature* **127**, 704 (1932).
5. Lemaitre, G., *Rev. Mod. Phys.* **21**, 357 (1949).
6. Swordy, S. P., in *Proc. 23rd Int'l. Cosmic Ray Conf. (Calgary)*, eds. D. A. Leahy, R. B. Hicks, & D. Venkatesan (World Scientific, Singapore, 1994), p. 243.
7. NRA 96-OSS-03, "New Mission Concepts in Space Science."
8. NRA 97-OSS-13, "Detector Definition and Instrument Assessment for an Advanced Cosmic-ray Composition Experiment on the Space Station (ACCESS)."
9. JSC ACCESS TIM #1, JSC Accommodation Study Team (Lunar and Planetary Institute, Houston, October 14-15, 1997).
10. JSC ACCESS TIM #2, JSC Accommodation Study Team (Lunar and Planetary Institute, Houston, October 7-8, 1998).
11. ACCESS Working Group (AWG) Meeting (Goddard Spaceflight Center, Greenbelt, Maryland, May 13-14, 1998).
12. Simpson, J. A., *Ann. Rev. Nucl. Part. Sci.* **33**, 323 (1983).
13. Gaisser, T. K., *et al.*, *Opportunities in Cosmic-Ray Physics and Astrophysics*, National Research Council, National Academy Press, Washington, D. C. (1995).
14. Waddington, C. J., *et al.*, *Galactic Origin and the Acceleration Limit (GOAL)*, NASA Headquarters, Code SS, Washington, DC, (1992).
15. Blandford, R. D. and Ostriker, J. P., *Ap. J.* **237**, 793 (1980).
16. Ellison, D. C., *et al.*, *Publ. Astron. Soc. Pacific* **106**, 780 (1994).
17. Lagage, P. O. and Cesarsky, C. J., *A & Ap.* **118**, 223 (1983).
18. Biermann, P. L., in *Proc. 23rd Int'l. Cosmic Ray Conf.*, (Calgary), eds. D. A. Leahy, R. B. Hicks, & D. Venkatesan, (Singapore, 1994, World Scientific), p. 45.
19. Asakimori, K. *et al.*, *Ap. J.* **502**, 278 (1998).
20. Engelmann, J. J., *et al.*, *A & Ap.* **233**, 96 (1990).
21. Müller, D., Swordy, S. P., Meyer, P., L'Heureux, J., & Grunsfeld, J. M., *Ap. J.* **374**, 356 (1991).
22. Wefel, J. P., in *Genesis and Propagations of Cosmic Rays*, eds. M. M. Shapiro and J. P. Wefel, NATO ASI C220, (D. Reidel Co., Dordrecht, 1988), p. 1.
23. Binns, W. R., *et al.*, *Adv. Space Res.* **4**, 25 (1984); *Ap. J. Lett.* **267**, L93 (1983); *Ap. J. Lett.* **247**, L115 (1981).
24. Fowler, P. H. *et al.*, *Proc. 19th Int'l Cosmic Ray Conf.* **2**, 115; **2**, 117 (1985); *Nature*, **291**, 45 (1981).
25. García-Muñoz, M., *et al.*, *Ap. J. Suppl.* **64**, 269 (1987).
26. Swordy, S. P., *et al.*, *Ap. J.* **349**, 625 (1990).
27. Wefel, J. P., in *Cosmic Rays, Supernovae and the Interstellar Medium*, eds. M. M. Shapiro, R. Silberberg and J. P. Wefel, NATO ASI C337, (D. Reidel Co., Dordrecht, 1991), p. 29.
28. Meyer, J. P., Drury, L. O'C., and Ellison, D. C., *Ap. J.* **487**, 182 (1997).
29. Ellison, D. C., Drury, L. O'C., and Meyer, J. P., *Ap. J.* **487**, 197 (1997).
30. Ahlen, S., *et al.*, *Nucl. Instrum. Meth. A* **350**, 351 (1994).
31. *Feasibility Study of USS for ACCESS*, GSFC ACCESS TIM #1, Lockheed Martin, (Goddard Space Flight Center, December 8, 1997).
32. CR 1135-Rev. A, "S3/P3 Attached Payload & Logistics Sites Interface Performance Requirements," Mark A. Foster, Boeing-Utilization Office (April 24, 1998).
33. "ISS S3 Attached Payload Center of Gravity Definition," G. Martin, McDonnell-Douglas Aerospace, SSP PAIT-PG-1 (October 1995).
34. *Structural Assessment for the JSC Accommodation Study of ACCESS*, JSC ACCESS TIM #2, Lockheed Martin (Lunar and Planetary Institute, Houston, October 7-8, 1998).
35. Thorn, V., "ISS Flight Attitudes for Design, Rev D Configuration / Assembly Sequence, Change 1334", Mission Integration Office – VIPER, NASA/JSC (September 1998).

36. Laubach, J. G.; "ISS AC thermal environments for ACCESS", Personal Communication, Lockheed Martin (December 1998).

37. Gilmore, D. G, et al.; Satellite Thermal Control Handbook (The Aerospace Corporation Press, El Segundo, California, 1994).

38. Badhwar, G., et al., Adv. Spac. Res. 22, 501 (1998); ibid. 22, 485 (1998).

39. Messenger, G.C., and Ash, M.S., Single Event Phenomena (Chapman & Hall, New York, 1997).

40. O'Neill, P.M., ISS Ionizing Radiation Effects Assessment for ACCESS, in Ref. 10.

41. O'Neill, P.M., Badhwar, G., and Culpepper, W.X., IEEE Trans. Nucl. Sci. 46, 2467 (Dec. 1998).

42. Badwar, G., MARIE-Mars 2001, Preliminary Design Review (JSC, August 1998).

43. Johnson, N. J., Sci. Amer. 279.2, 62 (1998); Kessler, D. J., et al., A Computer-based Orbital Debris Environment Model for Spacecraft Design and Observations in Low-Earth Orbit (NASA Technical Memorandum TM-104825, November, 1996). Available at Orbital Debris website.

44. Christiansen, E.L., Meteoroid/Debris Shields for ACCESS, in Ref. 10.

45. Micrometeoroid/Orbital Debris (M/OD) Analysis for M/OD Critical Items, Vol. 2, RD97-606-V2, ISS Product Group 2, Boeing Purchase Contract HX3211 (Boeing, Canoga Park, CA, August 6, 1997), 62 pages.

46. Xenon Tank Specification, RC2849 (Rockwell-Rocketdyne Division, August 13, 1996), 30 pages.

47. Tank, Xenon Gas Feed System, Drawing No. RE2849 (Boeing-Rocketdyne Division, February 2, 1997).

48. Bromberg, Marcelo (Boeing-Canoga Park), private communication with Thomas L. Wilson (January 4, 1999). The verbal quote from Arde (the tank manufacturer) is $25K per tank, while an actual cost three years ago was $70K per tank.

49. The Space Science Enterprise, NASA Strategic Plan.
(1997 @ http://www.hq.nasa.gov/office/oss/strategy/1997/sseplanm.htm).

50. Hughes, E. B., et al., Nucl. Instr. and Meth. 75, 130 (1969).

51. Whiteside, H., et al., Nucl. Instr. and Meth. 109. 375 (1973).

52. Barish, B. C., et al., Nucl. Instr. and Meth. 116, 413 (1974).

53. Cheshire, D. L., Huggestt, R. W., and Jones, W. V., Nucl. Instrum Meth. 141, 219 (1977).

54. Jones, W. V., Ormes, J. F., and Schmidt, W. K. H., Nucl. Instrum. Meth. 140, 557 (1977).

55. Adeva, et al. (The L3 Collaboration), Nucl. Instrum. Meth. A289, 35 (1990).

56. Seo, E. S. et al., Proc. SPIE (Denver) 2806, 134 (1996).

57. Simon, M., et al., Ap. J. 239, 712 (1980).

58. Ellsworth, R. W., et al., Astrophys. and Space Sci. 52, 415 (1977).

59. Grigorov, N. L., et al., 12th Int'l. Cosmic Ray Conf, (Tasmania) 5, 1746 (1971).

60. Beuville, E., et al., Nuc. Instr. & Meth. A288, 157 (1990).

61. Beuville, E., et al., IEEE Trans. on Nucl. Sci. 39, No. 4, 766 (1992).

62. Kleinfelder, S. A., and Kipnis, I., LBNL, Berkeley, CA, private conversation (1996).

63. "ACE," Nova R & D, Inc., www.pe.net/~NOVA.

64. Asakimori, K., et al., Proc. 23rd ICRC (Calgary) 2, 25 (1993).

65. Ichimura, M., et al., Phys. Rev. D 48, 1949 (1993).

66. Binns, W. R., et al., "ZIM Instrument Description" (Draft, Washington University, St. Louis, October 18, 1998).

67. Grunsfeld, J.M., et al., Ap. J. Lett. 327, L31 (1988).

68. L'Heureux, J., et al., Nucl. Instr. and Methods A295, 246 (1990).

69. Ginzburg, V.L. and Frank, I.M., JETP 16, 15 (1946).

70. Hartman, G., et al., Phys. Rev. Lett. 38, 1368 (1977).

71. Prince, T., et al., Ap. J. 227, 676 (1979).

72. Müller, D. and Tang, K., Ap. J. 312, 183 (1987).

73. Cherry, M.L. and Müller, D., Phys. Rev. Lett. 38, 5 (1977).

74. Cherry, M.L., Phys. Rev. D. 17, 2245 (1978).

75. Ter-Mikaelian, M.L., High-Energy Electromagnetic Processes in Condensed Media (Wiley, New York, 1972).

76. Ter-Mikaelian, M.L., Nucl. Phys. 24, 43 (1961).

77. Garibian, G.M., Sov. Phys.-JETP 33, 23 (1971).

78. Wang, J.Z. and Seo, E.S., ACCESS TechNote UMD 98-1-2, University of Maryland, unpublished (1998).

79. Heikkila, W.J., EOS 54, 764 (1973).

80. Frooninckx, T.B., and Sojka, J.J., JGR 97, 2985 (1992).

81. Gussenhoven, M.S., *et al., JGR* **90**, 11009 (1985).
82. Feynman, J. Spitale, G., Wang, J., and Gabriel, S., *JGR* **98**, 13281 (1993).
83. IGRF 1965.0, *JGR* **74**, 4407 (1969); IGRF 1987, *J. Geomag. Geoelectr.* **39**, 773 (1987).
84. Bilitza, D., *Radio Science* **21**, 343 (1986); NSSDC/WDC-A-R&S 90-22 (November 1990).
85. Arquilla, R., *J. Spacecraft Rockets* **33**, 167 (1996); NSSDC/WDC-A-R&S 76-06; 76-04; 74-03; 72-12.
86. Gardner, B.M., *et al., Environmental Workbench (EWB)*, Version 3.0 (NASA-Lewis Contract NAS3-25347 with S-Cubed Division of Maxwell Labs, La Jolla, California 92038, April 11, 1994).
87. 1998 Workshop on Balloon-Borne and Space-Based Calorimetry, Sill, A., and Wigmans, R., convenors (Texas Tech University, Lubbock, Texas, October 21-24, 1998).

Notes

1) Procurement Notice (PN) 97-19. Government regulations are now silent as to titles, definitions, or how many phases can be used in phased procurement. PN 97-19 does switch from alphabetic to numeric designations. The NASA FAR Supplement 1817.7300(b) simply defines "phase acquisition" as "an incremental acquisition implementation comprised of several distinct phases where the realization of program/project objectives requires a planned, sequential acquisition of each phase. The phases may be acquired separately, in combination, or through a down-selection strategy." Because PN 97-19 creates infinite possibilities for confusion, the ACCESS Accommodation Study Team has adopted the following definitions. These are not to be confused with the safety review phasing in Table 19 of the main text of this report. For example, Phase 0 (zero) cannot be used under PN 97-19 because it has a strong heritage in the NASA safety review process. Roman numerals and Arabic numerals both use the same zero.

Previous Phasing Terminology	*Terminology - This Report*
• *Phase A/B*	• *Phase 1 (Formulation)*
• *Phase C/D (DDT&E)*	• *Phase 2 (Implementation)*
• *Phase E (MO&DA)*	• *Phase 3 (Deployment to ISS)*
• *Phase E (MO&DA)*	• *Phase 4 (On-orbit MO&DA).*
• *Phase E (MO&DA)*	• *Phase 5 (Post-flight retrieval)*

2) At the final JSC Technical Interchange Meeting for this Accommodation Study, Dr. James H. Adams of the Naval Research Laboratory introduced the suggestion that ACCESS might include a battery in its conceptual design[10]. This could enhance the science data return by allowing the experiment to continue operating even during the keep-alive conditions on ISS. Batteries, however, raise additional safety issues. Because this discussion occurred late in the Accommodation Study, it was decided to defer the feasibility of an augmented keep-alive condition using a battery to a trade study in Phase 2 (DDT&E, Note 1). Dr. Adam's suggestion was handed over to the Goddard instrument team[8] at the ACCESS calorimeter workshop two weeks later[87].

3) The authors express their gratitude to Luanne Jorewicz at JSC for her assistance in editing this report for final publication.

Appendices

Appendix A. Historical Background and Scope of Study

ACCESS began in 1996 as a new mission concept in NASA's Office of Space Science to perform fundamental cosmic-ray astrophysics investigations from the ISS using a calorimeter. It was selected with the proviso that a TRD module should be combined with the proposed CAL so that the composite instrument would provide measurements of the elements from H-Fe at the highest practical energies. In addition, the capability to measure UH (Z>28) cosmic rays was to be included. This was a natural merger of techniques and requirements since the separate modules complement one another and each requires a large-area detector and long exposure time to make significant measurements of the very rare ultra-high energy and UH cosmic-ray nuclei, as described in this report.

An Accommodation Study was to be performed by the science team in collaboration with the engineering team at JSC to assess the feasibility of flying ACCESS both in the Space Shuttle as transportation system, and on the ISS. The JSC team completed such a study several years ago for the AMS experiment, and currently works with the AMS team that successfully launched that payload on its precursor flight (STS-91) in June 1998. It was the AMS that led to the ACCESS concept, and one of the questions in the study was the degree to which ACCESS might utilize the expertise and, possibly, the hardware developed for AMS to reduce cost.

A study team to define a preliminary model for the ACCESS instrument was convened, involving JSC, Louisiana State University (lead for the calorimeter and the precursor balloon experiment, advanced thin ionization calorimeter [ATIC]), University of Chicago (lead for the TRD and the balloon experiment, transition radiation array for composition of energetic radiation [TRACER]), Washington University (lead for the UH and the balloon experiment, trans-iron galactic element recorder [TIGER]) and the collaborators on these projects plus other members of the community (University of Maryland, Naval Research Laboratory, University of Michigan, Caltech, Jet Propulsion Laboratory, and Kanagawa University). This study team refined the science goals for ACCESS, identified constraints and interoperability, and defined a baseline instrument concept to go forward into the detailed Accommodation Study. This stage of the process was coordinated with the Cosmic Ray Roadmapping Committee, which NASA Headquarters initiated.

In parallel, NASA Headquarters established a Project Formulation Office for ACCESS at GSFC and funded definition studies for alternate instrumentation concepts and needed technology development. The two studies have been coordinated with GSFC personnel participating in JSC technical interchange meetings and JSC personnel participating in the GSFC working group meetings.

The science goals for ACCESS require maximizing the exposure to the rare ultra-high energy particles and UH nuclei. As the science team pointed out, achieving a large detector area is important to mission success. Therefore, a second objective for this study was to look into larger (and heavier) configurations. For study purposes, these alternate configurations were derived by scaling the area and the weight and using these to establish the appropriate envelopes and mass properties. In this part of the study, it was necessary to consider a number of ECS options.

The most basic question that has been addressed in this report is "Can ACCESS be accommodated on the ISS (and STS) within the currently known constraints, requirements, and attached payload site data for the Space Station?" The answer appears to be "Yes," as explained above. At another level, this study was intended to

(i)   define areas of major engineering concern and develop a plan to resolve the concerns.

(ii) provide a baseline engineering design (and cost estimate) for the accommodation work that can be utilized in assessing mission viability and schedule constraints.

(iii) develop a management structure for interfacing between STS/ISS and the instrument developer.

(iv) provide feedback and suggestions to the ACCESS science team, the ACCESS Working Group, and the ACCESS instrument developer.

All of these goals are addressed within the main body of this report.

Appendix B. Detailed Instrument Descriptions

Summary

The ACCESS project derives from the greatly renewed interest in measurements of cosmic-ray composition and energy spectra, particularly measurements approaching the "knee" region (Figure 1). The enthusiasm stems from the recent confluence of (1) theoretical developments related to cosmic-ray origin and acceleration; (2) exciting new data indicating both different rigidity spectral indices for protons and heavier nuclei and possible bend(s) in the proton spectrum; and (3) an opportunity to expose large experimental payloads on the ISS.

As described previously, the ACCESS payload for ISS combines three instruments, each of which is derived from a balloon flight prototype. Figure 3 showed the payload schematically. At the bottom is the hadron calorimeter (CAL) composed of a target/tracking section followed by a BGO energy detector. Above the calorimeter is a TRD composed of fiber radiators and proportional tubes to detect the transition radiation X-ray photons. And at the top is the CM designed to measure the rare UH cosmic-ray nuclei. With the addition of avionics, a thermal control system, gas resupply, a debris shield, and a carrier structure including the PAS interface, these three baseline instruments form the total ACCESS payload as shown previously in Figure 21. In the following subsections, each of the instruments is described in some detail.

B.1 The hadron calorimeter

Achieving the ACCESS science goals requires measurements of all of the elements (H......Ni) to as high an energy as possible. This objective necessitates the combination of the TRD and a CAL. The science requirements are derived directly from the mission goals, namely: (a) to combine CAL, TRD, and CM into one functional instrument; and (b) to meet the GOAL (Galactic Origin and the Acceleration Limit) report measurement objectives[14]. The latter call for the measurement of 10 events above 10^{15} eV for each of the major charge groups: H, He, CNO, Ne-S, Ar-Ni. For the CAL, the focus is on H and He since the TRD cannot measure these two groups. [In addition, an objective is to cross-calibrate the CAL and TRD techniques by measuring a subsample of high-Z events in both sub-instruments.] The GOAL report[14] calls for an accumulated exposure in excess of 300 m^2-sr-days for H and He and 600 m^2-sr-days for the higher-Z nuclei. Since not all particles passing through the CAL generate measurable events, the exposure necessary to meet the GOAL objective must be increased by the interaction factor, IF. For IF = 63%, the required minimum CAL exposure is 476 m^2-sr-days. Thus, of necessity, the TRD must be at least 25% greater in collecting power than the CAL.

A diagram of the baseline CAL is shown in Figure B.1-1. This instrument may be divided functionally into two parts: the top "target/tracking" section measures the incident particle's charge and trajectory, provides a first level trigger, and causes the particle to interact inelastically; the lower, "BGO" section measures the energy of the ensuing cascade of particles. The highly segmented Si matrix detector measures the incident particle charge in the presence of background generated by backscatter from the shower. The C (carbon) target layers (T1, T2, T3, T4) are each
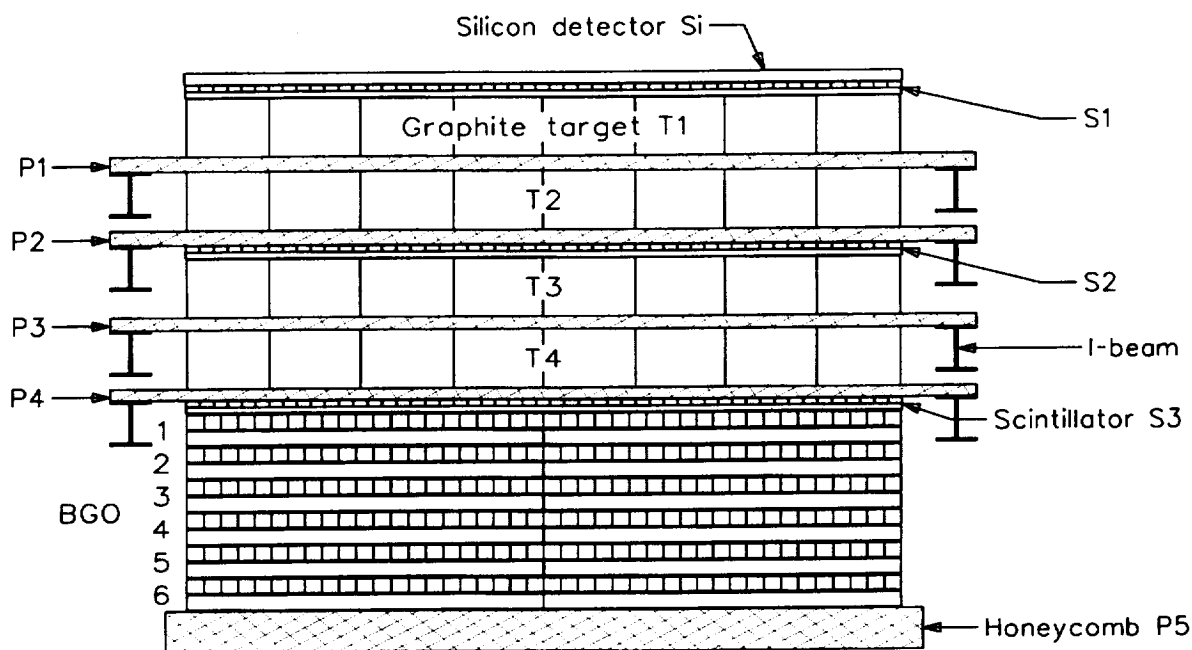
Figure B.1-1. The baseline hadron calorimeter for ACCESS.

10 cm thick and together provide ~one interaction length to cause incident particles to interact without substantially developing a shower. The active calorimeter consists of twelve layers of BGO crystals, each of which has dimensions 2.5 cm by 2.5 cm by 100 cm long. The twelve layers provide > 26 radiation lengths for the shower development and alternate layers are mounted at right angles so that the trajectory of the shower core can be determined. Scintillator hodoscopes (S1, S2, S3) between layers of target material provide the event trigger, and honeycomb structure (P1-P5) provides support for the detectors/materials.

The full device has an area of 1 m^2 and a height of 0.8 m, resulting in a geometrical factor of $\leq$ 0.8 m^2 steradian. Taking into account a ~63% interaction rate in the target and assuming a 1000-day exposure on board the ISS, the CAL's effective collecting power is 500 m^2-sr-days. We have also considered designs in which the target/tracking section is expanded at the top into a cone shape and the BGO is reduced in area to maintain the same weight. Such an arrangement (c.f. Figures 3, 17, and B.4-1, or Appendix E) accepts particles at larger zenith angles, which can yield an increase in collecting power.

The instrument requirements for the CAL necessitate that it must: (a) force the particles to interact, (b) measure the charge of each incident event, (c) determine the trajectory through the instrument, and (d) measure a signal proportional to the total energy of the incident particle. These requirements, and the ensuing instrument design, are explained in more detail below.

B.1.1. Ionization calorimetry: target and BGO

At the ultra-high energies to be studied by ACCESS, the practical method to measure H and He, and other elements, in the cosmic rays is ionization calorimetry. In an ionization calorimeter, a particle's energy is deposited inside a medium via a cascade of nuclear and electromagnetic particles. At each step of the cascade, the energy of the primary particle is subdivided among

many secondary particles. The integral of the deposited energy versus depth is a measure of the energy of the incident hadron. In principle, a device that is tens of interaction lengths deep will provide energy resolution limited only by the statistical nature of the cascade process and the measuring technique. Such "thick" calorimeters are possible for ground-based experiments, but instruments for space applications are necessarily "thin." In this case, the calorimeter resolution depends, as well, on the fluctuations in the energy transferred to secondary particles in the first few interactions. Thus, an optimal calorimeter would have a target as thick as possible in interaction lengths, to force interactions of both the incoming primary and secondary hadrons, while remaining thin in terms of radiation lengths, so the cascade development occurs not in the target but in the calorimeter material. The calorimeter material should be thick in terms of both radiation length, to absorb the cascades, and interaction length, to force additional interactions of both secondary and primary particles. The energy resolution improves as the calorimeter is made deeper because additional interactions occur, which results in a larger portion of the incident energy appearing in the electromagnetic component. Finally, if the calorimeter is sensitive over its full volume, it will observe the total deposited energy. From Monte Carlo simulations and detailed investigations using accelerators, there is a good understanding of how the energy resolution depends on depth, materials, particle species, and primary energy[50-55].

Practical instruments for balloon or space applications must necessarily be limited in absorber thickness in order to have a reasonable cross-sectional area, i.e. geometrical factor, for collecting the particles. The minimum depth depends on the energy resolution acceptable for a particular experiment. A thin CAL to measure the spectra of galactic cosmic rays must meet two basic requirements: (1) the primary nucleus must undergo at least one inelastic interaction; and (2) the electromagnetic energy resulting from the interaction(s) must be measured with good resolution. An optimal design would have a target thickness of about one proton interaction length located upstream of an electromagnetic calorimeter, which must be sufficiently thick in radiation lengths to develop the photon cascades ensuing from the neutral pions produced in the interactions.

Considering these requirements, C is a nearly ideal target material since this element has 2.02 radiation lengths per proton interaction length (38 cm at a density of 2.265 g cm^{-3}) and is readily available. For the calorimeter material, BGO is also nearly ideal with a radiation length equal to 1.12 cm, with a density of 7.1 g cm^{-3} and about 20 radiation lengths per interaction length. BGO is an inert, non-hygroscopic scintillation crystal that has no tendency to cleave or shatter and is radiation resistant. It is widely used in accelerator experiments and is appropriate for exposure on the ISS. The other advantage of BGO is that it is a scintillator and, thus, the calorimeter can be made fully active, thereby avoiding transition effects. For these reasons the ACCESS calorimeter adopted for the baseline study uses C as the target and the ionization measurement is made by BGO crystals.

The anticipated integral cascade curves, i.e. the mean energy deposited as a function of increasing BGO thickness, for an ACCESS-type CAL is illustrated in Figure B.1-2 for protons at 10, 100, 10^3, 10^4 and 10^5 GeV incident vertically on the top of the target section. These results were generated with the GEANT Monte-Carlo code for a 25-cm-thick stack of BGO. The mean energy deposition for protons is about 30%-40% of the incident energy, and is almost linear with the incident energy. The energy resolution (the ratio of the standard deviation of the energy deposit distribution to the mean energy deposit) varies from 30% to 40% below 10 TeV, but it

degrades to about 60% at 100 TeV. This is due to the limited thickness of the BGO in these calculations. For ACCESS, the BGO will be at least 30 cm in depth, sufficient to achieve resolution of <50% at all energies. For heavier nuclei, the situation improves with increasing charge. For He, the calculated resolution is 30%-40%, while for Fe it is 10%-20% [56].
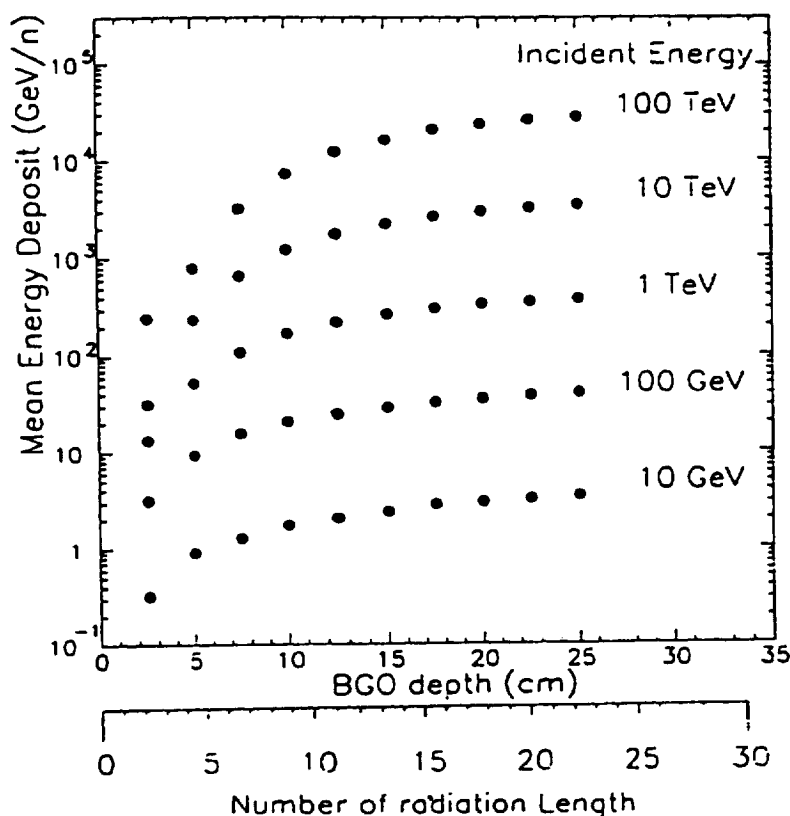
Figure B.1-2. Monte-Carlo calculated integral cascade curves for a C-BGO instrument.

B.1.2. Charge, backscatter, and tracking

In a calorimeter experiment, particles are backscattered from the calorimeter into the upper hemisphere[57]. These albedo particles consist mostly of relativistic (several MeV) electrons that result from gamma rays scattered into the backward hemisphere of the calorimeter. They also include non-relativistic particles, which may result either directly from nuclear interaction products emitted into the backward hemisphere or from albedo neutrons produced in the interactions. Simulations confirm that as the energy increases, the number of backscattered particles per unit area increases, potentially adding to the charge signal of the incident cosmic ray and degrading the charge resolution, including distinguishing $Z=1$ and $Z=2$. In fact, it is rather widely accepted that backsplash from the calorimeter was responsible for confusing protons and He, leading to a claimed spectral break in previous experiments[58-59]. The magnitude and energy dependence of this albedo becomes smaller with an increase in the distance and the amount of matter between the point of the first interaction and the charge detector. For example, when the first interaction

occurs deeper in the target the average backscatter signal in the charge layers is much smaller than when the first interaction occurs near the top of the target.

In the baseline CAL of Figure B.1-1, the topmost layers are a Si detector followed by a scintillator layer (S1). S1 is formed from two layers of 2-cm-wide, 1-cm-thick scintillator strips, arranged orthogonally to provide both an x- and a y-measurement, as well as a fast trigger signal. Based upon simulations of the backscatter, the 2-cm-wide strips become inefficient at separating Z=1,2 at about 10 TeV, due to the presence, somewhere along the strips, of several albedo particles. To provide reliable charge identification at high energy, a detector with two-dimensional segmentation is needed. This is provided by the Si detector, which is a matrix of small individual detectors constructed so as to cover the full aperture of the instrument. Simulations show that, with this pixelation, the fraction of misidentified protons remains at the few-percent level. For ACCESS, we plan on pixels about 2 cm x 2 cm or smaller, which, combined with the strip scintillators and tracking information, should eliminate the backscatter ambiguity.

The Si-matrix also provides excellent charge resolution up to Ni to compensate for the saturation in the scintillator at high charges. In the case of a bare calorimeter instrument, the Si + S1 will provide the identity of the incident cosmic ray. In the ACCESS configuration, however, the particles observed at the top of the CAL must first penetrate the TRD and CM instruments. The mass in these instruments guarantees that some of the events will interact before reaching the CAL, fragmenting in the case of heavy ions, plus interacting and beginning to develop a cascade. For these events, it is vital that the incident particle's charge be determined at the top, in the CM, and that its position of incidence or trajectory be known, to compare to the data from the CAL instrument.

Particle tracking is required to correct for the angle of incidence effect in the cascade curves and in the charge detectors. In addition, the use of pixelated detectors requires tracking to point to the pixel containing the incident particle. The shower develops along the particle's trajectory, so determining the shower axis is equivalent to measuring the trajectory. In the ACCESS design of Figure B.1-1, every alternate BGO layer is oriented perpendicular to the adjacent layers, providing twelve measurements of the shower core. Analyzing the distribution of energy deposition across a single layer determines the centroid of the shower. Fitting these centroids determines the shower axis. In addition, there are two additional scintillator layers (S2 and S3) in the middle and at the bottom of the target/tracking section and each of these, like S1, are composed of an x-y pair of planes of scintillator strips. Signals are read from both ends of the strips providing a redundancy in determining the location of a particle's path or the axis of a developing shower. Combining the BGO, scintillators and Si-matrix provides the information to be compared to the data available from the TRD and CM. For events that enter at an angle and do not traverse the CM or the full TRD, the CAL has the ability to measure the charge, energy, and trajectory of the event.

It should be noted here that the scintillators (S1, S2 and S3) provide the first-level trigger for the CAL. This coincidence determines the geometrical acceptance of the instrument. If a particle does not interact and generate a cascade, the BGO would not provide the second-level shower trigger and the event would be discarded.

A refinement to the CAL concept, not included in the baseline, is the addition of layers of scintillating fibers, e.g. 1-2 mm^2 fibers, which would provide even finer resolution of the shower

core and thereby improve the trajectory resolution. Such an addition will be considered later, as the ACCESS project is developed further.

B.1.3. Detector readout electronics

There are a large number of channels to be read from the CAL, particularly when the large dynamic range is considered. For a 1-m × 1-m CAL, each of the scintillator layers consists of 100 strips, 50 in the X and 50 in the Y direction. Each strip is read out with a photomultiplier tube (PMT) on each end. To cover the dynamic range from Z=1 to Z=28, two dynodes from each PMT must be pulse height analyzed. This gives 400 channels of information per scintillator layer and 1200 channels in total for S1, S2 and S3. In addition, the 600 anode signals are utilized to form the first-level trigger to select events within the instrument acceptance.

For the Si-matrix, assuming each pixel is 2 cm x 2 cm (the exact size of a pixel may be less than this), there will be about 3200 separate detector units when the necessary overlap is taken into account. Each of these must be read out and then interrogated to determine which ones contain a signal to be pulse height analyzed. To cover the dynamic range from H to Ni, each pixel must be analyzed in two separate gain ranges, giving a total of 6400 channels.

The baseline BGO stack contains twelve layers, each of which has 40 crystals, each 2.5-cm x 2.5-cm x 100-cm crystals. These are read out on both sides via photodiode detectors, a sketch of which is shown in Figure B.1-3. The dynamic range extends from the energy deposit of several minimum ionizing particles to the maximum energy deposit that could occur in the center of the cascade due to the highest energy particle to be measured. This latter value has been determined from simulations, with the result that the dynamic range exceeds a factor of 10^6. This can only be handled by multiple readout channels, and Figure B.1-3 shows three separate photodiodes attached to one side of one crystal. This implies 240 channels per BGO layer and a total of
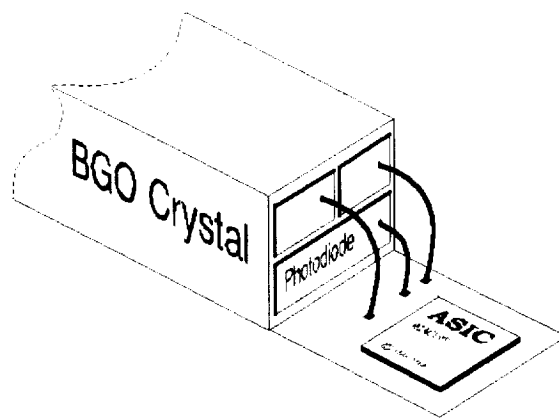
Figure B.1-3. Schematic representation of the readout of one side of a BGO crystal.

2880 channels for the full calorimeter. An alternative design, depending upon procurement limitations and mechanical packaging considerations, divides each crystal into two pieces, i.e. two 2.5-cm x 2.5-cm x 50-cm crystals, mounted adjacent to each other with a support structure in

the center. Each crystal is still read out with three photodiodes, so that the number of channels remains unchanged.

There is, however, some remaining ambiguity in these estimates since the final size of the calorimeter depends upon the total mass available to the CAL instrument. This mass varies depending upon the size and mass of the other two instruments and the estimated weight for the structure, avionics, radiators, etc. For example, in a lighter configuration, the CAL is reduced to 0.9 m x 0.9 m, which decreases the number of scintillator and BGO channels to 1080 and 2592, respectively. Similar scaling applies to the Si-matrix.

The overall CAL requires handling $\sim 10^4$ channels of information which, in turn, requires the use of application-specific integrated circuits (ASICs) to minimize the power consumption and the weight of the electronics. The use of ASICs then entails relatively sophisticated control logic and digital data handling. A schematic diagram of the readout system electronics is shown in Figure B.1-4. Beginning at the right side with the active detectors plus their PMT or photodiode readout, the chains proceed to the left to the DCU, which provides the event data for the instrument readout/ACCESS data interface unit to the ISS. The ASICs are contained in the blocks labeled FEMs (front end modules), which take the analog signals from the detectors and convert them to digital data. The ACLBs (ASIC control logic board) provide all of the setup, clock timing, and other signals required to operate the ASICs and pass the digital information to the digital interface module (DIM). The DIM/ACLB also passes command and control information to the FEMs. The division between functions in Figure B.1-4 indicates physical location as well. The FEMs must be physically close to the photodetector readout devices, while the ACLBs and DIMs can be mounted elsewhere and cabled to the FEMs. Note that one ACLB can service a number of FEMs; and, likewise, one DIM can handle multiple ACLBs.
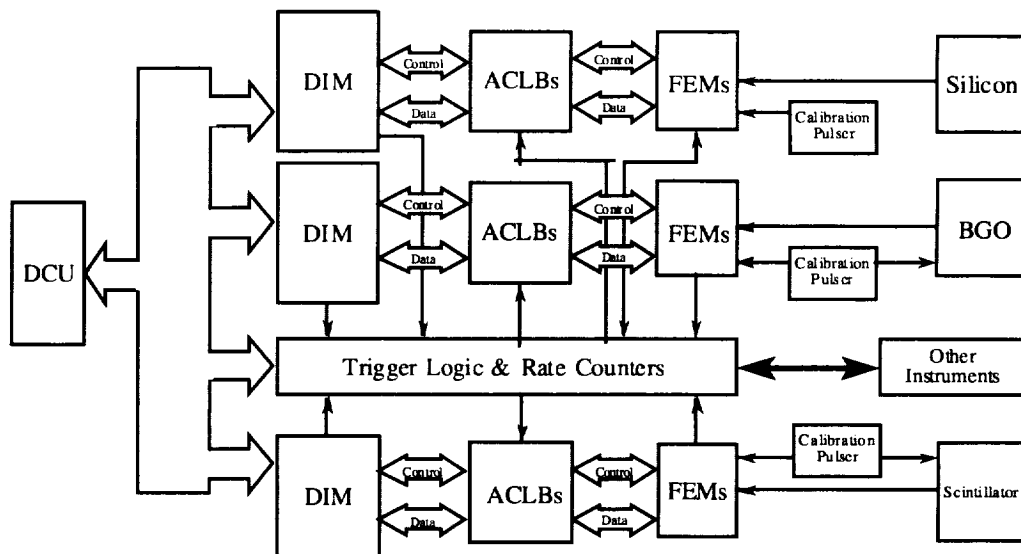
Figure B.1-4. Readout electronics for the CAL detector subsystems.

102

The readout of an event is inherently asynchronous, started by the arrival of a cosmic-ray particle. This is controlled by the trigger logic module, which also provides overall normalization through the use of rate counters. The trigger must start the readout based upon the first-level trigger derived from the scintillator signals. The somewhat slower BGO signals are used to determine the size of the shower, which then classifies the event. For low-priority classes (e.g. low energy) only a small fraction will be transmitted to the DCU. The rate counters will count the rest, but the readout will be terminated and the FEMs reset to await another cosmic ray. This reduces the data volume coming from the CAL and minimizes the deadtime of the instrument.

There are at least two separate types of ASICs involved in the readout. Based on the experience with the balloon prototype, ATIC, one ASIC should be able to handle the scintillators and BGO readouts while a second type of ASIC will be required for the Si-matrix detector. (The corresponding ACLBs will, of necessity, differ as well.)

In ATIC, the ASIC for the Si pixels is a new derivative of a chip originally developed for DESY called Amplex[60-61]. There is a whole family of Amplex derivatives used in high-energy physics. The one ATIC is developing is called CR1.4. This ASIC has 16 channels, each containing a charge-integrating preamplifier, a shaper, a hold circuit, and a discriminator. Each channel is multiplexed to an output buffer/driver. The gain of the output buffer can be switched from 1X to 10X. The dynamic range covers 1400 Mips (minimum ionizing particles in Si). Except for the discriminator and the hold circuit, this chip is analog; the output is a voltage level corresponding to the input charge of the selected channel. The conversion gain is about 5mV/Mip for the 1X buffer setting. An external ADC is required to switch each channel and digitize the signal.

The ASIC used in ATIC for the scintillators and BGO is a non-rad-hard version of a 16-channel chip developed for the ACE (advanced composition explorer) mission[62-63]. Each channel contains a charge-integrating preamplifier, a switched capacitor array (3 caps), a difference amplifier, and a Wilkinson-type run down/up analog-to-digital converter (ADC). In addition, each channel has a pickoff at the output of the preamp with a shaper and two discriminators. Each set of discriminators is OR'd for all 16 channels, giving effectively two discriminated output signals for the entire chip.

In "waiting-for-event mode," two capacitors of the array are switched into and out of the preamp output, basically switching one in while the other is out (called ping-pong). The third cap is continuously switched in at that time. An external trigger stops the ping-pong and switches the third cap from the preamp into holding mode. To digitize the signal, cap 3 and the cap that was switched off the preamp the longest time before the trigger occurred are switched to the two inputs of the difference amplifier. A constant current source begins to discharge cap 3 and a run down/up counter is started. Each channel individually stops the rundown/up once the difference amplifier reaches zero. The overall rundown/up is stopped after the maximum count of 4096 (12 bit) is reached. The ADC values are serially clocked out to the control circuit, the ACLB. The ping-pong is resumed and the process starts over, waiting for a new trigger.

B.1.4. Data rate

The data rate from the CAL is controlled by the threshold selected for full pulse height analysis. For a threshold at 5×10^{13} eV (0.5 TeV), there will be, on average, 0.26 events per second. We assume that the instrument data system will perform sparsification (eliminating

103

channels with no or low signal(s)), resulting in an average event reading out 5 strips per scintillator hodoscope layer, 4 BGO units per calorimeter layer, and 100 Si pixels. Each Si pixel requires an address plus two 10-bit ADC values; each scintillator readout involves an address plus two 12-bit ADCs; and each BGO readout requires an address plus three 12-bit ADC values. This gives 8752 bits per event and 2.3 kbps for the average event-generated data rate.

To this must be added (a) rate counter readout, (b) calibration data, and (c) housekeeping data. Assuming 64 rate counters, each of 24 bits, read every 10 seconds, the rate counter data rate is 0.2 kbps. We plan to incorporate an onboard calibration mode (pulsers) that will monitor the performance of the detectors and the electronic readout systems. Assuming a calibration "run" exercises all of the channels, there will be a high rate of 317 kbits. However, a calibration run will be needed, at most, every 10 minutes, giving an average calibration data rate of 0.5 kbps.

The housekeeping system to be developed for ACCESS will monitor voltages, currents, temperatures, and the like at various locations in the instrument and for each of the major subsystems. Periodically these data will be formatted and transferred to the data system for downlink. We estimate a volume of 3 kbits read every 5 minutes for an average data rate of 0.01 kbps.

Combining these three sources of data together, the average raw data rate from the CAL will be very modest, just over 3 kbps. These data will need to be formatted for transmission to the ISS and we are assuming use of CCSDS (Consultative Committee for Space Data Systems) encoding. We assume that housekeeping data are transmitted frequently via the ISS 1553B link. The event and calibration data may need to be buffered for infrequent transmission via the fiber optic link. Each of these requires some overhead. Allowing a 33% margin for overhead and growth, the CAL is not expected to average more than 4 kbps.

B.1.5. Power consumption

The total power required for the CAL instrument is composed of a number of parts, not all of which are fully specified at this time. In particular, the power involves (a) instrument operation, (b) data handling, (c) voltage conversion, and (d) thermal control (heaters). Several of these require further definition of the overall payload and its subsystems before accurate estimates can be assigned.

The power for instrument operation is perhaps the best known, but still depends upon the actual power consumption of the ASIC chips to be developed for the ACCESS program and assumptions about the needed ACLB. Based upon the balloon prototype, we assume ASICs can easily be developed with power consumption of 2 mW/channel for the Si-matrix and 10 mW/channel for the scintillators and BGO readouts. Further, we assume 8 W for ACLB to handle these ASICs (but this is only a first estimate). Combining these with detector bias, ADCs, and DIMs, we obtained the following estimates:

Si-matrix	27 W
Scintillators	32 W
BGO stack	36 W

for a total detector power of 95 W. (The uncertainty here may be a factor of two depending upon the ASIC, the complexity of the FEMs and ACLBs, and the actual layout of the flight systems.) To this must be added the power needed for the DCU, the housekeeping system, the control systems, trigger logic and rate counters, and the calibration system (pulsers and controls). The estimates here are also uncertain but a minimum requirement is 25-30 W. This gives a total instrument operating power of 120-125 W as a minimum (with ~200 W as the worst case).

The extent of the data system required by the CAL depends upon the capabilities of the avionics that interface with the ISS data systems. This remains undefined, so that the CAL may require a data system that can range from a simple buffer to a sophisticated large-scale memory and processing unit. Power consumption may range from 10-30 W, depending upon the complexity of the system.

This total of 130-155 W is actual power being consumed at the appropriate voltages. These voltages include ~1 kV for the PMTs, ~100 V for the Si and photodiode bias, and ±5, ±7.5, 12 and ±15 V for the electronics. Beginning with a 28 V power system (such as is used in the balloon payload) an average conversion efficiency utilizing commercial DC-to-DC converters is about 65%. This implies the need for 200-240 W of input power at 28 volts.

The ISS, however, provides power at 120 VDC, nominal, to the attached payloads. Converting this to 28 VDC involves another loss due to conversion efficiency. If such is to be done within the CAL instrument, the raw power input to the CAL increases by 20%-25%.

Finally, there is the question of thermal control. Almost certainly some heaters will be required to minimize gradients and to maintain the instrument temperature. Depending upon the thermal control system (TCS) capabilities, this heater power can range from 10 W to as high as 100 W. Specifying the TCS, and determining the level of heater power required, is one of the high-priority tasks for ACCESS.

B.1.6. Thermal considerations

The CAL instrument requires a relatively constant temperature with minimal thermal gradients throughout the BGO. This is because the light output from BGO is temperature dependent. We are planning to monitor the temperature continuously, but do not believe it is desirable to correct every event for a different temperature. Therefore, we are baselining a temperature variation of:

> < 1-2°C per orbit
> < 2-3°C per 45-50-day period
> < 5°C per year

where these apply specifically to the BGO volume.

The desired operating temperature for the CAL is ~10°C, with a desired range of 0-20°C. The full operating range limits are:

	Min. (°C)	Max. (°C)
Si Matrix	-25	+30
Hodoscopes	-25	+30
Calorimeter	-10	+30
DCU	- 5	+40
Instr. Control Elec.	-20	+50

The operating temperature gradients should be:

Si-matrix	< 2°C across the detector
Scintillators	< 5°C " " "
BGO	< 2°C " " "

Finally, the survival temperature ranges have been estimated to be:

	Min. (°C)	Max. (°C)
Si Matrix	-40	+40
Hodoscopes	-40	+50
Calorimeter	-40	+50
DCU	-45	+75
Instr. Control Elec.	-55	+85

The above are the initial estimates to be used in the early planning and development process. These will be refined as additional design work is performed and the hardware is developed.

B.1.7. Science results

The number of events to be observed by ACCESS have been estimated from fits to the available data above 50 GeV/nucleon. The proton differential energy spectrum at high energy is proportional to $E^{-2.75}$ while the He spectrum is flatter, proportional to $E^{-2.66}$. For heavier nuclei, (C, O....) we have assumed an energy dependence identical to He (i.e. $E^{-2.66}$) scaled by the relative abundance of the species relative to He.

Table B.1-1 gives the results for six different elements above four total energy thresholds for the CAL, assuming 1000 days of full exposure.

Recent results from the JACEE (Japanese-American cooperative emulsion experiment) measurements[19] indicate slightly larger spectral indices, -2.80 ± 0.04 for H and -2.68+0.04, -0.06 for He. The indices assumed above are within the quoted uncertainties on these new measurements, but the steeper spectra would reduce, slightly, the predicted number of events. Moreover, JACEE has reported[64] harder spectra for C-O and Ne-S than utilized in the above calculations. Such spectra would increase the predicted number of events in Table B.1-1 for nuclei heavier than He. Finally, the cosmic-ray nuclei (CRN) experiment[21,65] on Spacelab-2 observed a smaller number of Si at the highest energies, yielding a steep Si spectrum. This spectrum would reduce the expected number of Si events compared to the numbers in Table B.1-1. ACCESS will resolve many of these questions about the heavy element spectra.

Table B.1-1. Integral Counts for Continuous Spectra

	>50 TeV	> 100 TeV	> 500 TeV	> 1000 TeV
H	1487	442	26.4	7.9
He	1357	429	29.7	9.4
C	267	85	5.8	1.9
O	388	123	8.5	2.7
Si	148	47	3.2	1.0
Fe	279	88	6.1	1.9

Of interest for ACCESS is the limit of the SNR acceleration process. In the simplest model, the accelerator is predicted to "turn-off" at $Z \times 10^{14}$ eV. Thus, we expect a 'break' in the power law energy spectrum at about this energy. We have modified the calculations presented above to include a steepening in the spectrum by 0.3 at Z x 100 TeV (e.g. the proton spectrum

becomes $E^{-3.05}$ above 100 TeV). The expected numbers of events in this case are presented in Table B.1-2 for the same energy ranges as Table B.1-1.

Table B.1-2. Integral Counts Including Spectral Breaks

	>50 TeV	> 100 TeV	> 500 TeV	> 1000 TeV
H	1421	377	13.9	3.4
He	1336	409	19.1	4.9
C	267	84	5.2	1.3
O	387	122	7.9	2.1
Si	148	47	3.1	0.9
Fe	279	88	6.0	1.9

Note that the effects of the predicted spectral steepening are observed in the H and He event numbers at the highest energies, > 500 TeV, with a smaller effect for those > 100 TeV. For C and O, such a 'break' can just barely be observed at > 1000 TeV, and it will require the larger event statistics from the TRD at energies > 50 TeV/nucleon to establish such a spectral change. For still heavier nuclei, the assumed 'break' occurs at such a high energy that it will be difficult to observe.

Figure B.1-5 shows the anticipated results for H and He for the two cases presented in the tables. Plotted is the flux that would be measured by the CAL multiplied by $E^{2.5}$ and compared to a compilation of previous results. The solid squares show the effect of the spectral 'break' when compared to the open squares, which represent continuous spectra. The error bars are statistical uncertainty only and the flux values are multiplied by $E^{2.5}$. The open squares assume no break in the spectrum, while the filled squares assume that the spectral index steepens by 0.3 at a total energy of Z x 100 TeV.
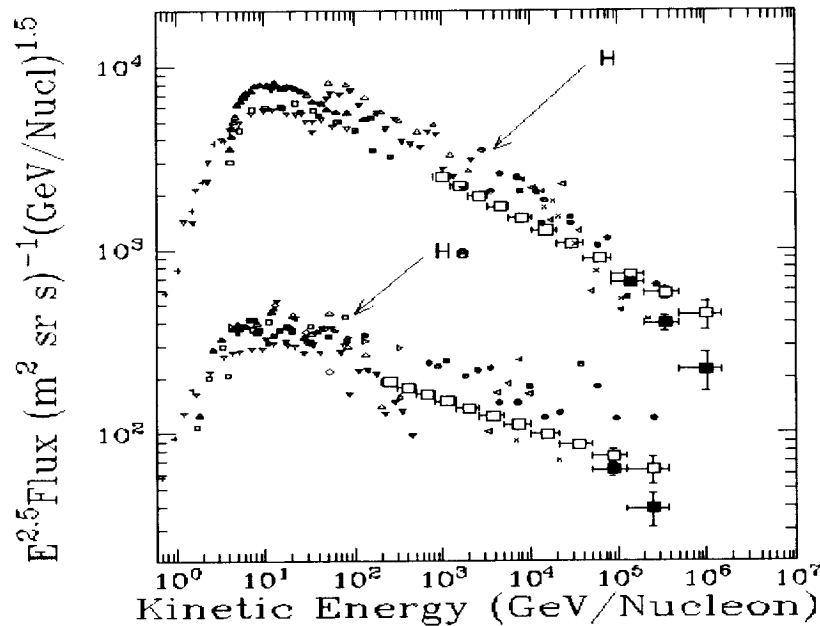

Figure B.1-5. H and He results (large squares) estimated for a 1000-day ACCESS mission compared with previous data.

Achieving good statistical precision at the highest energies is clearly necessary, and this is the goal for ACCESS on the ISS.

B.2. The charge identification module (ZIM)

The following description of the ZIM for ACCESS is adapted from a preliminary instrument description[66] prepared by the University of Washington instrument team in support of the two ACCESS program studies[7,8], as members of the Accommodation Study Team[7] and the science instrument definition team[8]. It has been shortened to fit the format of Appendix B for this report.

B.2.1 Instrument concept

The ZIM has as its primary objective the measurement of the cosmic-ray abundance of every individual element in the interval $26 \leq Z \leq 83$ with accurate element resolution and with sufficient collection power to give excellent statistical significance. This instrument will, for the first time, determine the full element-by-element composition of cosmic rays, throughout the heavy two-thirds of the periodic table. This will provide data for definitive tests of theories regarding sites and mechanisms for cosmic-ray acceleration. In addition to unambiguous determination of Z, the system will also define the energy E of the cosmic rays in the interval of approximately $0.3 \leq E \leq 20$ GeV/nucleon. Finally, the detectors will measure the actinide elements, $_{90}$Th and $_{92}$U, although limitations on the size of ACCESS will limit the statistical significance of these data.

The complement of detectors included in ZIM will also resolve individual charges in the interval $10 \leq Z \leq 26$. In this region, the instrument can determine energies up to at least 10 and possibly 100 GeV/nucleon, which will complement the higher-energy data from the TRD described in section B.3.

The UH configuration is also expected to serve as the CM for the full ACCESS instrument. The dynamic range of the Si detectors should permit measurements down to Z=1. These detectors should also serve the entire Z-range of high-energy measurement and thus provide complementary measurements to the ACCESS calorimeter (sectionB.1) and TRD modules.

B.2.1.1 Design drivers

There are a number of detector qualities that drive the design of the detector. This includes minimizing the weight, power, and bit rate without compromising experiment objectives. Other items that are important in the instrument design are:

1) Minimize material traversed by the cosmic rays. This will minimize the number of nuclear interactions, which increases the number of good particles that we can collect while reducing the number of interacted particles which must be effectively rejected in the data analysis.

2) The material in the beam must be as uniform as possible. Non-uniform materials result in the creation of differing amounts of knock-on electrons for particles traversing different locations within the detector. This results in variations of signal from the detectors and reduces the charge resolution that can be obtained.

3) The radiator or detector active area must be maximized, to maximize the number of particles that can be collected.

4) There are two light-collection boxes. These should have the maximum surface area possible covered by PMT photocathodes to optimize light collection. That is, as many 5-inch tubes as possible should ring each of the light-collection boxes.

5) The Si detectors will probably be pixelated, which will give the capability to detect and identify Z=1 nuclei. In addition, if a detector starts drawing a large leakage current, it usually would limit the detector loss to a single pixel.

B.2.1.2 Overall instrument description

The instrument under study utilizes Si dE/dx detector arrays, two Cerenkov counters with radiators of different refractive index to measure velocity, and a scintillating fiber hodoscope for trajectory determination. Figure B.2-1 shows a cross-sectional drawing of the baseline instrument. The overall dimensions of the detector are 2.5 meters square by 0.5 meters deep. This instrument provides a useful radiator area of ~206 cm square and a total geometry factor for entry in one direction of 8.7 m^2sr. The fiber outputs are only shown for the left half of the instrument so that the other detectors can be seen. Figures B.2-2 and B.2-3 illustrate an exploded three-dimensional view.
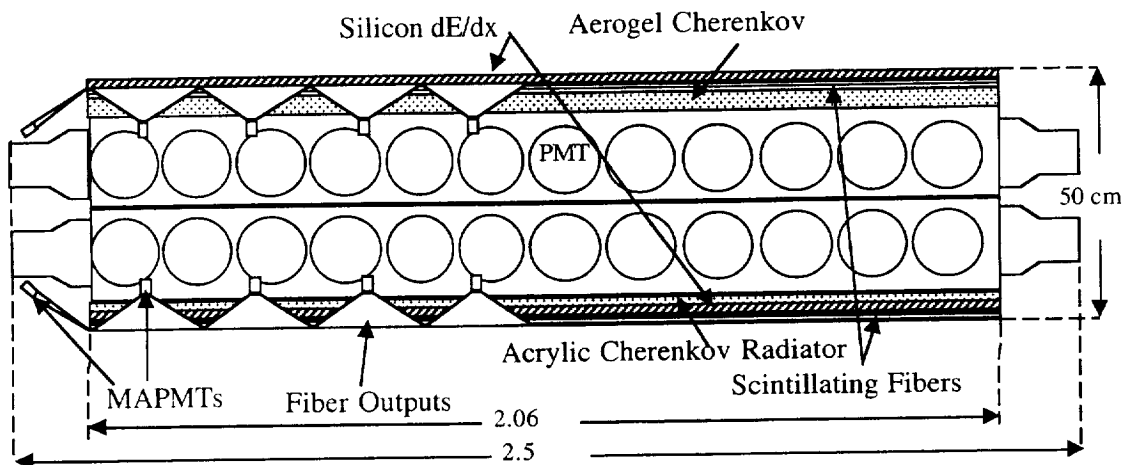
Figure B.2-1. ZIM instrument cross-sectional view. The fiber outputs (triangular regions) and MAPMT (multi-anode PMT) readouts are shown only on the left half of the instrument for clarity.
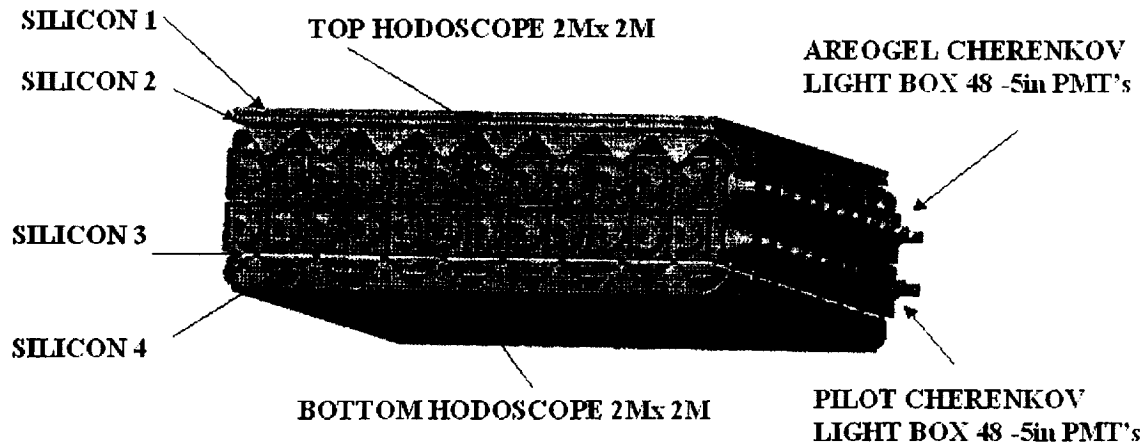
Figure B.2-2. A three-dimensional view of the ZIM instrument.
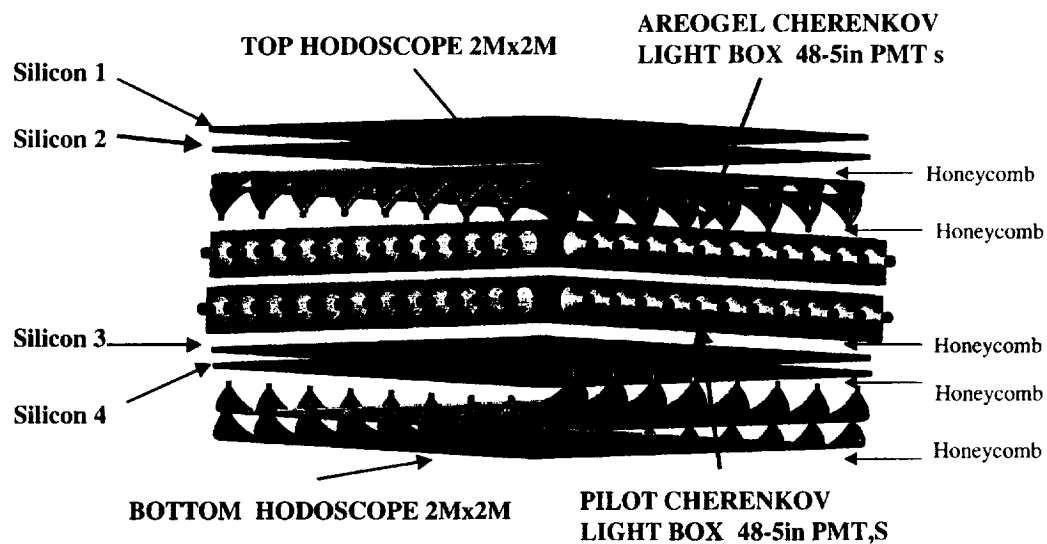
Figure B.2-3. An exploded three-dimensional view of Figure B.2-2 above.

Going from top to bottom, the order of the detectors is as follows:

1. Si detector layer 1
2. Si detector layer 2
3. Top fiber hodoscope (layers x and y)
4. Aerogel Cherenkov counter
5. Acrylic Cherenkov counter
6. Si detector layer 3
7. Si detector layer 4
8. Bottom fiber hodoscope (layers x and y)

B.2.1.3 Basic mechanical structure

Figure B.2-4 depicts the Cerenkov light box sidewall construction. In the current concept the sidewall is fabricated out of aluminum. The structure is hogged out of the aluminum and has the dimensions shown in the drawing. In this drawing the sidewalls for the two light boxes are shown as an integral unit. The weight of this wall is 22.2 lb. It is more likely, however, that these will be separate as shown in Figure B.2-3 to facilitate detector testing. Thus the sidewall for one light box would weigh around 12 lb. The strawman configuration assumes that these two boxes are separate and will be bolted together at their adjacent flanges.
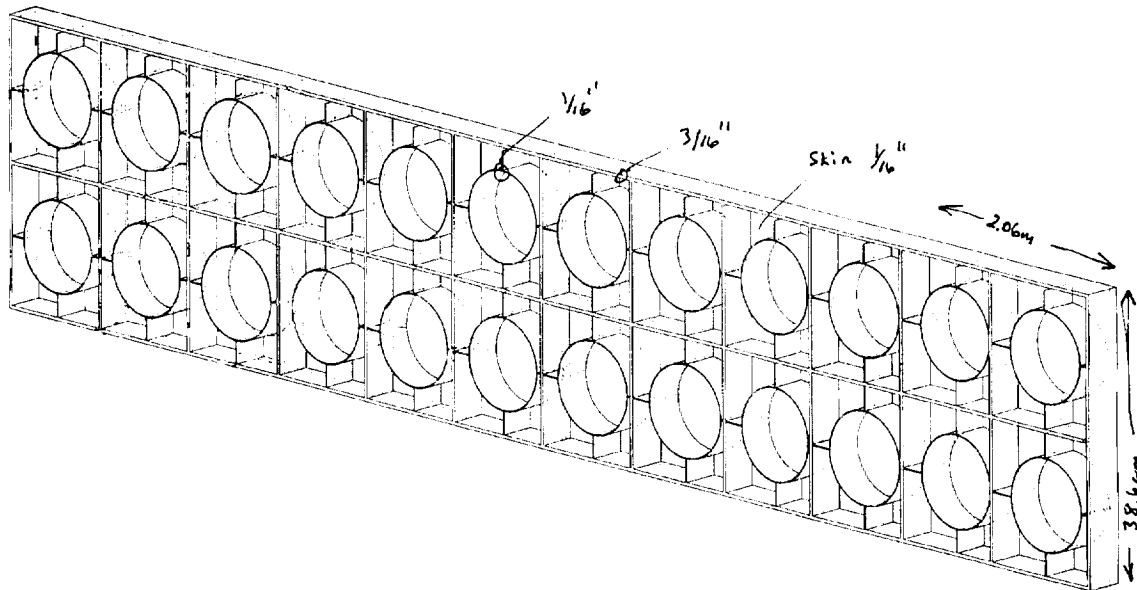
Figure B.2-4. The Cerenkov light box sidewall construction.

It is anticipated that the top Si and fiber hodoscope will require a support plate. It appears that it is not possible to use a lightweight foam support panel (which would provide the best material uniformity) since there appear to be none that is space-qualified. That being the case, the recommendation[8] is to use an aluminum honeycomb panel with thickness 0.5 inch, facesheets of 0.020-inch aluminum, a core web size of 3/8 inch, a web thickness of 0.002 inch, and an adhesive FM-73 made by Cytek. The adhesive has a nominal thickness of 0.0035-0.005 inch and has an average fillet thickness of 0.002-0.005 inch. (This corresponds to an areal density of 0.0122 g cm^{-3} for each adhesive layer and an adhesive density of 1.13 g cm^{-3}.) The weight of the adhesive is 0.020-0.030 lb ft^{-2}. It is preferred that the facesheets be made of 0.010-inch aluminum instead of 0.020 inch to minimize interactions. A 0.5-inch-thick core is assumed as the strawman for ZIM. To use a support plate this thin will probably require a center support post that runs vertically throughout the instrument. With that support post, the estimate is that the displacement under Space Shuttle loads would be ~0.01 inch, which at this time appears acceptable.

At present five such support plates are assumed to be required (locations indicated by the honeycomb label and arrows on Figure B.2-3). The first would be beneath the top two Si planes and would support them; the second would serve as the support for the top fibers and the top of the box for the aerogel Cerenkov (with a separate thin aluminum bladder for a light seal probably

111

on the aerogel box); the third would serve as the bottom of the box for the acrylic Cerenkov (again with a separate aluminum bladder for a light seal probably on the aerogel box); the fourth would be the support for the bottom Si planes; and the fifth would be the support for the bottom fiber planes.

Figure B.2-5 shows a corner support that would be used as the vertical structural member to tie the experiment together and as the mount to the TRD detector below. One of these would be located at each of the four corners of the ZIM instrument. These would also serve as the
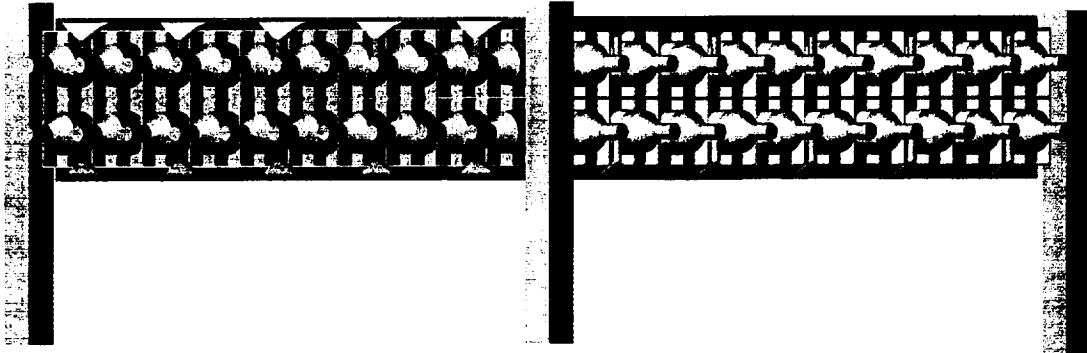
Figure B.2-5. Illustration of a corner ZIM support.

attach points for ZIM to the Space Shuttle and Space Station payload support carrier. The JSC/Lockheed Martin Accommodation Study has suggested additional attachment between the center of each of the ZIM sidewalls and the mounting structure. It appears that four such attach points, each of which would be centered both vertically and horizontally on the ZIM instrument, can be accommodated.

B.2.2 Instrument detectors

B.2.2.1 Silicon detector

The ZIM instrument uses arrays of Si detectors for dE/dx measurements. There are four planes of Si arrays with two planes on top and two near the bottom of the detector stack (Figures B.2-1 through B.2-3). Each plane of Si detectors is composed of an array of 10-cm-square Si wafers with thickness 380 μm. For the two top and two bottom detectors, each 10-cm wafer in the second plane is located directly below the detector in the first plane in the strawman concept. (On the bottom two Si planes, the two planes may be offset in X and Y to achieve 100% coverage if it is important, but at present this is not being done.) The result will be an incomplete coverage ($\geq$90% coverage) but will provide a known, uniform thickness for all particles that traverse the active area of the top (and bottom) Si planes. Each of the 10-cm wafers will be segmented into a 7x7 pixel array (other segmentation may be considered) with each pixel having dimensions 1.4 cm square. This reduces the capacitive noise on the Si detector, thus making it possible to extend the dynamic range down to Z=1. This will be useful for calorimeter events in distinguishing the primary particle from backsplash particles and in identifying the charge of the primary particle. In addition to providing dE/dx measurements, the Si detectors also serve as a coarse hodoscope which will be used for consistency checks on the fiber hodoscope described below.

112

A top view of a 1-m^2 panel for a single Si plane would show each plane consisting of four 50-cm subpanels, each of which hold a 5x5 array of 10-cm-square Si detectors. The plan is to mount the detectors on a C fiber substrate that is supported by a support frame. Because this is a secondary instrument structure, such a lightweight material is not subject to the more stringent safety review criteria discussed under Table 3 in the main text of this report. The 50-cm frame would also be a C composite frame. The two Si planes on top (or bottom) would be stacked and optically decoupled. The stacking method is TBD. This concept is described in more detail in Table B.2-1.

Table B.2-1. Silicon Detector Layout Concepts‡

Module configuration	0.5 m x 0.5 m tray with individual G-10 mounts;
	C fiber frame
Circuitry location	On C frame or on bottom of substrate
Si Detector size	10 cm x 10 cm
Active area	-9.6 cm x 9.6 cm
Detector thickness	0.38 mm
Number of detectors	100
Number of pads/detector	49
Pad size	1.4 cm x 1.4 cm
Total channels per m^2	4900
Readout	New VLSI
Threshold	0.5 mips (70keV)
Full Scale	20K mips (3 GeV)
Power per ADC	≤1 mW
ADC power per m^2	≤10 W
Leakage current/pad	< 1 mA
Bias	-100 V
Leakage current power per m^2	< 1 W
Coverage	90% top and 90% bottom
dE/dx measurements	2 top and 2 bottom for ≥90% area
Uniformity	100%
Detector mass	0.9 kg
G-10 mass	2.7 kg
C mass	0.3 ?
Detector cost per m^2	$0.3M

‡ All quantities are per square meter and one layer of coverage.

The possibility of offsetting one of the Si layers in the bottom Si detector to provide 100% coverage for calorimeter events has also been considered. Although this is still a possibility, it is not included in the baseline concept since it is not clear how important that change is to the calorimeter and its implementation is somewhat more difficult.

To measure cosmic rays of atomic number 10 to 100 at all energies above 300 MeV/nucleon at incident angles from 0 to 60 degrees requires a dynamic range of approximately 300. The charge-sensitive preamplifier must provide adequate dynamic range while minimizing the contributions

from electronic noise. Existing ASIC designs now in space on ACE and in the ATIC balloon payload have solved these dynamic range and noise problems. With such ASICs the power requirement will not exceed about 4 mW per channel. These and other ASICs are now being evaluated for use on ACCESS. It is expected that the dynamic range can be extended down to Z=1 through the use of two to three ADCs for each signal.

B.2.2.2 Fiber hodoscope/time of flight (TOF)

Just inside of the top Si array and at the bottom of the detector stack are two planes of a coded scintillating fiber hodoscope. Each plane of fibers is composed of two layers of ~0.5-mm fibers, one layer for x- and one for y-coordinate measurements. Each of the four hodoscope layers has fibers combined into eight modules, each with width ~26 cm. The fibers in each module are read out using a 16-element MAPMT (Hamamatsu 5900-016) at either end of the fibers. Adjacent fibers are grouped in pairs (elements) and are coded differently at opposite ends such that the position of a particle traversing the ~26-cm width of 512 fibers (256 pairs) can be unambiguously resolved to within 0.3 mm. Thus, to read out the four fiber layers, 64 MAPMTs with a total of 1024 channels are required. The possibility of using the ACE-ASIC (16 channels/ chip) to read out the MAPMTs is under study. The bottom fiber hodoscope is identical to the top hodoscope.

There is a possibility that the Space Station may be pointed such that the vertical axis of ACCESS may be pointing at angles of 10 to 20 degrees from the zenith in its torque equilibrium attitude (TEA). This will result in an increased number of particles entering the detector from the Earth side of the instrument. In view of this, a TOF counter that measures time of flight with precision sufficient to distinguish upward from downward moving particles is probably needed. It is included in the strawman ZIM instrument. The sensor for the TOF counter would be identically the same fibers and MAPMTs as used for the hodoscope. There is a single dynode signal that is brought out for each MAPMT. One way of implementing the TOF would be to use that dynode signal for the TOF measurement. The electronics downstream of the dynode signal is TBD.

B.2.2.3 Aerogel Cerenkov counter

A Cerenkov counter with a 3-cm-thick aerogel (n~1.04) radiator in a light-collection box is to be mounted just below the top fiber detector. The aerogel radiators that Caltech has in-house are 55 cm square in size. Thus the radiator would probably be a 4x4 array with the individual radiator cut to fit. A graphite-epoxy frame will be used to support the aerogel. The aerogel would be supported in the frame using ~1-mm-thick Silgard pads for dynamic isolation. The aerogel density is 0.22 g cm^{-3}. The interior of the box must be white. The light box is viewed by 48 five-inch PMTs as shown in Figures B.2.1-B.2.3. The PMTs that have been assumed for the purpose of size and weight estimates were the Hamamatsu R877-04 tube used on the high-energy X-ray telescope experiment (HEXTE). The actual tube that would be used is TBD. The weight, including potting and magnetic shielding, would be ~1.2 kg/tube. The threshold energy for this detector would be 2.4 GeV/nucleon, and thus could enable it to distinguish nuclei that have energy higher than minimum ionizing from those that are on the low energy branch. Two or three ADCs for each PMT to cover the required dynamic range would probably be required. The aerogel detector weight estimate is 29 kg for the aerogel itself, 4.1 kg for the mounting frame, plus ~2.5 kg for adhesive and miscellaneous hardware. Table B.2-2 gives a more detailed weight breakdown.

Table B.2-2. ACCESS Aerogel Mounting Weight Estimate

Aerogels	55 cm x 55 cm x 3 cm
Volume	9075 cm^3 per block
x 16 blocks	$\cong$ 145,200 cm^3 total volume
x 0.2 gm cm^{-3}	$\cong$ 29 kg (~ 64 lbs) total mass
Mounting frame	
Volume	2,344 cm^3
Density	1.76 gm cm^{-3}
Mass	4.1 kg (~ 9 lbs)
Additional items:	
Top CFRP constraints	~ 1 kg
Sylgard coating	~ 1 kg
Assembly hardware	~ 0.5 kg
Total aerogel mounting weight	6.6 kg (~ 15 lbs)

A NASTRAN structural analysis of the aerogel holding frame and the aerogels themselves mounted in the frame, under 1-G traverse loading has been carried out. The modulus of the C fiber frame was adjusted to keep the maximum center deflection at 0.3 mm without a center support. The current frame design will support the aerogels with no handling fixture to move the frame from storage to the counter.

B.2.2.4 Acrylic Cerenkov counter

A second Cerenkov counter located immediately below the aerogel Cerenkov counter uses an acrylic-based radiator with a refractive index of about 1.5 in an essentially identical light-collection box to the aerogel box. The radiator which we plan to use is composed of ultraviolet-transmitting acrylic with Bis-multi-sideband waveshifter dye added to isotropize the light and shift the ultraviolet component of Cerenkov light to longer wavelengths where PMTs have greater sensitivity. The density of the acrylic material is 1.18 g cm^{-3}. This counter would also be viewed by 48 five-inch PMTs. The threshold energy for this detector is 0.3 GeV/nucleon. Signals from this counter will be used as the primary charge identification for nuclei with a saturated aerogel Cerenkov signal. We would also expect to use two or three ADCs for each PMT to cover the required dynamic range.

B.2.3 Weight estimate

The current weight estimate is given in Table B.2-3. The instrument vertical height estimate is given in Table B.2-4. As one can see, it adds up to 56 cm, not the allotted 50 cm for the ZIM baseline. This is being worked at the time of writing this report.

Table B.2-3. ACCESS ZIM Instrument Mass Estimate

PMT (cm)	16						
Length (cm)	206						
Width (cm)	206						
Height (cm)	20	(light box)					
C0	PMTs	mass (kg)				Total (kg)	
	40	1.3				52.00	
	radiator	density (g cm^{-3})	thickness(cm)	mass (kg)			
	1	0.2	3	25.46		25.46	
	box						
	0.5					23.00	
							100.5
C1	PMTs	mass (kg)			detectors		
	40	1.3			1	52.00	
	radiator	density (g cm^{-3})	thickness(cm)	mass (kg)			
	1	1.18	1.27	63.59	1	63.59	
	box						
	0.5					23.00	
							138.6
Hodoscope	PMTs	mass (kg)					
	2	0.06			32	3.84	
	fibers	density (g cm^{-3})	thickness(cm)	mass (kg)			
	panel	1.05	0.05	0.36	32	11.51	
	support	0.08	1.27	0.54	32	17.25	
							32.6
Si							**50.0**
Electronics							**15.0**
Misc. Structure							**25.0**
TOTAL							**361.6**

Table B.2-4. ACCESS ZIM Instrument Height Estimate‡

Detector	Vertical Height (cm)
Si	3
Honeycomb	1.3
Fiber	1.3
Honeycomb	1.3
C0	22.7
C1	19.3
Honeycomb	1.3
Si	3
Fibers	1.3
Honeycomb	1.3
Total	**55.8**

‡ Aerogel and holding fixture take up 3.4 cm vertical space.

B.2.4 Electronics system

The electronics block diagram is shown in Figure B.2-6. The ZIM electronics subsystem provides science sensor data acquisition and control, instrument status monitoring, event trigger information for the ACCESS facility, and C&DH functions. Interfaces to the ACCESS facility include a data bus and command interface with the ZIM as a remote terminal, a dedicated trigger interface for coordinating triggers with the other instruments on ACCESS, and a 120 VDC power interface.
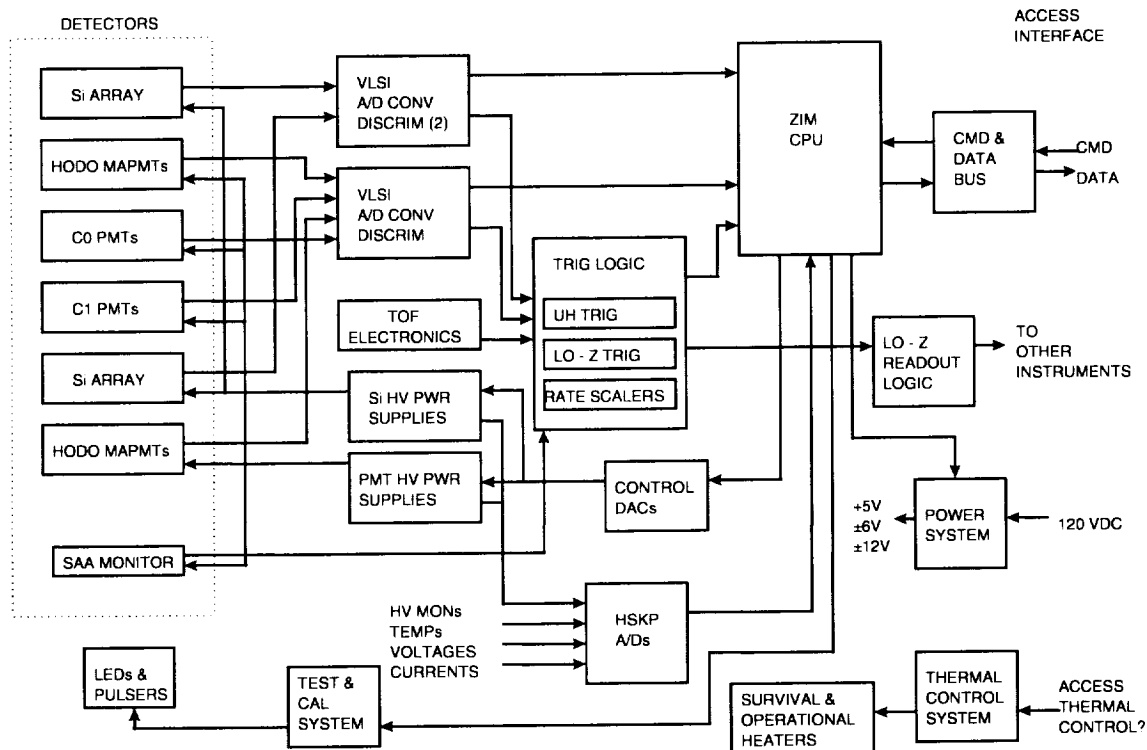
Figure B.2-6. ZIM electronics block diagram.

There will also be an interface for heater power, both active and survival (keep-alive). All data will be transmitted over the data bus to the ACCESS command and data handler for final packetization, storage, and telemetry. All commands to the ZIM will be via the data bus. The ZIM central electronics unit (CEU) will be based on a central processing unit (CPU) and will perform all command and data processing functions. We anticipate that the CEU software will be written in the C-language. The front-end electronics will include three distinct ASICs for sensor readout. The ASIC for the PMT pulse-height analysis will be based on a commercially available circuit originally used in the ACE. The Si detector ASIC is currently being designed by the California Institute of Technology, GSFC, Jet Propulsion Library, and Naval Research Laboratory collaborators. A third ASIC will be used for the TOF system and is in preliminary design by GSFC collaborators. The trigger logic unit will make extensive use of field-programmable gate arrays for trigger definition and ASIC control during event readout. An extensive electronic and light-stimulation calibration system will also be provided to monitor the performance of the

117

sensors, both in test and on orbit. The high-voltage power supplies will provide bias voltages to the PMTs, ranging from 800V - 1800V. The current requirements are minimal and these supplies can be similar to those flown on previous missions. The nominal Si bias voltage is 100V, which is compatible with the bus voltage of 120V.

B.2.5 Power and data

The power estimate is shown in Table B.2-5. Total power is 120 W. The power dissipation in the Si detector is assumed to be uniform over the top and bottom Si planes. Power is dissipated in detector leakage current and front-end electronics. For the two Cerenkov counters (C0 and C1) power is dissipated mainly in tube bases and front-end electronics. For the fiber hodoscope, power is dissipated in tube bases and front-end electronics. The CPU, logic and power conversion electronics can be located wherever it is most convenient or wherever it optimizes overall ACCESS thermal control.

Table B.2-5. ACCESS ZIM Instrument Power Estimate

	# Devices	Device power (W)	# HVPS	HVPS power (W)	# Channels	Channel Power (W)	Total (W)
C0	40	0.02	4	0.2	80	0.007	2.2
C1	40	0.02	4	0.2	80	0.007	2.2
Hodoscope	64	0.04	16	0.16	1024	0.007	12.3
TOF							20.0
Si pixel	1600	0.00005	16	0.005	78400	0.0005	39.4
Digital							20.0
Subtotal							96.0
Power Conversion							24.0
Total							**120.0**

Several approaches have been discussed regarding the data readout. A decision is pending further study. Preliminary analysis showed a data rate in the vicinity of 15 kbps, but this could change.

B.2.6 Performance and results

The Si detectors in the CM are critical for obtaining individual element resolution up to the highest charge in the UH region of the spectrum. Fortunately, the Brookhaven National Laboratory (BNL) accelerates gold ions to several GeV/nucleon and these can be used to study the response of the detectors to high-energy UH nuclei. The results from one such experiment are illustrated in Figure B.2-7, which shows the charge histogram obtained in a run in which the primary beam was fragmented to obtain ions of all charges.

Note that individual element peaks are well resolved down to the region of the Fe peak elements. This demonstrates, experimentally, that the Si detectors will provide the needed charge resolution for the UH nuclei studies to be performed by ACCESS.

For a 1000-day exposure on the ISS, an estimate of the number of UH nuclei that will be observed by the CM is shown in Figure B.2-8.
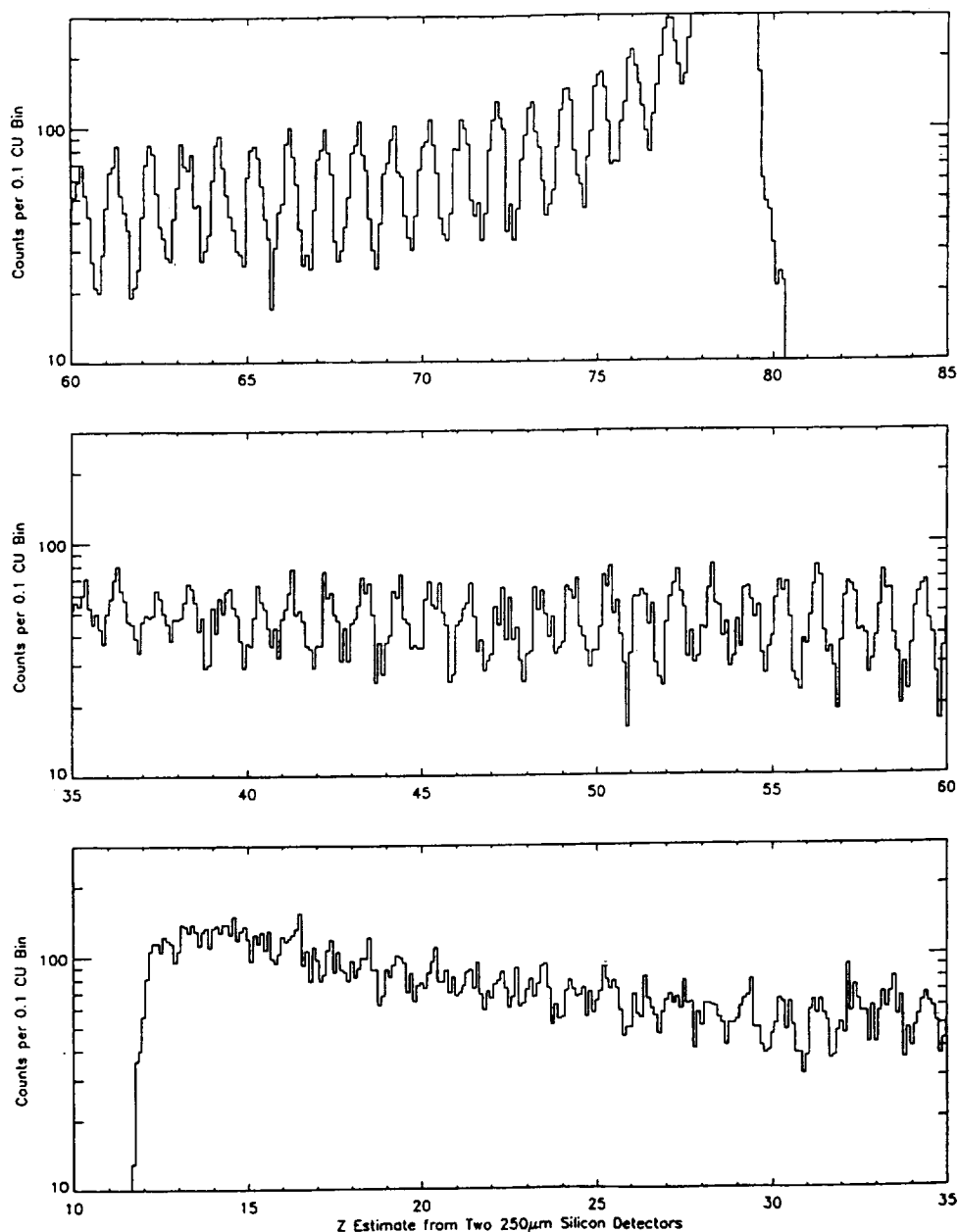
Figure B.2-7. Charge resolution in prototype Si detectors as measured at BNL using a 10.6 GeV/nucleon gold beam.

In the region up to Z=60 there will be several hundred events even for the least abundant elements and many more for the more abundant species. Significant numbers of Pt and Pb nuclei will be observed along with a few actinide elements (Th, U). Overall, these ACCESS results will be a major advance over current measurements in this important charge range.

119
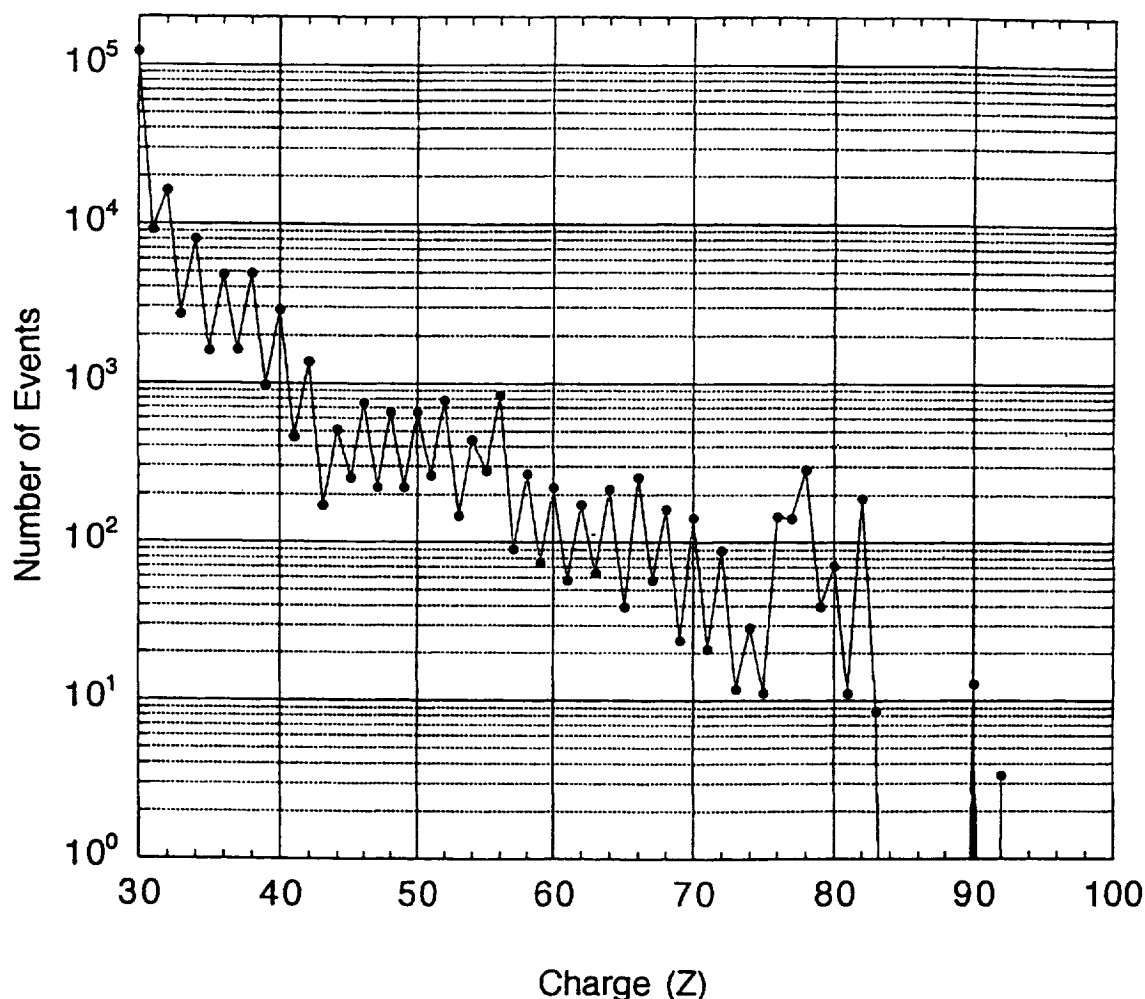
Figure B.2-8. Estimated numbers of UH events as a function of Z expected to be observed by ZIM.

B.3. Transition radiation detector

The TRD on ACCESS is intended to measure the charge and velocity (the Lorentz factor, γ) for heavy nuclei up through the Fe peak at the highest energies. The low particle fluxes at high energy make mandatory a very large exposure (geometric factor times flight time). The largest instruments used previously for observations at high energy, either on balloons or in space, had exposure factors of a few m^2sr days. Extrapolating from lower energy, for the major primary nuclei C, O, Fe we require exposure factors of ~12 m^2sr days for measurements up to 10^{14} eV/particle, but ~600 m^2sr days up to 10^{15} eV/particle. The requirements for measurements of the rare secondary nuclei are even more severe. If the B/C ratio, for example, continues to fall as steeply above 10^{12} eV/particle as it does at lower energies, (i.e. decreasing about as $E^{-0.6}$), precise measurements of the spectra to 10^{13} eV would require an exposure factor of about 60 m^2 sr days and of about 10,000 m^2 sr days for measurements to 10^{14} eV per particle.

120

Achieving large exposure factors requires a combination of long flight time, as is proposed for ACCESS on ISS, and large collecting area. The detector must measure the charge of each incident cosmic ray as well as the transition radiation signal. The need for a large area plus low weight precludes the use of a pressurized container, such as in our previous CRN experiment which flew successfully on the Spacelab-2 mission[67-68,26,21]. Much of the TRD instrument concept for ACCESS is derived from this previous space mission.

The TRD concept for ACCESS is sketched in Figure B.3-1 and consists of: (a) two square scintillators on top and bottom, (b) an array of proportional tubes of approximately 2 cm diameter and 250 cm length with alternate pairs arranged at right angles to provide measurements in both X and Y directions, and (c) A TRD consisting of 6 radiator/detector pairs. The radiator may consist of polyethylene fiber mats, and each detector would be a double layer of proportional tubes.
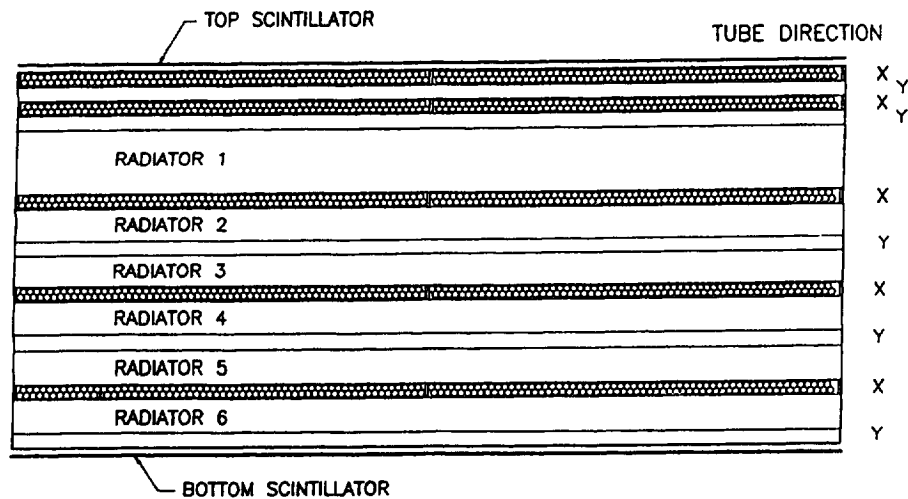
Figure B.3-1. The baseline TRD for ACCESS.

This detector can be made as large as 2.5 m x 2.5 m at a weight of about 750 kg and having a geometric factor of 8.5 m^2 sr.

B.3.1 Transition radiation

A charged particle moving through a medium radiates energy, the most common of which are bremsstrahlung and Cerenkov radiation. A related phenomenon is transition radiation, which occurs when the incident particle crosses a sharp interface between two different media and rapidly rearranges its electromagnetic field, both in intensity and spatial extent[69]. In the case of a highly relativistic ($\gamma = E/mc^2 \gg 1$) particle, most of the transition radiation is emitted at X-ray frequencies. The energy dependence of the radiation intensity is very different from that of bremsstrahlung or Cerenkov radiation. Typically, a strong increase of the transition radiation intensity is observed with increasing particle Lorentz factor γ, up to extremely high values of γ. This feature makes x-ray transition radiation very useful for the detection of highly relativistic charged particles and for measuring the particle's total energy.

121

The intensity of the transition radiation emitted at a single interface is weak and contributes a negligible amount to the energy loss of the particle. Therefore, for practical detector applications[67-68,70-72,26,21], the radiator must consist of a large number of thin foils, or a large number of transitions. Radiation is produced at each of the interfaces. The total intensity is not just the sum of the intensities from the individual interfaces, since interference effects must be taken into account, as well as absorption. In the case of a single interface, the intensity per unit frequency decreases monotonically with increasing frequency, and the total intensity is proportional to the Lorentz factor. However, for a radiator consisting of many foils, the interference effects lead to a frequency spectrum which exhibits strong oscillations, and to a saturation in the total intensity[73-75]. The detailed calculations show that the positions of the interference maxima in the spectrum are governed largely by the radiator foil thickness, and that the onset of saturation is determined by both the thickness and the spacing of the radiator foils. In order to optimize the TRD radiator for high energies, it is necessary to tune the radiator dimensions and frequency spectrum.

The theoretical expressions for the intensity in the general case of many interfaces are quite complicated. However, the key features may be summarized as follows: (a) X rays are emitted at frequencies below $\gamma\omega_r$, where ω_r is the plasma frequency of the radiator material; (b) the total emitted transition radiation increases with particle energy, approximately linear with γ, up to a saturation value, γ_s, which depends upon the radiator material (ω_r), the radiator thickness and the size of the gaps between the radiator layers; and (c) The transition radiation yield is proportional to Z^2 for a heavy particle. Explicit predictions must involve detailed theoretical calculations[74-75]. Experimentally, the observed quantity is most often the intensity integrated over all angles for which there are analytic treatments available[76-77]. For other situations, e.g. non-uniform radiator thickness or variable spacings, it is necessary to integrate the equations numerically.

One of the advantages of transition radiation is that the response depends solely on the Lorentz factor γ of the particle, and therefore can be perfectly well studied with beams of electrons and pions that are readily available at accelerators. Transition radiation is a purely electromagnetic effect and has been shown to scale perfectly with Z^2 of the primary particle. The calibration of the response for heavy nuclei can, therefore, be established without ambiguity at accelerators. Thus, radiator concepts can be readily studied experimentally as well as theoretically.

An example of the transition radiation response is shown in Figure B.3-2, where the data points represent calibration measurements made at accelerators or from CRN flight data. The signal was recorded in a multi-wire proportional chamber (MWPC). Note the Y-axis is signal/Z^2 which allows heavy ion data to be included on the same plot. The radiator in this case was a collection of polyethylene fibers (much like the fiber filling in some types of ski jackets) which provided a random set of interfaces to the particle.

The transition radiation X rays undergo photoelectric conversion in the MWPC to produce the transition radiation signal. This signal is superimposed upon the ionization signal of the particle. The straight line in the figure shows the ionization signal (measured by removing the radiator). The transition radiation signal becomes observable for $\gamma > 400$ and increases with γ until saturation is reached around $\gamma = 4 \times 10^4$. Thus, the response curve of the TRD is characterized by a signal due only to ionization loss at low energies, but increasing rapidly for $\gamma > 400$. This increase with increasing γ makes possible an accurate measurement of γ, i.e. of the energy. In units of total energy per particle, the Lorentz factor range $400 \le \gamma \le 40,000$ corresponds to about 6×10^{12} to 6×10^{14} eV for oxygen, and 2×10^{13} to 2×10^{15} eV for Fe.
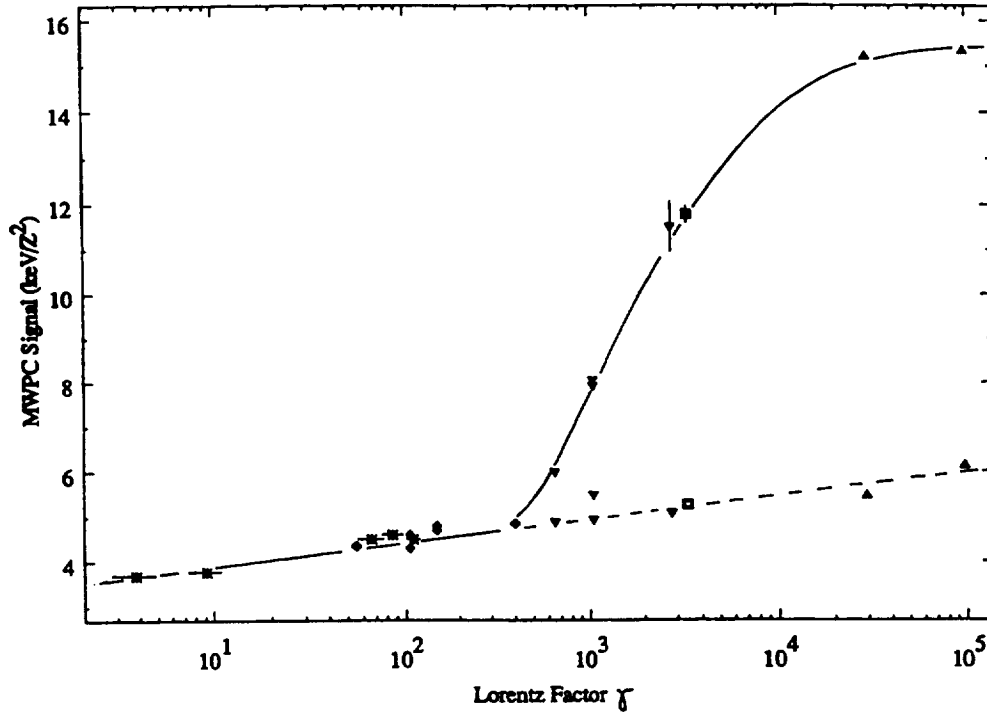
Figure B.3-2. Transition radiation signal in a MWPC as a function of the Lorentz factor, γ.

The yield for singly charged particles may be only a single photoelectron in the detector, and is subject to large fluctuations, which can be studied at accelerators. In flight, however, the yield will increase by Z^2 for heavy nuclei, thereby reducing fluctuations. Moreover, the design of Figure B.3-1 envisions many independent measurements of the transition radiation signal in the six radiator and detector layers shown. This will allow fluctuations to be analyzed from the actual flight data.

In order to determine the response of the detector quantitatively, a full Monte Carlo simulation of the TRD has been performed. The simulation assumes an isotropic flux of nuclei, reconstructs the particle trajectories, determines the ionization signals in each tube layer, and determines the X-ray signals deposited in the tubes, assuming Poisson fluctuations in the number of photons. The simulation uses the calibration curve of Figure B.3-2 for the yield of X-rays for each particle trajectory through the radiator stack. The result is shown in Figure B.3-3 for C and Fe nuclei at three different values of γ.

At low γ, the ionization signal is observed and is very sharp. As γ increases, the total signal increases with the addition of the transition radiation component. From the widths of these distributions, the energy resolution of the detector, which depends on both Z and γ, can be assessed.

For a given application, devising a radiator plus detector system to cover the needed range in γ involves optimizing many parameters, i.e. radiator material and structure, overall thickness, size of detectors, and composition of the gas. This is a task that is under way for ACCESS and involves both theoretical calculations and accelerator testing of prototype devices.
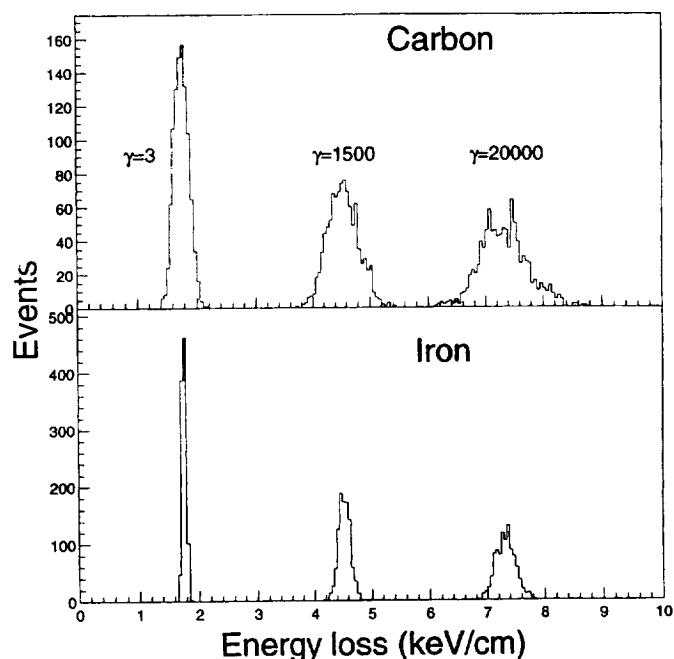
Figure B.3-3. **Simulated energy loss signal for C (top) and Fe (bottom) for different Lorentz factors.**

B.3.2 Detector design and construction

The centerpiece of this module is the TRD for energy measurements. Without a pressurized shell as was used for CRN, we cannot utilize MWPCs or drift chambers, since, pressurized at one atmosphere, these devices would not withstand external vacuum. To resolve this problem, the TRD design utilizes arrays of cylindrical single wire proportional tubes. Such tubes, with thin walls of aluminized Mylar, are inexpensive to make, simple to operate, and, most importantly, can easily work at zero outside pressure. These tubes are quite rigid when pressurized, can be several meters long, and can be easily arranged to form lightweight arrays of several square meter area. A sketch of such a proportional tube-radiator subassembly is shown in Figure B.3-4.

Each proportional counter tube has a laminated Mylar wall made conductive with an aluminum coating on the inside. The tube diameter is 2 cm, and its length is 2.5 m. A 50 μm thick stainless steel wire along the axis of the tube forms the anode of the counter. Filled with a Xe/methane mixture, these tubes operate in the proportional regime at an absolute pressure of 1.5 atmosphere. These tubes are extremely lightweight, and are commercially available at relatively low cost. They are manufactured by spiral-winding, and laminating, two or more strips of plastic foil, and are available in arbitrary dimensions, with high-precision mechanical tolerances. Laboratory tests have shown that: (a) no gas leaks or outgassing problems compromise their performance as proportional counters at low gas flow rates; (b) the Al coating provides good electrical conductivity, with a typical resistance of 100 Ω over 5 m length; (c) the tube walls are transparent to low energy X-rays as required for the detection of transition radiation: the measured attenuation of X rays in a 50-μm-thick tube wall is 9% at 6 keV, and 4% at 8 keV; and (d) the

tube walls withstand over-pressures of several atmospheres; even for tubes with the lowest wall thickness (50 μm) the burst pressure is larger than 5 atmospheres.
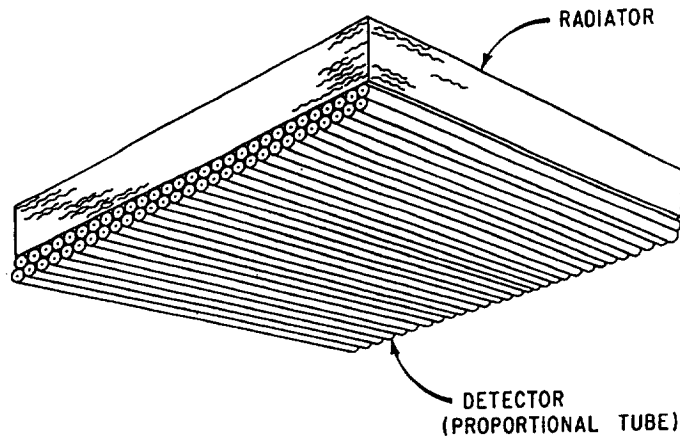
Figure B.3-4. Radiator and proportional tube assembly.

The consequence of using the proportional drift tubes for the ACCESS mission is that the payload must include a gas supply and a circulation system, if a flow rate is to be maintained. The size of this reservoir will be determined by the exact level of the (small) gas leakage, both from around the end caps of the tubes and through the walls of the tubes. This gas reservoir will require a pressurized tank that must be safety-certified for launch on the Shuttle. Whether or not a tank refill will be necessary during the life of the ACCESS mission is one of the important issues for study as the project develops.

A preliminary baseline concept for a gas-handling system for the ACCESS TRD module is shown in Figure B.3-5 and involves a circulating pump to maintain the flow rate through the
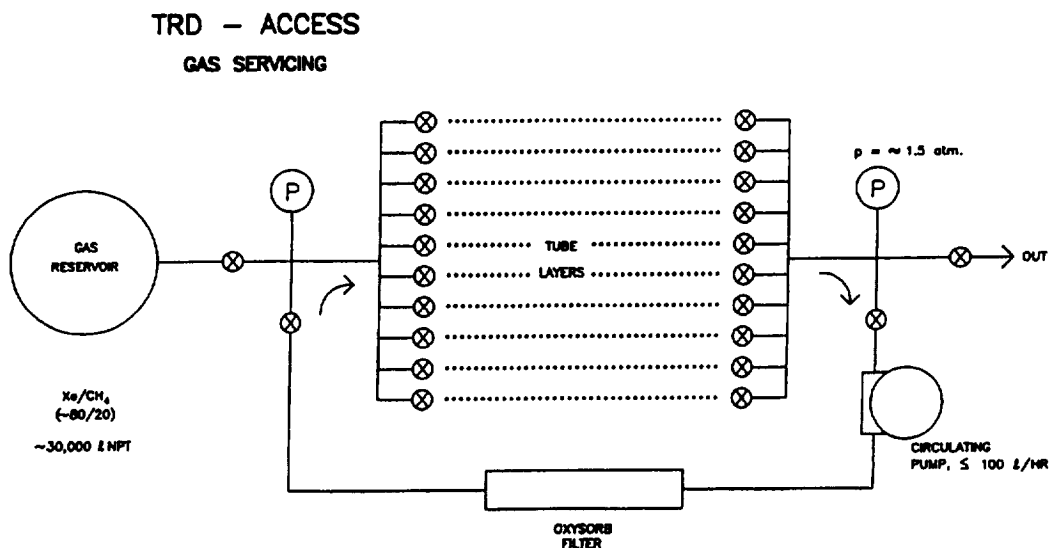
Figure B.3-5. Gas system for TRD proportional tubes.

125

tubes as well as in-line filters to remove any contaminants that are introduced into the gas mixture. As long as the leak rate is low, such a system could keep the Xe-methane gas operating for the life of the mission.

Alternative scenarios for the gas system involve operation in a fill-purge-refill mode rather than a recirculating system. A trade study will be needed to decide upon the best method for handling the gas system requirement for the TRD.

The use of a gas mixture such as Xe-methane, however, provides a thermal constraint. At low temperatures (about 0 °C) the two components of the gas can separate. Once this has happened, they do not readily remix even when the temperature is increased. Thus, the thermal environment for the gas reservoir must be designed carefully, and, probably, heaters will be necessary to avoid component separation in the gas.

The other detectors involved in the TRD module are the top and bottom scintillators. Here we envision a relatively simple design such as is sketched in Figure B.3-6.
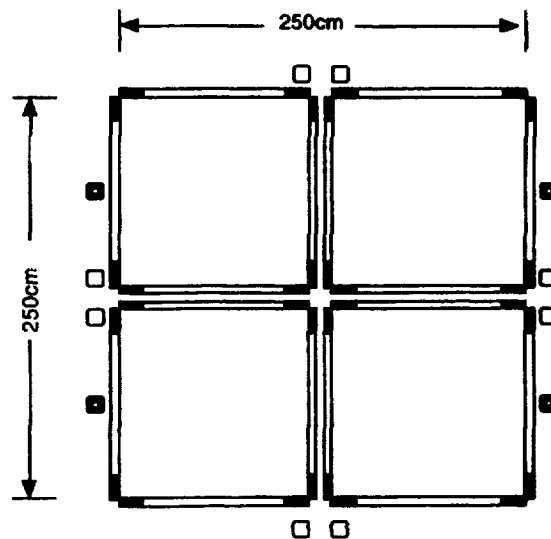
Figure B.3-6. TRD scintillator concept.

The scintillator is divided into four pieces, each side of each piece being connected to a bar of wave-shifter material. Both ends of each wave-shifter bar are viewed by PMTs, indicated by the dark sections of the bars in Figure B.3-6. These PMTs are read out via preamps and shapers (open squares) and fast summing amplifiers (closed squares with open dot in center). These electronics are located on the edges of the detector, and signals are passed to the digital electronics, which may be located nearby.

B.3.3 Charge and trajectory measurements

The particle charge is first measured by the top and bottom scintillators with an expected resolution of about a quarter charge unit. Comparison of the top and bottom scintillators determines if a particle has fragmented in traversing the TRD module.

126

Charge can also be measured from the ionization signal in the proportional tubes, particularly those at the top of the stack. However, the ionization signal increases logarithmically with increasing γ (the "relativistic rise"), amounting to roughly a 50% increase in the ionization signal from minimum ionizing to highly relativistic particles. This increase is a desirable feature since it provides a means of removing minimum ionizing particles, e.g. an event will only be accepted if a TRD signal is accompanied by a pulse height in the proportional tubes well above the minimum ionizing level. As the flux of low-energy cosmic rays traversing the instrument is much higher than the flux of those in the TRD region ($\gamma > 400$), this discrimination against low-energy background is important.

On the other hand, the relativistic rise compromises the uniqueness of the charge determination since a highly relativistic particle of charge Z may not be distinguishable from a minimum ionizing particle of higher Z, if just the tubes are used for charge identification. However, the relativistic rise in a solid, e.g. the scintillator, is much smaller than in a gas (the "density effect"), so the scintillator is able to resolve the ambiguity. Thus, by combining measurements from the scintillator layers with the proportional tubes, an accurate charge measurement for all of the elements can be obtained.

It is also necessary to know the trajectory of the particle through the instrument in order to correct for the angle of incidence and the corresponding actual pathlength in the detectors. Here information from the CM (ZIM) at the top can be helpful for the heaviest events.

The proportional tubes are arranged, alternately, in orthogonal directions to permit trajectory determination in the TRD module. Using a tracking algorithm based on the fact that, within fluctuations, tube signals are proportional to the pathlength within each tube, the trajectory which best reproduces the signals found in all tubes can be determined. Simulating this procedure with a Monte Carlo code, assuming a stack of six double layers of tubes, as in Figure B.3-1, results in trajectory reconstruction that is accurate to about 0.4 mm in both the X- and Y-directions for C nuclei. For Fe, the reconstruction (one sigma) improves to about 0.3 mm. This excellent trajectory reconstruction allows us to normalize the total ionization signal measured in the stack to the total pathlength traversed by the particle in order to determine the specific ionization dE/dx, and therefore the charge Z of the particle.

B.3.4 Readout, electronics, power, and data

There are two types of detectors to be read out in the TRD module, the PMTs associated with the scintillators and the proportional tubes. There are only 64 PMTs to be analyzed, which can be accomplished with standard electronics. There are many more proportional tubes to sample, and these require the use of ASICs to conserve power. A typical ASIC for the proportional tubes may involve a preamp, shaping amp and track/hold circuit. The held pulse is then shifted out to an ADC circuit for digitization. A schematic block diagram of the electronics for the TRD is shown in Figure B.3-7, with the necessary location of the modules indicated at the bottom.

TRD Electronics Block Diagram
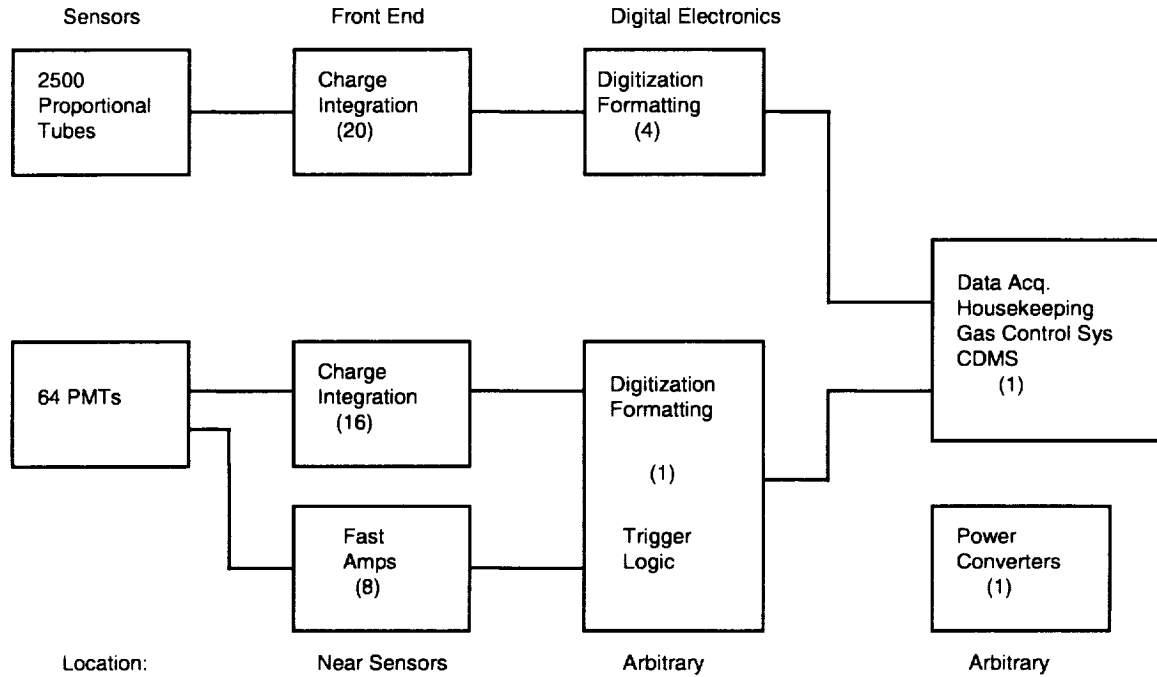
Figure B.3-7. Electronics block diagram for baseline TRD on ACCESS.

The estimated power required for the TRD is summarized below:

REGULATED POWER ESTIMATE:

64 PMT @ 0.12w	-	7.7
16 Scin. preamp & shaper	-	1.6
8 Scin. fast sum amp	-	1.2
20 Prop. Tube linear ass'y	-	32
4 Prop. Tube ADC ass'y	-	48
1 Scintillator rack	-	14
1 Main rack	-	60
SUB-TOTAL	-	165 W
1 Power Converter (assume 75% efficient)	-	55 W
TOTAL		220 W

To this must be added the power involved in (a) the gas handling system and (b) heaters (if needed) for thermal control. These latter remain undefined at this time, so power estimates are not possible.

The estimated event rate for the TRD module is about 100 events per second. Each event readout requires about 2100 bits. This gives an event data rate of 210 kbps. To this must be added housekeeping data, rates, calibration frames and the like which all-together are estimated to add another 2 kbps. Thus, the anticipated data rate from the TRD module is 212 kbps.

B.3.5 Anticipated results

The baseline TRD for ACCESS will measure events with Z > 3. Projecting the results from a 1000-day exposure of the instrument on the ISS, Figure B.3-8 shows the expected results for the B/C ratio, compared to lower energy results and to two theoretical curves for different models. Even if the ratio continues to fall as in the "leaky box" model, the ACCESS data can trace the energy dependence to nearly 10^{13} eV/nucleon. (It should be noted that Figure B.3-8 shows but one of the several secondary-to-primary ratios that ACCESS will be able to measure.)
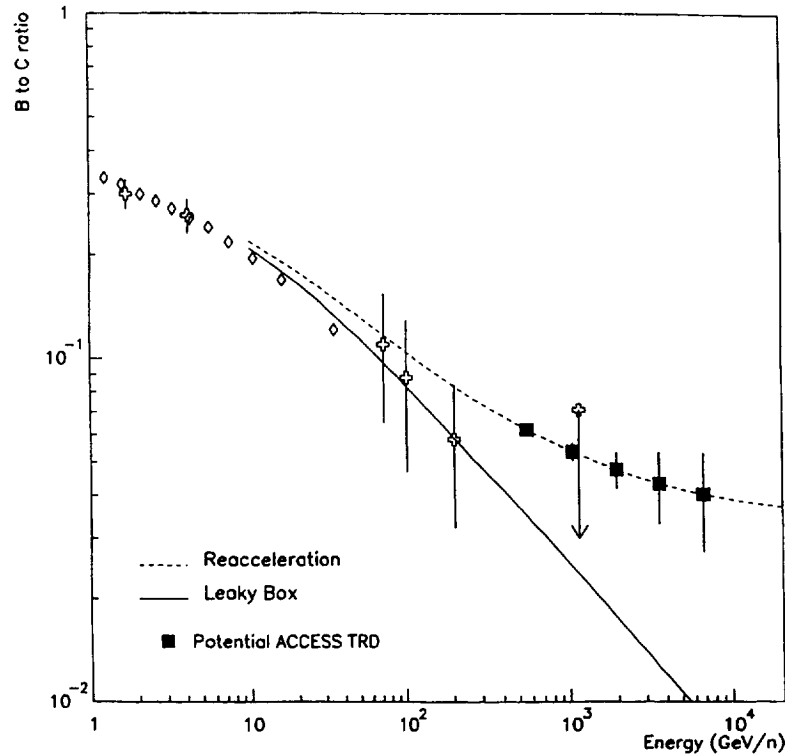
Figure B.3-8. B/C measurements expected from the ACCESS TRD compared to previous measurements.

Turning next to the primary elements, Figure B.3-9 shows the type of results anticipated for the CNO nuclei and the Fe group. Here, again, two models are shown, the leaky box and the residual pathlength, the latter being similar to the upper curve in the previous figure. In addition, all-particle spectrum measurements are indicated, and the scale is total energy per particle. Error bars on the calculated values (large solid points) are statistical, demonstrating that the number of events observed by ACCESS will not limit the interpretation. Thus, ACCESS data will be able

to resolve the discrepancies in the previous results and trace the energy spectra of the elements to close to the knee region of the all-particle spectrum.
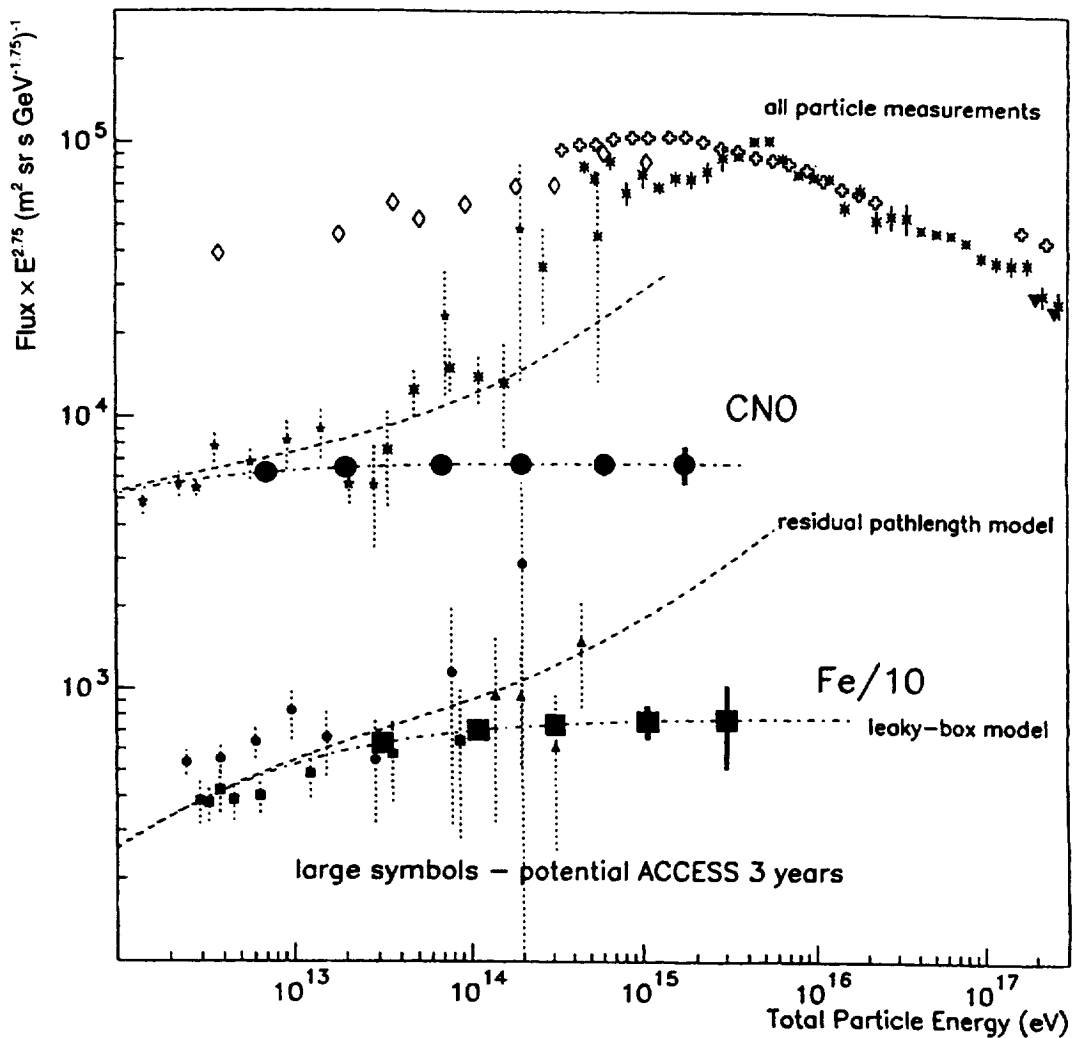
Figure B.3-9. Potential results for CNO and Fe from the TRD on ACCESS compared to previous results and models.

B.4. Composite detail of the ACCESS instrument

The three experiments, CAL, TRD, and CM (ZIM), together form the overall ACCESS instrument. A conceptual cross section of the instrument is shown in Figure B.4-1.

This composite was created by the University of Maryland group[78] for the ACCESS simulation team. It is based upon the USS/ACCESS configuration (see Figure 14 and Figure E.1) and does not include some of the evolution in the experiment designs that has occurred since beginning this study. However, Figure B.4-1 provides a perspective of the overall ACCESS instrument concept that is the basis for this accommodation study.

Figure B.4-1. Cross section of the composite ACCESS instrument.

Appendix C. ISS Assembly Sequence

For reference, the following is a flight-to-flight detail of the currently planned ISS assembly sequence [SSP-50110, Rev. Db]. Phase 1 was the joint U.S.-Russian *Mir* program. See the ISS 10/2/98 planning reference at the Assembly Sequence website.

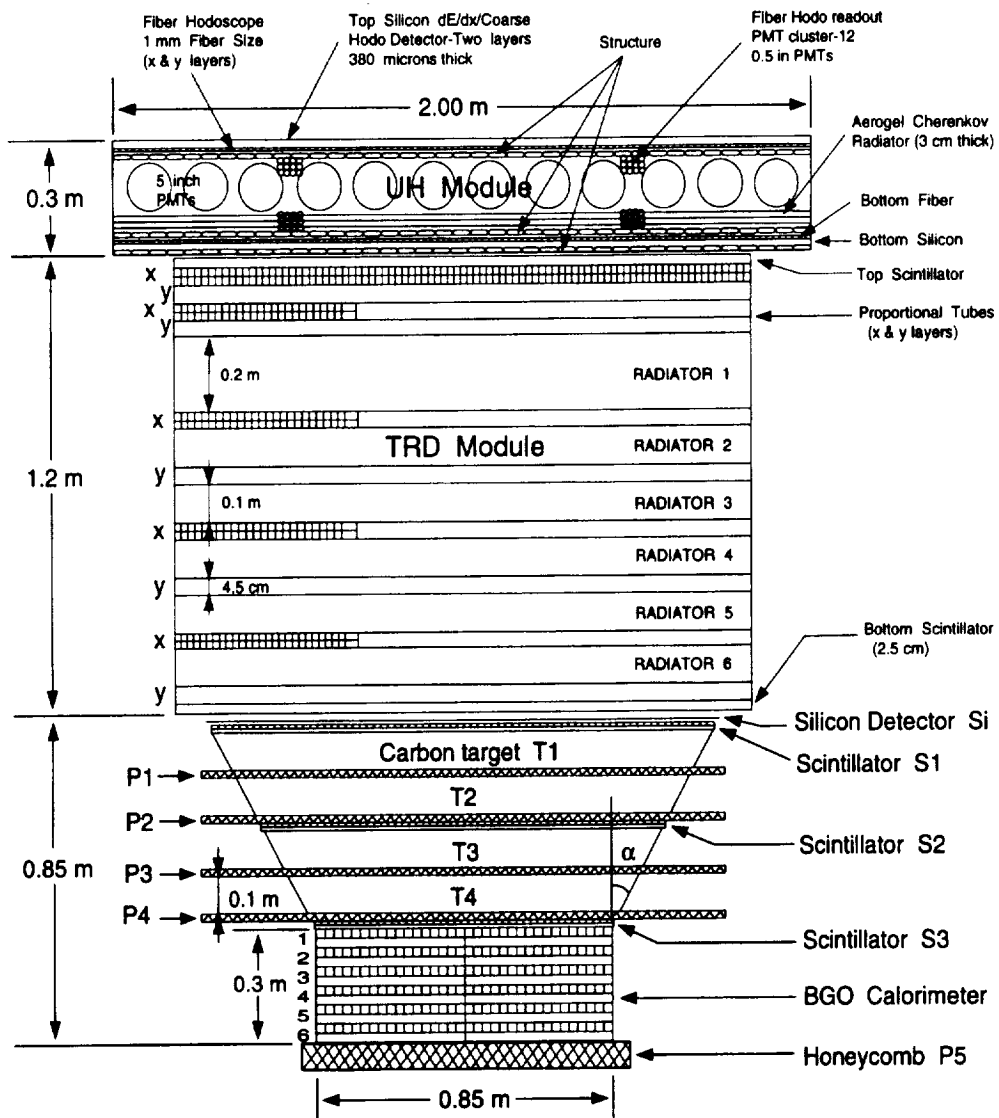| Launch Date	Flight	Delivered Elements
Nov-98	1A/R	FGB (Launched on PROTON launcher)
Dec-98	2A	Node 1 (1 Stowage rack), PMA1, PMA2, 2 APFRs (on Sidewalls)
May-99	2A.1	Spacehab Double Cargo Module, OTD (on Sidewall), RS Cargo Crane
Jul-99	1R	Service Module (Launched on PROTON launcher)
Aug-99	1P	Progress M1
Aug-99	2A.2	Spacehab Double Cargo Module
Oct-99	2P	Progress M1
Oct-99	3A	Z1 truss, CMGs, Ku-band, S-band Equip, PMA3, EVAS (SLP), 2 Z1 DDCUs (Sidewall)
Dec-99	4A	P6, PV Array (6 battery sets) / EEATCS radiators, S-band Equipment
Jan-00	2R	Soyuz - TM - (a)
Feb-00	5A	Lab (5 Lab System racks), PDGF (on Sidewall)
Feb-00	3P	Progress M
Mar-00	5A.1	Lab Outfitting (Sys racks, RSRs), (on MPLM)
Apr-00	4P	Progress M1
Apr-00	6A	Lab Outfitting (Payload Racks, RSPs, RSRs) (on MPLM), UHF, SSRMS (on SLP) - (b)
Jun-00	2S	Soyuz - TMA
Jul-00	7A	Airlock, HP gas (2 O2, 2 N2) (on SLDP)
Jul-00	5P*	Progress M
Aug-00	4R*	Docking Compartment 1 (DC1), RS Cargo Crane
Aug-00	7A.1*	4 RSRs, 6 RSPs, ISPRs (on MPLM), OTD, APFR (on Sidewall)
Sep-00	6P*	Progress M1
Oct-00	7P*	Progress M1
Nov-00	UF1*	ISPRs, 2 RSRs, 2-RSP-2s (on MPLM), Spares Warehouse
Dec-00	8P*	Progress M1
Dec-00	3S*	Soyuz - TM
Jan-01	8A*	S0, MT, GPS, Umbilicals, A/L Spur
Mar-01	UF2*	ISPRs, 3 RSRs, 1 RSPs, 1 RSP-2s, MELFI (MPLM), MBS, PDGF (Sidewalls)
May-01	9A*	S1 (3 rads), TCS, CETA (1), S-band
Jul-01	9A.1*	Science Power Platform w/4 solar arrays and ERA
Aug-01	11A*	P1 (3 rads), TCS, CETA (1), UHF
TBS	3R*	Universal Docking Module (UDM)
Sep-01	12A*	P3/4, PV Array (4 battery sets), 2 ULCAS
TBS	5R*	Docking Compartment 2 (DC2)
Dec-01	12A.1*	ISPR, 3 RSRs, 1-RSP-2s, 1 RSP-1 (MPLM), P5, Radiator OSE
Jan-02	13A*	S3/4, PV Array (4 battery sets), 4 PAS
Apr-02	10A*	Node 2 (4 DDCU racks), NTA (on Sidewall)
May-02	10A.1*	Propulsion Module

* - Sequence and schedule after Flight 7A are under review.

(a) - 3 Person Permanent International Human Presence Capability

(b) - Microgravity Capability

Appendix C. ISS Assembly Sequence
(continued, page 2)

Launch Date	Flight	Delivered Elements
Jul-02	1J/A*	ELM PS (4 Sys, 3 ISPRs, 1 Stow), 2 SPP SA w/ truss, Conform. Shields (ULC)
Sep-02	1J*	JEM PM (4 JEM Sys racks), JEM RMS
TBS	9R*	Docking & Stowage Module (DSM) (FGB module type)
Oct-02	UF3*	ISPRs, 1 JEM rack, 1 RSP, 1 RSP-2 (on MPLM), 1 Express Pallet w/ PL
Nov-02	UF4*	Truss Attach Site P/L, Express Pallet w/ Payloads, ATA, SPDM (SLP)
Feb-03	2J/A*	JEM EF, ELM-ES w/ Payloads, 4 PV battery sets (on Spacelab Pallet)
Mar-03	14A*	2 SPP SA w/ truss, 4 SM MMOD Wings (ULC), Cupola (SLP), Port Rails (ULC)
TBS	8R*	Research Module #1 (RM-1)
Jun-03	UF5*	ISPRs, 1 RSP, 1 RSP-2 (on MPLM), Express Pallet w/ Payloads
Jul-03	20A*	Node 3 (2 Avionics, 2 ECLSS racks)
TBS	10R*	Research Module #2 (RM-2)
Sep-03	17A*	1 Lab Sys, 4 Node 3 Sys, 3 CHeCS, 2 RSP-2s, ISPRs (MPLM) - (c)
Oct-03	1E*	APM (5 ISPRs)
Dec-03	18A*	CRV #1, CRV adapter - (d)
Jan-04	19A*	5 RSP-2, 1 RSR, ISPRs, 4 Crew Qtrs. (on MPLM), S5 - (e)
Mar-04	15A*	S6, PV Array (4 battery sets), Stbd MT/CETA rails
Apr-04	UF6*	3 RSP-2s, 1 RSP, ISPRs (on MPLM), 2 PV battery sets (on SLP)
May-04	UF7*	Centrifuge Accommodations Module (CAM), ISPRs (TBD)
Jul-04	16A*	Hab (6 Hab sys racks, 2 RSRs, ISPRs) - (f)

* - Sequence and schedule after Flight 7A are under review.

(c) - 6 Person USOS ECLSS Capability

(d) - 6 Person Permanent International Human Presence Capability

133

Appendix D. Space Station Program and Space Shuttle Documentation

The following SSP documentation should be retrievable as a download from the Program Automated Library System (PALS) website in Appendix K.

Space Station Program (SSP)

SSP 30000	SSP Definitions and Requirements
SSP 30233	SS Requirements for Materials and Processes
SSP 30237	SS Electromagnetic Emission and Susceptibility Requirements
SSP 30238	SS Electromagnetic Techniques
SSP 30240	SS Grounding Requirements
SSP 30242	SS Cable/Wire Design and Control Requirements for Electromagnetic Compatibility
SSP 30243	SS Requirements for Electromagnetic Compatibility
SSP 30245	SS Electrical Bonding Requirements
SSP 30242	Space Station Cable/Wire Design
SSP 30425, Rev. B	SSP Natural Environment Definition for Design
SSP 30426	SS External Contamination Control Requirements
SSP 30482	Electrical Power Specification and Standards
SSP 30512, Rev. C	SS Ionizing Radiation Environment for Design
SSP 30513	SS Ionizing Radiation Environment Effects Test and Analysis Techniques
SSP 41000	System Specification for the International Space Station
SSP 42131	S3/P3 to AP/UCC ICD (under revision, CR 1135)
SSP 50005	International Space Station Flight Crew Integration Standard
SSP 50110	Multi-Increment Manifest Document
SSP 50184	HRDL Physical Media, Physical Signaling and Protocol Specification
SSP 50513	
SSP 52000-A04	Payload Command and Data (C&D) Integration Data File
SSP 52050	Software ICD
SSP 57000-IRD-TAP	IRD, Truss Attached Payloads
SSP 57000-PAH-LSP	PAH, Launch Site Processing
SSP 57000-PAH-TAP	PAH , Truss Attached Payloads
SSP 57003	Attached Payloads IRD
SSP 57010	Payload EMI/EMC Control Plan

Appendix D. Space Station Program and Space Shuttle Documentation
(continued)

Shuttle Program (NSTS)

NSTS-07700, Vol. XIV Appendix 1	Space Shuttle System Payload Accommodations
NSTS 1700.7B	Safety Policy and Requirements for Payloads Using the Space Transportation System
NSTS 1700.7B, ISS Addendum	Safety Policy and Requirements for Payloads Using the International Space Station (ISS Addendum)
NSTS/ISS 18798B	Interpretations of NSTS/ISS Payload Safety Requirements
NSTS-13820	Implementation Procedure for NSTS Payloads System Safety Requirements
NSTS/ISS 13830C	Payload Safety Review and Data Submittal Requirements For Payloads Using the Space Shuttle/International Space Station
NSTS-14046	Payload Interface Verification Requirements
NSTS-21000-IDD-ISS	International Space Station Interface Definition Document
JSC 73642	
JSC SC-C-0005C	
KHB 1700.7B	Space Shuttle Payload Ground Safety Handbook

ISS Telecommunications, Ground Segment

HOSC-DOC-237, Rev. A	ISS HOSC: Payload Commanding (Marshall Whitepaper, November 17, 1998)
MSFC-SPEC-2123B	Payload Data Services System (PDSS) Development Specification (Fall, 1998)

Military Standards

MIL-STD-5G	Military Handbook 5G
MIL-STD-210	Climatic Extremes for Military Equipment
MIL-STD-461	Electromagnetic Emission and Susceptibility Requirements for the Control of Electromagnetic Interference
MIL-STD-1576	Electro-Explosive Subsystem Safety Requirements and Test Methods for Space Systems
MIL-STD-1553b	Digital Time Division Command/Response Multiplex Data Bus
MIL-STD-1776	Air Crew Station and Passenger Accommodations
MIL-STD-2073	Standard Practice for Military Packaging

Appendix E. ACCESS Structural Options

ACCESS on USS
Integration Option 1

Total Average Payload Mass Estimate: 4968 kg (10952 lbs.)

Overall approximate weights and dimensions for the preliminary structural assessment of the ACCESS Experiment integrated on the existing Unique Support Structure (USS) design developed for the Alpha Magnetic Spectrometer (AMS) Experiment.
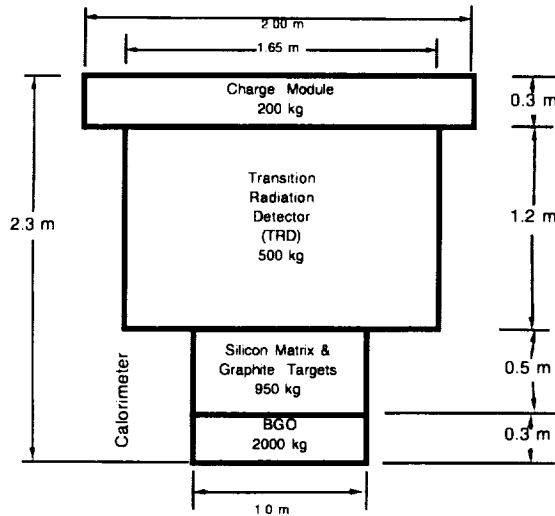
All envelopes are squares in the X-Y plane.

Orbiter coordinate system.
+X is out of the paper.

There is another 200 kg of avionics, thermal control system, gas resupply system, debris shields, and contingency mass for a total ACCESS Experiment mass of 3850 kg (8488 lbs).
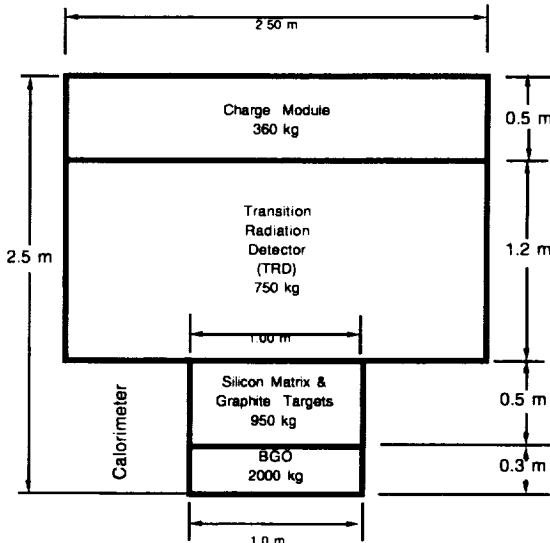
For this preliminary assessment, all mass is assumed to be uniformly distributed throughout each of the envelopes shown.

118 to 163 kg (260 to 359 lbs) is required to adapt ACCESS to the USS. 132 to 159 kg (291 to 351 lbs) is required to make the USS deployable and to attach it to the PAS. With an existing USS weight of 832 kg (1834 lbs) the total integration hardware mass is 1082 to 1154 kg (2385 to 2544 lbs). Therefore the total ACCESS Payload mass is 4932 to 5004 kg (10873 to 11032 lbs) with an average of 4968 kg (10952 lbs).

ACCESS on ECS
Integration Option 2

Total Average Payload Mass Estimate: 5041 kg (11113 lbs.)
(Using total weights from the payload on structures 1, 6, and 9.)

Orbiter coordinate system.
+Z is out of the paper.

There is another 140 kg of avionics, thermal control system, gas resupply system, debris shields, and contingency mass for a total ACCESS Experiment mass of 4200 kg (9259 lbs).

For this preliminary assessment, all mass is assumed to be uniformly distributed throughout each of the envelopes shown.
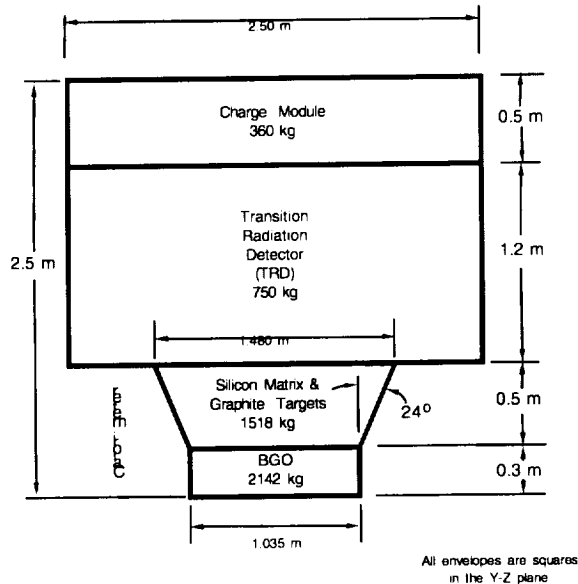
An ECS to carry this experiment mass would weigh 658 to 819 kg (1450 to 1805 lbs). 102 to 114 kg (225 to 251 lbs) is required to make the ECS deployable and to attach it to the PAS. Therefore the total ACCESS Payload mass is 4960 to 5133 kg (10934 to 11316 lbs).

Figure E.1. The four options addressed in the JSC/Louisiana State University (LSU) Accommodation Study.
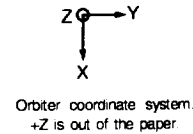
Appendix E. ACCESS Structural Options

(continued)

ACCESS on ECS

Total Payload Mass Estimate: 6014 kg (13232 lbs.)

Charge Module
360 kg — 0.5 m

Transition
Radiation
Detector
(TRD)
750 kg — 1.2 m

2.5 m

1.480 m

Silicon Matrix &
Graphite Targets
1518 kg — 24° — 0.5 m

BGO
2142 kg — 0.3 m

1.035 m

All envelopes are squares
in the Y-Z plane

Z⊙→Y
↓
X

Orbiter coordinate system.
+Z is out of the paper.

There is another 250 kg of avionics, thermal control system, gas resupply system, debris shields, and contingency mass for a total ACCESS Experiment mass of 5031 kg (11069 lbs)

For this preliminary assessment, all mass is assumed to be uniformly distributed throughout each of the envelopes shown

An ECS to carry this experiment mass would weigh 865 kg (1903 lbs) 118 kg (260 lbs) is required to make the ECS deployable and to attach it to the PAS. Therefore the total ACCESS Payload mass is 6014 kg (13232 lbs)

ACCESS on ECS
Integration Option 4

Total Average Payload Mass Estimate: 6807 kg (15006 lbs.)
(Using total weights from the payload on structures 1, 6, and 9.)

2.50 m

Charge Module
360 kg — 0.5 m

Transition
Radiation
Detector
(TRD)
750 kg — 1.2 m

2.5 m

1.604 m

Silicon Matrix &
Graphite Targets
1829 kg — 24° — 0.5 m

Calorimeter

BGO
2687 kg — 0.3 m

1.159 m

All envelopes are squares
in the Y-Z plane

Z⊙→Y
↓
X

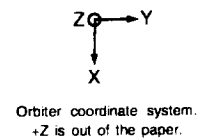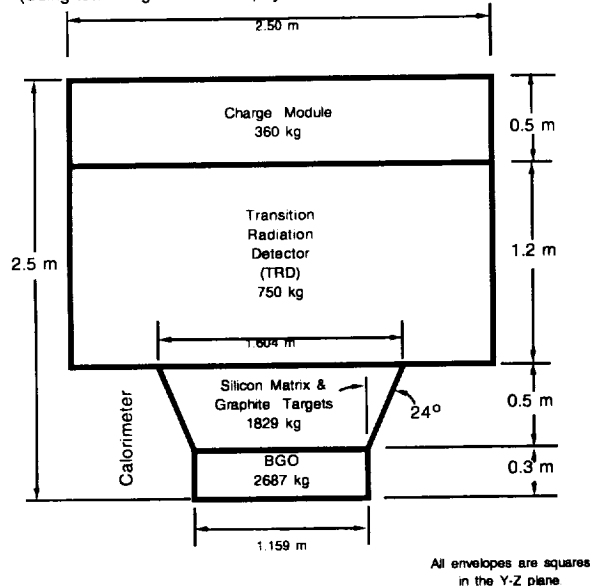Orbiter coordinate system.
+Z is out of the paper.

There is another 250 kg of avionics, thermal control system, gas resupply system, debris shields, and contingency mass for a total ACCESS Experiment mass of 5876 kg (12954 lbs).

For this preliminary assessment, all mass is assumed to be uniformly distributed throughout each of the envelopes shown.

An ECS to carry this experiment mass would weigh 758 to 913 kg (1672 to 2012 lbs). 109 to 121 kg (240 to 267 lbs) is required to make the ECS deployable and to attach it to the PAS. Therefore the total ACCESS Payload mass is 6743 to 6909 kg (14866 to 15233 lbs).

Figure E.1. (continued) The four options addressed in the JSC/LSU Accommodation Study.

Appendix E. ACCESS Structural Options
(continued)

STRUCTURE 1   STRUCTURE 2   STRUCTURE 3

STRUCTURE 4   STRUCTURE 5   STRUCTURE 6

STRUCTURE 7   STRUCTURE 8   STRUCTURE 9

STRUCTURE 10   STRUCTURE 11   STRUCTURE 13
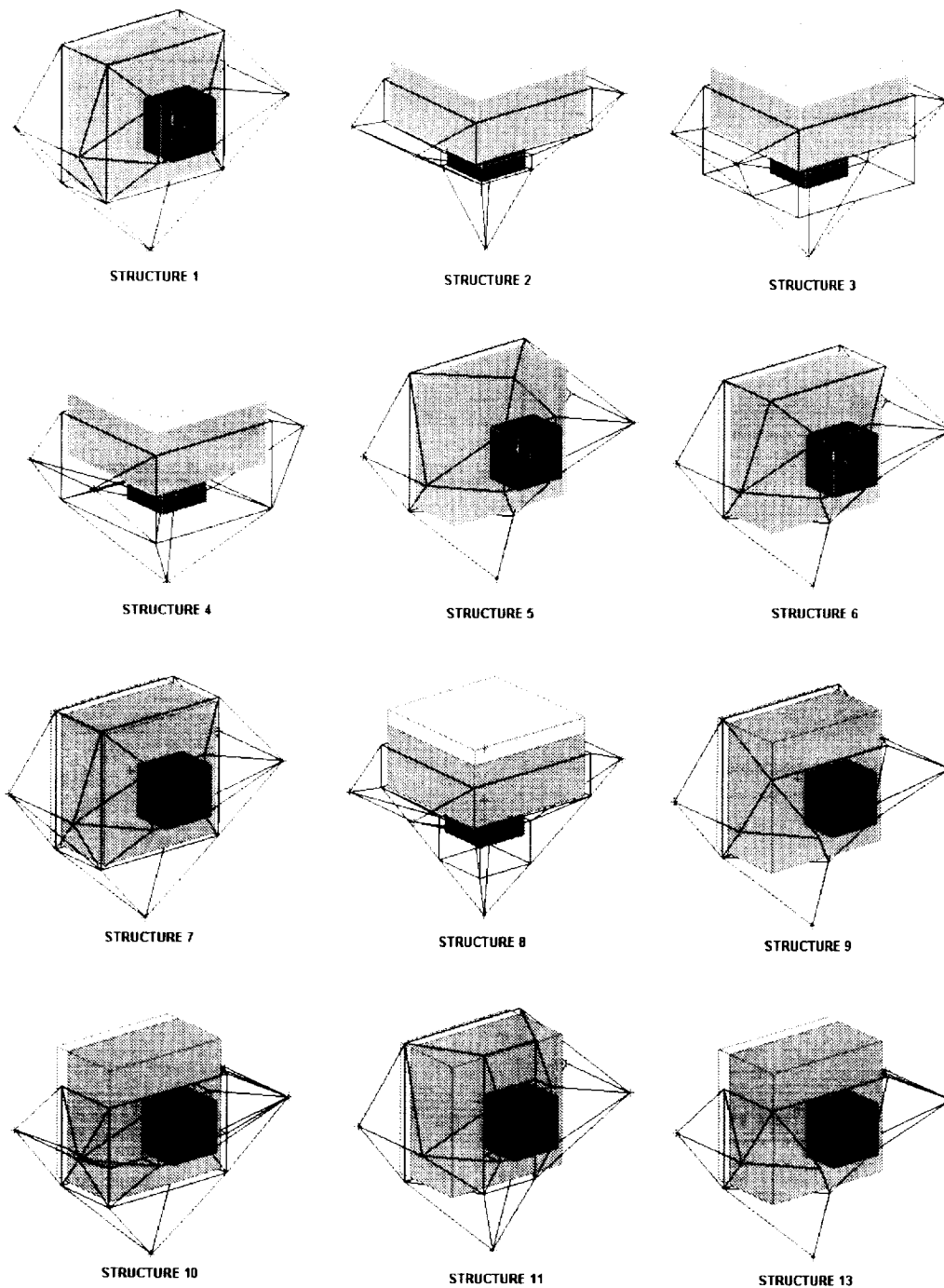
Figure E.2. The thirteen Option 2 ECS structures analyzed under the JSC/LSU Accommodation Study (with emphasis on Structures 1, 6, and 9). Options 3 and 4 are very similar. Not shown is Structure 12, which is much like Structure 7.

Appendix F. ISS CG Restraints

Shell for 11000 lbs.

$$Z_{cg} < 78.21 - 2.34E\text{-}04*abs(X_{cg}) - 1.09E\text{-}02*X_{cg}^2 - 2.70E\text{-}03*abs(Y_{cg}) - 4.85E\text{-}02*Y_{cg}^2 + 5.79E\text{-}06*X_{cg}^2*Y_{cg}^2$$
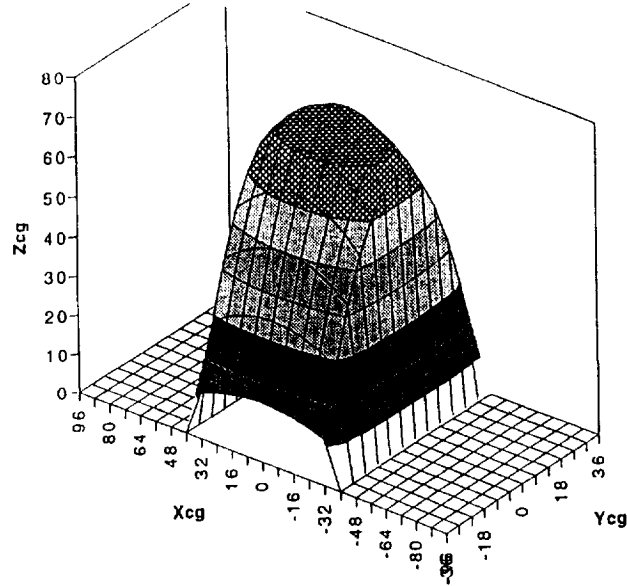
Figure F.1. CG envelope.

Shell for 13000 lbs.

$$Z_{cg} < 69.88 - 2.24E\text{-}04*abs(X_{cg}) - 9.88E\text{-}03*X_{cg}^2 - 2.70E\text{-}03*abs(Y_{cg}) - 4.85E\text{-}02*Y_{cg}^2 + 5.79E\text{-}06*X_{cg}^2*Y_{cg}^2$$
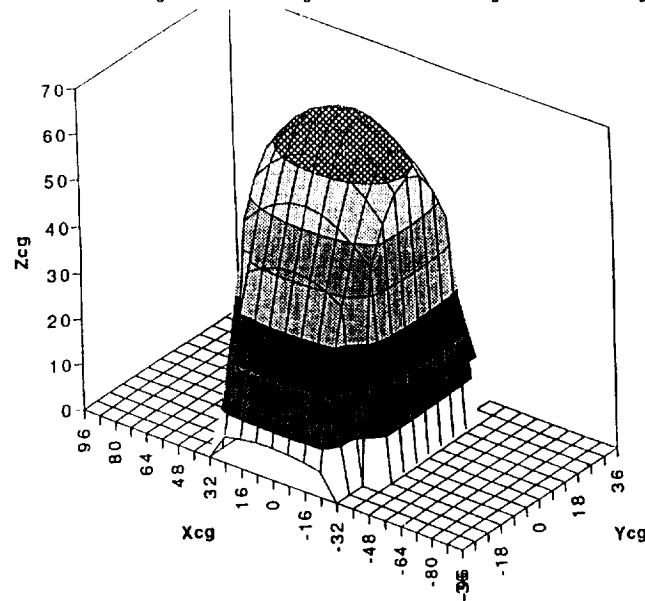
Figure F.2. CG envelope.

139

Appendix F. ISS CG Restraints (continued)

Shell for 15000 lbs.

$$Z_{cg} < 64.16\text{-}2.07\text{E-}04*abs(X_{cg})\text{-}8.23\text{E-}03*X_{cg}^2\text{-}2.70\text{E-}03*abs(Y_{cg})\text{-}4.85\text{E-}02*Y_{cg}^2\text{+}4.66\text{E-}06*X_{cg}^2*Y_{cg}^2$$

Figure F.3. CG envelope.

Payload Weight (lbs)	Z-axis CG (inches)
19,060	57.41
17,000	62.89
15,000	64.16
13,000	69.88
11,000	78.21
9,000	90.77
7,000	110.14
5,000	143.95
3,060	222.13

Acceptable Region

PAS CG Z-axis (inches)

Maximum Payload Weight At S3 and P3 PAS Site (lbs)

Figure F.4. Weight-and-balance problem for ISS attached payloads, prior to CR 1135, (assuming $X_{CG} = Y_{CG} = 0$ in PAS coordinates).

140

Appendix G. ISS Environments

There are a number of environments that affect the ISS payload. These can be distinguished according to mission phase: (1) ground operations; (2) ascent, orbital payload transfer and deployment; (3) on-orbit operations; and (4) payload retrieval, descent, and landing. The on-orbit environments relevant to ISS payload design include the following:

- Gravitation
- Neutral atmosphere
- Thermal
- Plasma
- Ionizing radiation
- MMOD
- EMI
- Contamination
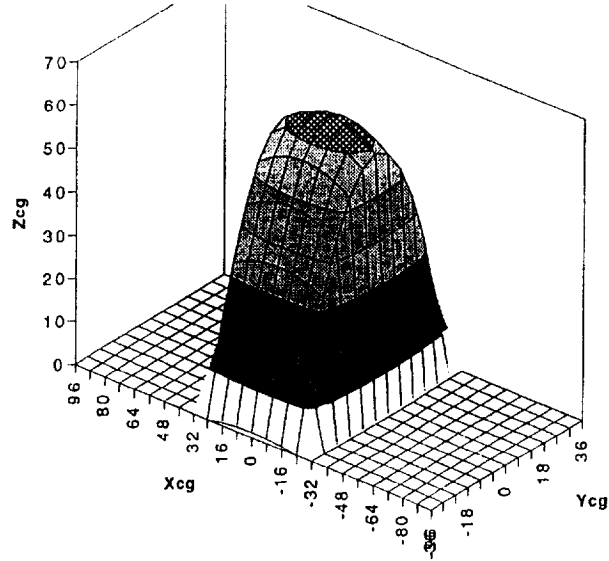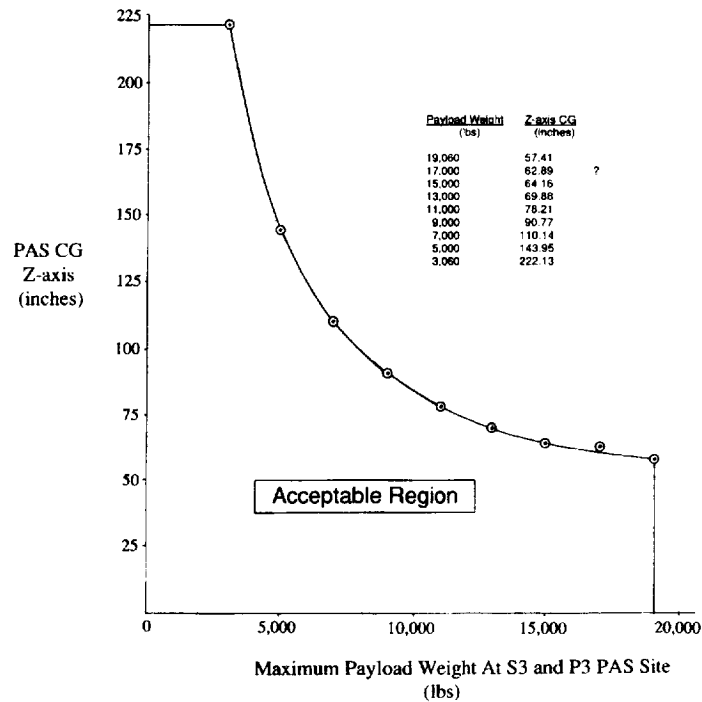- Acoustics, stress, and vibration

A general ISS baseline reference on this subject is SSP 30425, available for download from the PALS website.

Gravitation

At altitudes of 350-500 km, ISS will orbit through the Earth's gravitational field, with perturbations from the Moon and Sun. Due to the pear-shaped and irregular form of mass distribution in the Earth, the ISS orbit precesses in space as a result of the gravitational torques acting upon its orbital angular momentum. As this happens, the ISS attitude control system attempts to maintain its own pointing attitude by modulating its resultant angular momentum using control moment gyros (CMGs). The dynamic consequence of all external torques such as gravitation, the ISS instrinsic mass properties (such as moments of inertia and total weight), and the desired pointing attitude in inertial space, is a TEA.

Relevant documentation is: Any publication on orbital dynamics, the U.S. Skylab Program (CMGs), and the Russian *Mir* Program (gyrodynes).

Neutral atmosphere

As the ISS moves about LEO, it interacts with the Earth's upper tenuous atmosphere and experiences effects that influence payload structural design, material selection, and operations. Two features of this atmospheric environment are particularly relevant: (1) atmospheric density; and (2) atmospheric composition. They both vary as a function of solar activity and altitude above the Earth. Density generates orbital drag and decay which reduce altitude, in addition to external aerodynamic torques which the ISS attitude control system must account for in its TEA. To compensate for the orbital decay, the ISS orbit (Figure G.1) will undergo a periodic re-boost

(Figure G.2). Atmospheric composition (Figures G.3 and G.4) manifests itself as molecular and atomic components with differing scale-heights as a function of solar activity. The presence of atomic oxygen produces atmospheric erosion of payload material, its oxidation, and its surface contamination over long periods.
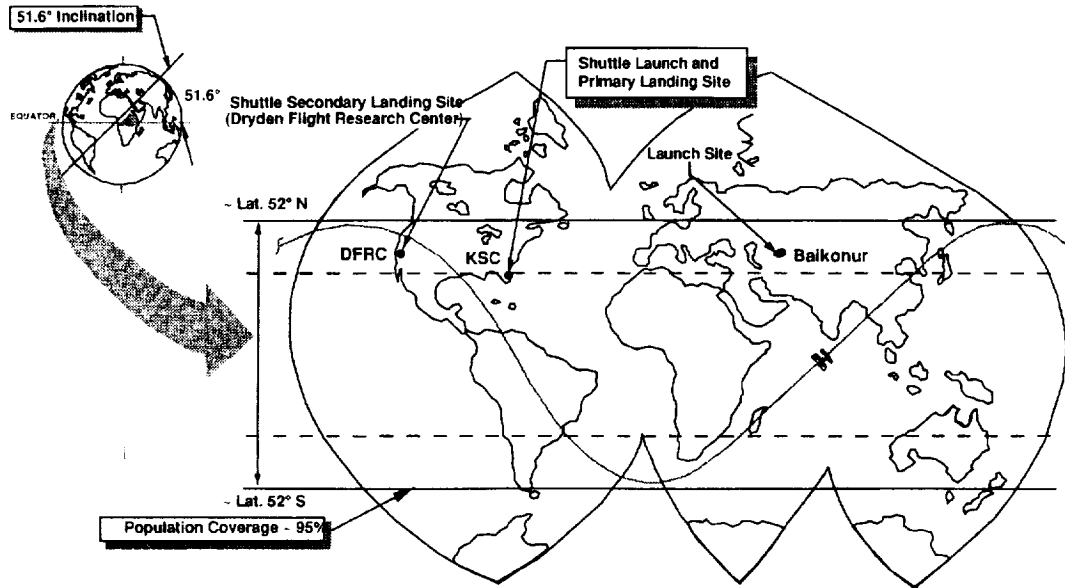
Figure G.1. Geographic perspective of typical ISS groundtrack.
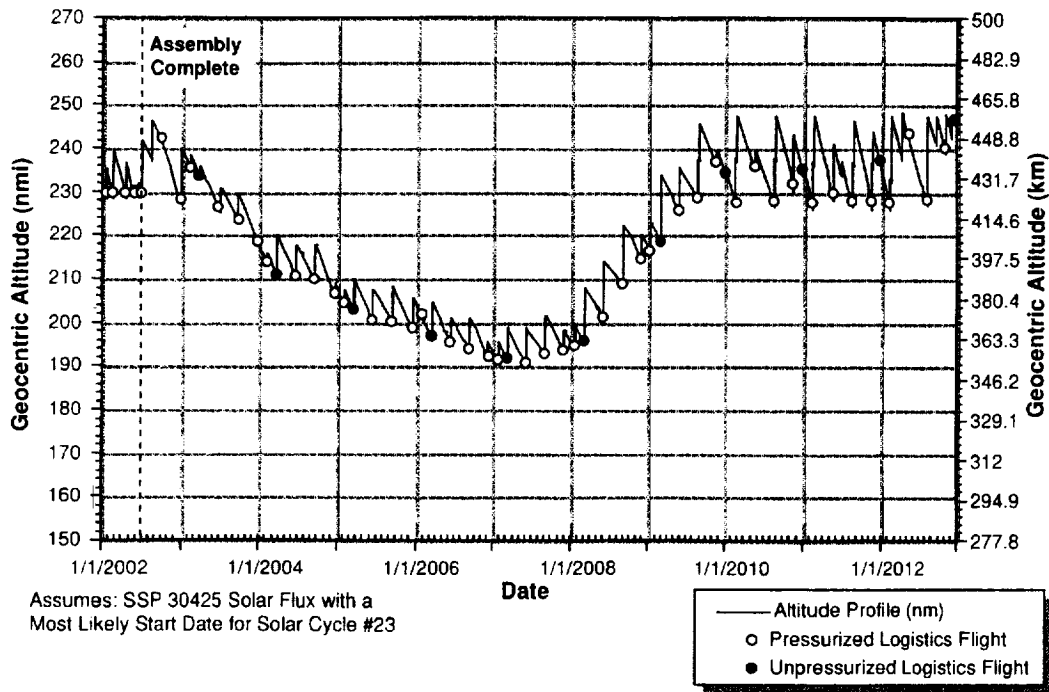
Figure G.2. Generic ISS re-boost profile, using a previous assembly sequence and launch ephemeris.
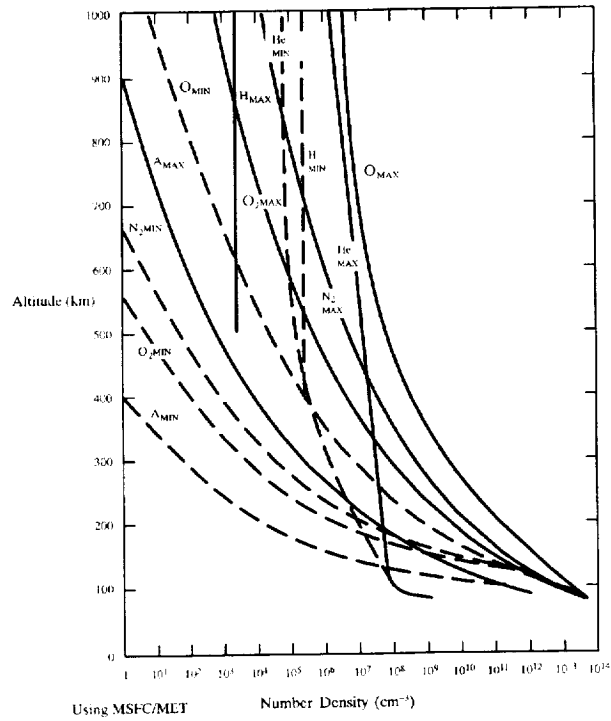
Dashed Lines Represent Solar Minimum Conditions; 0400hrs. Using $F_{10.7} = 70$ and $A_p = 0$

Solid Lines Represent Solar Maximum Conditions; 1400hrs. Using $F_{10.7} = 230$ and $A_p = 140$

Figure G.3. Number density of atmospheric constituents (after SSP 30425).

Figure G.4. Typical atmospheric mass density profiles at high and low solar activity.

143

Relevant documentation is: SSP 30425, Rev. A and B; NASA TM 100351; the Marshall Engineering Thermosphere (MET) model; the Mass Spectrometer Incoherent Scatter (MSIS) model; and Global Reference Atmosphere Model (GRAM).

Thermal

The on-orbit ISS thermal environments are natural and induced. Natural sources of thermal variation and fluctuation include the sun (solar constants for cold, mean, and hot solar activity), the Earth's albedo, the Earth's thermal radiation, and deep space temperatures. These are all influenced by ephemeris (season and time), solar cycle, cloud cover, and orbital state vector (inclination and altitude). The consequence is payload surface temperature variation, thermal stress, heat rejection, and electrical power fluctuation. Induced sources of thermal variation derive from the coupled thermal performance of the ISS constituents themselves. These range from orbital characteristics (flight attitude and state vector) and ISS geometry, to material thermal and optical properties (absorptivity, emissivity, and transmissivity). Examples include thruster plume impingement, contamination of payload thermal coatings, and Shuttle Orbiter shadowing.
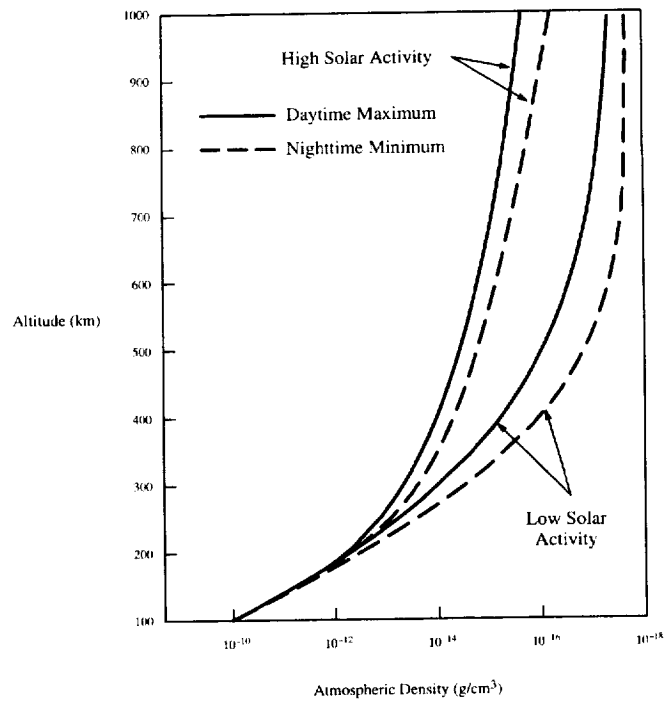
Relevant documentation and modeling is: SSP 30425, Rev. B; the MET model; the MSIS model; and the GRAM.

Plasma

The on-orbit ISS plasma environment is likewise natural and induced. LEO is a complex state of ionized gas (plasma) generating electric fields and electric potentials (and voltages) which affect the ISS performance and behavior. Natural sources (Figure G.5) include the Earth's trapped radiation belts, auroral charging, equatorial and meridional electrojets, the Earth's magnetosphere and plasmasphere, and the presence of the Earth's geomagnetic field. There also is a day-night effect as the ISS orbits in and out of a daytime and nightime plasma environment each of its orbital periods. Induced plasma sources include ISS and Shuttle thruster firings, thruster plumes, and venting of gases. In order to control the electric potential variations of this complex plasma environment, the ISS electrical system includes a plasma contactor, which attempts to equalize potential gradients appearing across it, as well as a thorough electrical grounding system. The natural and induced plasma environments are coupled together by means of well-understood space plasma physics: (1) plasma waves and magnetohydrodynamics; (2) sparking, arching, and sputtering; (3) spacecraft charging in the auroral and SAA (South Atlantic Anomaly) zones; (4) spacecraft corona and electrostatic discharge; (5) spacecraft rendezvous and docking; and (6) geomagnetic electrojet effects. All of these combined plasma phenomena (natural and induced) contribute to payload material degradation and enhanced EMI. Risk mitigation is the plasma contactor which attempts to control the ISS potential differences to within ± 40 volts of the ionospheric plasma potential, and grounding architecture.

Relevant documentation is: *JGR* **97**, 2985 (1992), Ref. 80; *JGR* **90**, 11009 (1985), Ref. 81; SSP 41000; SSP 30425; SSP 30420; SSP 30240; SSP 30245; IGRF (Ref. 83); IRI (Ref. 84); AP-8 and AE-8 (Ref. 85); EWB 3.0 (Ref. 86).
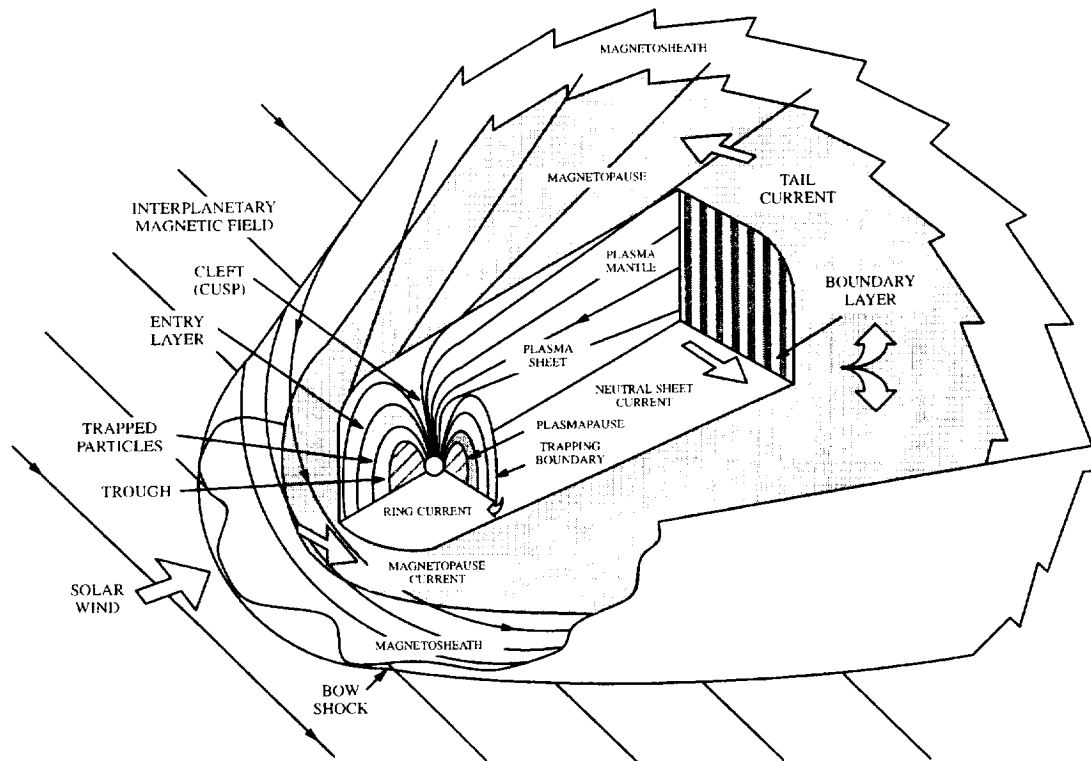
Figure G.5. Earth's plasma environment, adapted from Heikkila[79].
(reprinted by permission of the AGU)

Ionizing radiation

ISS payloads are continuously exposed to charge particle radiation and cosmic rays (ionized nuclei) which vary with solar activity (Figure G.6) and geomagnetic activity (Figure G.7). Sources include: (1) inner trapped radiation belts of the Earth (Figures G.8-G.11); (2) Galactic cosmic rays; and (3) energetic solar event particles. The consequences include material degradation, electronic microcircuit and avionics single-event effects (SEEs), human radiation exposure, and payload experiment anomalies. SEEs include single-event upset (SEU), transients, latch-up, burnout, and gate rupture. The highly energetic events can even result in total avionics failures and partial or total loss of payload electronic circuitry functions. Risk mitigation against space radiation includes some shielding (~ 250 mils) as beneficial for the low-energy particles (Figures G.12-G.14), ops work-arounds (such as power-off during energetic solar events or possibly presence in the SAA), and multipath redundancy design in avionics such that hard failures are compensated for and are multi-fault tolerant. Figures G.6-G.14 are adapted from SSP 30512C.

Relevant documentation is: Messenger & Ash, *Single Event Phenomena* (Ref. 39); *JGR* **98**, 13281 (1993), Ref. 82; SSP 30000, Sec. 3, M1; SSP 30420B; SSP 30425B; SSP 30512C; SSP 30513A,B; SSP 50005; IGRF (Ref. 83); IRI (Ref. 84); AP-8 and AE-8 (Ref. 85); EWB 3.0 (Ref. 86).

145
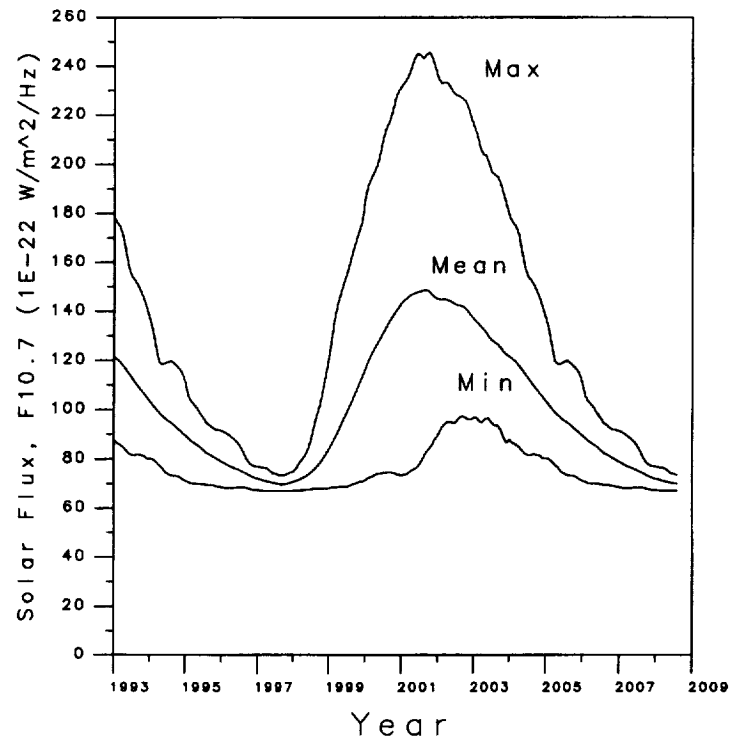
Figure G.6. Solar flux model ($F_{10.7}$) over the mean solar cycle.
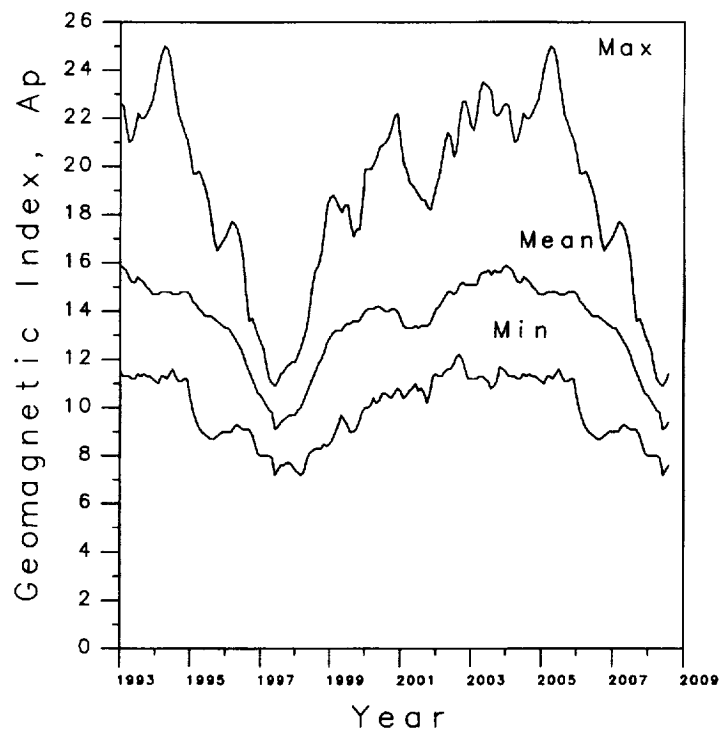
Figure G.7. Geomagnetic activity index (A_p) over the mean solar cycle.

146
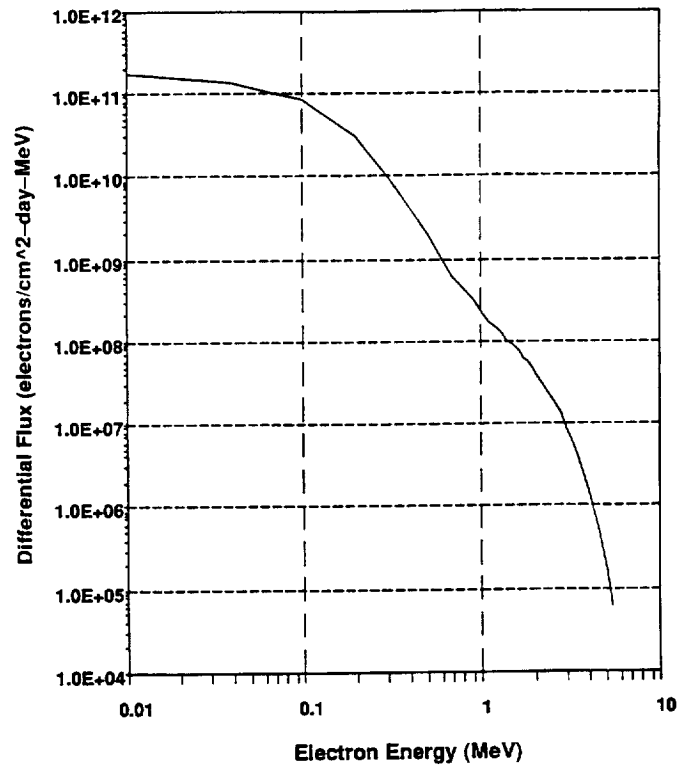
Figure G.8. AE8MAX electron differential flux at 500-km altitude.
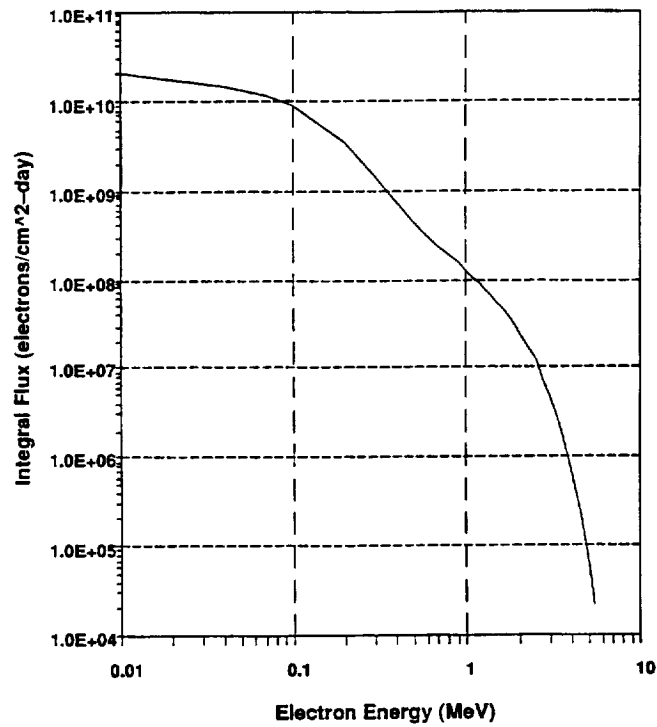
Figure G.9. AE8MAX electron integral flux at 500-km altitude.

147
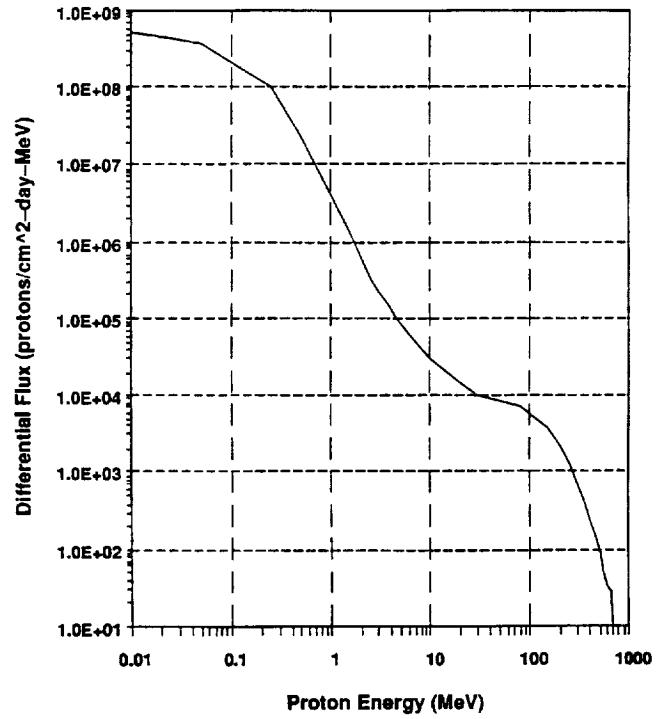
Figure G.10. AP8MAX proton differential flux at 500-km altitude.
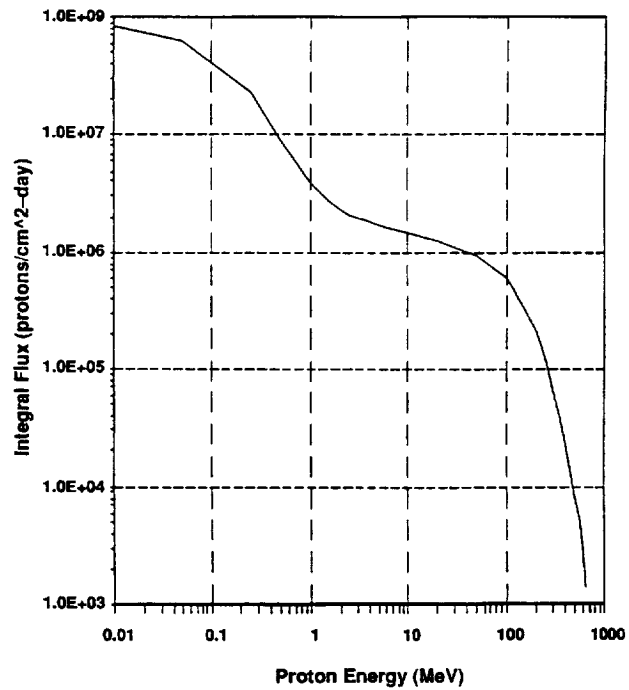
Figure G.11. AP8MAX proton integral flux at 500-km altitude.

148
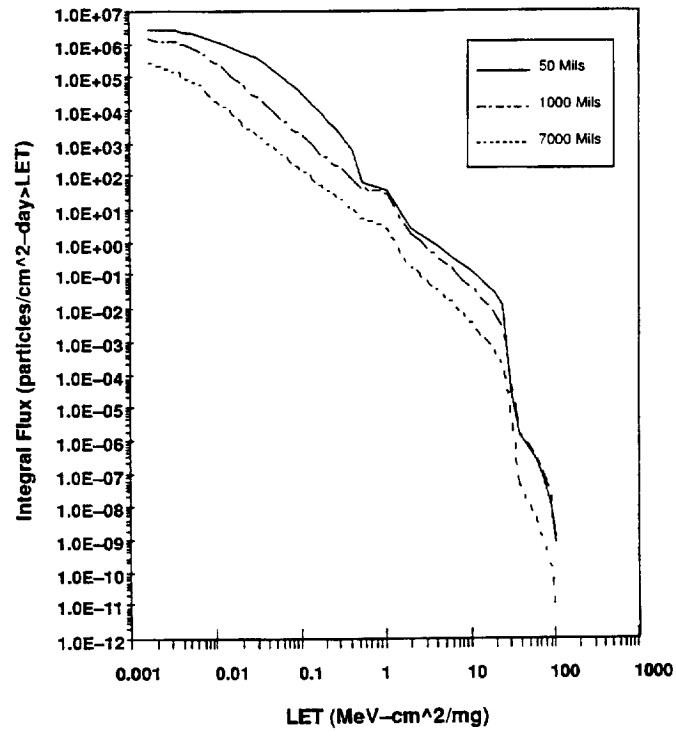
Figure G.12. Combined integral flux LET spectra, no solar flare component.
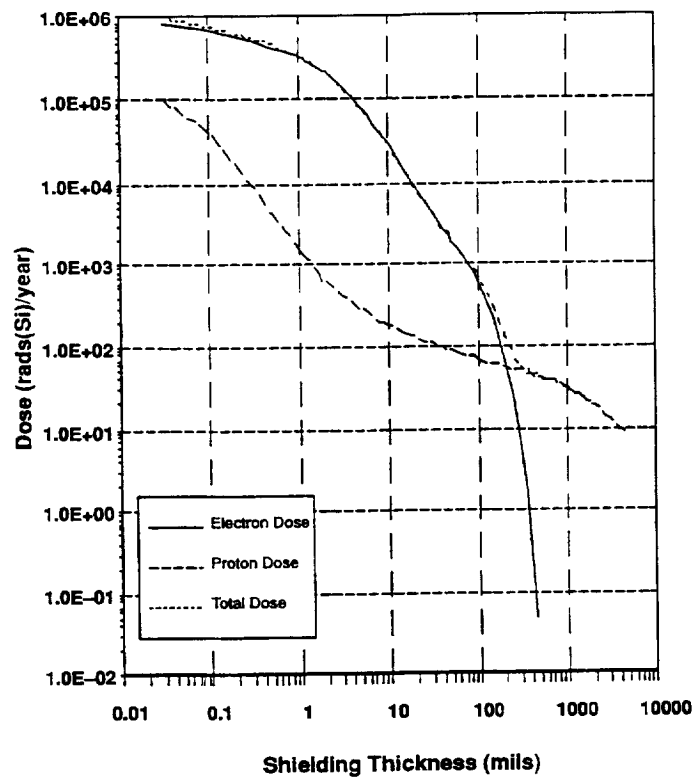
Figure G.13. One-year dose at the center of a solid aluminum sphere.

149
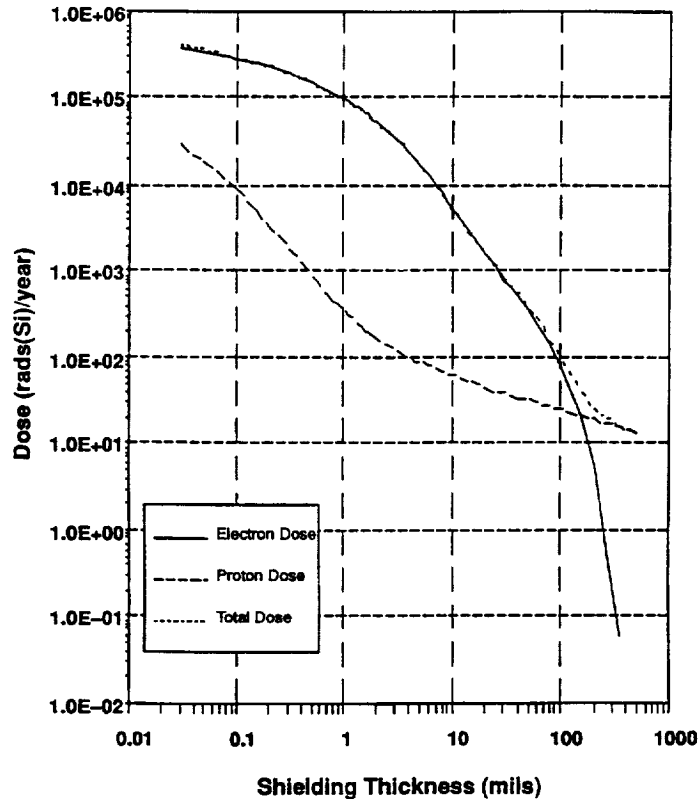
Figure G.14. One-year dose in a semi-infinite aluminum medium.

Relevant computer transport codes and radiation simulation models include: IRI86 and IRI90, AP8MAX/MIN, AE8MAX/MIN, BREM, PDOSE, HZETRN, VETTE, CREME, Proton Vector Flux model, CADRays, IBM SEU Code, Shieldose, GEANT, and FLUKA.

Relevant websites include Boeing's Radiation Effects Laboratory.

Micrometeoroids and orbital debris

Orbiting in LEO, the ISS will undergo collisions with natural micrometeoroids and man-made orbital debris (space junk) left over from spacecraft collisions and explosions. Highly improbable catastrophic collisions are not considered here. However, NASA's surveillance programs in conjunction with the Air Force Defense Command have measured and determined the collisional cross sections and collisional probabilities. These data in turn show that the ISS will be "hit" with a certain flux (Figure G.15) and frequency over its lifetime. Some of the collisions with micron-sized particles can necessarily result in the degradation of unshielded ISS components and equipment (e.g., solar arrays). Typical impact velocities are 8-14 km/sec for debris and as much as 19 km/sec for micrometeoroids. Risk mitigation is debris shields or "bumpers" placed in the ram direction for debris and in the zenith direction for micrometeoroids. Calculation of such shielding is supported by the JSC orbital debris program (with website @ sn-callisto) and the JSC HITF, with website @ hitf. Because pressurized vessel penetration is a potential consequence, crew safety can be jeopardized by a rupturing vessel. Any pressurized "tank" intended for the ISS must therefore pass adequate safety reviews, and actually becomes a "tank system" with the tank enclosed in a debris shield box, which prevents vessel rupture. An

150

example would be the gaseous tank supply system required for the baseline ACCESS TRD instrument.

COMPARATIVE DEBRIS AND METEOROID FLUXES
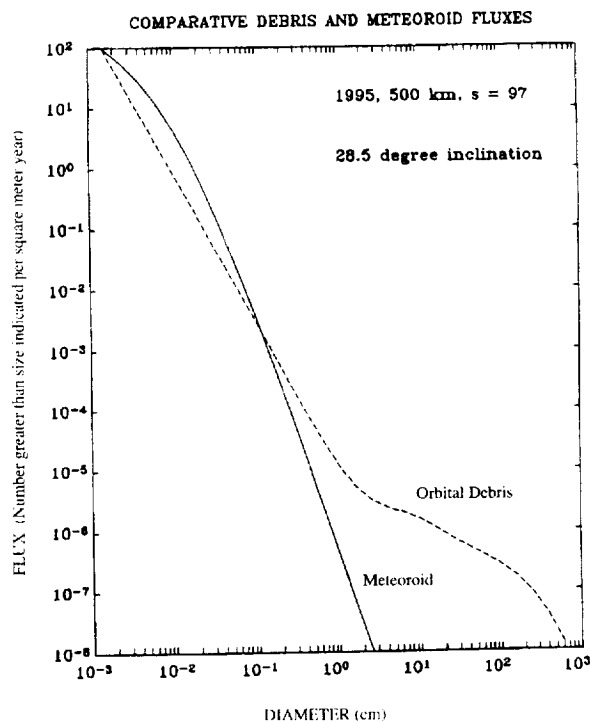
Figure G.15. Meteoroid and orbital debris flux.

Relevant documentation is: SSP 30425, Sec. 8; Ref. 43.

Relevant websites include: Orbital Debris Lab and Hypervelocity Impact Facility.

Electromagnetic interference

The STS and ISS electromagnetic environments are particularly relevant for science payload function and operation. It is important that instrumentation and avionics systems function without degradation due to interference from other payloads and spacecraft activity, in the presence of a radio-frequency background emitted by the Earth. One obvious source of such environmental conflict is the potential for EMI or noise generated by other payloads or neighboring equipment. Examples of EMI would include inadvertent radiation or emissions from electrical power systems, switching devices, motors, and avionics circuitry. Other examples are transmitters and receivers, cabling geometry, wiring configuration, grounding schemes, and bonding methods. Consequences of EMI include fundamental noise and interference, ground loops, cross-talk in cabling, sporadic behavior and equipment upsets, static charge buildup, and sporadic sources of electromagnetic radiation. Risk mitigation includes EMI safety review, emission and susceptibility limits with margins, wiring and cabling separation, electromagnetic shielding, EMI testing, adequate grounding, electromagnetic isolation, and appropriate bonding methods. EMC and the EMI control plan are the subject of SSP57010, Appendix G. A general discussion of natural EMI sources is given in SSP 30425B, Figure 7.1.

151

Relevant documentation is: SSP 57010G, SSP 30237, SSP 30242, MIL-STD-461, SSP 30243, SSP 30238, MIL-STD-1576, SSP 30240, and SSP 30245.

Contamination

Degradation of ISS payload performance through contamination of external surfaces is another environmental concern. This is usually defined as molecular or particulate deposits which, in combination with solar ultraviolet radiation, atomic oxygen, and the ambient plasma, can alter the optical, thermal, and surface properties of payload surfaces. Floating contamination could obstruct the FOV, degrade visibility, and possibly compromise certain science payload objectives. Surface contamination includes any molecular or particulate releases from the STS and ISS during operations. An example was urea from flight crew urine dumps during proximity operations for Long-Duration Exposure Facility retrieval, discovered to be coating the entire payload during postflight analysis. Other potential contamination sources include outgassing. Some consequences are change in thermal control performance, degradation of solar array efficiency, obstruction of FOV, and instrument clogging. Risk mitigation includes prelaunch contamination control, appropriate prox ops procedures regarding plume impingement, venting, and dumps, and safety reviews.

Relevant documentation is: SSP 30426, ASTM-E595-84, JSC SC-C-0005C, NSTS 07700-Vol. XIV, Appendix 1, MCR-86-2004.

Acoustics, Stress, and Vibration

The subject of acoustical interference, stress, and vibration is pertinent to all STS and ISS mission phases in both the ground and space segments. Audible noise from operating equipment and instrumentation is an issue of crew and personnel safety. Acoustical noise transmitted by phonon propagation, resonance, and structural vibration can result in degradation of payload performance, falling into the categories of EMI discussed above. Stress and vibration are the subject of rigorous safety review and were the basis of the ACCESS carrier analysis described in the body of this report. All can result in mission failure. Risk mitigation is a thorough safety review process.

Relevant documentation is: SSP 50005, MIL-STD-5G, NSTS-14046, JSC 73642, NSTS-1700.7B, SSP 50021.

Appendix H. Interface Hardware, Kits, and Incompatibilities

The hardware *per se* will be discussed in section H.1, while functional incompatibilities which impact power and data interfaces are presented in section H.2.

H.1 Hardware per se

The following Table is a preliminary assessment of ISS interface hardware that may be required for the ACCESS payload. All of the hardware should be provided government-furnished equipment (GFE) to the payload at no cost. All deliverables are compatible with the 36-month schedule template for launch.

NASA-ISS Provided Hardware	Interface Definition Provided	Deliver HDWR for prelim IVTs (if req'd)	Deliver Flight Hardware
PAS/UMA "Kit"	L-42	L-24	L-18
Grapple Fixtures	L-36	L-20	L-14
ROEU	L-34	L-18	L-13
Video Cameras, Targets	L-24	L-16	L-12
EVA Handrails, Tether Attach	L-24	L-14	L-11
PFR Attach Points	L-24	L-14	L-11

Prototypes, qualification units, or special test equipment required for mechanical fit-checks and electrical or data IVTs should also be provided when required. This Table must be revised as the ISS and PAS interface requirements are defined.

Passive PAS/UMA "kit"

NASA-ISS will probably provide all flight hardware components for attached payloads in a standard adaptable "kit" that would include the passive half of the PAS and UMA. This would also include the EVA unloadable or removable capture bar mechanism that is now required for all payloads since NASA-ISS eliminated the redundant motors on the PAS capture latch assembly. If a standard passive PAS/UMA kit were provided, it might also eliminate the need for a ground adjustable capture bar that would allow the proper preload to be imposed by the PAS capture latch. All the other components listed above should be provided in the attached payload "kit."

Grapple fixtures

When the Accommodation Study Team proposed the ACCESS USS option[7] in 1996, the original scenario was to remove it from the payload bay with the Shuttle RMS (SRMS), pass it off to the Space Station RMS (SSRMS), and install it on the S3 upper inboard PAS site without translating the mobile transporter (MT). If there were no problems, this would take a few hours and ACCESS would not need keep-alive power. Originally, this was to be accomplished using at

least two relatively inexpensive, unpowered FRGFs supplied by the ISS Program. In other words, this was a mechanical interface only.

However, since the PAS weight and CG envelopes have been considerably reduced, a retractable keel trunnion assembly mechanism(s) will probably be required on the USS option with EVA contingency operation. Otherwise, ACCESS must go with the ECS.

Therefore, an ACCESS-with-USS option would require at least one EFGF to operate and control the retractable keel mechanism from the SRMS after the payload is unberthed from the Shuttle. Once the keel is moved to expose the passive PAS, a FRGF is still needed for the SSRMS to grab and install ACCESS/USS on the PAS. If this operation were to take several hours or even days due to equipment or logistical problems, ACCESS (ECS or USS) would need to be handed back to the SRMS to get keep-alive power (via an EFGF) or get power from the SSRMS (via a power and data grapple fixture, or PDGF).

This would mean replacing the relatively cheap FRGF with an expensive (≈$700K) PDGF because the EFGF is not currently compatible with the SSRMS. The PDGF is an ISS orbital replacement unit (ORU) that could be removed from the ECS or USS via EVA and recycled while ACCESS is on the ISS if necessary.

If ACCESS were to need to be moved on the MT at some point, a third grapple fixture (FRGF or PDGF?) may be needed somewhere else on the ECS or USS.

Remotely operated electrical umbilical

NASA/ISS may consider performing a post-launch functional test of the ACCESS experiment prior to unberthing from the payload bay of the Shuttle. This way, problems that may lead to a return-to-Earth decision can be detected prior to installation on the ISS truss. Also, if the rendezvous and docking with the ISS takes longer than expected, or problems with other payloads and logistics carriers delay ACCESS installation on the PAS, ACCESS may require keep-alive power in the payload bay of the Shuttle to stabilize the temperature of its TRD gas system.

For any of these scenarios, NASA-ISS should provide one complete ROEU payload half, compatible with the Space Shuttle half. Depending upon the ACCESS payload interface design (Appendix H.2 below), an assembly power conversion unit (APCU) may also be required.

Video cameras or targets

NASA-ISS must provide any video cameras or targets if required for berthing the ACCESS payload on the active half of the PAS. ACCESS would integrate the targets.

EVA handrails and tether attach points

NASA-ISS should provide any EVA handrails and tether attach points needed to allow passage around areas that will be blocked by the ECS or USS on the S3 truss segment PAS due to new EVA translation envelope requirements. These may also be required because the reduced PAS weight and CG envelopes will cause the payload to be located lower on the truss, thus causing an EVA translation corridor path blockage.

Portable foot restraint attach points

NASA-ISS should provide any PFR attach points required on the ECS or USS to provide coverage for areas of the S3 Truss Segment that may be blocked by the ECS or USS. This is to maintain the capability to service ISS ORUs in the area.

Schedule

The Table is a preliminary estimate in L-months of the lead time needed to incorporate the design, manufacturing, and installation of each of the hardware components into the ACCESS payload.

Interface definition requirements (specifically IRD SSP 57003 and CR 1135[32] which modifies it) for the PAS and UMA, whether they are in a "kit" or not, will have the greatest impact on the overall payload configuration. It is these requirements that will define the position and orientation of the payload on the PAS as well as in the Space Shuttle. There is a reasonable chance that the completely new carrier structure will be required in order to comply with CR 1135. This is why the interface definition needs to be provided as early as possible. Other components, like video cameras, EVA handrails, and PFR attach points, will have less impact and can be incorporated into the design later.

Presently, 11 months lead time is required from submittal of a planning purchase request to delivery of an FRGF. For an EFGF, 14 months lead time is needed and 20 months is needed for a PDGF and its cable harness. Since the flight hardware must be ready for installation at L-14 months, these need to be ordered at L-25 to L-34 months.

H.2 STS functional incompatibilities

As mentioned under "ACCESS Accommodation on STS" in the main text of this report, there are three distinguishing features about STS accommodations, summarized in Table H.2-1.

Table H.2-1. STS-ISS Accommodation Incompatibilities

- *STS power is 28 VDC while ISS PAS power is 120 VDC.*
- *STS high-rate data travels via copper wire while the ISS uses fiber optics.*
- *STS low-rate data and command is via the payload signal processor (PSP) and payload data interleaver (PDI), while the ISS uses 1553 data bus.*

Figure H.2-1 functionally illustrates the STS power and data accommodation interface. The ROEU provides the physical connection between the Shuttle cabin and its payload bay for transferring power (28 VDC) and data (low-rate 1553 data bus and high-rate copper wire). From Table H.2-1, additional hardware may be required, depending upon the functional STS requirements to support the ISS ACCESS payload and the design of ACCESS itself. Table H.2-2 summarizes the STS accommodation situation.

STS Power and Data Accommodations
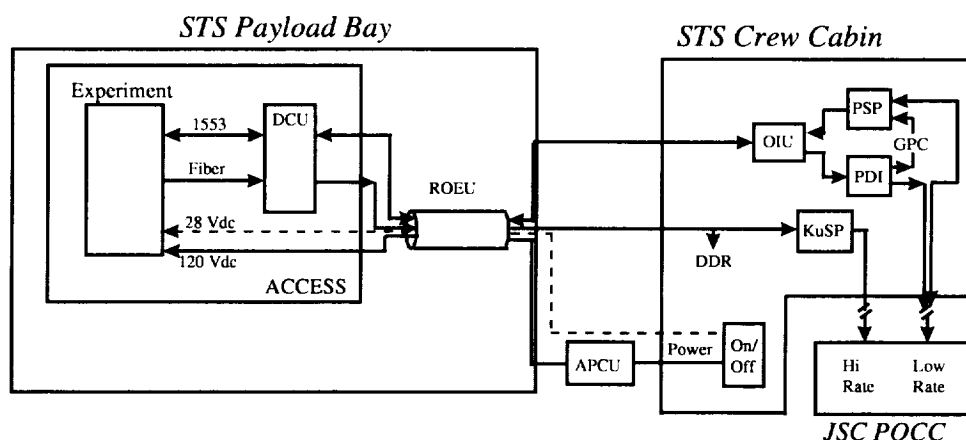
Figure H.2-1 STS accommodation interfaces.

Table H.2-2. Examples of STS Accommodation Requirements

Requirement	*Outfitting*
• *Provide power at 28 VDC.*	• *ROEU*
• *Provide power at 120 VDC.*	• *ROEU and APCU*
• *Provide low-rate data via S-band.*	• *ROEU and OIU*
• *Provide high-rate data via Ku-band*	• *DCU and ROEU*
• *Provide all of the above.*	• *DCU, ROEU, APCU, OIU*

Only the ROEU in Table H.2-2 is GFE. The others are costs incurred by the payload.

If the STS payload bay accommodation requirement is only power in order to activate the ACCESS heaters in its thermal control system for stabilizing the TRD gas system (Appendix B.3, Figure B.3-5), only an ROEU is required. From Figure H.2-1, the APCU, DCU, and OIU are not necessary if the payload heater system for the thermal control can function using the STS 28 VDC power available in the ROEU interface.

If the ACCESS payload is designed to operate on both 28 VDC and 120 VDC power (Figure 27 in the main text), the APCU in Figure H.2-1 and Table H.2-2 is unnecessary. A redundant heater system or internal power conversion (28 VDC $\Leftrightarrow$ 120 VDC) in Figure 27 can accomplish this.

If no live science data downlink functional test is required before unberthing the ACCESS payload from the Shuttle bay, and the previous paragraph above is complied with, then only the ROEU in Figure H.2-1 is required for STS power accommodations.

H.3. Functional PAS and UMA interfaces
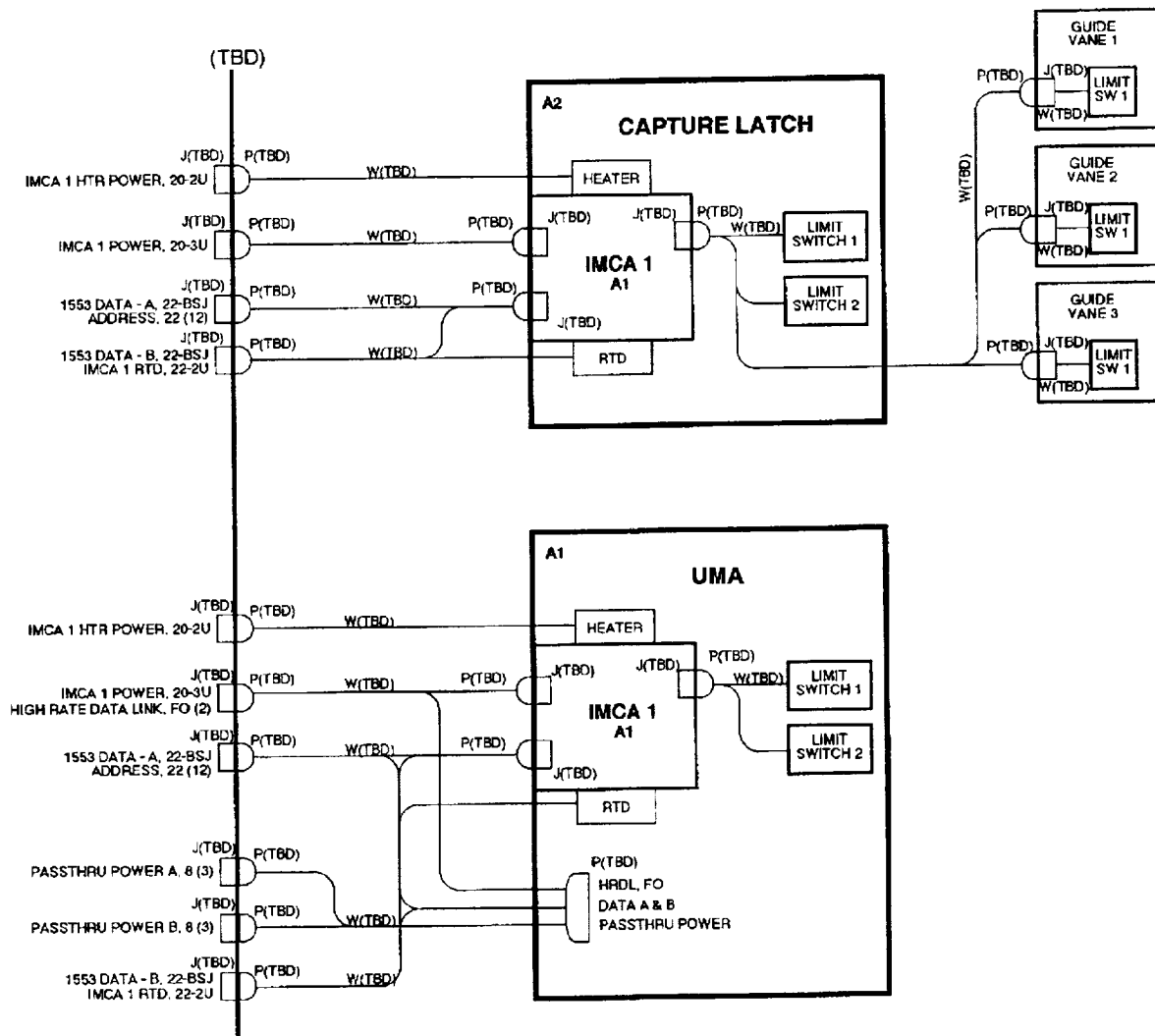
Figure H.3-1. PAS interface block diagram.

Appendix I. PCU Tank System, Details
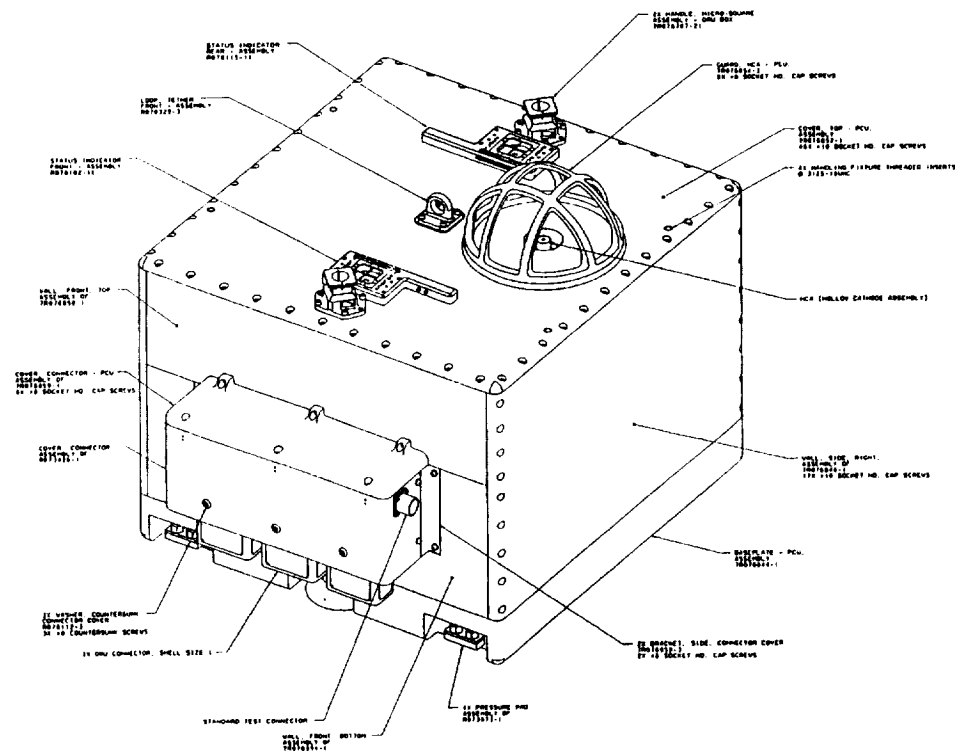
Figure I-1. PCU box.
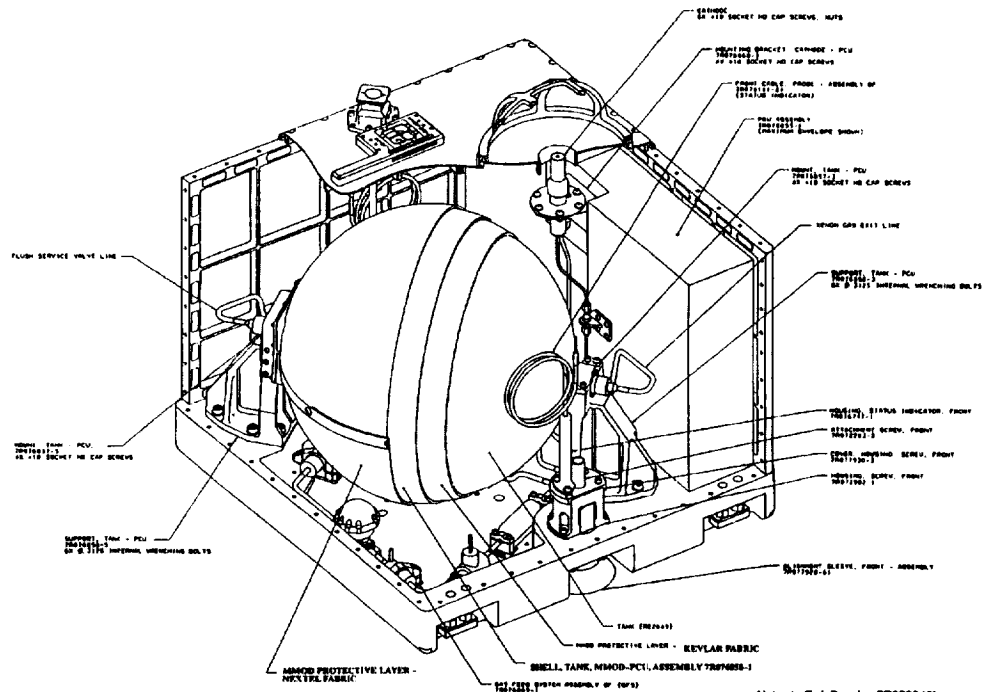
Figure I-2. Cut-away configuration of PCU box.

Appendix J. Acronyms, Symbols, and Definitions

Acronym	Meaning
ACCESS	Advanced Cosmic-Ray Composition Experiment for Space Station
AC	Assembly Complete
ACE	advanced composition explorer
ACLB	ASIC control logic board
A/D	analog-to-digital
ADC	analog-to-digital converter
AE8MAX(MIN)	trapped electron flux computer code
AGU	American Geophysical Union
Al	aluminum
AMS	alpha magnetic spectrometer
AP	attached payload
AP8MAX(MIN)	trapped proton flux computer code
APCU	assembly power converter unit (ISS)
APCU	auxiliary power conversion unit (Shuttle)
APFR	Avionics Planning Flight Review
APL	approved parts list
APLSS	attached payload support structure
APM	attached pressurized module
APS	automated payload switch
Ar	argon
As	arsenic
ASIC	application-specific integrated circuit
Assy, ASSY	assembly
ATC	aerogel threshold counter
ATP	Acceptance Test Plan
ATIC	advanced thin ionization calorimeter
Avionics	aviation electronics
Avionics	aerospace electronics
B	boron
Be	beryllium
BGO	bismuth germanate ($Bi_4Ge_3O_{12}$ - chemical formula)
B/L	baseline
BLKT	blanket
BOL	beginning of life
Br	bromine
C	carbon
CAL	calorimeter
Caltech	California Institute of Technology
CAM	centrifuge accommodations module
cap	capacitor
C&C MDM	command and control MDM
C&D	command and data
C&DH	command and data handling
CCF	consolidated communications facilities
CCSDS	Consultative Committee for Space Data Systems
CDR	comprehensive design review
CETA	crew and equipment translation aid
CEU	control electronics unit
Cert	certification

c.f.	confer, compare
CG	center of gravity
CIR	cargo integration review
CITE	cargo integration test equipment
CLA	capture latch assembly
cm	centimeter
cm^2	cm^2
CMD	command
CMG	control moment gyro
CMOS	complementary metal oxide semiconductor
CNO	carbon, nitrogen, oxygen element group
CONTAM	contamination
COR	communications outage recorder
COTS	commercial-off-the-shelf
CPDS	charged particle differential spectrometer
CPU	central processing unit
CR	change request
CREME	Cosmic Ray Effects on Micro-Electronics (computer code)
CRF	Canister Rotation Facility
CRN	cosmic-ray nuclei (Experiment, Spacelab-2)
CRV	crew return (rescue) vehicle
Cs	cesium
CSR	customer support room
DC	direct current (power)
DC	docking compartment
DC&I	design, certification, & integration
DCU	data conversion unit
DDCU	DC-to-DC converter unit
DDR	digital data recorder
DDT&C	design, development, test, and certification
DDT&E	design, development, test, and evaluation
DESY	Deutsche Electonishen Synchrotron
DIM	digital interface module
DNY	Downey
DSM	docking and stowage module
E	energy
E-net	Ethernet
ECLSS	environmental control and life support system
ECS	experiment carrier structure
EDAC	error detection and correction
EDO	extended-duration orbiter
EEE	electrical, electronic, and electromechanical
EF	Exposure Facility
EFGF	electrical flight releasable grapple fixture
E.g., e.g.	for example
EGSE	electrical ground support equipment
ELM	experiment logistics module
EMC	electromagnetic compatibility
EMCS	enhanced mission communications system
EMI	electromagnetic interference
EMICP	EMI control plan
EMU	extravehicular mobility unit
ENG	engineering
EOL	end of life

ERA	European robotic arm
ESA	European Space Agency
ESTL	Electronic Systems Test Laboratory
etc.	et cetera
ETE	end-to-end
EUV	extreme ultraviolet
EVA	extravehicular activity
EVAL	evaluation
EWB	environmental workbench
EXP	experiment
F	fluorine
Fab	fabrication
FAR	flight acceptance review
FAR	Federal Acquisition Register
FAWG	Flight Assignment Working Group
FDRD	Flight Definition Requirements Document
Fe	iron
FEM	finite element model
FEM	front-end module
FEMA	failure modes and effects analysis
FGB	functional cargo block (Russian control module, Zarya)
FIP	first ionization potential
Flt, FLT	flight
FLUKA	Fluctuating Cascade (German) computer code
FOR	flight operations review
FORTRAN	formula translator
FOV	field of view
FPSR	flight planning and stowage review
FRGF	flight releasable grapple fixture
FRR	flight readiness review
FSE	flight support equipment
FUNCT	functional
g	gram
G	giga-
GC	generally clean
GEANT	Giant (French), simulation computer code
GFE	government-furnished equipment
GHE	ground handling equipment
GN&C	guidance, navigation, and control
GOAL	galactic origin and acceleration limit
GOWG	Ground Operations Working Group
GPC	general purpose computer (Shuttle)
GPS	global positioning satellite
GRAM	global reference atmosphere model (MSFC)
GRND	ground
GSE	ground support equipment
GSFC	Goddard Space Flight Center
H	hydrogen
Hab	habitation
HCOR	operational version of COR
He	helium
HEAO	High-Energy Astrophysics Observatory
HEXTE	high-energy X-ray telescope experiment
HITF	Hypervelocity Impact Facility
HMP	hazard mitigation plan

HODO	hodoscope
HORIZ	horizontal
HOSC	Huntsville Operations Support Center
HQ	Headquarters
HSKP	housekeeping
HST	Hubble Space Telescope
HTR	heater
HV	high voltage
HVI	hypervelocity impact
I	inboard
ICD	Interface Control Document
ICRC	International Cosmic Ray Conference
ID	identification
IDD	Interface Definition Document
IEEE	Institute for Electrical and Electronic Engineers
I/F	interface
IF	interaction factor
IGRF	international geomagnetic reference field
IMCA	integrated motor control assembly
In	indium
INST'LN	installation
INTG	integration
IR	infrared
IRD	Interface Requirements Document
IRI	international reference ionosphere
ISPR	international standard payload rack
ISS	International Space Station
ITA	integrated truss assembly
ITA-S	ITA-starboard
ITA-P	ITA-port
IVT	interface verification test
IV&T	integration, verification, and test
JACEE	Japanese-American cooperative emulsion experiment
JAM	joint airlock module
JCP	Japanese Control Program
JEM	Japanese equipment module
JEM	Japanese experiment module
JGR	Journal of Geophysical Research
JIS	joint integrated simulation
JSC	Johnson Space Center
kbps	kilobits per second
KSC	Kennedy Space Center
KuSP	Ku-band signal processor
L-34	launch minus 34 months (or weeks)
L-months	time prior to launch, in months
lb	pound, pounds
LBNL	Lawrence Berkley National Laboratory
LDEF	Long-Duration Exposure Facility
LED	light-emitting diode
LEO	low Earth orbit
LEPS	low-energy particle shield
LET	linear energy transfer (Ref. 39, $MeV\text{-}cm^2/mg$)
LM, L-M	Lockheed Martin
LMES	Lockheed Martin Engineering and Sciences
LPIS	launch processing integration stand

LRR	launch readiness review
LSFR	launch site final review
LSM	life support module
LSP	launch site processing
LSRR	launch site readiness review
M	mega-
m	meter
MAG	magnet
MAPMT	multi-anode PMT
MARIE	Martian radiation environment experiment
Mbps	megabits per second
MBS	MRS base system
MCC	Mission Control Center
MCC	master control computer
MDF	minimum duration flight
MDM	multiplexer-demultiplexer
MECH	mechanical
MECH INT & PROC	mechanical integration and processing
MET	Marshall Engineering thermosphere model
Mfg, MFG	manufacturer
mg	milligram
Mg	magnesium
Mil	10^{-3} inch
MIL-STD	Military Standard
Mip	minimum ionizing particle
MIP	mission integration plan
Mips	Mip in silicon
Mission-00	Shuttle/ISS mission, TBD
MLI	multilayer insulation
mm	millimeter
MMC	(APM) mission management computer
MMO	Mission Management Office
MMOD	micrometeoroid and orbital debris
MMPF	Microgravity and Materials Processing Facility
MMPTD	Manufacturing Materials and Processing Technical Division
MPLM	multipurpose logistics module
MPPF	Multi-Payload Processing Facility
MRS	mobile remote servicer
MSB	multi-sideband
MSC	mobile servicing center
MSFC	Marshall Space Flight Center
MSIS	mass spectrometer incoherent scatter model
MSU	mass storage unit
mV	millivolt
MT	mobile transporter
MTBF	mean-time between failures
MTG, Mtg	meeting
Mux	multiplexer
MWPC	multi-wire proportional counter/chamber
n	index of refraction
NASA	National Aeronautics and Space Administration
NASDA	National Space Development Agency of Japan
NASTRAN	NASA structural analysis computer program (cf. FORTRAN)
NATO	North Atlantic Treaty Organization
Ne	neon

Ni	nickel
NISN	NASA Information Services Network
NRA	NASA Research Announcement
NSSDC	National Space Science Data Center
NSTS	National Space Transportation System
NTA	network test adapter
NTA	nitrogen tank assembly
φ	Phase (see Phase below)
φ II	Phase "Two" safety review
O	oxygen (atomic)
O2	oxygen (molecular)
Off-line	payload at KSC but not turned over to NASA
OIU	Orbiter interface unit
On-line	payload at KSC and turned over to NASA
OPF	Orbiter Processing Facility
OPS, Ops	operations (flight crew in conjunction with flight controllers)
OR	logic summing gate (electronics)
ORU	orbital replacement unit
OSE	orbital support equipment
OTD	ORU transfer device
OV	Orbiter vehicle
P	proton
P3	port 3
P/L	payload
PAH	Payload Accommodations Handbook
PAIT	Payload Accommodations Integration Team
parsec	3.258 light years
PAS	payload attach system
Pb	lead
PC	personal computer
PCS	portable computer system
PCU	plasma contactor unit
PCU	power conversion unit
PDGF	power and data grapple fixture
PDI	payload data interleaver
PDLU	payload data interleaver unit
PDM	payload data multiplexer
PDR	preliminary design review
PDSS	Payload Data Services System
PETS	Payload Environmental Transfer System
PFR	portable foot restraint
PGSC	payload general support computer
Phase	designated by "φ" (safety-review phase designation)
PIA	Program Initiation Agreement
PIP	payload integration plan
PL	payload
PLBD	payload bay doors
PLCU	payload control unit
PYLD	payload
PM	propulsion module
PMA	pressurized mating adapter
PMT	photo-multiplier tube
PNP	probability of no penetration
POCC	Payload Operations Control Center

POIC	Payload Operations Integration Center
PPL	preferred parts list
PR	purchase request
PREP(s)	preparation(s)
PRIM	primary
PROG MGR	program manager
PROM	programmable read-only memory
Prox Ops	proximity operations (on-orbit)
PSP	payload signal processor
PSV	pressure safety valve
Pt	platinum
PUP	partner utilization plan
PV	photovoltaic
PVLR	pre-VLR
Pwr	power
Q1	first quarter, etc.
Qual	qualification
R&D	research and development
RACU	Russian-American converter unit
Rad-hard	radiation hardened
RAM	random access memory
Rb	rubidium
req'd	required
RI	Rockwell International
RM	research module
RMS	remote manipulator subsystem
ROEU	remotely operable electrical umbilical
RSA	Russian Space Agency
RY	real-year (dollars)
s	second
S	sulfur
S3	starboard 3 (etc.)
SAA	South Atlantic Anomaly
SAAMD	stand-alone acceleration measurement device
Sc	scandium
Scar	placeholder interface
SCHED	schedule
SEE	stand end effector
SEE	single event effects
SEU	single-event upset
SFWR	software
Si	silicon
Sim	simulation
SLF	Shuttle Landing Facility
SLP	Spacelab pallet
SM	service module (Russian)
S/MM-09	Shuttle-*Mir* mission No. 9
SN	supernova
SNR	supernova remnant
SOI	silicon-on-sapphire insulator
SPDM	special purpose dexterous manipulator
SPIE	The International Society for Optical Engineering
SPP	science power platform
Sr	steradian
SRAG	Space Radiation Analysis Group

SRMS	Shuttle remote manipulator subsystem
SS	Space Station
SSE	Space Science Enterprise
SSP	Space Station Program
SSPF	Space Station Processing Facility
SSRMS	Space Station remote manipulator subsystem
STA	structural test article
STE	special test equipment
STS	space transportation system (Space Shuttle)
STS-00	STS flight, TBD
STS-TBD	STS flight, TBD
SWH	Spares Warehouse
S-Wire	safety wire
T	tera-
TAP	truss attached payloads
TBD	to-be-determined
TCP/IP	transfer command protocol/Internet protocol
TCP/IP	transmission command protocol/Internet protocol
TCS	thermal control system
TDRS	tracking data relay satellite
TeV	tera-electron-volt
Th	thorium
TIGER	trans-iron galactic element recorder
TIM	technical interchange meeting
TM	telemetry
TM	task/technical manager
TMA	Technical Management Area
TOF	time-of-flight
TPEC	tissue-equivalent proportional counter
TRACER	transition radiation array for composition of energetic radiation
TRD	transition radiation detector
TRIG	trigger
TRR	test readiness review
Turnkey	utilization of existing JSC DC&I methodology, personnel, & templates
T/V	test and verification
U	uranium
U	upper
UCC	unpressurized cargo carrier
UCCAS	UCC attach system
UDM	universal docking module
UF	utilization (utility) flight
UH	ultra-heavy
UI	upper inboard
ULC	unpressurized logistics carrier
ULCAS	ULC attach system
UMA	umbilical mechanism assembly
UO	upper outboard
UOF	User Operations Facility
URL	uniform resource locator
U.S.	United States of America
USOC	United States Operations Center
USOS	United States on-orbit segment
USS	unique support structure
UV	ultraviolet
V	vanadium

V	volt
VAB	Vehicle Assembly Building
VAR	verification analysis review
VDC	volts direct current
VES	vacuum exhaust system
VIB	vibration
VLA	verification loads analysis
VLR	verification loads review
VLSI	very large-scale integration
W	watts
WBS	work breakdown structure
WETF	Weightless Environment Training Facility
WG	working group
WSC	White Sands Complex
Wt	weight
WBSAAMD	wide-band stand-alone acceleration measurement device
WYE	work-year equivalent
Xe	xenon
Z	electric charge of the nucleus (atomic number)
Z1	Zenith 1
ZIM	"Z" (charge) identification module
Zn	zinc
&	and (ampersand)
1-G	one Earth-gravity (9.80665 m s^{-2})

Appendix K. Websites and Internet Access

Various ACCESS-related websites:

◆Goddard   http://www701.gsfc.nasa.gov/access/access.htm
◆Johnson Space Center   http://cass.jsc.nasa.gov
◆Office of Space Science, Headquarters   http://www.hq.nasa.gov/office/oss/
◆University of Maryland   http://www.atic.umd.edu/access.html
◆University of Chicago   http://hep.uchicago.edu/~swordy/access.html
◆Louisiana State University   http://phacts.phys.lsu.edu/access
◆Washington University, St. Louis   http://cosray2.wustl.edu/access

Various Space Station-related websites:

◆Program Automated Library System   http://iss-www.jsc.nasa.gov/cgi-bin/dsql+/ORAP?-h+pl_search
◆SSP Released documents   http://iss-www.jsc.nasa.gov/ss/issapt/payofc/documents/ozdocs.html
◆ISS Program Team   http://iss-www.jsc.nasa.gov/ss/issapt/
◆Image of ISS   http://station.nasa.gov/gallery/animstills/fin22.jpg
◆Boeing, Radiation Effects Lab   http://www.boeing.com/assocproducts/radiationlab/data.htm
◆GSFC Preferred Parts List   http://misspiggy.gsfc.nasa.gov
◆Orbital Debris Lab   http://sn-callisto.jsc.nasa.gov/model/ordem96.html
◆Hypervelocity Impact Facility   http://hitf.jsc.nasa.gov/hitfpub/main/index.html
◆ISS Assembly Sequence   http://iss-www.jsc.nasa.gov/ss/issapt/mio/mioissably.htm

Office of Space Science (OSS) websites:

◆OSS images   http://www.hq.nasa.gov/office/oss/images.html
◆Space Science Enterprise (SSE)   http://www.hq.nasa.gov/office/oss/strategy/1997/sseplanm.htm

ACCESS Study Participants

(in alphabetical order)

Institutions
◆NASA Goddard Space Flight Center
◆NASA Headquarters
◆NASA Jet Propulsion Laboratory
◆NASA Johnson Space Center
◆NASA Marshall Space Flight Center
◆California Institute of Technology
◆Louisiana State University
◆Naval Research Laboratory
◆New Mexico State University
◆Pennsylvania State University
◆Texas Tech University
◆University of Alabama
◆University of Chicago
◆University of Maryland
◆University of Michigan
◆Washington University in St. Louis
◆Institute for Theoretical and
      Experimental Physics, Moscow
◆Italian National Institute of
      Nuclear Physics (INFN)
◆Kanagawa University, Japan
◆Seoul National University, Korea
◆University of Siegen, Germany

ACCESS Project Principals:
◆Program Scientist: W. Vernon Jones
◆Project Formulation Manager: Elizabeth A. Park
◆Project Study Scientist:
      Robert E. Streitmatter
◆JSC Accommodation Study Scientist:
      Thomas L. Wilson
◆LSU Baseline Principal Investigator:
      John P. Wefel

ACCESS Baseline Principal Investigators
◆W. Robert Binns, CM
◆Dietrich Müller, TRD
◆John P. Wefel, BGO calorimeter

Cal Tech
◆Richard A. Mewaldt
◆Mark E. Wiedenbeck

Louisiana State University
◆Gary Case
◆Michael L. Cherry
◆T. Gregory Guzik
◆Joachim Isbert
◆John P. Wefel

Naval Research Laboratory
◆James H. Adams
◆Richard A. Kroeger

University of Chicago
◆Wayne C. Johnson
◆Dietrich Müller
◆Simon P. Swordy

University of Maryland
◆Eun-Suk Seo

University of Michigan
◆Gregory Tarle

Washington University, St. Louis
◆W. Robert Binns
◆John Epstein
◆Paul L. Hink
◆Martin H. Israel

JSC Legal Office, Code AL
◆Joyce R. Simmons

*JSC Earth Science and Solar System
Exploration Division, Code SN3*
◆Gautam Badhwar
◆Douglas P. Blanchard

◆Eric L. Christiansen
◆Jane H. MacGibbon

JSC Mission Management Office, Code SM2
◆Charlotte S. Hudgins
◆Karen M. Morrison
◆Michael L. Richardson
◆Fred R. Spross

JSC Safety, Reliability, and Quality Assurance
Office, Code NC4
◆Chris Cottrill

JSC Systems Integration Office, Code EA4
◆Patrick M. O'Neill

JSC Avionics and Test Analysis Branch, Code EV4
◆William X. Culpepper

Space Station Program Office, Code OM
◆Joseph K. LaRochelle
◆Nancy A. Wilks

Space Station Program Office, Code OZ
◆Gene Cook
◆David G. Corcoran
◆Dean B. Eppler
◆Robert S. Harris
◆Ned J. Penley
◆Mark Pestana

◆Rob Suggs
◆Stephen A. Voels

Lockheed-Martin
◆Gary Deardorff
◆Carolina Godoy
◆Lollie Lopez
◆Robert R. J. Mohler
◆David J. Posek
◆Don S. Probe
◆Ken S. Reightler, Jr.
◆Thomas H. See
◆Robert Stonestreet
◆A. D. Travis
◆Jerry H. Wagstaff
◆Patricia Winn

Boeing-Houston
◆Paul Boeder
◆Fred Henderson
◆Bob Martinson
◆Doug Paige

Boeing-Rocketdyne
◆Marcelo Bromberg
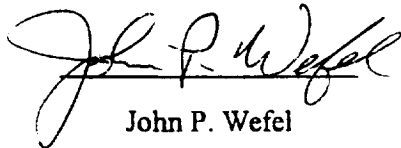
McDonnell-Douglas-Houston
◆Mark Foster
◆Janella Youmans

REPORT DOCUMENTATION PAGE

1. AGENCY USE ONLY *(Leave Blank)*	2. REPORT DATE June 1999	3. REPORT TYPE AND DATES COVERED Technical Paper

4. TITLE AND SUBTITLE
Advanced Cosmic-Ray Composition Experiment for Space Station (ACCESS) - ACCESS Accommodation Study Report

5. FUNDING NUMBERS

6. AUTHOR(S)
Thomas L. Wilson & John P. Wefel*, editors

7. PERFORMING ORGANIZATION NAME(S) AND ADDRESS(ES)

Lyndon B. Johnson Space Center
Houston, Texas 77058

8. PERFORMING ORGANIZATION REPORT NUMBERS
S-846

9. SPONSORING/MONITORING AGENCY NAME(S) AND ADDRESS(ES)

National Aeronautics and Space Administration
Washington, DC 20546-0001

10. SPONSORING/MONITORING AGENCY REPORT NUMBER
TP-1999-209202

11. SUPPLEMENTARY NOTES
* Louisiana State University

12a. DISTRIBUTION/AVAILABILITY STATEMENT

Available from the NASA Center for AeroSpace Information (CASI)
7121 Standard
Hanover, MD 21076-1320   Subject Category: 93

12b. DISTRIBUTION CODE

13. ABSTRACT *(Maximum 200 words)*
    In 1994 NASA Administrator selected the first high-energy particle physics experiment for the Space Station, the Alpha Magnetic Spectrometer (AMS), to place a magnetic spectrometer in Earth orbit and search for cosmic antimatter. A natural consequence of this decision was that NASA would begin to explore cost-effective ways through which the design and implementation of AMS might benefit other promising payload experiments.
    The first such experiment to come forward was Advanced Cosmic-Ray Composition Experiment for Space Station (ACCESS) in 1996. It was proposed as a new mission concept in space physics to attach a cosmic-ray experiment of weight, volume, and geometry similar to the AMS on the International Space Station (ISS), and replace the latter as its successor when the AMS is returned to Earth. This was to be an extension of NASA's suborbital balloon program, with balloon payloads serving as the precursor flights and heritage for ACCESS. The balloon programs have always been a cost-effective NASA resource since the particle physics instrumentation for balloon and space applications are directly related.
    The next step was to expand the process, pooling together expertise from various NASA centers and universities while opening up definition of the ACCESS science goals to the international community through the standard practice of peer review. This process is still ongoing, and the accommodation study presented here will discuss the baseline definition of ACCESS as we understand it today.

14. SUBJECT TERMS

spectrometers, cosmic rays, antimatter, International Space Station, observatories, calorimeters, accelerators, extraterrestrial radiation

15. NUMBER OF PAGES
193

16. PRICE CODE

17. SECURITY CLASSIFICATION OF REPORT	18. SECURITY CLASSIFICATION OF THIS PAGE	19. SECURITY CLASSIFICATION OF ABSTRACT	20. LIMITATION OF ABSTRACT
Unclassified	Unclassified	Unclassified	Unlimited

Authentication of Costs and Schedules

The estimated costs presented in this report for the accommodation of ACCESS as an ISS payload represent values arrived at by Lockheed-Martin as the support contractor for our Science Payloads Management Division, Code SM, at the Johnson Space Center in Houston, Texas. This payload accommodation study activity has been funded through the Office of Space Science as NRA 96-OSS-03 (New Mission Concepts in Space Science), under which it was agreed to determine an estimate of the end-to-end costs for the Mission Management Office (MMO) function here at JSC as a part of this ACCESS Accommodation Study Report. The assumptions involved in both the costs and the schedules for the MMO function are given in the text of this report. They basically treat ACCESS as a follow-on payload for the STS and ISS programs in the same fashion as we are currently handling the alpha magnetic spectrometer (AMS).

Both the costs and the schedules are acceptable, being valid estimates derived from JSC actuals for AMS.
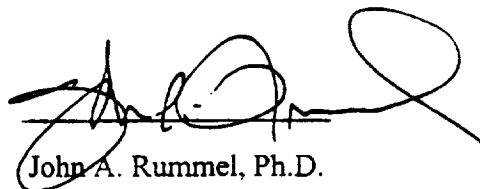
Prepared by:

John P. Wefel

Principal Investigator
Department of Physics and Astronomy
Nicholson Hall
Louisiana State University

Thomas L. Wilson

Co-Investigator
Earth Science and Solar System
Exploration Division
Johnson Space Center

Approved:

John A. Rummel, Ph.D.

Deputy Director
Space and Life Sciences
Johnson Space Center

Date